

*PURE AND RANDOM POTTS-LIKE MODELS:  
REAL-SPACE RENORMALIZATION-GROUP  
APPROACH*

Constantino TSALLIS

Centro Brasileiro de Pesquisas Físicas – CBPF/CNPq

Rua Dr. Xavier Sigaud, 150, 22290-180 – Rio de Janeiro – RJ, Brazil

and

Department of Chemistry, Baker Laboratory, Cornell University

Ithaca, NY 14853-1301, USA

and

A.C.N. de MAGALHÃES

Centro Brasileiro de Pesquisas Físicas – CBPF/CNPq

Rua Dr. Xavier Sigaud, 150, 22290-180 – Rio de Janeiro – RJ, Brazil

**Abstract**

The present status of knowledge on the pure and random Potts models and various related systems (resistor network, directed bond percolation, Ising-like frustrated models,  $Z(q)$  model and the discrete cubic model) is reviewed. The available real-space renormalization group techniques which can further enlighten this picture are tutorially presented and discussed.

**Key-words:** Potts model; Real space renormalization group; Critical phenomena; Random models.

# Contents

<b>1</b>	<b>INTRODUCTION</b>	<b>4</b>
1.1	The Potts Model . . . . .	5
1.2	Related Models . . . . .	6
1.2.1	Bond percolation and similar problems . . . . .	6
1.2.2	Resistor network . . . . .	8
1.2.3	Directed bond percolation . . . . .	9
1.2.4	$Z(q)$ model . . . . .	10
1.2.5	Random models . . . . .	13
<b>2</b>	<b>SOME EXACT OR ACCURATE RESULTS</b>	<b>15</b>
2.1	The Pure Potts Model . . . . .	16
2.1.1	$d=1$ . . . . .	16
2.1.2	$d \rightarrow 1$ . . . . .	16
2.1.3	$d=2$ . . . . .	16
2.1.4	$d=3$ . . . . .	18
2.1.5	$d \geq 4$ . . . . .	18
2.1.6	Bethe lattice . . . . .	19
2.2	The Bond-Random Potts Ferromagnet . . . . .	20
2.2.1	$d=2$ . . . . .	20
2.2.2	Bethe lattice . . . . .	21
2.3	Resistor Network . . . . .	21
2.3.1	$d=2$ . . . . .	22
2.3.2	$d \geq 3$ . . . . .	22
2.4	$Z(q)$ Model . . . . .	22
2.4.1	Isotropic $Z(4)$ ferromagnet on the square lattice . . . . .	23
2.4.2	Duality . . . . .	23
<b>3</b>	<b>TRANSMISSIVITIES AND THE BREAK-COLLAPSE METHOD</b>	<b>25</b>
3.1	Bond Percolation . . . . .	25

3.1.1	Break-collapse method and other properties . . . . .	27
3.1.2	Extension to multi-rooted graphs . . . . .	31
3.2	Potts Model . . . . .	32
3.2.1	Thermal transmissivity . . . . .	32
3.2.2	Break-collapse method and other properties . . . . .	36
3.2.3	Extension to multi-rooted graphs . . . . .	45
3.2.4	Bond-random model . . . . .	48
3.3	Related Models . . . . .	52
3.3.1	Resistor network . . . . .	52
3.3.2	Directed bond percolation . . . . .	54
3.3.3	Models with frustration . . . . .	55
3.3.4	Z(q) model . . . . .	61
3.3.5	The Discrete Cubic Model . . . . .	69
<b>4</b>	<b>REAL-SPACE RENORMALIZATION-GROUP APPROACHES</b>	<b>73</b>
4.1	Phase diagram and critical exponents . . . . .	76
4.1.1	Correlation function preserving RG . . . . .	77
4.1.2	Other real space RG approaches . . . . .	94
4.1.3	Connection between the correlation function preserving RG and the phenomenological one . . . . .	97
4.2	Equation of states and other thermodynamical quantities . . . . .	99
4.2.1	Free energy, internal energy and specific heat . . . . .	100
4.2.2	Equations of states . . . . .	102
4.2.3	Surface tension . . . . .	104
4.2.4	Correlation length . . . . .	105
4.3	Interface effects . . . . .	106
<b>5</b>	<b>FINAL REMARKS</b>	<b>109</b>
	<b>APPENDIX</b>	<b>111</b>
	<b>REFERENCES</b>	<b>130</b>

# 1 INTRODUCTION

The  $q$ -state Potts model [1] is a quite interesting classical system as it presents a remarkable richness from both theoretical and experimental standpoints. It was formulated to Potts by Domb as a PhD research subject [2]. This model has been reviewed by Wu [3] (see also [4] for developments after 1981): the reader is referred to these excellent works for information mainly concerning exact results (static properties); several experimental realizations are also discussed in [3]. Further related relevant theoretical work can be found in Ref. [5].

In the present review we mainly deal with the available real-space renormalization-group (RG) approaches of the pure and various random Potts models, its particular cases and its extensions. The properties on which we essentially focus are the phase diagram, critical exponents and amplitudes, free and internal energies, specific heat, equations of states, surface tension, correlation length, and finally some quite rich surface and interface effects.

The review has been prepared with every care for *exactness* but not necessarily for *rigor*. It is organized as follows. In Section 1 we introduce the various models we are interested in. In Section 2 we briefly recall most of the available exact (or nearly so) results; this information will be frequently used as tests for the approximate frameworks which we shall develop. In Section 3 we introduce convenient variables (*thermal transmissivities*) and present a quite performant operational procedure (referred to as the *Break-collapse method* (BCM)) which enables, through simple topological operations, the exact calculation of correlations as well as zero-field partition functions. In Section 4 we present the main existing RG approaches (with special emphasis on those which use the procedures introduced in Section 3) for calculating relevant static quantities. Finally, in Section 5, we present possible lines which could further enlighten and expand the present status of knowledge.

## 1.1 The Potts Model

Slightly different notations are used to define the  $q$ -state Potts model Hamiltonian; we shall use the following one:

$$\mathcal{H} = -q \sum_{i,j} J_{ij} \delta_{\sigma_i, \sigma_j} \quad (\sigma_i = 1, 2, \dots, q, \forall_i) \quad (1)$$

where the sum runs over all pairs of “spins” located at the sites of an arbitrary lattice (finite or infinite, regular or not, translationally invariant, i.e., Bravais lattice, scale invariant, i.e., fractal lattice, etc.) and  $\delta_{\sigma_i, \sigma_j}$  is the Kroenecker’s delta.  $J_{ij}$  might be non-null only for first-neighbours (the notation  $\langle i, j \rangle$  will then be used) or might extend arbitrarily far away;  $J_{ij} > 0$  and  $J_{ij} < 0$  will be respectively referred to as *ferromagnetic* and *antiferromagnetic* couplings. The particular case  $q = 2$  is (through a trivial energy shift in the Hamiltonian) identical to the standard spin 1/2 Ising model. But for arbitrary  $q$ , the Potts model has to be clearly distinguished from the plain spin  $S$  Ising model with  $q \equiv 2S + 1$ , whose Hamiltonian is given by

$$\mathcal{H}^{Ising} = -\frac{1}{S^2} \sum_{i,j} J_{ij}^{Ising} S_i^z S_j^z \quad (2)$$

with  $S_i^z = S, S - 1, \dots, -S, \forall_i$ , where  $S$  is a fixed integer or half-integer positive number.

The elementary Potts interaction (single bond) yields a *two*-level spectrum: one level with energy  $-qJ_{ij}$  and degeneracy  $q$ , and the other one with energy 0 and degeneracy  $q(q - 1)$ . The elementary Ising interaction yields instead a complex spectrum which takes values in the interval  $[-|J_{ij}^{Ising}|, |J_{ij}^{Ising}|]$ , and which presents  $(S + 1/2)(S + 3/2)$  levels (with degeneracies 2 or 4) if  $S$  is a half-integer, and  $S(S + 1) + 1$  levels (with degeneracies 2 or 4 excepting for the vanishing energy level whose degeneracy is  $4S + 1$ ) if  $S$  is an integer. In spite of the relative complexity of this spectrum, the spin  $S$  Ising (ferromagnetic) model brings no deep novelty in the Critical Phenomena area as it belongs to the same universality class (i.e., it shares the same critical exponents) as the spin 1/2 Ising (ferromagnetic) model [6]. The Potts model instead exhibits, already for its ferromagnetic case, a rich criticality (due to the degeneracy of its lower-energy level), as will be seen later on.

Notice that if we add other terms to eq. (1), the Potts model can be formulated as a spin  $S = (q - 1)/2$  system whose Hamiltonian is more complex than the above eq. (2) (see section IV E of [3] for more details).

## 1.2 Related Models

The Potts (or Ashkin-Teller-Potts or standard, as sometimes referred to) model in its plain formulation (eq. (1)) or in a more general one with many-body interactions is placed at a privileged position in a complex network of relations and isomorphisms (or at least analogies) between important (and less important!) geometrical and/or thermal statistical models, in the same or in a related lattice structure. This network includes several types of uncorrelated and correlated, directed and non-directed (or isotropic, as sometimes referred to), bond, site, bond and/or site, multisite and mixed percolation problems [7–22], antipercolation [23, 24], generalized resistor and diode network problems [25–28] (including Kirchhoff 1847 laws), the  $Z(q)$  model [29–34], the planar (or vector or clock, as sometimes referred to) Potts model (chiral or not) [35, 36], the Potts lattice gas [37], polychromatic Potts model [38], polychromatic majority model [39], the classical and quantum, finite or infinite spin length, n-vector models [40] (including the Ising, XY, Heisenberg and spherical models), the discrete cubic model [41–50], the  $(N_\alpha, N_\beta)$  model [51], polymer problems [52, 53], quenched and annealed bond and/or site random problems [54, 55], various vertex models [5, 56, 57] (including the ice-rule vertex models), spin glass models [58], the Blume-Capel [59, 60] and the Blume-Emery-Griffiths [61] models.

It is completely out of the scope of the present review to give an exhaustive description of the ensemble of models involved in this network and to analyze their intricated relationships (such an effort would require a review exclusively dedicated to this task!). Herein we restrict our attention to those few (but relevant) models that attracted considerable and fruitful RG effort.

### 1.2.1 Bond percolation and similar problems

The *bond percolation* problem [62, 7, 8, 14] consists in considering a lattice (typically a regular d-dimensional Bravais lattice) whose bonds might be independently *present* (or

*active*) with probability  $p$ , or *absent* (or *blocked*) with probability  $1 - p$ . It is known that, for  $p > p_c$  ( $p_c \equiv$  *critical probability or concentration*), two infinitely distant lattice sites are connected with *finite* probability, whereas this probability vanishes for  $p \leq p_c$  (by “connected” we mean that, between those two sites, exists at least one path constituted by present bonds). For  $0 < p < p_c$ , the system is exclusively constituted by a large number of *finite* clusters (cluster  $\equiv$  connected ensemble of bonds); for  $p > p_c$ , one (and only one under standard conditions) [63] *infinite* cluster appears as well (for  $p = 1$ , the infinite cluster essentially coincides with the entire lattice). The *mean linear size* (or *correlation length*)  $\xi$  of the (infinite) set of *finite* clusters behaves, in the neighbourhood of  $p_c$ , as follows:  $\xi \sim A_{\pm}/|p - p_c|^{\nu_p}$ . The *critical amplitudes*  $A_+$  and  $A_-$  respectively correspond to  $p \rightarrow p_c + 0$  and  $p \rightarrow p_c - 0$ ; the *critical exponent*  $\nu_p$  depends on  $d$  but not on the particular Bravais lattice, whereas  $p_c$ ,  $A_+$  and  $A_-$  depend on both.

A notorious connection [16] exists between the general *bond* percolation problem in a given lattice (e.g., Bravais, Bethe, hierarchical [64–66] lattices), all the bonds of which have (possibly different) independent occupancy probabilities  $\{p_{ij}\}$  (between sites  $i$  and  $j$ ), and the  $q \rightarrow 1$  limit of the  $q$ -state Potts *ferromagnet* on the same lattice with bonds representing Potts coupling constants  $\{J_{ij}\}$ . All relevant statistical quantities in one model have their equivalent in the other one provided that

$$p_{ij} = 1 - e^{-J_{ij}/k_B T} \quad (3)$$

where  $k_B$  and  $T$  are the Boltzmann constant and the temperature respectively. Immediate consequences of this connection are that

$$p_c = 1 - e^{-J/k_B T_c(1)} \quad (4)$$

and

$$\nu_p = \nu_t(1) \quad (5)$$

where  $J$  is the  $q$ -state isotropic Potts coupling constant,  $T_c(q)$  is the para-ferromagnetic critical temperature, and  $\nu_t(q)$  the corresponding correlation length critical exponent (the sub-index  $t$  stands for “thermal”).

A problem very similar to the one under consideration is *site percolation*, where, instead of the bonds, we randomly and independently *occupy* (or *activate*) the *sites* of a given

lattice. Its connection with a multisite-interaction Potts model is described in [19, 20]. General and important site percolation results are the following:  $p_c(\text{site}) \geq p_c(\text{bond})$ , and  $\nu_p(\text{site}) = \nu_p(\text{bond})$ .

More general percolation problems can be formulated (which contain both site and bond percolations as particular cases) by assuming that *both* sites and bonds are randomly and independently occupied with occupancy probabilities  $p_S$  and  $p_B$  respectively. We may then define *site-and-bond* ( $S \cap B$ ) and *site-or-bond* ( $S \cup B$ ) percolations: in the  $S \cap B$  ( $S \cup B$ ) problem, two points are said to be connected if a sequence of occupied sites *and* (*or*) bonds joins them. The  $S \cap B$  problem is frequently referred to as *site-bond* percolation [67]. Standard site (bond) percolation is recovered as the  $p_B = 1$  ( $p_S = 1$ ) case of the  $S \cap B$  problem, as well as the  $p_B = 0$  ( $p_S = 0$ ) case of the  $S \cup B$  problem. The phase diagrams (which we characterize by  $\phi_{S \cap B}(p_S, p_B) = 0$  and  $\phi_{S \cup B}(p_S, p_B) = 0$  respectively) of the  $S \cap B$  and  $S \cup B$  problems on any  $d > 1$  lattice hopefully are, qualitatively, as indicated in Fig. 1; their universality class presumably is the same as that of the standard bond percolation. Later on (see section 1.2.5) we shall recover the  $S \cap B$  problem as the  $T \rightarrow 0$  limit of a quite general random q-state Potts ferromagnet.

### 1.2.2 Resistor network

The system which is focused is a random distribution of conductances  $\sigma$  on the bonds of an infinite array (typically a regular Bravais d-dimensional lattice). The most frequent case is the *quenched* one, in which the distribution laws over the bonds are independent among themselves. By assuming one and the same distribution law  $P(\sigma)$  for all the bonds, and more precisely

$$P(\sigma) = (1 - p)\delta(\sigma - \sigma_1) + p\delta(\sigma - \sigma_2) \tag{6}$$

we encounter a variety of interesting situations according to the value of the ratio  $\sigma_1/\sigma_2$ . The extreme situations are the *random insulator-resistor mixture* ( $\sigma_1 = 0$  and  $\sigma_2$  finite) and the *random superconductor-resistor mixture* ( $\sigma_1 \rightarrow \infty$  and  $\sigma_2$  finite); the particular case  $\sigma_1 = \sigma_2$  clearly corresponds to the *non-random resistor network*, largely studied in the context of the Theory of Linear Circuits. The central inquiry for random resistor networks is the conductivity as a function of parameters such as  $p$  and  $\sigma_1/\sigma_2$ . We address



this question later on.

It can be shown that the  $q \rightarrow 0$  limit of the Potts ferromagnetic model is isomorphic to the resistor problem. A detailed discussion is available in Wu's review [3]. Here we shall only present an alternative way of looking at this isomorphism. The Potts dimensionless coupling constant  $K \equiv J/k_B T$  can be conveniently handled (as we shall see in Section 3) through the *thermal transmissivity* defined [68] as  $t \equiv [1 - e^{-qK}]/[1 + (q - 1)e^{-qK}]$ . In the  $0 < q \ll \frac{k_B T}{J} \ll 1$  limit we obtain  $t \sim 1 - 1/K$ . The transmissivity  $t_s$  of a series array of two bonds (characterized by  $t_1$  and  $t_2$ ) is given (see Section 3) by  $t_s = t_1 t_2$ . In the limit we are interested in, this implies  $1 - 1/K_s \sim (1 - 1/K_1)(1 - 1/K_2)$ , hence

$$\frac{1}{K_s} \sim \frac{1}{K_1} + \frac{1}{K_2} \quad (\text{series}) \quad (7)$$

On the other hand, for a parallel array of bonds, we obviously have

$$K_p = K_1 + K_2 \quad (\text{parallel}) \quad (8)$$

But the composition laws (7) and (8) are precisely those of conductances if we identify  $K$  with  $\sigma/\sigma_0$  ( $\sigma_0 \equiv$  conventional conductance unit). In other words, in the limit where  $q \rightarrow 0$  and  $K \rightarrow \infty$  with  $qK \rightarrow 0$ , the Potts ferromagnetic interactions compose as conductances with the transformations  $1 - t \leftrightarrow \sigma_0/\sigma$ .

### 1.2.3 Directed bond percolation

We briefly mention here the *directed bond percolation* since it is closely related to the bond percolation. Indeed, its formulation is completely analogous to that of bond percolation, but the bonds can be active *only* along one of their two senses. A physical realization of such a system can be a random network of *diodes* (instead of conductances): for example, diodes randomly distributed on the bonds of a d-dimensional hypercubic lattice, and conducting only along the positive directions of the crystalline axes. Very few exact (or almost exact) results are available in the literature [69–77],[28], one of them being the fact that the upper critical dimensionality  $d_u$  (see Section 4) is equal to 5 (whereas for standard percolation it is  $d_u = 6$ ). Related mixed systems can be such that the bonds are isotropic along some of the crystalline axes and directed along the rest of them. Later on we shall address one problem similar to this kind.

### 1.2.4 $Z(q)$ model

The  $Z(q)$  model is a quite rich generalization of the  $q$ -state Potts model [30, 31]. The site random variable can still take  $q$  values: let us characterize it by  $n_i = 0, 1, 2, \dots, q-1, \forall i$ . But the energy associated with a pair  $(n_i, n_j)$  might be different for different values of  $|n_i - n_j|$ , the difference  $(n_i - n_j)$  being measured modulus ( $q$ ). For example, for  $q = 4$ , the two-site configurations such that  $n_i - n_j = 0$ ,  $|n_i - n_j| = 1$  and  $|n_i - n_j| = 2$  correspond to energies which are not necessarily equal. In other words, and by conventionally assuming  $n_i = 0$ , the state  $n_j = 0$  corresponds to a certain energy, the states  $n_j = 1, 3$  to a (possibly) different one, and finally  $n_j = 2$  to a third one. Since the zero of energy has no physical meaning in the present context (it might have in different ones [78–80]), the  $Z(4)$  model involves 2 independent coupling constants. See Fig. 2 for convenient representations of the  $Z(4)$  and  $Z(5)$  interactions. Generically speaking, the spectrum of the  $Z(q)$  model presents, if  $q$  is even (odd),  $\frac{q}{2} + 1$  ( $\frac{q+1}{2}$ ) levels, two (one) of them being  $q$  times degenerate and the other  $\frac{q}{2} - 1$  ( $\frac{q-1}{2}$ ) levels being  $2q$  times degenerate. Or more synthetically, and by introducing  $\bar{q} \equiv$  integer part of  $q/2$ , the  $Z(q)$  spectrum has  $\bar{q} + 1$  levels:  $2(\bar{q} + 1) - q$  of them have degeneracy  $q$ , the other  $q - \bar{q} - 1$  levels have degeneracy  $2q$ . To generate such a spectrum it suffices  $\bar{q}$  independent coupling constants.

The  $Z(q)$  pair Hamiltonian might be written in various equivalent manners. We shall adopt the following one:

$$\mathcal{H}_{ij}(n_i - n_j) = J_1 - 2 \sum_{\beta=1}^{\bar{q}} J_\beta \cos \left[ \frac{2\pi\beta}{q}(n_i - n_j) \right] \quad (9)$$

The  $q$ -state Potts model is recovered as the particular case  $J_1 = J_2 = \dots = J_{\bar{q}-1} = \frac{1}{2}[3 + (-1)^q]J_{\bar{q}}$ , in which case the Hamiltonian becomes  $\mathcal{H}_{ij} = -qJ_1\delta_{n_i, n_j} + 2J_1$ . For  $q \leq 3$  the Potts model coincides with the  $Z(q)$  one. Another interesting particular case is  $J_\beta = 0$  if  $\beta \neq 1$  (*clock model*), in which case the Hamiltonian becomes  $\mathcal{H}_{ij} = J_1 - 2J_1 \cos[\frac{2\pi}{q}(n_i - n_j)]$ ; its  $q \rightarrow \infty$  limit recovers the classical spin planar model ( $S \rightarrow \infty XY$  model).

Another model which is contained in the  $Z(q)$  one is the *discrete N-vector model* [41–50] (sometimes referred to as the *discrete cubic model*). Consider a classical  $N$ -dimensional unit vector  $\vec{S}_i$  which can be aligned only along  $N$  orthogonal axes (hence  $2N$  configurations), and assume the pair Hamiltonian  $\mathcal{H}_{ij} = -NJ_1 \vec{S}_i \cdot \vec{S}_j - NJ_2(\vec{S}_i \cdot \vec{S}_j)^2$ . It is

easy to verify that this model is a particular case of the  $Z(2N)$  one (see [47]). Within this context let us mention the existence of the  $(N_\alpha, N_\beta)$  *model* [51] which generalizes the cubic one, and reduces to the symmetric Ashkin-Teller model [81] and to the  $Z(6)$  model in the respective cases where  $(N_\alpha, N_\beta) = (2, 2)$  and  $(3, 2)$ .

In fact this is a good stage for realizing that the  $Z(q)$  is itself included into the following largest  $q$ -state classical model. Consider the site variable  $\sigma_i = 1, 2, \dots, q, \forall i$ , and assume that the pair interaction Hamiltonian is given by the set  $\{\varepsilon_{\sigma_i, \sigma_j}\}$  of  $q^2$  real numbers. The interaction matrix  $\mathbf{W}(\{\varepsilon_{ij}\})$  is defined by:

$$\mathbf{W} = \begin{pmatrix} W_{11} & W_{12} & \cdots & W_{1q} \\ W_{21} & W_{22} & \cdots & W_{2q} \\ \vdots & \vdots & & \vdots \\ W_{q1} & W_{q2} & \cdots & W_{qq} \end{pmatrix} \quad (W_{ij} \equiv e^{-\varepsilon_{\sigma_i, \sigma_j}/k_B T}) \quad (10.a)$$

This matrix contains (at most)  $q^2 - 1$  independent coupling constants due to the irrelevance of the zero of energy.

In practically all spin models of physical interests each row and column of the above matrix contain the same set of numbers, i.e.

$$\sum_{i=1}^q W_{ij} = \sum_{j=1}^q W_{ij} = \lambda_0 \quad (10.b)$$

where  $\lambda_0$  is independent of  $i$  and the matrix  $\mathbf{W}$  is not necessarily symmetric. Models such as the spin  $S = 1/2$  Ising, Potts, chiral Potts [82, 83, 22, 35], clock, Ashkin-Teller,  $(N_\alpha, N_\beta)$ , discrete cubic and  $Z(q)$  are described by Hamiltonians which satisfy condition (10b).

The  $Z(q)$  model is recovered with the restriction that  $\varepsilon_{ij}$  only depends on  $|i - j|$  where  $(i - j)$  is measured modulus  $q$  (consequently  $W_{ii} = W_{jj}$  and  $W_{ij} = W_{ji}, \forall (i, j)$ ). The Potts model is reobtained for  $W_{ii} = W_{11}, \forall i$ , and  $W_{ij} = W_{12}$  for all  $i \neq j$  (the usual choice is  $\varepsilon_{11} = -qJ$  and  $\varepsilon_{12} = 0$ ). The chiral Potts model corresponds to  $\varepsilon_{\sigma_i, \sigma_j} \propto \cos[2\pi(\sigma_i - \sigma_j - \Delta)/q]$  with arbitrary  $\Delta$ ;  $\Delta = 0$  reproduces the clock model.

Before closing this subsection let us illustrate the interaction matrix (10) through a few examples.

$q = 3$ : The 3-state Potts model (coincident with the  $Z(3)$  model) corresponds to

$$\begin{pmatrix} W_{11} & W_{12} & W_{12} \\ W_{12} & W_{11} & W_{12} \\ W_{12} & W_{12} & W_{11} \end{pmatrix} \quad (\lambda_0 = W_{11} + 2W_{12}) , \quad (11)$$

the spin 1 Ising model corresponds to

$$\begin{pmatrix} W_{11} & 1 & W_{11}^{-1} \\ 1 & 1 & 1 \\ W_{11}^{-1} & 1 & W_{11} \end{pmatrix} \quad (12)$$

and the chiral 3-state Potts model is described by

$$\begin{pmatrix} W_{11} & W_{12} & W_{13} \\ W_{13} & W_{11} & W_{12} \\ W_{12} & W_{13} & W_{11} \end{pmatrix} \quad (\lambda_0 = W_{11} + W_{12} + W_{13}) \quad (13)$$

(chirality vanishes with  $(\varepsilon_{13} - \varepsilon_{12})$ ).

$q = 4$ : The  $Z(4)$  model corresponds to

$$\begin{pmatrix} W_{11} & W_{12} & W_{13} & W_{12} \\ W_{12} & W_{11} & W_{12} & W_{13} \\ W_{13} & W_{12} & W_{11} & W_{12} \\ W_{12} & W_{13} & W_{12} & W_{11} \end{pmatrix} \quad (\lambda_0 = W_{11} + 2W_{12} + W_{13}) \quad (14)$$

and the spin 3/2 Ising model is characterized by the matrix:

$$\begin{pmatrix} W_{11} & W_{11}^{1/3} & W_{11}^{-1/3} & W_{11}^{-1} \\ W_{11}^{1/3} & W_{11}^{1/9} & W_{11}^{-1/9} & W_{11}^{-1/3} \\ W_{11}^{-1/3} & W_{11}^{-1/9} & W_{11}^{1/9} & W_{11}^{1/3} \\ W_{11}^{-1} & W_{11}^{-1/3} & W_{11}^{1/3} & W_{11} \end{pmatrix} \quad (15)$$

Notice that the spin 1-and 3/2-Ising models do not fulfill condition (10b). The multi-component spin model characterized by the interaction matrix (10a) with the condition (10b) has been considered by Wang and Wu [84] and more recently by Maillard et al [85]. In ref. [84] the duality transformation on two-dimensional lattices and the thermodynamics on a Cayley tree for this model have been derived. In ref. [85] it is shown how the

eigenvalues of the interaction matrix are related to the convenient *vector transmissivity* which will appear, for certain particular cases of this multi-component spin model, in section 3. As far as we know, the general model described by (10a) (but without the restriction (10b)) has never been studied. The renormalization group techniques presented in this review are powerful enough to enable such a study (which is therefore welcome!). This comes from the fact that the model (10a) is necessarily closed under renormalization since it is the most general q-state one.

### 1.2.5 Random models

A great variety of physical situations exist (e.g., alloys and glasses) in which one-body terms and/or the coupling constants themselves are random variables. A typical case is the *bond random model*: the two-body coupling constant  $J_{ij}$  (between sites  $i$  and  $j$ ) is a random variable, which might take, for instance, two different values (binary distribution) or a continuous spectrum of values (e.g., Gaussian distribution, centered or not in  $J_{ij} = 0$ ). Another typical case is the *site random model*: the spins  $S_i$  themselves might be randomly present or absent. Mixed situations with simultaneous bond and site randomness are possible as well.

The bond and/or site randomness yields configurations (of coupling constants and presence or absence of spins) which might be either frozen once for ever (*quenched model*) or completely free to evolve subject to those particular external conditions such as temperature and applied fields (*annealed model*). Many realistic situations are *intermediate* in the sense that bonds and/or sites are neither completely frozen nor completely free to evolve. Several works have been dedicated to the analysis of the thermostistical implications of the quenched and annealed limits [86–90], [55]. The quenched limit involves *independent* local probability distributions (say of  $J_{ij}$ ) and is physically a very rich case.

To fix ideas let us consider a random Potts model. Its dimensionless Hamiltonian is given by

$$-\beta\mathcal{H} = \sum_{i,j} K_{ij} \varepsilon_i \varepsilon_j \delta_{\sigma_i, \sigma_j} \quad (\sigma_i = 1, 2 \dots, q) \quad (16)$$

where  $\{K_{ij}\}$  and  $\{\varepsilon_i\}$  are random variables and  $(i, j)$  runs over all bonds of a given arbitrary lattice; the site disorder variable  $\varepsilon_i$  takes the values 1 (*present* spin) and 0

(*absent spin*). The sets  $\{K_{ij}\}$  and  $\{\varepsilon_i\}$  are weighed with the law  $P(\{K_{ij}\}, \{\varepsilon_i\})$ .

In the annealed limit (for *both* bonds and sites),  $P(\{K_{ij}\}, \{\varepsilon_i\})$  can in principle be obtained from the Boltzmann factor  $\exp(-\beta\mathcal{H})$ . The corresponding free energy is given by

$$F_{annealed} = -k_B T \ln \sum_{\sigma_i, \varepsilon_i, K_{ij}} e^{-\beta\mathcal{H}} \quad (17)$$

In the quenched limit (for *both* bonds and sites),  $P(\{K_{ij}\}, \{\varepsilon_i\})$  has to be known (in practice, it depends on the procedure of preparation of the sample). If bonds and sites are *independently* distributed we have that  $P(\{K_{ij}\}, \{\varepsilon_i\}) = P_B(\{K_{ij}\})P_S(\{\varepsilon_i\})$ , where  $P_B$  and  $P_S$  are the bond and site distributions respectively. The pure bond-random problem corresponds to  $P_B(\{K_{ij}\}) \neq \prod_{(i,j)} \delta(K_{ij} - K_{ij}^0)$  ( $\{K_{ij}^0\}$  is a set of fixed values) and  $P_S(\{\varepsilon_i\}) = \prod_i \delta(\varepsilon_i - 1)$ ; the pure site-random problem corresponds to  $P_B(\{K_{ij}\}) = \prod_{(i,j)} \delta(K_{ij} - K_{ij}^0)$  and  $P_S(\{\varepsilon_i\}) \neq \prod_i \delta(\varepsilon_i - 1)$ . In the quenched-bond limit  $P_B(\{K_{ij}\}) = \prod_{(i,j)} P_{ij}(K_{ij})$ , where  $\{P_{ij}(K_{ij})\}$  are independent laws (i.e., no correlation exists in the disorder). On the other hand, the quenched-site limit corresponds to  $P_S(\{\varepsilon_i\}) = \prod_i \{P_i(\varepsilon_i)\}$  where  $\{P_i(\varepsilon_i)\}$  are independent laws. The free energy corresponding to the quenched case is given by

$$F_{quenched} = -k_B T \int P(\{K_{ij}\}, \{\varepsilon\}) \left( \prod_i d\varepsilon_i \right) \left( \prod_{i,j} dK_{ij} \right) \ln \sum_{\{\sigma_i\}} e^{-\beta\mathcal{H}} \quad (18)$$

An important particular case of the quenched limit is the bond-and-site diluted ferromagnet. It corresponds to

$$P_{ij}(K_{ij}) = (1 - p_B)\delta(K_{ij}) + p_B\delta(K_{ij} - K) \quad (K > 0) \quad (19)$$

and

$$P_i(\varepsilon_i) = (1 - p_S)\delta(\varepsilon_i) + p_S\delta(\varepsilon_i - 1) \quad (20)$$

Its schematic phase diagram (for  $d > 1$ ) is depicted in Fig. 3. The  $T = 0$  line is precisely that of Fig. 1 ( $S \cap B$  percolation). The critical curve of a *bond*-diluted annealed ferromagnet is similar to the particular case  $p_s = 1$  of Fig. 3. Typical annealed *site*-diluted ferromagnets do not show percolation effects due to aggregation at low temperatures (see [55]), and, therefore, their phase diagrams are not qualitatively similar to the  $p_b = 1$  curve of Fig. 3.

## 2 SOME EXACT OR ACCURATE RESULTS

We present here a large set of exact or accurate (series, Monte Carlo, RG, conjectures and others) results concerning mainly critical frontiers (points, lines, surfaces) and critical exponents ( $\nu, \alpha, \beta$ , crossover exponent  $\phi$ , etc). The models that we consider are essentially those of Section 1 on Bravais lattices. Most of these models are such that the knowledge of two independent critical exponents (say  $\nu$  and  $\beta$ ) determines all of them (hence, the universality class) through the scaling and hyperscaling relations. We briefly recall the most important among them:

$$\alpha + 2\beta + \gamma = 2 \quad (21)$$

$$\gamma = \beta(\delta - 1) \quad (22)$$

$$\gamma = \nu(2 - \eta) \quad (23)$$

and

$$2 - \alpha = d\nu \quad (\text{hyperscaling}) \quad (24)$$

where, for standard ferromagnets (and analogously for various other models),

$$M \equiv \text{order parameter} \propto (T_c - T)^\beta \quad (T \rightarrow T_c, H = 0) \quad (25)$$

$$C \equiv \text{specific heat} \propto |T - T_c|^{-\alpha} \quad (T \rightarrow T_c, H = 0) \quad (26)$$

$$\chi_T \equiv \text{isothermal susceptibility} \propto |T - T_c|^{-\gamma} \quad (T \rightarrow T_c, H = 0) \quad (27)$$

$$\xi \equiv \text{correlation length} \propto |T - T_c|^{-\nu} \quad (T \rightarrow T_c, H = 0) \quad (28)$$

$$M \propto H^{1/\delta} \quad (T = T_c, H \rightarrow 0) \quad (29)$$

$$\begin{aligned} \Gamma(R) &\equiv \text{correlation function (between two spins at distance } R) \\ &\propto \frac{1}{R^{d-2+\eta}} \quad (T = T_c, H = 0, R \rightarrow \infty) \end{aligned} \quad (30)$$

$H$  being the external parameter thermodynamically conjugate of the order parameter associated with the phase transition. In what follows, whenever new quantities (e.g., crossover exponents) or departures from the above general trend (e.g., more than two independent critical exponents, first-order phase transitions) appear, we shall specifically discuss them.

## 2.1 The Pure Potts Model

Unless otherwise stated, we refer to the ferromagnetic case, the interactions only existing between first-neighbours ( $J \equiv$  coupling constant).

### 2.1.1 $d=1$

For the linear chain we have

$$\frac{k_B T_c}{qJ} = 0 \quad (\forall q) \quad (31)$$

and

$$\nu = 1 \quad (32)$$

with the definition  $\xi \propto (e^{-qJ/k_B T})^{-\nu}$  (instead of Eq. (28)) in the limit  $T \rightarrow T_c = 0$ .

### 2.1.2 $d \rightarrow 1$

For the  $d$ -dimensional hypercubic lattice in the  $d \rightarrow 1 + 0$  limit and  $q > 1$  we have [25]

$$\frac{qJ}{k_B T_c} \sim \frac{1}{d-1} \quad (33)$$

and

$$\nu \sim \frac{1}{d-1} \quad (34)$$

Notice that  $\nu$  diverges in the  $d \rightarrow 1$  limit in contrast with the result indicated in Eq. (32): this discrepancy is due to the fact that  $\nu$  has been defined here via the standard variable (28).

### 2.1.3 $d=2$

The isotropic square-lattice Potts ferromagnetic critical points (see [3]) and critical exponents  $\nu$  [91] and  $\beta$  [92] are given by

$$\frac{k_B T_c}{qJ} = \frac{1}{\ln(\sqrt{q} + 1)} \quad (\forall q) \quad (35)$$

$$\nu = \frac{2}{3} \left\{ 2 + \pi / \left[ \arccos \left( \frac{1}{2} \sqrt{q} \right) - \pi \right] \right\}^{-1} \quad (q \leq 4) \quad (36)$$



and

$$\beta = \frac{1}{12} \left\{ 1 + \frac{2}{\pi} \arccos \left( \frac{\sqrt{q}}{2} \right) \right\} \quad (q \leq 4) \quad (37)$$

These results have been represented in Figs. 4 and 5. Eqs. (36) and (37) hold only for  $q \leq 4$  because the transition becomes of the first-order for  $q > 4$ . As a matter of fact, the common belief is that the Potts ferromagnetic phase transition is a continuous (first-order) one for  $q \leq q_c(d)$  ( $q > q_c(d)$ ): see Fig. 6 for a tentative representation of  $q_c(d)$  which takes into account various results [93-97,3] available in the literature. It is suggested that  $d = 6$  ( $d = 4$ ) separates critical and classical regimes for  $0 < q < 2$  ( $q = 2$ ): this is in variance with Fig. 2 of Ref. [3]

Eq. (35) is generalized, for the anisotropic square lattice (arbitrary  $J_x$  and  $J_y$ ), into (see [3])

$$(e^{qJ_x/k_B T_c} - 1)(e^{qJ_y/k_B T_c} - 1) = q \quad (38)$$

which is represented in Fig. 7. We may define the  $d = 1 \leftrightarrow d = 2$  crossover exponent  $\phi_{12}$  as follows:

$$e^{-qJ_x/k_B T_c(J_y/J_x)} \propto \left( \frac{J_y}{J_x} \right)^{\phi_{12}} \quad (J_y/J_x \rightarrow 0) \quad (39)$$

Then Eq. (38) implies

$$\phi_{12} = 1 \quad (\forall q) \quad (40)$$

The critical surface for the anisotropic triangular lattice (arbitrary  $J_x, J_y$  and  $J_z$  along the corresponding crystalline axes) is given by [98, 99]

$$\begin{aligned} & (e^{qJ_x/k_B T_c} - 1)(e^{qJ_y/k_B T_c} - 1)(e^{qJ_z/k_B T_c} - 1) + (e^{qJ_x/k_B T_c} - 1)(e^{qJ_y/k_B T_c} - 1) + \\ & + (e^{qJ_y/k_B T_c} - 1)(e^{qJ_z/k_B T_c} - 1) + (e^{qJ_z/k_B T_c} - 1)(e^{qJ_x/k_B T_c} - 1) = q \end{aligned} \quad (41)$$

If we take  $J_x = 0$  (or  $J_y = 0$  or  $J_z = 0$ ) we reproduce Eq. (38).

For the anisotropic honeycomb lattice (dual of the triangular lattice) we have [98, 99]

$$\begin{aligned} & q^2 + q(e^{qJ_x/k_B T_c} - 1) + q(e^{qJ_y/k_B T_c} - 1) + q(e^{qJ_z/k_B T_c} - 1) - \\ & - (e^{qJ_x/k_B T_c} - 1)(e^{qJ_y/k_B T_c} - 1)(e^{qJ_z/k_B T_c} - 1) = 0 \end{aligned} \quad (42)$$

If we take  $J_x \rightarrow \infty$  (or  $J_y \rightarrow \infty$  or  $J_z \rightarrow \infty$ ) we reproduce oncemore Eq. (38). In Ref. [100] critical points (with an expected good accuracy) associated with various other  $d = 2$

isotropic lattices are conjectured. Finally we present below the critical point corresponding to the anisotropic Potts *antiferromagnet* ( $J_x, J_y < 0$ ) on the square lattice [101]:

$$(e^{qJ_x/k_B T_c} + 1)(e^{qJ_y/k_B T_c} + 1) = 4 - q \quad (q \leq 3) \quad (43)$$

whose isotropic case is also represented in Fig. 8 (this figure contains also the ferromagnet case given by eq. (35)).

### 2.1.4 $d=3$

The approximate value of the Potts ferromagnetic critical points on isotropic simple cubic lattice (SC) and on other  $d = 3$  lattices can be found in Ref. [93]. These phase transitions are believed to be of the continuous type for  $q < q_c$  with  $q_c \lesssim 3$  [102]. Concerning the  $d = 3$  Ising ferromagnet ( $q = 2$ ), accurate estimates of critical exponents can be found in [103] and references therein.

The critical surface associated with the anisotropic Potts ferromagnet on the *SC* lattice (arbitrary coupling constants  $J_x, J_y$  and  $J_z$  along the three axes) is known with quite good precision (see [104] and reference therein). We may define the  $d = 1 \leftrightarrow d = 3$  and the  $d = 2 \leftrightarrow d = 3$  crossover exponents  $\phi_{13}$  and  $\phi_{23}$  respectively through

$$e^{-qJ_x/k_B T_c(J_y/J_x=J_z/J_x)} \propto \left(\frac{J_y}{J_x}\right)^{\phi_{13}} \quad (J_y/J_x = J_z/J_x \rightarrow 0) \quad (44)$$

and

$$\frac{k_B T_c(J_z/J_x; J_x = J_y)}{J_x} - \frac{k_B T_c(0; J_x = J_y)}{J_x} \propto \left(\frac{J_z}{J_x}\right)^{\phi_{23}} \quad (J_z/J_x \rightarrow 0) \quad (45)$$

Then we have that (see [104] and references therein)

$$\phi_{13} = 1 \quad (\forall q) \quad (46)$$

and

$$\phi_{23} \simeq \begin{cases} 1.75 & \text{if } q = 1 \\ 7/4 & \text{if } q = 2 \end{cases} \quad (47)$$

### 2.1.5 $d \geq 4$

Approximate Potts ferromagnetic critical points corresponding to several  $d \geq 4$  hypercubic (as well as some others) isotropic lattices are presented (many of them on conjectural grounds) in Ref. [93]. For  $d \geq 4$ ,  $q_c = 2$ .

### 2.1.6 Bethe lattice

Here we shall follow Baxter's terminology [5] concerning the distinction between Cayley tree and the Bethe lattice with coordination number  $z$ . Both are constructed from a central point which is connected to  $z$  points forming the first shell; in general, the  $n^{\text{th}}$  shell ( $n > 1$ ) is created by connecting  $(z - 1)$  new points to each of the points in the  $(n - 1)^{\text{th}}$  shell. In the Bethe lattice only sites far from the boundary in the limit  $n \rightarrow \infty$  are considered, while in the Cayley tree sites close to or on the boundary are also taken into account. The ferromagnetic Potts model on the Cayley tree presents some quite unusual properties (see, e.g., [84] and references therein) and we shall not consider it herein.

The critical point of the Potts ferromagnet on a  $z$ -coordinated Bethe lattice is given by (see [93] and references therein)

$$\frac{1 - e^{-qJ/k_B T_c}}{1 + (q - 1)e^{-qJ/k_B T_c}} = \frac{1}{z - 1} \quad (\forall q) \quad (48)$$

This result can be extended to anisotropic Bethe lattices where the  $z$  bonds (arriving on each site) are partitioned as follows:  $n_1$  with coupling constant  $J_1$ ,  $n_2$  with coupling constant  $J_2, \dots$  and  $n_N$  with coupling constant  $J_N$  such that  $\sum_{i=1}^N n_i = z$  (the partition is one and the same for all sites). The critical hypersurface is (conjecturally) given by [93]

$$\begin{vmatrix} 1 - t_1(n_1 - 1) & -t_1 n_2 & \cdots & -t_1 n_N \\ -t_2 n_1 & 1 - t_2(n_2 - 1) & \cdots & -t_2 n_N \\ \vdots & \vdots & & \vdots \\ -t_N n_1 & -t_N n_2 & \cdots & 1 - t_N(n_N - 1) \end{vmatrix} = 0 \quad (49)$$

with

$$t_i \equiv \frac{1 - e^{-qJ_i/k_B T_c}}{1 + (q - 1)e^{-qJ_i/k_B T_c}} \quad (i = 1, 2, \dots, N) \quad (50)$$

Eq. (49) recovers, as particular cases, all the exact results available in the literature.

With respect to the universality class, all Bethe lattices present classical values for the critical exponents, in particular  $\nu = 1/2$  and  $\beta = 1$  for  $q = 1$  [105],  $\nu = 1/2$  and  $\beta = 1/2$  for  $q = 2$  (see, e.g., [5]), and first order phase transitions for  $q > 2$  (see [106]).

## 2.2 The Bond-Random Potts Ferromagnet

We refer here to the *quenched* model unless specifically stated otherwise.

### 2.2.1 d=2

We consider, for each bond, the following independent probability law for the coupling constant:

$$P(J_{ij}) = (1 - p)\delta(J_{ij} - J_1) + p\delta(J_{ij} - J_2) \quad (51)$$

with  $0 \leq p \leq 1$  and  $J_1 \geq 0, J_2 > 0$ .

An accurate critical surface  $k_B T_c(p, J_1/J_2)/qJ_2$  for the isotropic square lattice [107] is represented for  $q = 2$  and different values of  $J_1/J_2$  in Fig. 9. The results for the triangular and honeycomb lattices are completely analogous [108]. Although known with high numerical accuracy (see [109, 108, 107]), the exact analytic expressions for these critical surfaces are not yet available. However some partial exact results can be presented [110–112]

$$\frac{1}{T_c(1, 0)} \left[ \frac{dT_c(p, 0)}{dp} \right]_{p=1} = \frac{2\sqrt{q}}{(1 + \sqrt{q}) \ln(1 + \sqrt{q})} \quad (\forall q) \text{ (square lattice)} \quad (52)$$

$$\left[ \frac{d \exp(-qJ_2/k_B T_c(p, 0))}{dp} \right]_{p=p_c} = \frac{\ln q}{(q - 1)p_c} \quad (\forall q) \quad (53)$$

(square, triangular and honeycomb lattices;  $p_c \equiv$  bond percolation threshold)

$$\begin{aligned} & \left[ 1 + (q - 1) \exp(-qJ_1/k_B T_c \left( \frac{1}{2}, \frac{J_1}{J_2} \right)) \right] \times \\ & \times \left[ 1 + (q - 1) \exp(-qJ_2/k_B T_c \left( \frac{1}{2}, \frac{J_1}{J_2} \right)) \right] = q \quad (\forall q) \text{ (square lattice)} \quad (54) \end{aligned}$$

The exact values for the  $p = 1$  slopes for the diluted case ( $J_1 = 0$ ) on the triangular and honeycomb lattices [111] are indicated in Table I. The slopes at  $p = 1$  for the quenched and annealed models coincide (see [113]) for *any* given lattice (not necessarily two-dimensional).

With respect to the critical exponents for any  $d = 2$  lattice it is believed that (see, e.g., [55]):

(i) At  $T_c = 0$ , the universality class is that of percolation;

- (ii) At  $T_c > 0$  and  $q > 4$  the phase transition is a first-order one;
- (iii) At  $T_c > 0$  and  $2 < q \leq 4$ , the universality class is that of the pure model if  $p = 1$ , and a new one (“random”) if  $p < 1$ ;
- (iv) At  $T_c > 0$  and  $q = 2$ , the universality class is that of the pure model if  $p = 1$ , and unknown if  $p < 1$ ;
- (v) At  $T_c > 0$  and  $q < 2$ , the universality class is that of the pure model,  $\forall p$ .

### 2.2.2 Bethe lattice

We consider, on each bond of a  $z$ -coordinated Bethe lattice, an arbitrary independent probability law  $P(J_{ij})$  for the coupling constant, with the unique restriction that  $P(J_{ij})$  vanishes for  $J_{ij} < 0$ . The critical frontier is (conjecturally) given by [93]

$$\langle \frac{1 - e^{-qJ/k_B T_c}}{1 + (q-1)e^{-qJ/k_B T_c}} \rangle_{P(J)} = \frac{1}{z-1} \quad (\forall q) \quad (55)$$

where  $\langle \dots \rangle$  stands for the average value with the law  $P(J)$ . Eq. (55) recovers, as particular cases, all the exact results available in the literature [111, 55].

## 2.3 Resistor Network

We consider a quenched random distribution of *conductances*  $g$  on a given lattice, each bond distribution law being given by

$$P(g) = (1-p)\delta(g-g_1) + p\delta(g-g_2) \quad (56)$$

with  $0 \leq p \leq 1$  and  $g_1, g_2 \geq 0$ . We denote  $\sigma(p)$  the *conductivity* of the random medium, and  $\alpha \equiv g_1/g_2$ . In the  $\alpha = 0$  and  $\alpha \rightarrow \infty$  limits (diluted resistor network and diluted superconductor network respectively), we define the following critical exponents

$$\sigma(p) \propto (p-p_c)^t \quad (\alpha = 0, p \rightarrow p_c + 0) \quad (57)$$

and

$$\sigma(p) \propto (p-p_c)^{-s} \quad (\alpha \rightarrow \infty, p \rightarrow p_c + 0) \quad (58)$$

$p_c$  being the critical point for bond percolation.

### 2.3.1 $d=2$

The following results are exact for the square lattice [114–116]:

$$\frac{1}{\sigma(1)} \left. \frac{d\sigma(p)}{dp} \right|_{p=0} = \frac{2\alpha(1-\alpha)}{1+\alpha} \quad (59)$$

and consistently

$$\frac{1}{\sigma(1)} \left. \frac{d\sigma(p)}{dp} \right|_{p=1} = \frac{2(1-\alpha)}{1+\alpha} \quad (60)$$

as well as

$$\sigma(0)/\sigma(1) = \alpha \quad (61)$$

and, more generally,

$$\frac{\sigma(p)}{\sigma(1)} \frac{\sigma(1-p)}{\sigma(1)} = \alpha \quad (\forall p) \quad (62)$$

hence

$$\sigma(1/2)/\sigma(1) = \sqrt{\alpha} \quad (63)$$

For the square lattice (and for any other  $d = 2$  lattice) we have ([117], [118] and references therein)

$$t = s \approx 1.3 \quad (64)$$

### 2.3.2 $d \geq 3$

The following results are exact for the  $d$ -dimensional hypercubic lattice [115]:

$$\frac{1}{\sigma(1)} \left. \frac{d\sigma(p)}{dp} \right|_{p=0} = \frac{d\alpha(1-\alpha)}{1+(d-1)\alpha} \quad (65)$$

and consistently

$$\frac{1}{\sigma(1)} \left. \frac{d\sigma(p)}{dp} \right|_{p=1} = \frac{d(1-\alpha)}{d-1+\alpha} \quad (66)$$

Also, for any  $d = 3$  lattices we have [115, 119]  $t \simeq 1.7$  and  $t/(t+s) \simeq 0.7$

## 2.4 $\mathbf{Z}(\mathbf{q})$ Model

Unless otherwise stated, we refer to the ferromagnetic case, the interactions only existing between first-neighbours.

### 2.4.1 Isotropic Z(4) ferromagnet on the square lattice

The pair Hamiltonian given by eq. (9) can be rewritten, for  $q = 4$ , in terms of two coupled Ising variables  $\sigma_i$  and  $\tau_i$ , namely [120]

$$\mathcal{H}_{ij} = J_1 - J_1(\sigma_i\sigma_j + \tau_i\tau_j) - 2J_2\sigma_i\sigma_j\tau_i\tau_j \quad (\sigma_i = \pm 1, \tau_i = \pm 1) \quad (67)$$

The phase diagram presents, for  $J_1 \geq 0$  and  $J_1 + 2J_2 \geq 0$ , three phases namely the *paramagnetic* ( $P$ ), *ferromagnetic* ( $F$ ) and *intermediate* ( $I$ ) ones. We show in Fig. 10 an accurate approximation [121] for it which recovers all the exact results available for the square lattice. The  $P - F$  critical line satisfies the duality condition given by

$$e^{-4K_1} + 2e^{-2(K_1+2K_2)} = 1 \quad (K_\alpha = J_\alpha/k_B T; \alpha = 1, 2) . \quad (68)$$

Its universality class is a *continuous* function of  $J_1/J_2$  (a fact which is not reproduced in [121]). For instance, its critical exponent  $\nu$  is given by [122]:

$$\nu = \left\{ 2 - \frac{\pi}{2} \cos^{-1}[\tanh(4K_2)/(\tanh(4K_2) - 1)] \right\}^{-1} \quad (-1/2 \leq J_2/J_1 \leq 1/2) \quad (69)$$

The  $IP$  and  $IF$  critical lines belong to the Ising universality class, but their analytical expressions are yet unknown, though they are closely related (through duality). Their  $J_2/J_1 \rightarrow \infty$  limits are known, namely

$$\lim_{J_2/J_1 \rightarrow \infty} \frac{k_B T^{IP}}{J_2} = \frac{4}{\ln(1 + \sqrt{2})} = 2 \times 2.269 \dots \quad (70)$$

and

$$\lim_{J_2/J_1 \rightarrow \infty} \frac{k_B T^{IF}}{J_1} = \frac{4}{\ln(1 + \sqrt{2})} = 2 \times 2.269 \dots \quad (71)$$

thus reproducing the Ising critical point.

### 2.4.2 Duality

Since Kramers and Wannier [123] derived a duality transformation for the Ising model on the square lattice (i.e., a relation connecting the partition functions in the high-and low-temperature regions) there has been many generalizations of this transformation to different statistical systems (see [31] and references therein).

For the  $Z(q)$  ferromagnet on the square lattice, the duality transformation leaves invariant the following hypersurface (which becomes a point for  $q = 2, 3$ , a line for  $q = 4, 5$ , a surface for  $q = 6, 7$ , and so on): [32, 124, 125]

$$x_\alpha^D = x_\alpha \tag{72.a}$$

where

$$x_\alpha \equiv \exp \left\{ \sum_{\delta=0}^{q-1} K_\delta \left[ \cos \left( \frac{2\pi\alpha\delta}{q} \right) - 1 \right] \right\} \tag{72.b}$$

and its dual variable  $x_\alpha^D$  is given by

$$x_\alpha^D = \frac{\sum_{\eta=0}^{q-1} \exp(2\pi i\alpha\eta/q) x_\eta}{\sum_{\eta=0}^{q-1} x_\eta} \tag{72.c}$$

hereafter referred to as *self-dual hypersurface* (*not all the points of which are themselves self-dual*; see [125]). If an odd (even) number of phase transitions exists when  $T$  increases from zero to infinity, necessarily one (none) of them lies on the self-dual hypersurface; all the others, if any, being strictly related two by two through duality (to each phase transition existing *below* the self-dual temperature corresponds one and only one *above* that temperature related through the duality transformation; i.e., if there are, for example, three phase transitions, then one necessarily coincides with the self-dual temperature and the other two are transformed through duality one into the other). This statement is correct for all  $q > 0$  and for arbitrary values of the coupling constants along the x-and y-axes; it implies *nothing* concerning the *nature* of the transitions (continuous or of the first-order, with or without spontaneous symmetry breaking, universality class, etc).

The same type of arguments can be extended to other planar lattices (e.g., triangular and honeycomb) by adding duality to other convenient transformations (e.g., star-triangle), but this is out of the present scope.



### 3 TRANSMISSIVITIES AND THE BREAK-COLLAPSE METHOD

This Section is devoted to the *exact* calculation, using the Break-collapse method, of correlation-like quantities for finite (connected) *graphs* (i.e., connected arrays of edges joining vertices) associated with bond percolation, Potts model and other classical physical systems. These calculations constitute the basis on which are constructed the RG's presented in Section 4.

#### 3.1 Bond Percolation

Let us consider a *series* array of two bonds whose independent occupancy probabilities are  $p_1$  and  $p_2$ . The equivalent probability  $p_s$  is given by

$$p_s = p_1 p_2 \tag{73}$$

where “equivalent” is used in the sense that the array can be replaced by a single bond connecting the two *terminal sites* (or *external sites*, noted  $\circ$ , to distinguish them from the *internal sites*, noted  $\bullet$ ). If the array is a *parallel* one, the equivalent probability  $p_p$  can be obtained through analysis of the 4 possible configurations; it is given by

$$p_p = p_1 p_2 + p_1(1 - p_2) + p_2(1 - p_1) \tag{74}$$

hence

$$p_p = p_1 + p_2 - p_1 p_2 . \tag{75}$$

This equation can be rewritten in a series-like form, namely

$$p_p^D = p_1^D p_2^D \tag{76}$$

with

$$p^D \equiv 1 - p \tag{77}$$

The variable  $p^D$  plays a role, as shown in [126], similar to the dual variable of the duality transformation for the partition function of the Ising model [123]. Furthermore as

we shall see below, the geometric dual of two edges in series is two edges in parallel if we consider the terminal sites as *roots* (roots are specially distinguished vertices of a graph). These two facts justify the use of the superscript  $D$  standing for dual in eqs. (76) and (77). A rooted graph is said to be *planar* if it can be embedded in the plane in such a way that no edge crossing exists except at a vertex. Any possible embedding of a planar graph represents a *plane* graph. In Fig. 11 we show a few two-rooted plane (a-d), planar (a-e) and non-planar (f,g) graphs. Let us consider a connected two-rooted plane graph  $G$  which has the following characteristics: i) it does not contain any single-edge loop or any unrooted vertex which has a coordination number 1 (i.e., which is connected to a unique vertex), ii) its articulation points (an articulation point is one that if we remove it together with its incident edges the graph becomes disconnected), if any, are not rooted iii) the roots are on the boundary of the infinite (exterior) face. Examples of such graphs  $G$  can be seen in Fig. 11 (a-d). Now imagine a boundary line running from each root out to infinity; these two non-intersecting lines divide the infinite face into two regions which we shall picture as being the “two (imaginary) infinite faces” of  $G$ . The dual  $G^D$  of such a graph  $G$  is defined [127–129] as another two-rooted graph constructed as follows:

- i) place one unrooted vertex of  $G^D$  on each of the finite (or inner) faces of  $G$
- ii) place each rooted vertex of  $G^D$  on each “imaginary infinite face”
- iii) draw an edge joining the vertices of  $G^D$  which lie in the faces adjoining an edge of  $G$  (which implies that each edge of one graph crosses one and only one of the other and that each unrooted vertex of one graph is surrounded by an elementary mesh of the other).

In Fig. 12 we have represented a few couples of two-rooted dual graphs ((a), (c) and (d) are *self-dual*). The extension of this duality construction to graphs with *any* number of roots has been done in this decade [129], while the dual of a lattice (which can be seen as an infinite unrooted graph) and that of an unrooted or one-rooted (the root residing in the infinite face) graph has been established much earlier (see [130, 131]). For example, the triangular (Kagomé) lattice is the dual of the honeycomb (diced) lattice; the square lattice is self-dual. The self-duality of the anisotropic bond percolation on the square lattice (arbitrary  $p_x$  and  $p_y$ ) enables, following along the lines of refs. [123] and [6] for the Ising model, the immediate calculation of its bond percolation critical line. The full

discussion and derivation was first done by Sykes and Essam [126], but a quick derivation can be done as follows: self-duality yields  $p_x^D = p_y$ , which, together with definition (77), provides the exact result  $p_x + p_y = 1$ .

If we have a series or parallel array of  $\ell$  bonds, the respective eqs. (73) and (76) are immediately generalized into

$$p_s = \prod_{i=1}^{\ell} p_i \tag{78}$$

and

$$p_p^D = \prod_{i=1}^{\ell} p_i^D \tag{79}$$

hence

$$p_p = 1 - \prod_{i=1}^{\ell} (1 - p_i) \tag{80}$$

The use of algorithms (78) and (80) enables, *without performing the configurational analysis*, the calculation of the equivalent probability of *any* two-rooted graph *sequentially reducible in series and parallel operations* (e.g., graphs appearing in Figs. 12 (b,e,f)), but not of the irreducible ones (e.g., graphs appearing in Figs. 11(b-g)). We now describe the Break-collapse method (BCM) which applies to *any* two-rooted graph.

### 3.1.1 Break-collapse method and other properties

We consider an arbitrary connected two-rooted graph  $G$  with roots 1 and 2, the edges of which are respectively associated with probabilities  $\{p_i\}$ . In many cases *all* the edges of  $G$  are *relevant* in the sense that the deletion of any of them modifies the connectivity properties between the roots, or equivalently that the graph coincides with its *backbone* (if we assume that *arbitrary* finite electrical conductances are placed on the edges of the graph, the *backbone* is the set of edges along which current flows when a voltage is applied between the roots of the graph). See, in Fig. 13, graphs which include at least one *irrelevant* edge. We note  $P_{12}(\{p_i\}, G)$  the probability that the root 1 and 2 be connected (this is the *pair connectedness* introduced by Essam [7]), i.e, that at least one path of active bonds connects the roots.  $P_{12}(\{p_i\}, G)$  is a polynomial of the  $\{p_i\}$ ; if the graph includes irrelevant edges,  $P_{12}$  will not depend on their occupancy probabilities (if all edges have the same probability  $p$ ,  $P_{12}$  will be a polynomial in  $p$  with degree  $N_b \equiv$  number

of relevant edges). In general  $P_{12}(\{p_i\}, G)$  satisfies  $P_{12}(\{p_i = 0\}) = 0$  and  $P_{12}(\{p_i = 1\}) = 1$ , and is a *multilinear* function of  $\{p_i\}$ , i.e., it can always be written as follows:  $P_{12}(\{p_i\}) = A(\{p_i\}') + B(\{p_i\}')p_j$ , where  $p_j$  is the probability associated with an arbitrarily chosen bond, and the set  $\{p_i\}'$  excludes  $p_j$ . We note  $P_{12}(\{p_i\}', G_j^b)(P_{12}(\{p_i\}', G_j^c))$  the pair connectedness probability associated with the *j-broken (j-collapsed)* graph, defined as the one obtained from  $G$  by taking  $p_j = 0$  ( $p_j = 1$ ).  $G_j^b$  is the graph obtained from  $G$  by deleting the edge  $j$  of  $G$ , while  $G_j^c$  is obtained from  $G$  by contracting (i.e., by deleting the edge  $j$  and indentifying its incident vertices) the edge  $j$  of  $G$ .  $A$  and  $B$  are trivially evaluated in terms of the pair connectedness of  $G_j^b$  and  $G_j^c$ , and the following algorithm holds:

$$P_{12}(\{p_i\}, G) = (1 - p_j)P_{12}(\{p_i\}', G_j^b) + p_jP_{12}(\{p_i\}', G_j^c) \quad (81)$$

The iterative use of this algorithm, which we shall call the break-collapse equation, together with (78) and (79) will lead eventually to an *effective edge j* whose pair connectivity is a multilinear function of some  $p_i'$ s. In order to include this case one should regard  $p_j$  as being, in fact, the effective probability of the edge  $j$  given by the pair connectivity of the subgraph which generated it. Similarly, the  $p_i'$ s and  $p_i^{D'}$ s which appear in eqs. (78) and (79) should be considered as effective probabilities.

Besides eqs. (81), another valuable property is the factorization rule for articulated graphs; this refers to a situation where there is an articulation point  $i$ . In this case the graph  $G$  becomes the union of two subgraphs,  $G_1$  and  $G_2$ , which intersect at only  $i$  (we say that  $G_1$  and  $G_2$  are in series). We have, thus, to consider two cases according to the distribution of the roots:

1) If  $G_1$  contains one root, say 1, and  $G_2$  contains the other root, then the following factorization occurs [132]

$$P_{12}(G_1UG_2) = P_{1i}(G_1)P_{i2}(G_2) \quad (82.a)$$

2) If all the roots belong to only one subgraph (including the case where one of the roots coincides with the articulation point itself), say  $G_1$ , then all the edges of  $G_2$  are irrelevant for the pair connectedness  $P_{12}$  and the following relation holds

$$P_{12}(G_1UG_2) = P_{12}(G_1) \quad (82.b)$$

which is a particular case of eq. (6.6a) of ref. [133].

An example of the first situation is the following:

$$P_{12} \left( \begin{array}{c} \circ 1 \\ | \\ \bullet i \\ | \\ \bullet \\ | \\ \bullet \\ | \\ \circ 2 \end{array} \right) = P_{1i} \left( \begin{array}{c} \circ 1 \\ | \\ \circ i \end{array} \right) P_{i2} \left( \begin{array}{c} \circ i \\ | \\ \bullet \\ | \\ \bullet \\ | \\ \circ 2 \end{array} \right) \quad (83)$$

where we have illustrated the fact that the articulation point generates in this situation a root on each of the subgraphs.

An example where eq. (82b) applies is the graph of Fig. (13a).

We shall refer to the iterative use of eqs. (78), (80), (81) and (82) as many times as needed for calculating  $P_{12}(\{p_i\}, G)$  as the *Break-collapse method (BCM)*; it enables the full calculation of the pair connectedness of *any* two-rooted graph *without any configurational analysis*. The BCM is operationally very convenient, can be analytically implemented in computer, and enables consequently the treatment of quite large arrays, practically untractable within more traditional procedures. Eq. (81) coincides with eq. (3.11) of Essam [132], referred to as the edge substitution equation for the pair connectedness. Later on we shall present successive extensions (Potts, resistor, directed percolation,  $Z(q)$  and cubic model), where specific variables and operations will be described. However we can already anticipate that *all* these procedures essentially rely on a single very simple property: *multilinearity* (in appropriate variables) of the relevant quantities.

Before going on, let us perform a brief illustration of the BCM to the graph  $G$  shown on the left of Fig. 12c with  $p_1 = p_2 = p_3 = p_4 = p_5 = p$ :

$$\begin{aligned} P_{12}(p, G) &= (1 - p)P_{12}(G_5^b, p) + pP_{12}(G_5^c, p) = \\ &= (1 - p)(2p^2 - p^4) + p(2p - p^2)^2 = 2p^2 + 2p^3 - 5p^4 + 2p^5 \end{aligned} \quad (84)$$

where the 5-broken  $G_5^b$  (5 collapsed  $G_5^c$ ) graph is shown in the left (right) of Fig. 12f with each edge having probability  $p$ .

This result was first obtained, through configurational analysis, by Reynolds et al. (Eq. (12) of [134]).

We list now several interesting properties:

- (i) Equation (81) reproduces Eqs. (73) and (75) as particular cases.

(ii) As an immediate corollary of Eq. (81) we obtain

$$\frac{\partial P_{12}}{\partial p_j}(\{p_i\}, G) = P_{12}(\{p_i\}', G_j^c) - P_{12}(\{p_i\}', G_j^b) \quad (85)$$

(iii) Algorithm (81) can be generalized into a kind of binominal expression if we break-collapse more than one bond simultaneously. If we note  $G_{jk}^{bb}, G_{jk}^{bc}, G_{jk}^{cb}$  and  $G_{jk}^{cc}$  the graphs obtained from a given graph  $G$  by simultaneously breaking-collapsing (as indicated in the superscript) its  $j$ -th and  $k$ -th edges, we verify

$$\begin{aligned} P_{12}(\{p_i\}, G) &= (1-p_j)(1-p_k)P_{12}(\{p_i\}'', G_{jk}^{bb}) \\ &+ (1-p_j)p_k P_{12}(\{p_i\}'', G_{jk}^{bc}) \\ &+ p_j(1-p_k)P_{12}(\{p_i\}'', G_{jk}^{cb}) + p_j p_k P_{12}(\{p_i\}'', G_{jk}^{cc}) \end{aligned} \quad (86)$$

where the set  $\{p_i\}''$  excludes  $p_j$  and  $p_k$ . This relation is trivially extended to the case where we operate on three or more edges simultaneously. Let us illustrate this property on the following example (where all bonds have occupancy probability  $p$ ):

$$P_{12} \left( \begin{array}{c} \circ \\ \bullet \bullet \bullet \\ \circ \end{array} \begin{array}{c} 1 \\ \\ 2 \end{array} \right) = (1-p)^2 P_{12} \left( \begin{array}{c} \circ \\ \bullet \bullet \bullet \\ \circ \end{array} \right) + 2p(1-p) P_{12} \left( \begin{array}{c} \circ \\ \bullet \bullet \\ \circ \end{array} \right) + p^2 P_{12} \left( \begin{array}{c} \circ \\ \bullet \\ \circ \end{array} \right) \quad (87)$$

(iv) A pair of dual two-rooted graphs, whose associated pair connectedness are respectively  $P_{12}(\{p_i\}, G)$  and  $P_{12}(\{p_i^D\}, G^D)$  where the sets  $\{p_i\}$  and  $\{p_i^D\}$  are such that each bond of one graph has an occupancy probability which is the dual of that of the corresponding bond in the other graph (see various illustrations in Fig. 12), satisfy

$$P_{12}(\{p_i^D\}, G^d) = 1 - P_{12}(\{p_i\}, G) \equiv [P_{12}(\{p_i\}, G)]^D \quad (88)$$

In short we could say that “the dual of the (associated) pair connectedness on a graph is equal to the (associated) pair connectedness of the dual”. An immediate corollary is that *any* self-dual two-rooted graph (e.g., those appearing in Figs. 11 (a-d)), all the bonds of which have  $p_i = 1/2$  (hence  $p_i = p_i^D$ ), satisfies  $P_{12}(G) = 1/2$ . This property (and the similar ones for the Potts and other models expressed in the transmissivity variables) is the basis for using self-dual clusters in the RG approach of the square lattice (self-dual itself).

(v) If we have a pair of dual two-rooted graphs, noted  $G$  and  $G^D$ , and break-collapse the  $j$ -th bond of each of the graphs, we verify that

$$(G_j^b)^D = (G^D)_j^c \quad (89)$$

and

$$(G_j^c)^D = (G^D)_j^b \quad (90)$$

consequently, if  $G = G^D$ , then  $G_j^b$  and  $G_j^c$  are dual (if  $G$  is given by Fig. 12(c) and  $j = 5$  then Fig. 12 (f) illustrates this property). Also we have that a graph is series/parallel reducible if and only if the same happens with its dual. Eqs. (89) and (90) being topological (and not functional) relations, they are model independent (i.e., they hold for bond percolation, Potts model, etc.).

### 3.1.2 Extension to multi-rooted graphs

Within the context of bond percolation it is interesting to define multi-rooted ( $n$ -rooted) graphs (whose edges have occupancy probabilities  $\{p_i\}$ ) which contain  $n \geq 1$  roots. We note  $P_{12\dots n}(\{p_i\}, G)$  the multi-connectedness function, i.e., the probability that *all* the  $n$  roots  $1, 2, 3 \dots, n$  of  $G$  be connected.  $P_{12\dots n}(\{p_i\}, G)$  vanishes if the graph contains one or more disconnected roots.  $P_{12\dots}(\{p_i\}, G)$  equals 1 for any graph with  $n = 1$ , and reproduces the pair connectedness [7] (discussed in Section 3.1.1) for  $n = 2$ . Examples with  $n \geq 3$  are presented in Fig. 14. Configurational analysis yields

$$\begin{aligned} P_{123}(p_1, p_2, p_3, G_\Delta) &= p_1 p_2 p_3 + (1 - p_1) p_2 p_3 + (1 - p_2) p_1 p_3 \\ &+ (1 - p_3) p_1 p_2 = p_1 p_2 + p_2 p_3 + p_3 p_1 - 2 p_1 p_2 p_3 \end{aligned} \quad (91)$$

and

$$P_{123}(p_1^D, p_2^D, p_3^D, G_Y) = p_1^D p_2^D p_3^D \quad (92)$$

respectively associated with Figs. 14(a) and 14(b).

The break-collapse equation (Eq. (81)) *stands precisely as before* (i.e., as for  $n = 2$ ) [133], with the following supplementary rules:

(i) the collapse of two or more vertices yields a root if at least one of them is a root (consequently, it yields an unrooted vertex only if *all* of them are unrooted ones);

(ii) articulation points can be indistinctively considered as roots or unrooted vertices if the connection of the other roots requires paths containing necessarily these articulation points. For example, Eq. (91) can be recovered as follows if we apply the break-collapse equation to bond 1 of graph  $G_\Delta$ :

$$P_{12}(p_1, p_2, p_3, G_\Delta) = p_1(p_2 + p_3 - p_2p_3) + (1 - p_1)p_2p_3 \quad (93)$$

Another illustration is indicated in Figs. 14 (d-f).

Before going on, it is worth noting that Eqs. (91) and (92) enable a quick derivation of the anisotropic bond percolation exact critical frontiers for the triangular and honeycomb lattices (with occupancy probabilities  $p_1, p_2$  and  $p_3$  respectively along the three crystalline axes), first obtained by Sykes and Essam [126]. The equations, which implicitly involve the well known star-triangle and duality transformations (see details in [54, 126]), are respectively given by

$$P_{123}(p_1, p_2, p_3, G_\Delta) = P_{123}(p_1^D, p_2^D, p_3^D, G_Y) \quad (\text{triangular lattice}) \quad (94)$$

and

$$P_{123}(p_1^D, p_2^D, p_3^D, G_\Delta) = P_{123}(p_1, p_2, p_3, G_Y) \quad (\text{honeycomb lattice}) \quad (95)$$

Let us finally mention that the factorization rules (eq. 82) (see [133]) and the properties (ii) and (iii) of Section 3.1.1 hold similarly for multi-rooted graphs.

## 3.2 Potts Model

In the present Section we extend to the  $q$ -state Potts model the results and methods of Section 3.1, herein recovered as the  $q \rightarrow 1$  limit.

### 3.2.1 Thermal transmissivity

We first consider a *series* array of two edges (with Potts coupling constants  $J_1$  and  $J_2$ ) and three vertices (see Fig. 15(a)). The corresponding Hamiltonian is given by  $\mathcal{H}_{123} = -qJ_1\delta_{\sigma_1, \sigma_3} - qJ_2\delta_{\sigma_3, \sigma_2}$ , and the associated canonical density operator  $\rho_{123}$  is proportional to



$\exp(-\mathcal{H}_{123}/k_B T)$ . All possible thermal equilibrium statistical quantities associated with this system can be calculated in terms of  $\rho_{123}$ . An important subset of these quantities involve canonical averages of functions of  $\sigma_1$  and/or  $\sigma_2$ , *but not*  $\sigma_3$ ; we refer herein to all those resulting from interactions (with the system) through  $\sigma_1$  and/or  $\sigma_2$ , but not directly through  $\sigma_3$ . For this subset of quantities, we can perform the calculations by using  $\rho_{123}$  or, better,  $Tr_{\sigma_3}\rho_{123}$ . Consistently we next propose a trial Potts Hamiltonian  $\mathcal{H}_{12}^s = -qJ_s\delta_{\sigma_1,\sigma_2} - qJ'_0$ , and check whether the following equality can be imposed:

$$e^{-\mathcal{H}_{12}^s/k_B T} = Tr_{\sigma_3} e^{-\mathcal{H}_{123}/k_B T} \quad (96)$$

where  $J'_0$  (zero-energy shift) and  $J_s$  are quantities to be found. By using the property  $e^{\lambda\delta_{\sigma_i,\sigma_j}} = 1 + \delta_{\sigma_i,\sigma_j}(e^\lambda - 1)(\forall\lambda)$ , and performing the sum  $\sum_{\sigma_3=1}^q$ , one straightforwardly obtain (see [2]):

$$t_s = t_1 t_2 \quad (\text{series}) \quad (97)$$

and

$$e^{qK'_0} = (q - 2) + e^{qK_1} + e^{qK_2} \quad (98)$$

where

$$t \equiv \frac{1 - e^{-qK}}{1 + (q - 1)e^{-qK}} \quad (99)$$

and, for all  $J'_i$ s,

$$K_i \equiv J_i/k_B T \quad (100)$$

We first note that equality (96) is indeed possible, no coupling proliferation occurring (i.e., no other interaction is needed than the Potts pair one, with an *equivalent* coupling constant  $J_s$  and a trivial zero-energy shift). This convenient property is, in some sense, a quite rare one, most many-body interactions not remaining, in this type of array composition, closed into themselves. The  $t$ -variable (hereafter referred to as *thermal transmissivity* [68]) will prove to be an extremely useful one for the present purposes; in particular, it recovers, in the  $q \rightarrow 1$  limit, transformation (3). This variable was first introduced (with no particular denomination) by Domb in 1974 [2] in the context of high-temperature series expansions; it was, since then, practically forgotten (as well as the algorithm (97), also first established by Domb [2]). More recently, the variable was independently rediscovered in

Oxford [135] and Rio de Janeiro [68], and since then intensively used in the context of RG treatments and related subjects [112, 109, 93, 108, 107, 104][136–152][133]. Its particular case for the Ising model (where the transmissivity reduces to  $t = th(K)$ ) becomes the high-temperature expression variable noted sometimes  $w$  by Domb [154] which has been introduced much earlier than the general definition (99); it has been widely used not only in the context of series expansions (see [154] and references therein) but also in RG approaches [155–180].

In the ferromagnetic case ( $J > 0$ ) and for all  $q > 0$ ,  $t$  monotonously increases from 0 to 1 while  $J/k_B T$  increases from zero (completely *uncorrelated* spins) to infinity (completely *correlated* spins). In the antiferromagnetic case ( $J < 0$ ), and for all  $q \geq 1$ , it monotonously decreases from 0 to  $-1/(q - 1)$  while  $|J|/k_B T$  increases from zero to infinity. Finally, if  $J < 0$  and  $0 < q < 1$  (analytic extension), the variation interval of  $t$  is a disconnected one, namely  $(-\infty, 0]$  and  $[1/(1 - q), \infty)$ .

Last but not least, let us make clear that imposition of equalities like that of Eq. (96) is equivalent [139] to preserving, through array composition, the two-body correlation function  $\Gamma_{12}$  between the rooted sites 1 and 2. Indeed if we have two sites ( $i$  and  $j$ ) connected through the Potts dimensionless coupling constant  $K_{ij}$ , we immediately verify, for the corresponding thermal transmissivity, that

$$t_{ij} = \Gamma_{ij} \equiv \frac{q \langle \delta_{\sigma_i, \sigma_j} \rangle - 1}{q - 1} \quad (101)$$

where  $\langle \dots \rangle$  denotes canonical thermal mean value.

Note that this expression has a form totally similar to that of the commonly defined Potts ferromagnet order parameter  $m \equiv (q \langle \delta_{\sigma_i, 0} \rangle - 1)/(q - 1)$ , which varies from 1 to 0 while  $T$  increases from 0 to the critical temperature  $T_c$ , and remains zero for all  $T > T_c$ .

If we have a series array of  $\ell$  bonds, Eq. (97) is generalized into

$$t_s = \prod_{i=1}^{\ell} t_i \quad (\text{series}) \quad (102)$$

If all bonds have the same transmissivity  $t$ , we obtain the well known two-end correlation function for the linear chain  $t_s = t^\ell = e^{-\ell/\xi}$ , with the correlation length  $\xi = 1/\ln(1/t)$ , which diverges at  $t = 1$  (i.e.,  $T_c = 0$ ) with a critical exponent  $\nu_t = 1, \forall q$ .

We consider now a *parallel* array of two edges (with coupling constants  $J_1$  and  $J_2$ ), as indicated in Fig. 15(b). The corresponding Hamiltonian is  $-qJ_1\delta_{\sigma_1,\sigma_2}-qJ_2\delta_{\sigma_1,\sigma_2}$ , therefore the equivalent coupling constant  $J_p$  is given by

$$J_p = J_1 + J_2 \quad (103)$$

hence

$$t_p = \frac{t_1 + t_2 + (q - 2)t_1 t_2}{1 + (q - 1)t_1 t_2} \quad (\text{parallel}) \quad (104)$$

which was first derived by Domb [2]. Eq. (104) can be rewritten as:

$$t_p^D = t_1^D t_2^D \quad (\text{parallel}) \quad (105)$$

with

$$t^D \equiv \frac{1 - t}{1 + (q - 1)t} \quad (106)$$

where again D stands for *dual* since eq. (106) provides the same relation between the coupling constants for dual lattices as that one which appeared in the duality transformation for the partition function of the Potts model, first derived for the square lattice by Potts [1]. Let us point out that the form (106) is the most general ratio of linear functions of  $t$  which vanishes for  $t = 1$ , equals unity for  $t = 0$ , and which applied twice leaves the argument invariant. We also note that, in the  $q = 1$  case, Eqs. (104) and (106) respectively recover Eqs. (75) and (77). The exact [98, 181] ferromagnetic critical line corresponding to the anisotropic square lattice (with transmissivities  $t_x$  and  $t_y$  along the  $x$  and  $y$  axes) is quickly derived by using definition (106): it is given by  $t_x = t_y^D$ .

The neutral element for parallel composition is  $t = 0$  ( $t_2 = 0$  implies, in Eq. (104),  $t_p = t_1, \forall t_1$ ); in the same way, the neutral element for series composition is  $t = 1$  (see Eq. (97)). Also, it is not without interest to mention a similarity with Special Relativity in a parallel array.  $t_2 = 1$  implies  $t_p = 1, \forall t$  (see Eq. (104)), in analogy with the relativistic composition of velocities (the total speed is that of light if one of the speeds is that of light, no matter the other one). In fact, algorithm (104) becomes, for  $q = 1$ , absolutely isomorphic to the relativistic composition of speeds, the correspondence being  $t \leftrightarrow v/c$  ( $v$  and  $c$  respectively are the speeds of the system and that of light).

If we have a parallel array of  $\ell$  bonds, Eq. (105) is generalized into

$$t_p^D = \prod_{i=1}^{\ell} t_i^D \quad (107)$$

hence

$$t_p = \frac{1 - \prod_{i=1}^{\ell} \frac{1 - t_i}{1 + (q-1)t_i}}{1 + (q-1) \prod_{i=1}^{\ell} \frac{1 - t_i}{1 + (q-1)t_i}} \quad (108)$$

Similarly to the case of bond percolation, algorithms (102) and (108) enable, *without performing any partial tracings*, the calculation of the pair correlation functions for *any* two-rooted graph *sequentially reducible in series and parallel operations*. We describe in the next Section how to deal with the irreducible ones.

### 3.2.2 Break-collapse method and other properties

Analogously to Section 3.1.1 we consider here an arbitrary connected two-rooted graph  $G$ , the edges of which are respectively associated with transmissivities  $\{t_i\}$ . The equivalent transmissivity between the roots 1 and 2 of the graph  $G$ , noted  $T_{12}(\{t_i\}, G)$ , is the transmissivity of an effective single edge  $e_{eff}$  joining 1 and 2 whose effective dimensionless coupling constant  $K_{eff}$  is obtained analogously to eq. (96) by using the Hamiltonian  $\mathcal{H}(G)$  associated with the graph  $G$  instead of  $\mathcal{H}_{123}$ , i.e.:

$$T_{12}(\{t_i\}, G) = \frac{1 - e^{-qK_{eff}}}{1 + (q-1)e^{-qK_{eff}}} \quad (109.a)$$

with  $K_{eff}$  being given by:

$$e^{qK'_0} e^{qK_{eff}\delta_{\sigma_1, \sigma_2}} = Tr' \{ e^{-\mathcal{H}(G)/k_B T} \} \quad (109.b)$$

wher  $Tr'$  refers to the trace over the configurations of only the internal spins located on the unrooted vertices, and  $K'_0$  is due to the renormalization of the zero-energy.

Some years ago it was proved [139] that for any graph  $G$  one has:

$$T_{12}(\{t_i\}, G) = \Gamma_{12}(\{t_i\}, G) \quad (110)$$

where  $\Gamma_{12}(\{t_i\}, G)$  is the correlation function between  $\sigma_1$  and  $\sigma_2$  on the graph  $G$  expressed in the  $t_i$  variables whose definition is given by eq. (101), where now the thermal average involves all the spins on the graph  $G$ .

$T_{12}(\{t_i\}, G)$  is, in fact, a ratio of polynomials in  $\{t_i\}$ , i.e.,  $T_{12}(\{t_i\}, G) = N_{12}(\{t_i\}, G)/D(\{t_i\}, G)$ , where both  $N_{12}$  and  $D$  are *multilinear* functions of  $\{t_i\}$ .

The denominator  $D$  is independent of the roots 1 and 2 and also determines the partition function  $Z(\{t_i\}, G)$ , i.e. [139]

$$Z(\{t_i\}, G) \equiv Tr[e^{-\mathcal{H}(G)/k_B T}] = AD(\{t_i\}, G) \quad (111.a)$$

with

$$A = q^{N_s(G)} \prod_i [1 - t_i]^{-1} \quad (111.b)$$

where the trace is over all the spin configurations of the  $N_s(G)$  sites of the graph  $G$ , and the product in (111b) is over all the  $N_b(G)$  bonds of  $G$ .

Furthermore, it has been shown [139] that both  $D$  and  $N_{12}$  can be written as “percolation averages” (noted as  $\langle \dots \rangle_{G,t}$ ) of certain quantities in a bond percolation problem defined on  $G$  where each edge  $i$  has an independent bond occupancy probability  $t_i$ , namely

$$D(\{t_i\}, G) = \langle q^c \rangle_{G,t} \quad (112)$$

and

$$N_{12}(\{t_i\}, G) = \langle q^c \gamma_{12} \rangle_{G,t} \quad (113)$$

where  $c(G')$  is the cyclomatic number of a graph  $G'$ , i.e., the number of independent circuits (which, for a plane graph, is equal to the number of finite faces); it satisfies the Euler law  $c(G') = N_b(G') - N_s(G') + n(G')$  with  $n(G')$  being the number of clusters of  $G'$  (each isolated vertex counts also as a cluster;  $n = 1$  for a connected graph).  $\gamma_{12}(G')$  is defined as 1 if the roots 1 and 2 are connected on  $G'$  and zero otherwise. “The percolation average” of a quantity  $Q$  is given by:

$$\langle Q \rangle_G = \sum_{G' \subseteq G} Q(G') \mathcal{P}(G') \quad (114)$$

where the sum is over all the subgraphs  $G'$  of  $G$  which have the same  $N_s(G)$  vertices of  $G$  and only  $N_b(G')$  edges ( $N_b(G') \leq N_b(G)$ ) of an edge subset  $E(G')$  contained in the edge

subset  $E(G)$  of  $G$ .  $\mathcal{P}(G')$  is the probability of occurrence of a subgraph  $G'$  given by the product of the transmissivities  $t_i$  of the edges of  $G'$  times the product of the probabilities of absence  $(1 - t_i)$  of the edges of  $G$  which do not appear in  $G'$ .

Before mentioning the break-collapse equation, let us focus on some factorization rules, namely:

1) if  $G$  is the union of two subgraphs, say  $G_1$  and  $G_2$ , which have zero or at most one vertex in common and if the roots 1 and 2 belong both to  $G_1$  (including the case where one of the roots coincides with the articulation point) then [139]:

$$N_{12}(G) = N_{12}(G_1)D(G_2) \tag{115.a}$$

and

$$D(G) = D(G_1)D(G_2) \tag{115.b}$$

If  $G_2$  is a loop with transmissivity  $t_\ell$  then

$$D\{t_\ell, G_2\} = 1 + (q - 1)t_\ell \tag{115.c}$$

From eqs. (115a) and (115b) it follows immediately that

$$T_{12}(G) = T_{12}(G_1) \tag{115.d}$$

This means that the subgraph  $G_2$  contains only irrelevant bonds in the sense defined in section 3.1.1. The fact that irrelevant edges do not affect the equivalent transmissivity of a graph happens only for classical models, but not for quantum ones (this point is explicitly raised by Suzuki and Takano [182], is relevant for many  $RG$  approaches [183–190], and is fully illustrated by Mariz et al [187]). Similarly this is true for *uncorrelated* percolation, but not necessarily for various forms of correlated percolation [191–193].

2) if  $G$  is the union of two subgraphs, say  $G_1$  and  $G_2$ , which intersect at only the articulation point  $i$  and if  $G_1$  contains the root 1 and  $G_2$  contains the other root then the following *series algorithm for  $G_1$  and  $G_2$*  holds [133]

$$N_{12}(G) = N_{1i}(G_1)N_{i2}(G_2) \tag{116.a}$$

and

$$D(G) = D(G_1)D(G_2) \quad (116.b)$$

and consequently

$$T_{12}(G) = T_{1i}(G_1)T_{i2}(G_2) \quad (116.c)$$

which contains, as a particular case, the algorithm eq. (97) of two edges in series.

3) if  $G_1$  and  $G_2$  are disjoint graphs (i.e., without any intersection) and each of them contains one root then [139]

$$N_{12}(\{t_i\}, G) = T_{12}(\{t_i\}, G) = 0 \quad (117)$$

and eq. (116b) continues valid for this case.

Multilinearity of  $N_{12}(\{t_i\}, G)$  and  $D(\{t_i\}, G)$  immediately yields the following algorithm for the equivalent transmissivity  $T_{12}(\{t_i\}, G) \equiv N_{12}(\{t_i\}, G)/D(\{t_i\}, G)$  of an arbitrary graph:

$$N_{12}(\{t_i\}, G) = (1 - t_j)N_{12}(\{t_i\}', G_j^b) + t_jN_{12}(\{t_i\}', G_j^c) \quad (118.a)$$

and

$$D(\{t_i\}, G) = (1 - t_j)D(\{t_i\}', G_j^b) + t_jD(\{t_i\}', G_j^c) \quad (118.b)$$

where the set  $\{t_i\}'$  excludes the transmissivity  $t_j$  of an arbitrarily chosen bond  $j$ , and where  $T_{12}(\{t_i\}', G_j^b) \equiv N_{12}(\{t_i\}', G_j^b)/D(\{t_i\}', G_j^b)$  and  $T_{12}(\{t_i\}', G_j^c) \equiv N_{12}(\{t_i\}', G_j^c)/D(\{t_i\}', G_j^c)$  are the equivalent transmissivities of the  $j$ -*broken* ( $t_j = 0$ ) and  $j$ -*collapsed* ( $t_j = 1$ ) graphs respectively. The iterative use of this algorithm, together with Eqs. (102) and (108), can lead to an *effective edge*  $j$ , whose transmissivity is, in fact, a ratio,  $t_j = N_j/D_j$ , of multilinear functions of some  $t'_i$ s. Therefore one should use, instead of eqs. (118), the more general case given by [133]

$$N_{12}(G) = (D_j - N_j)N_{12}(G_j^b) + N_jN_{12}(G_j^c) \quad (119.a)$$

and

$$D(G) = (D_j - N_j)D(G_j^b) + N_jD(G_j^c) \quad (119.b)$$

where  $N_j$  and  $D_j$  are the respective numerator and denominator of the transmissivity  $t_j$  of the effective edge, which is equal to the equivalent transmissivity of the subgraph

which generated the edge  $j$ . Similarly, the transmissivity which appeared in eqs. (102) and (108) should be regarded as effective ones. The respective equivalent transmissivities  $N_s/D_s$  and  $N_p/D_p$  corresponding to a series and a parallel array of  $\ell$  edges should thus be

$$N_s = \prod_{i=1}^{\ell} N_i \quad (\text{series numerator}) \quad (120.a)$$

$$D_s = \prod_{i=1}^{\ell} D_i \quad (\text{series denominator}) \quad (120.b)$$

$$N_p = \left\{ \prod_{i=1}^{\ell} [D_i + (q-1)N_i] - \prod_{i=1}^{\ell} [D_i - N_i] \right\} / q \quad (\text{parallel numerator}) \quad (121.a)$$

and

$$D_p = \left\{ \prod_{i=1}^{\ell} [D_i + (q-1)N_i] + (q-1) \prod_{i=1}^{\ell} [D_i - N_i] \right\} / q \quad (\text{parallel denominator}) \quad (121.b)$$

In spite of the aspect of Eqs. (121) (see [133]), it can be verified that they *always* ( $\forall \ell, \forall \{N_i/D_i\}$ ) provide a  $q$ -factor in their numerators which cancels that one appearing in their denominators. For example, for  $\ell = 2$ , we obtain

$$N_p = N_1 D_2 + N_2 D_1 + (q-2)N_1 N_2 \quad (\text{parallel numerator}) \quad (122.a)$$

and

$$D_p = D_1 D_2 + (q-1)N_1 N_2 \quad (\text{parallel denominator}) \quad (122.b)$$

The iterative use of the factorization rules (eqs. 115-117), the series (eqs. 120) and parallel algorithms (eqs. 122) together with the break-collapse equation (eqs. 119) constitutes the BCM and enables the full calculations of the pair correlation function of the Potts model on *any* two-rooted graph. To be more explicit, the imposition given by (109b) is possible and *automatically satisfied* within the BCM, *algebraically complex tracing operations being thus replaced by simple topological ones.*

This BCM is a particular case of the subgraph break-collapse method introduced in [133] for computing more complicated equivalent transmissivities which arise in the calculation of many-spin correlation functions (see [140]). In order to implement the



BCM in a computer one should treat the transmissivity of each edge  $i$  as an ordered pair of quantities (i.e.,  $\{N_i, D_i\}$  where  $t_i = N_i/D_i$ ; for an original edge of  $G$ ,  $N_i = t_i$  and  $D_i = 1$ ) and *not* as ratios  $\{N_i/D_i\}$ . The numerator and denominator of  $T_{12}(\{t_i\}, G)$  satisfy necessarily the following equalities (see [139]):

$$N_{12}(\{t_i = 0\}, G) = 0 \quad , \quad D(\{t_i = 0\}, G) = 1 \quad (\forall G) \quad (123)$$

and

$$N_{12}(\{t_i = 1\}, G) = q^{c(G)} \quad , \quad D(\{t_i = 1\}, G) = q^{c(G)} \quad (\forall G) \quad (124)$$

In the  $q = 1$  limit, which corresponds to the bond percolation limit (see Kasteleyn and Fortuin [16]), the transmissivity coincides with the  $p$ -variable of ref. [16] (i.e.,  $t_i = p_i = 1 - e^{-K_i}$ ),  $D(\{t_i\}, G) = 1$  and  $N_{12}(\{t_i\}, G)$  reduces to the pair connectivity  $P_{12}(\{p_i = t_i\}, G)$  of section 3.1 (see [140]).

Before going on, let us briefly illustrate the BCM for the Potts model. We want to calculate  $T_{12}(t, G)$  of the graph  $G$  shown on the left of Fig. 12c where, instead of  $p_i (i = 1, 2, \dots, 5)$ , we associate the transmissivity  $t$  to each of its edges. We first choose an arbitrary bond, say the central one (edge 5), then calculate (by using the series and parallel composition laws expressed in Eqs. (120) and (122)):

$$T_{12}(t, G_5^b) \equiv \frac{N_{12}(t, G_5^b)}{D(t, G_5^b)} = \frac{2t^2 + (q-2)t^2}{1 + (q-1)t^4} \quad (125)$$

and

$$T_{12}(t, G_5^c) \equiv \frac{N_{12}(t, G_5^c)}{D(t, G_5^c)} = \frac{4t^2 + 4(q-2)t^3 + (q-2)^2t^4}{1 + 2(q-1)t^2 + (q-1)^2t^4} \quad (126)$$

where the 5-broken  $G_5^b$  (5-collapsed  $G_5^c$ ) graph is drawn in the left (right) of Fig. 12f with each edge having transmissivity  $t$ . Finally, using algorithms (119), we obtain:

$$N_{12}(t, G) = (1-t)N_{12}(t, G_5^b) + tN_{12}(t, G_5^c) \quad (127.a)$$

and

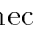

$$D(t, G) = (1-t)D(t, G_5^b) + tD(t, G_5^c) \quad (127.b)$$

and consequently,

$$T_{12}(t, G) = \frac{2t^2 + 2t^3 + 5(q-2)t^4 + (q-2)(q-3)t^5}{1 + 2(q-1)t^2 + (q-1)t^4 + (q-1)(q-2)t^5} \quad (128)$$

This result was first obtained, through conventional tracing operations, by Yeomans and Stinchcombe (the homogeneous case of Eq. (3) of ref. [135]) in a treatment of the dilute Potts ferromagnet on the square lattice (notice that  $T_{12}(1/(\sqrt{q}+1), G) = 1/(\sqrt{q}+1), \forall q$ ; this property will lead, within an appropriate RG framework, to the *exact* critical point). The  $q=1$  case of Eq. (128) reproduces Eq. (84) as it should be.

We now list some interesting properties, namely:

- (i) Eqs. (118) reproduce Eq. (97) if we associate  $t/1$  with a single edge (  ) and  $0/1$  with a disconnected two-rooted graph (  ), and they also reproduce Eq. (104) if we associate [139]  $[1 + (q-1)t]/[1 + (q-1)]$  with an elementary loop (  ).
- (ii) As an immediate corollary of Eqs. (118) we obtain for  $T_{12}(\{t_i\}, G) \equiv N_{12}(\{t_i\}, G)/D(\{t_i\}, G)$ ,

$$\begin{aligned} \frac{\partial T_{12}(\{t_i\}, G)}{\partial t_j} &= \tag{129} \\ &= \frac{N_{12}(\{t_i\}', G_j^c) - N_{12}(\{t_i\}', G_j^b) - T_{12}(\{t_i\}, G)[D(\{t_i\}', G_j^c) - D(\{t_i\}', G_j^b)]}{D(\{t_i\}, G)} \end{aligned}$$

which recovers eq. (85) for  $q = 1$ .

- (iii) Analogously to the bond percolation case, algorithms (118) can be generalized into a kind of binominal expansion if we break-collapse  $r$  bonds simultaneously ( $r \geq 1$ ).

We verify that

$$\begin{aligned} N_{12}(\{t_i\}, G) &= \left[ \prod_{s=1}^r (1 - t_{j_s}) \right] N_{12}(\{t_i\}'', \dots', G_{j_1 j_2 \dots j_r}^{t b b \dots b}) \\ &+ t_{j_1} \left[ \prod_{s=2}^r (1 - t_{j_s}) \right] N_{12}(\{t_i\}'', \dots', G_{j_1 j_2 \dots j_r}^{t c b \dots b}) + \dots \\ &+ \left[ \prod_{s=1}^r t_{j_s} \right] N_{12}(\{t_i\}'', \dots', G_{j_1 j_2 \dots j_r}^{t c c \dots c}) \quad (2^r \text{ terms}) \tag{130.a} \end{aligned}$$

and

$$D(\{t_i\}, G) = \left[ \prod_{s=1}^r (1 - t_{j_s}) \right] D(\{t_i\}'', \dots', G_{j_1 j_2 \dots j_r}^{t b b \dots b})$$

$$\begin{aligned}
 &+ t_{j_1} \left[ \prod_{s=2}^r (1 - t_{j_s}) \right] D(\{t_i\}'' \dots, G_{j_1 j_2 \dots j_r}^{c \ b \dots b}) + \dots \\
 &+ \left[ \prod_{s=1}^r t_{j_s} \right] D(\{t_i\}'' \dots', G_{j_1 j_2 \dots j_r}^{c \ c \dots c}) \quad (2^r \text{ terms}) \quad (130.b)
 \end{aligned}$$

where the notation is self-explanatory and the set  $\{t_i\}'' \dots'$  excludes  $(t_{j_1}, t_{j_2}, \dots, t_{j_r})$ , the transmissivities of  $r$  arbitrarily chosen bonds of the graph  $G$  whose equivalent transmissivity  $T_{12}(\{t_i\}, G) \equiv N_{12}(\{t_i\}, G)/D(\{t_i\}, G)$  we are looking for. The appropriate use of this property (for  $r \geq 2$ ) might lead to a considerable saving of operational time. A similar property in the  $\{p_i\}$  variables ( $p_i \equiv 1 - e^{-q\kappa_i}$ ) was derived by Kasteleyn and Fortuin [16]. As a matter of fact, they used this property to prove that the pair correlation function can be written as a ratio of percolation averages (where a bond has an occupancy probability  $p_i$ ) in a similar way as the ratio between eqs. (113) and (112).

- (iv) Analogously to the bond percolation case, an arbitrary pair of two-rooted dual graphs whose equivalent transmissivities are  $T_{12}(\{t_i\}, G)$  and  $T_{12}(\{t_i^D\}, G^D)$  satisfies (see proof in [129])

$$T_{12}(\{t_i^D\}, G^D) = \frac{1 - T_{12}(\{t_i\}, G)}{1 + (q - 1)T_{12}(\{t_i\}, G)} = [T_{12}(\{t_i\}, G)]^D \quad (131)$$

or, in a more symmetric form,

$$[1 + (q - 1)T_{12}(\{t_i\}, G)][1 + (q - 1)T_{12}(\{t_i^D\}, G^D)] = q \quad (132)$$

or even, in a probability-like form (see Eq. (77)),

$$s(\{t_i\}, G) + s^D(\{t_i\}, G) = 1 \quad (133)$$

with

$$s(t) \equiv \frac{\ln[1 + (q - 1)t]}{\ln q} \quad (\forall q) \quad (134)$$

and

$$s^D(t) \equiv s(t^D) \quad (\forall t) \quad (135)$$

The  $s$ -variable transforms, under duality and *for all values of  $q$* , like a probability; in the  $q \rightarrow 1$  limit, it becomes  $s = t$  and is strictly a probability (bond occupancy



### 3.2.3 Extension to multi-rooted graphs

The useful role that  $n$ -rooted graphs ( $n \geq 2$ ) played in bond percolation can be extended to the Potts model. The corresponding equivalent transmissivity  $T_{12\dots n}(\{t_i\}, G)$  among the roots  $1, 2, \dots, n$  of a graph  $G$  is defined as follows [140]:

$$T_{12}(\{t_i\}, G) = \frac{1}{q-1} \langle q\delta_{\sigma_1, \sigma_2} - 1 \rangle \quad (n = 2) \quad (138)$$

$$T_{123}(\{t_i\}, G) = \frac{(q-2)^{1/2}}{(q-1)} \langle q^3\delta_{\sigma_1, \sigma_2}\delta_{\sigma_2, \sigma_3}\delta_{\sigma_1, \sigma_3} - q^2(\delta_{\sigma_1, \sigma_2} + \delta_{\sigma_2, \sigma_3} + \delta_{\sigma_3, \sigma_1}) + 2 \rangle \quad (n = 3) \quad (139)$$

where  $\langle \dots \rangle \equiv \{Tr_{1,2,\dots,N_s} e^{-\beta\mathcal{H}_{12\dots N_s}(\dots)}\} / Tr_{1,2,\dots,N_s} \{e^{-\beta\mathcal{H}_{12\dots N_s}}\}$ . The definition in terms of *body correlations* becomes more and more complex for higher values of  $n$  (see [140]); however, in all cases, it is simply equal to a ratio of percolation averages [140] which generalizes the case  $n = 2$  (see eqs. 112 and 113), namely:

$$T_{12\dots n}(\{t_i\}, G) = \frac{N_{12\dots n}(\{t_i\}, G)}{D(\{T_i\}, G)} \quad (140.a)$$

with  $D(\{t_i\}, G)$  being given by eq. (112) and the numerator being the generalization of eq. (113), namely:

$$N_{12\dots n}(\{t_i\}, G) = \langle q\gamma_{12\dots n} \rangle_{G,t} \quad (140.b)$$

where the connectedness indicator  $\gamma_{12\dots n}(G')$  is 1 if all the  $n$  roots are connected among themselves on the graph  $G'$  and zero otherwise. Let us mention a few general properties of  $T_{12\dots n}$ :

(i) For  $n \geq 2$ ,

$$T_{12\dots n}(\{t_i = 0\}, G) = 0 \quad (\forall G) \quad (141)$$

or more generally,  $T_{12\dots n}(\{t_i\}, G) = 0$  if any of the roots is not connected to all the others.

(ii) For any connected graph  $G$  and  $n \geq 2$ :

$$N_{12\dots n}(\{t_i = 1\}, G) = D(\{t_i = 1\}, G) = q^c(G) \quad (142)$$

and therefore

$$T_{12\dots n}(\{t_i = 1\}, G) = 1 \quad (143)$$

(iii) the factorization rules in eqs. (115) continue to be valid if all the roots belong to  $G_1$ , with  $N_{12}$  and  $T_{12}$  being replaced by  $N_{12\dots n}$  and  $T_{12\dots n}$  respectively;

(iv) the factorization rules given by eqs. (116) generalize to:

$$N_{12\dots n}(G) = N_{12\dots \ell i}(G_1)N_{i\ell+1\dots n}(G_2) \quad (144.a)$$

and

$$T_{12\dots n}(G) = T_{12\dots \ell i}(G_1)T_{i\ell+1\dots n}(G_2) \quad (144.b)$$

where we supposed that the roots  $1, 2, \dots, \ell$  belong to  $G_1$  and the remaining ones  $(\ell + 1, \dots, n)$  belong to  $G_2$ .

(v) in the  $q = 1$  limit,  $T_{12\dots n}(\{t_i\}, G)$  reduces to the multi-connectedness  $P_{12\dots n}(\{t_i\}, G)$  defined in section 3.1.2 where  $t_i = p_i$ .

To illustrate the present generalized definition of equivalent transmissivity we calculate those of the three-rooted graphs of Figs. 14(a) and 14(b) (with  $\{p_i\}$  and  $\{p_i^D\}$  replaced by  $\{t_i\}$  and  $\{t_i^D\}$  respectively), and obtain

$$T_{123}(t_1, t_2, t_3, G_\Delta) \equiv \frac{N_{123}(t_1, t_2, t_3, G_\Delta)}{D(t_1, t_2, t_3, G_\Delta)} = \frac{t_1 t_2 + t_2 t_3 + t_3 t_1 + (q - 3)t_1 t_2 t_3}{1 + (q - 1)t_1 t_2 t_3} \quad (145)$$

and

$$T_{123}(t_1^D, t_2^D, t_3^D, G_Y) \equiv \frac{N_{123}(t_1^D, t_2^D, t_3^D, G_Y)}{D(t_1^D, t_2^D, t_3^D, G_Y)} = t_1^D t_2^D t_3^D \quad (146)$$

which recover eqs. (91) and (92) respectively for  $q = 1$ .

The break-collapse algorithm (Eqs. (119)) *stands precisely as for*  $n = 2$  replacing  $N_{12}$  by  $N_{12\dots n}$ , with the same supplementary rules as for bond percolation (i.e., the collapse of two or more vertices yields a root if at least one of them is a root, and articulation points can indistinctively be considered unrooted or not if the connection of the other roots requires paths containing necessarily these articulation points. For example Eq.

(145) can be quickly reobtained as follows [68]:

$$\begin{aligned}
 N_{123} \left( \begin{array}{c} \textcircled{3} \\ t_1 \triangle t_2 \\ \textcircled{2} \text{---} t_3 \text{---} \textcircled{1} \end{array} \right) &= (1 - t_1) N_{123} \left( \begin{array}{c} \textcircled{3} \\ t_2 \text{---} \textcircled{1} \\ t_3 \text{---} \textcircled{2} \end{array} \right) + t_1 N_{12} \left( \begin{array}{c} \textcircled{2} \equiv \textcircled{3} \\ t_2 \text{---} \textcircled{1} \\ t_3 \end{array} \right) \quad (147) \\
 &= (1 - t_1) t_2 t_3 + t_1 [t_2 + t_3 + (q - 2) t_2 t_3] \\
 &= t_1 t_2 + t_2 t_3 + t_3 t_1 + (q - 3) t_1 t_2 t_3
 \end{aligned}$$

and

$$\begin{aligned}
 D &= \left( \begin{array}{c} \textcircled{3} \\ t_1 \triangle t_2 \\ \textcircled{2} \text{---} t_3 \text{---} \textcircled{1} \end{array} \right) (1 - t_1) D \left( \begin{array}{c} \textcircled{3} \\ t_2 \text{---} \textcircled{1} \\ t_3 \text{---} \textcircled{2} \end{array} \right) + t_1 D \left( \begin{array}{c} \textcircled{2} \equiv \textcircled{3} \\ t_2 \text{---} \textcircled{1} \\ t_3 \end{array} \right) \quad (148) \\
 &= (1 - t_1) 1 + t_1 [1 + (q - 1) t_2 t_3] = 1 + (q - 1) t_1 t_2 t_3
 \end{aligned}$$

which immediately provides  $T_{123}(G_\Delta) \equiv T_{123} \left( \begin{array}{c} \textcircled{3} \\ \triangle \\ \textcircled{2} \text{---} \textcircled{1} \end{array} \right) = N_{123} \left( \begin{array}{c} \textcircled{3} \\ \triangle \\ \textcircled{2} \text{---} \textcircled{1} \end{array} \right) / D \left( \begin{array}{c} \textcircled{3} \\ \triangle \\ \textcircled{2} \text{---} \textcircled{1} \end{array} \right)$  as given by Eq. (145).

It is worthy noting that Eqs. (145) and (146) enable a quick derivation (implicitly involving the star-triangle and duality transformations) of the anisotropic Potts ferromagnet exact critical frontier for the triangular and the honeycomb lattices, first obtained independently by Baxter et al. [98] and by Burkhardt and Southern [99] (see also [163]). The equations are respectively given by

$$T_{123}(t_1, t_2, t_3, G_\Delta) \equiv T_{123}(t_1^D, t_2^D, t_3^D, G_Y) \quad (\text{triangular lattice}) \quad (149)$$

and

$$T_{123}(t_1^D, t_2^D, t_3^D, G_\Delta) = T_{123}(t_1, t_2, t_3, G_Y) \quad (\text{honeycomb lattice}) \quad (150)$$

Properties (ii) (eq. (129)) and (iii) (eqs. (130)) appearing in Section 3.2.2 hold for multi-rooted graphs.

Furthermore, it can be shown [140] that the numerator  $N_{12\dots n}(\{t_i\}, G)$  (denominator  $D(\{t_i\})$ ) of the equivalent transmissivity  $T_{12\dots n}(\{t_i\}) \equiv N_{12\dots n}(\{t_i\}, G) / D(\{t_i\}, G)$  of an arbitrary graph  $G$  depends (does not depend) on the number and location of the roots. The denominator contains, besides unity, only ‘‘cycle’’ terms (i.e. every edge belongs to a

cycle); the numerator contains only terms which join all the roots. These properties can be verified in the following examples:

$$\begin{aligned}
 T_{12} \left( \begin{array}{c} 1 \\ \circ \\ t_1 \quad t_2 \\ \diagup \quad \diagdown \\ t_5 \\ \bullet \quad \bullet \\ \diagdown \quad \diagup \\ t_3 \quad t_4 \\ \circ \\ 2 \end{array} \right) &= [t_1 t_3 + t_2 t_4 + t_1 t_4 t_5 + t_2 t_3 t_5 \\
 &+ (q-2)(t_1 t_2 t_3 t_4 + t_1 t_2 t_3 t_5 + t_1 t_2 t_4 t_5 + t_1 t_3 t_4 t_5 + t_2 t_3 t_4 t_5) \\
 &+ (q-2)(q-3)t_1 t_2 t_3 t_4 t_5] / [1 + (q-1)(t_1 t_2 t_5 + t_3 t_4 t_5 + t_1 t_2 t_3 t_4) + \\
 &+ (q-1)(q-2)t_1 t_2 t_3 t_4 t_5] \tag{151}
 \end{aligned}$$

and

$$\begin{aligned}
 T_{1234} \left( \begin{array}{c} 1 \\ \circ \\ t_1 \quad t_2 \\ \diagup \quad \diagdown \\ t_5 \\ \circ \quad \circ \\ 3 \quad 4 \\ \diagdown \quad \diagup \\ t_3 \quad t_4 \\ \circ \\ 2 \end{array} \right) &= [t_1 t_2 t_3 + t_1 t_2 t_4 + t_1 t_3 t_4 + t_2 t_3 t_4 + t_1 t_3 t_5 + t_2 t_4 t_5 + \\
 &+ t_1 t_4 t_5 + t_2 t_3 t_5 + (q-3)(t_1 t_2 t_3 t_5 + t_1 t_2 t_4 t_5 + t_1 t_3 t_4 t_5 + t_2 t_3 t_4 t_5) + \\
 &+ (q-4)t_1 t_2 t_3 t_4 + (q^2 - 5q + 8)t_1 t_2 t_3 t_4 t_5] / [1 + (q-1)(t_1 t_2 t_5 + t_3 t_4 t_5 + \\
 &+ t_1 t_2 t_3 t_4) + (q-1)(q-2)t_1 t_2 t_3 t_4 t_5] \tag{152}
 \end{aligned}$$

Eq. (151) plays, as we shall see later on, a central role for certain RG approaches [135, 107] of the bond-random Potts ferromagnet on the square lattice.

### 3.2.4 Bond-random model

In this subsection we present another type of extension in the sense that the transmissivity itself is allowed to become a random variable with an arbitrary probability law  $P(t)$  satisfying

$$\int dt P(t) = 1 \tag{153}$$

The reason for this generalization (which recovers, for  $P(t) = \delta(t - t_0)$ , the previous case where the transmissivity was single-valued) clearly is to describe bond-random systems in the *quenched* limit (the probability laws associated with different edges of a graph are assumed to be strictly *independent*). Typical examples are the *binary distribution*, given by

$$P(t) = (1 - p)\delta(t - t_1) + p\delta(t - t_2) \tag{154}$$



( $0 \leq p \leq 1; t_1, t_2 \stackrel{\geq}{\leq} 0$ ), and the *gaussian distribution*, given by

$$P(t) = \frac{1}{\sqrt{2\pi\tau}} e^{-(t-t_0)^2/2\tau^2} \quad (155)$$

( $t_0 \stackrel{\geq}{\leq} 0; \tau \geq 0$ ); they both contain the single-valued distribution as a limiting case.

If we consider a *series* array of two bonds respectively associated with  $P_1(t)$  and  $P_2(t)$ , the equivalent probability law  $P_s(t)$  will be given by

$$\begin{aligned} P_s(t) &= \int \int dt' dt'' P_1(t') P_2(t'') \delta(t - t't'') \\ &= \int_t^1 \frac{dt'}{t'} P_1(t') P_2(t/t') \equiv P_1 \circledS P_2 \end{aligned} \quad (156)$$

where we have used Eq. (97); also, at the second step where the limits of the integral have been specified, we have assumed for simplicity that  $P(t)$  takes non-zero values only for  $0 \leq t \leq 1$ . The product defined in Eq. (156), and hereafter referred to as *series-product* [127], generalizes Eq. (97), and has the structure of a commutative monoid (no inverse), the neutral element being  $I_s(t) \equiv \delta(t - 1)$  (see [127] for details and examples). It can be shown that this product is isomorphic to the convolution product through the transformation  $t = e^{-x}$ . If our series array had  $\ell$  bonds, Eq. (156) would generalize into

$$P_s = P_1 \circledS P_2 \circledS \cdots \circledS P_\ell \equiv \prod_{i=1}^{\ell} \circledS P_i \quad (157)$$

If our array of two bonds is a *parallel* one, the equivalent probability law  $P_p(t)$  will be given by

$$\begin{aligned} P_p(t) &= \int \int dt' dt'' P_1(t') P_2(t'') \delta\left(t - \frac{t' + t'' + (q-2)t't''}{1 + (q-1)t't''}\right) \\ &= \int_0^t dt' \frac{1 + (q-2)t' - (q-1)t'^2}{[1 + (q-2)t' - (q-1)t't']^2} P_1(t') P_2\left(\frac{t-t'}{1 + (q-2)t' - (q-1)t't'}\right) \\ &\equiv P_1 \circledP P_2 \end{aligned} \quad (158)$$

where we have used Eq. (104). The product just defined, and hereafter referred to as *parallel-product* [127], generalizes Eq. (104). It is isomorphic to the series-product, the neutral element of the monoid now being  $I_p(t) \equiv \delta(t)$ . If the parallel array has  $\ell$  bonds, Eq. (157) generalizes into

$$P_p(t) = P_1 \circledP P_2 \circledP \cdots \circledP P_\ell \equiv \prod_{i=1}^{\ell} \circledP P_i \quad (159)$$

Let us next introduce the *dual distribution*  $P^D(t)$  through

$$P^D(t^D)dt^D = -P(t)dt \quad (160)$$

where the minus sign is introduced because  $t^D$  monotonously *decreases* with  $t$  (see definition (106)). Relation (159) (and definition (106)) leads to the following expression

$$P^D(t) = \frac{q}{[1 + (q-1)t]^2} P\left(\frac{1-t}{1+(q-1)t}\right) \quad (161)$$

This expression recovers, for  $q = 1$ , definition (24) of ref. [127], and, for  $q = 2$ , definition (6) of ref. [159]. It is straightforward to prove that

$$(P_1 \oplus P_2)^D = P_1^D \otimes P_2^D \quad (162)$$

or, more generally,

$$\left(\prod_{i=1}^{\ell} P_i\right)^D = \prod_{i=1}^{\ell} P_i^D \quad (163)$$

which respectively generalize Eqs. (105) and (107).

Let us mention two useful properties concerning duality:

(i) the dual of the following *discrete* distribution

$$P(t) = \sum_{j=1}^J p_j \delta(t - t_j) \quad (164)$$

( $j \geq 1$ ;  $\sum_{j=1}^J p_j = 1$ ;  $\{t_j\} \equiv$  set of arbitrary transmissivities) is given by

$$P^D(t) = \sum_{j=1}^J p_j \delta(t - t_j^D) \quad (165)$$

(ii) if  $f(t)$  is an arbitrary function of the transmissivity  $t$ , and  $P(t)$  an arbitrary distribution such that  $\langle f(t) \rangle_P \equiv \int dt f(t) P(t)$  is well defined, then

$$\langle f(t) \rangle_P = \langle f(t^D) \rangle_{P^D} \quad (166)$$

Algorithms (156) and (158) enable the calculation of the distribution associated with any two-rooted graph reducible in series and parallel operations. A break-collapse algorithm would be very convenient to treat irreducible graphs. We have not succeeded in establishing it for arbitrary  $q$ , but we have for  $q=1$ : let us present it here.

We note  $\{P_i(t)\}$  the set of distributions respectively associated with the  $N_b$  (relevant) edges of the graph  $G$ ; let  $P_j(t)$  be an arbitrarily chosen distribution of that set. The distribution  $P_G(t)$  associated with the graph  $G$  is given by

$$P_G(t) = \int \left\{ \prod_{i=1}^{N_b} [dt^{(i)} P_i(t^{(i)})] \right\} \delta(t - T(\{t^{(i)}\})) \quad (167)$$

where  $T(\{t^{(i)}\})$  is the equivalent transmissivity corresponding to the set  $\{t^{(i)}\}$  of edge transmissivities. The integral appearing in (167) can be extremely heavy to handle in practical applications. We can take advantage of a generalized multilinearity property to make the problem sensibly easier from the operational standpoint.  $P_G(t)$  can be expressed as follows

$$P_G = A \star (B \otimes P_j) \quad (168)$$

where  $\star$  denotes the standard convolution product, and  $A$  and  $B$  are distributions which only depend on the set  $\{P_i\}'$  where  $P_j$  has been excluded. To determine  $A$  and  $B$  we *break* and *collapse* the  $j$ -th bond, i.e., we respectively consider  $P_j = I_p$  and  $P_j = I_s$ , and obtain

$$P_G^b = A \star (B \otimes I_p) = A \star I_p = A \quad (169)$$

and

$$P_G^c = A \star (B \otimes I_s) = A \star B \quad (170)$$

where  $P_G^b$  and  $P_G^c$  respectively denote the distributions associated with the broken and collapsed graphs. Eq. (170) implies

$$F(P_G^c) = F(A)F(B) \quad (171)$$

and hence

$$B = F^{-1}[F(P_G^c)/F(A)] = F^{-1}[F(P_G^c)/F(P_G^b)] \quad (172)$$

where we have used Eq. (169), and where  $F$  and  $F^{-1}$  respectively denote the direct and inverse Fourier-transformed distributions. Replacing Eqs. (169) and (172) into Eq. (168), we finally obtain

$$P_G = P_G^b \star \{F^{-1}[F(P_G^c)/F(P_G^b)] \otimes P_j\} \quad (173)$$

which, for  $q = 1$ , extends to distribution laws the BCM algorithm expressed in Eq. (81). This equation is herein recovered as the particular case where the set  $\{P_i(t)\}$  exclusively contains single-valued distributions. Let us work out explicitly this case.

We have  $P_i(t) = \delta(t - p_i), \forall i$ . Also  $P_G^b(t) = \delta(t - T(G_j^b))$  and  $P_G^c(t) = \delta(t - T(G_j^c))$ .

Therefore

$$F^c(\lambda) \equiv F(P_G^c) \equiv \int dt e^{-i\lambda t} P_G^c(t) = e^{-i\lambda T(G_j^c)} \quad (174)$$

and

$$F^b(\lambda) \equiv F(P_G^b) \equiv \int dt e^{-i\lambda t} P_G^b(t) = e^{-i\lambda T(G_j^b)} \quad (175)$$

hence

$$F^{-1}[F(P_G^c)/F(P_G^b)] = \delta(t - [T(G_j^c) - T(G_j^b)]) \quad (176)$$

We now use Eq. (173) to calculate  $P_G(t) \equiv \delta(t - T(G))$ :

$$\begin{aligned} \delta(t - T(G)) &= \delta[(t - T(G_j^b))] \star \{\delta(t - [T(G_j^c) - T(G_j^b)]) \otimes \delta(t - p_j)\} \\ &= \delta(t - T(G_j^b)) \star \delta(t - [(G_j^c) - T(G_j^b)]p_j) = \delta(t - [T(G_j^b) + T(G_j^c) - T(G_j^b)p_j]) \end{aligned} \quad (177)$$

hence

$$T(G) = (1 - p_j)T(G_j^b) + p_jT(G_j^c) \quad (178)$$

which reproduces Eq. (81).

Unfortunately the extension of Eq. (173) to arbitrary  $q$  is not available: it would of course be very welcome.

### 3.3 Related Models

In this subsection we extend the above notion to a few models directly related to the Potts one.

#### 3.3.1 Resistor network

A series (parallel) array of two conductances  $\sigma_1$  and  $\sigma_2$  provides the well known equivalent conductance algorithm

$$\sigma_s = \frac{\sigma_1 \sigma_2}{\sigma_1 + \sigma_2} \quad (\text{series}) \quad (179)$$

and

$$\sigma_p = \sigma_1 + \sigma_2 \quad (\text{parallel}) \quad (180)$$

By introducing the *dual conductance*  $\sigma^D$  through

$$\sigma^D \equiv \sigma_0^2/\sigma \quad (181)$$

( $\sigma_0 \equiv$  arbitrary reference conductance), algorithms (179) and (180) can be alternatively expressed as follows:

$$\sigma_s^D = \sigma_1^D + \sigma_2^D \quad (\text{series}) \quad (182)$$

and

$$\sigma_p^D = \frac{\sigma_1^D \sigma_2^D}{\sigma_1^D + \sigma_2^D} \quad (\text{parallel}) \quad (183)$$

To calculate the equivalent conductance  $\sigma_{12}(G) \equiv N/D$  between the terminals 1 and 2 associated with a graph  $G$  (with bond conductances  $\{\sigma_i\}$ ) which is irreducible in series and/or parallel operations, we can use the following algorithm [194]:

$$N_{12}(\{\sigma_i\}, G) = N_{12}(\{\sigma_i\}', G_j^b) + \sigma_j N_{12}(\{\sigma_i\}', G_j^c) \quad (184)$$

and

$$D(\{\sigma_i\}, G) = D(\{\sigma_i\}', G_j^b) + \sigma_j D(\{\sigma_i\}', G_j^c) \quad (185)$$

or more generally

$$N_{12}(G) = D_j N_{12}(G_j^b) + N_j N_{12}(G_j^c) \quad (186)$$

and

$$D(G) = D_j D(G_j^b) + N_j D(G_j^c) \quad (187)$$

where  $\sigma_{12}(G_j^b) \equiv N_{12}(G_j^b)/D(G_j^b)$  and  $\sigma_{12}(G_j^c) \equiv N_{12}(G_j^c)/D(G_j^c)$  respectively are the equivalent conductances of the broken and collapsed graphs,  $\{\sigma_i\}'$  being the set which excludes the arbitrarily chosen conductance  $\sigma_j \equiv N_j/D_j$ . By following along the same lines, it is trivial to formulate the BCM for resistances (instead of conductances).

Finally it is worth mentioning that it is possible to define a convenient variable  $s$  which plays, for conductance, the same role as that defined in Eq. (134) for the Potts model. We refer [194] to

$$s(\sigma) \equiv \frac{\sigma}{\sigma + \sigma_0} \quad (188)$$

which satisfies

$$s^D(\sigma) \equiv s(\sigma^D) = 1 - s(\sigma) \quad (189)$$

### 3.3.2 Directed bond percolation

If we are dealing with oriented graphs (e.g., see Fig. 16(a)) the BCM recursive equations becomes [28]

$$P_{12}(\{p_i\}, G) = (1 - p_j)P_{12}(\{p_i\}', G_j^b) + p_j P_{12}(\{p_i\}', G_j^c) \quad (190)$$

where  $P_{12}(G_j^b)$  and  $P_{12}(G_j^c)$  are respectively the pair connectedness (i.e., the probability that the roots 1 and 2 are connected by a path of bonds which can be traversed in the direction of the arrows) associated with the *j-broken* graph ( $p_i = 0$ ; see Fig. 16(b)) and the *j-precollapsed* one ( $p_j = 1$ ; see Fig. 16(c)). Note that the precollapsed, *-and not the collapsed* - graph, has to be considered in order that the information concerning the *sense* of possible flow is retained. For graphs containing precollapsed edges, Eq. (190) has to be recursively applied until a directed path appears which is entirely constituted by precollapsed bonds and joins the roots in the desired sense: the pair connectedness of such graph equals unity.

An interesting more general case is that in which each pair of neighbor sites is connected through a *double* opposite-directed bond (e.g., see Fig. 17(a)). We note  $p_i$  and  $q_i$  the *independent* occupancy probabilities respectively corresponding to each branch of the *i*-th double bond (the two branches being considered in a definite sense). In this problem, a two-rooted graph, (a definite root of which is chosen as “entrance”, the other one being the “exit”) is therefore characterized by the set  $\{p_i, q_i\}$ , and the pair connectedness  $P_{12}(\{p, q_i\}, G)$  satisfies [28]

$$\begin{aligned} P_{12}(\{p_i, q_i\}, G) &= (1 - p_j)(1 - q_j)P_{12}(\{p_i, q_i\}', G_j^{bb}) + (1 - p_j)q_j P_{12}(\{p_i, q_i\}', G_j^{bc}) \\ &+ p_j(1 - q_j)P_{12}(\{p_i, q_i\}', G_j^{cb}) + p_j q_j P_{12}(\{p_i, q_i\}, G_j^{cc}) \end{aligned} \quad (191)$$

where the set  $\{p_i, q_i\}'$  excludes the arbitrarily chosen  $(p_j, q_j)$ -bond, and where  $G_j^{bb}, G_j^{bc}, G_j^{cb}$  and  $G_j^{cc}$  correspond respectively to  $(p_j, q_j) = (0, 0), (0, 1), (1, 0)$  and  $(1, 1)$ . The *broken* ( $G_j^{bb}$ ), *collapsed* ( $G_j^{cc}$ ) and two *precollapsed* ( $G_j^{cb}$  and  $G_j^{bc}$ ) graphs, obtained from the graph  $G$  of Fig. 17(a) through operation on its central bond, are indicated in Figs. 17(b-e).

By making use of the property

$$P_{12}(G_j^{bc}) + P_{12}(G_j^{cb}) = P_{12}(G_j^{bb}) + P_{12}(G_j^{cc}) \quad (192)$$

we can alternatively rewrite eq. (191) in the following simpler forms:

$$P_{12}(\{p_i, q_i\}, G) = (1-p_j)P_{12}(\{p_i, q_i\}, G_j^{bb}) + q_j P_{12}(\{p_i, q_i\}', G_j^{cc}) + (p_j - q_j)P_{12}(\{p_i, q_i\}', G_j^{cb}) \quad (193)$$

or

$$P_{12}(\{p_i, q_i\}, G) = (1-q_j)P_{12}(\{p_i, q_i\}', G_j^{bb}) + p_j P_{12}(\{p_i, q_i\}', G_j^{cc}) + (q_j - p_j)P_{12}(\{p_i, q_i\}', G_j^{bc}) \quad (194)$$

Eq. (193) recovers, for  $q_i = 0$  ( $\forall i$ ), Eq. (190), and, for  $p_i = q_i$  ( $\forall i$ ), Eq. (81). The latter is not a trivial fact, as a double-oriented bond admits configurations which flow in one sense but not in the opposite, whereas such situation is impossible for a non-directed bond.

As an illustration of the double-bond problem, we consider the graph  $G$  of Fig. 17(a). It can be easily established that, for  $p_i = p$  and  $q_i = q \forall i$  [28]:

$$P_{12}(p, q, G) = p^5 - 3p^4 + p^3 + 2p^2 + (p^4 - 2p^3 + p^2)q \quad (195)$$

All these concepts are straightforwardly extended to cover n-rooted directed graphs, the roots of which have to be joined in a definite order. In particular, algorithm (190) remains as it stands.

### 3.3.3 Models with frustration

In order to discuss the  $T = 0$  properties of spin-glass systems of the spin 1/2 Ising type, it might be convenient to introduce a generalized bond [195] which can take four different configurations, namely the *ferromagnetic* (F) one ( $J_{ij} = J > 0$ ) with probability  $p$ , the *antiferromagnetic* (AF) one ( $J_{ij} = -J$ ) with probability  $q$ , the *absent* (A) one ( $J_{ij} = 0$ , non frustrated) with probability  $r$ , and the *frustrated* ( $\phi$ ) one ( $J_{ij} = 0$ , frustrated) with probability  $s$ ; obviously  $p + q + r + s = 1$ .

The *series* algorithm for two edges (denoted 1 and 2) is the following:

$$p_s = p_1 p_2 + q_1 q_2 \quad (196.a)$$

$$q_s = p_1 q_2 + p_2 q_1 \quad (196.b)$$

$$r_s = r_1 + r_2 - r_1 r_2 \quad (196.c)$$

$$s_s = (p_1 + q_1) s_2 + (p_2 + q_2) s_1 + s_1 s_2 \quad (196.d)$$

And the *parallel* algorithm is the following:

$$p_p = p_1 + p_2 - p_1 p_2 - p_1 q_2 - p_2 q_1 \quad (197.a)$$

$$q_p = q_1 + q_2 - q_1 q_2 - p_1 q_2 - p_2 q_1 \quad (197.b)$$

$$r_p = r_1 r_2 \quad (197.c)$$

$$s_p = p_1 q_2 + p_2 q_1 + r_1 s_2 + r_2 s_1 + s_1 s_2 \quad (197.d)$$

we can easily verify that  $p_s + q_s + r_s + s_s = p_p + q_p + r_p + s_p = 1$ . Eqs. (196a) and (197a) reproduce the standard bond percolation algorithms if  $q_1 = q_2 = 0$ . Eqs. (196.c) and (197.c) also reproduce the bond percolation algorithms with  $(1-r)$  playing the role of bond occupancy probability (this is related to the “hole effect” mentioned by Toulouse [196]). It is interesting also to notice that the  $r = 0$  subspace is a closed one (in the sense that  $r_1 = r_2 = 0$  is equivalent to  $r_s = r_p = 0$ ), as well as the  $q = 0$  subspace ( $q_1 = q_2 = 0$  is equivalent to  $q_s = q_p = 0$ ); the same property does not hold for the  $p = 0$  and the  $s = 0$  subspaces. Notice finally that frustration introduces great changes, which are reflected in the very different algorithms for composing the r-variables and the s-variables, in spite of the fact that the Ising coupling constant vanishes for *both* of them.

We illustrate now on the graph G of Fig. 18 the BCM corresponding to the present problem. It is sufficient to calculate  $p_G, q_G$  and  $r_G$  since  $s_G$  can be obtained through the relation  $p_G + q_G + r_G + s_G = 1$ . If we were to work through configurational analysis we should have to consider  $4^5 = 1024$  configurations ( $4^{N_b}$  in the general case). We proceed instead as follows. We arbitrarily choose one edge of the graph, say edge-5, and use multilinearity, therefore the probability  $P_G$  that the graph has a ferromagnetic equivalent bond is:

$$P_G \equiv p(G) = A p_5 + B q_5 + C r_5 + D s_5 \quad (198)$$

where we have used the fact that bond-5 has to be in one of its 4 possible configurations; A,B,C and D depend on all bonds *excepting bond-5*. Let us introduce the following



notation:  $\circ \cdots \circ$  ,  $\circ \text{---} \circ$  ,  $\circ \text{~~~~} \circ$  and will respectively indicate ferromagnetic ( $p = 1$ ), antiferromagnetic ( $q = 1$ ) and frustrated ( $s = 1$ ) bonds. It immediately comes that

$$A = \left( \begin{array}{c} \circ \quad \circ \\ \bullet \cdots \bullet \\ \circ \quad \circ \end{array} \right) \quad (199.a)$$

$$B = p \left( \begin{array}{c} \circ \quad \circ \\ \bullet \text{---} \bullet \\ \circ \quad \circ \end{array} \right) \quad (199.b)$$

$$C = p \left( \begin{array}{c} \circ \quad \circ \\ \bullet \quad \bullet \\ \circ \quad \circ \end{array} \right) \quad (199.c)$$

$$D = p \left( \begin{array}{c} \circ \quad \circ \\ \bullet \text{~~~~} \bullet \\ \circ \quad \circ \end{array} \right) \quad (199.d)$$

Therefore Eq. (198) can be rewritten as follows

$$p \left( \begin{array}{c} \circ \quad \circ \\ \bullet \text{---} \bullet \\ \circ \quad \circ \end{array} \right) = p_5 p \left( \begin{array}{c} \circ \quad \circ \\ \bullet \cdots \bullet \\ \circ \quad \circ \end{array} \right) + q_5 p \left( \begin{array}{c} \circ \quad \circ \\ \bullet \text{---} \bullet \\ \circ \quad \circ \end{array} \right) + r_5 p \left( \begin{array}{c} \circ \quad \circ \\ \bullet \quad \bullet \\ \circ \quad \circ \end{array} \right) + s_5 p \left( \begin{array}{c} \circ \quad \circ \\ \bullet \text{~~~~} \bullet \\ \circ \quad \circ \end{array} \right) \quad (200)$$

or even

$$p \left[ \begin{array}{c} \circ \quad \circ \\ \bullet \text{---} \bullet \\ \circ \quad \circ \end{array} \right] = p_5 p \left( \begin{array}{c} \circ \quad \circ \\ \bullet \cdots \bullet \\ \circ \quad \circ \end{array} \right) + q_5 p \left( \begin{array}{c} \circ \quad \circ \\ \bullet \text{---} \bullet \\ \circ \quad \circ \end{array} \right) + (1 - p_5 - q_5) p \left( \begin{array}{c} \circ \quad \circ \\ \bullet \quad \bullet \\ \circ \quad \circ \end{array} \right) \quad (201)$$

where we have used the fact that

$$p \left( \begin{array}{c} \circ \quad \circ \\ \bullet \text{~~~~} \bullet \\ \circ \quad \circ \end{array} \right) = p \left( \begin{array}{c} \circ \quad \circ \\ \bullet \quad \bullet \\ \circ \quad \circ \end{array} \right) \quad (202)$$

Property (202) holds in general and could be stated as follows: “In the calculations of  $p(G)$  of an arbitrary two-rooted graph, a fully frustrated bond ( $s = 1$ ) can be deleted if its deletion does not disconnected the roots”. This is due to the fact that *both* absent and frustrated bonds are associated to a vanishing coupling constant, consequently, the effective probability  $p$  of a graph being ferromagnetic is determined by the rest of the edges of the graph. This property can be verified on Eqs. (196.a) and (197.a), where it

can be noticed the absence of the variables  $r$  and  $s$ . Eq. (202) generalizes into

$$p(G_j^\phi) = p(G_j^b) \quad (203)$$

where  $j$  indicates that we are operating on the (arbitrarily chosen)  $j$ -th bond, and  $G_j^\phi$  and  $G_j^b$  denote respectively the  $j$ -th *frustrated-precollapsed* ( $s_j = 1$ ) and *broken* ( $r_j = 1$ ) graphs.

Eq. (201) is generalized into the following algorithm:

$$p(G) = p_j p(G_j^F) + q_j p(G_j^{AF}) + (1 - p_j - q_j) p(G_j^b) \quad (204)$$

where  $G_j^F$  and  $G_j^{AF}$  denote respectively the  $j$ -th *ferro-precollapsed* ( $p_j = 1$ ) and *antiferro-precollapsed* ( $q_j = 1$ ) graphs. This algorithm recovers, for  $q_j = 0$ , algorithm (81) with  $G_j^F$  becoming the collapsed graph  $G_j^c$ .

In a totally analogous manner we obtain for the probability  $q(c)$  that the graph  $G$  has an antiferromagnetic equivalent bond:

$$q(G) = p_j q(G_j^F) + q_j q(G_j^{AF}) + (1 - p_j - q_j) q(G_j^b) \quad (205)$$

where we have used the following property:

$$q(G_j^\phi) = q(G_j^b) \quad (206)$$

This equation is totally analogous to Eq. (202), and can be verified on the fact that Eqs. (196.b) and (197.b) do *not* contain the variables  $r$  and  $s$ .

Finally the algorithm for the  $r$ -variable is that of bond percolation (Eq. (81)), with bond occupancy probabilities  $(1 - r_i)$ , i.e.,

$$r(G) = (1 - r_j) r(G_j^c) + r_j r(G_j^b) \quad (207)$$

wheres it appears  $r$ -variables *only*.

The recursive use of Eqs. (204) (205) and (207) (together with Eqs. (196) and (197)) would enable the solution of an arbitrary graph, were it not for the fact that algorithms (204) and (205) eventually lead, as a final product, to irreducible graphs *exclusively constituted* by ferro- and antiferro-precollapsed bonds, whose solution we shall handle now.

We assume a F configuration on the roots of the graph G (i.e., the spins on both roots are *parallel*), and, considering all possible configurations for the *internal* spins (in general,  $2^{N_s-2}$  spin configurations), we obtain the *lowest* energy, noted  $E^F$ , and the corresponding degeneracy, noted  $g^F$ . We then assume an AF configuration on the roots (i.e., the spins on both roots are *antiparallel*), and consider oncemore all possible configurations for the *internal* spins, thus obtaining the lowest energy, now noted  $E^{AF}$ , and its degeneracy  $g^{AF}$ . We finally use the following set of rules (which will incidentally lead to a better understanding of the big difference existing between *absent* and *frustrated* bonds):

$$(i) \quad \text{if } E^F < E^{AF}, \text{ or if } E^F = E^{AF} \text{ and } g^F > g^{AF},$$

then the graph is equivalent to a fully F-bond (i.e.,

$$p(G) = 1 \text{ and } q(G) = r(G) = s(G) = 0); \tag{208.a}$$

$$(ii) \quad \text{if } E^F > E^{AF}, \text{ or if } E^F = E^{AF} \text{ and } g^F < g^{AF},$$

then the graph is equivalent to a fully AF-bond (i.e.,

$$q(G) = 1 \text{ and } p(G) = r(G) = s(G) = 0); \tag{208.b}$$

$$(iii) \quad \text{if } E^F = E^{AF} \text{ and } g^F = g^{AF},$$

then the graph is equivalent to a fully  $\phi$ -bond (i.e.,

$$s(G) = 1 \text{ and } p(G) = q(G) = r(G) = 0). \tag{208.c}$$

We illustrate these rules on Table II for the  $b = d = 2$  Wheatstone-bridge. The rules (208) together with Eqs. (196), (197), (204), (205) and (207) completely close the procedure. It is obviously much simpler than considering the  $4^{N_b}$  bond configurations and, for many among them, examining the spin configurations. However, it could in principle be even simpler because it does not completely avoids some configuration analysis; indeed the last step (rules (208)) demands, for each of the  $2^{N_b}$  (at most) bond configurations of an irreducible graph, the consideration of  $2^{N_s-2}$  (at most) spin configurations. An appreciable improvement would be a manner of connecting each bond configuration of the graph (first column of Table II) *directly* with is equivalent bond (third column of Table II) *without having to inspect the ground states* (intermediate column of Table II), as this is a quite time-consuming operator. We have not succeeded, and new attempts would be welcome. The observation of Table II yields the following hints:

- (i) The equivalent bond is frustrated if and only if an odd number of the  $2(c \equiv N_b - N_s + 1$  for a general connected graph) elementary plaquettes are frustrated, which in turn happens if and only if the plaquette perimeter contains an *odd* number of AF-bonds;
- (ii) Two configurations which can be obtained one from the other through F-bond  $\rightleftharpoons$  AF-bond interchanges, correspond to the same equivalent bond.

As an illustration, we have solved [195] the graph of Fig. 19 with the BCM (this two-rooted graph is self-dual, and will later on be used for RG applications for the square lattice). We obtain

$$\begin{aligned}
 p' &= 24pq^2 - 24pq^3 - 30pq^4 + 84pq^6 - 72pq^7 + 18pq^8 \\
 &- 30p^2q^2 - 50p^2q^3 + 84p^2q^4 + 262p^2q^5 - 394p^2q^6 \\
 &+ 140p^2q^7 + 8p^3 - 12p^3q - 26p^3q^2 + 36p^3q^3 + 398p^3q^4 \\
 &- 832p^3q^5 + 400p^3q^6 - 6p^4 - 28p^4q + 60p^4q^2 \\
 &+ 386p^4q^3 - 973p^4q^4 + 612p^4q^5 - 6p^5 + 12p^5q \\
 &+ 218p^5q^2 - 748p^5q^3 + 588p^5q^4 + 96p^6q \\
 &- 376p^6q^2 + 372p^6q^3 + 12p^7 - 100p^7q + 144p^7q^2 - 9p^8 + 28p^8q + 2p^9
 \end{aligned} \tag{209.a}$$

$$\begin{aligned}
 q' &= 8q^3 - 6q^4 - 6q^5 + 12q^7 - 9q^8 + 2q^9 - 12pq^3 - 28pq^4 \\
 &+ 12pq^5 + 96pq^6 - 100pq^7 + 28pq^8 + 24p^2q - 30p^2q^2 \\
 &- 26p^2q^3 + 60p^2q^4 + 218p^2q^5 - 376p^2q^6 + 144p^2q^7 \\
 &- 24p^3q - 50p^3q^2 + 36p^3q^3 + 386p^3q^4 - 748p^3q^5 \\
 &+ 372p^3q^6 - 30p^4q + 84p^4q^2 + 398p^4q^3 - 973p^4q^4 \\
 &+ 588p^4q^5 + 262p^5q^2 - 832p^5q^3 + 612p^5q^4 + 84p^6q \\
 &+ 394p^6q^2 + 400p^6q^3 - 72p^7q + 140p^7q^2 + 18p^8q
 \end{aligned} \tag{209.b}$$

$$r' = 8r^3 - 6r^4 - 6r^5 + 12r^7 - 9r^8 + 2r^9 \tag{209.c}$$

and

$$s' = 1 - p' - q' - r' \tag{209.d}$$

The generalization of the present procedure to *finite* temperatures presents [195] non trivial difficulties and will not be discussed herein.

### 3.3.4 Z(q) model

In this subsection we extend the transmissivity of the q-state Potts model in order to cover the Z(q) model where the transmissivity becomes a vector. The Hamiltonian of a single bond (between sites  $i$  and  $j$ ) is given by eq. (9). With that bond we associate the *vector transmissivity*  $\vec{t} \equiv (t_0, t_1, \dots, t_{q-1})$  defined through [120]:

$$t_\alpha = \frac{\sum_{\beta=0}^{q-1} \exp\left(\sum_{\gamma=1}^{\bar{q}} 2K_\gamma \cos \frac{2\pi\beta\gamma}{q}\right) \exp\left(\frac{i2\pi\alpha\beta}{q}\right)}{\sum_{\beta=0}^{q-1} \exp\left(\sum_{\gamma=1}^{\bar{q}} 2K_\gamma \cos \frac{2\pi\beta\gamma}{q}\right)} \quad (210)$$

with  $K_\alpha \equiv J_\alpha/k_B T$ .

We immediately verify that  $t_\alpha$  is a real number which satisfies

$$t_0 = 1 \quad (211)$$

$$t_\alpha = t_{q-\alpha} \quad (\alpha = 1, 2, \dots, q-1) \quad (212)$$

Consequently  $\vec{t}$  contains  $\bar{q}$  independent components. The Potts model corresponds to the particular case  $t_1 = t_2 = \dots = t_{q-1} \equiv t$ .

A *series* array of two bonds with transmissivities  $\vec{t}^{(1)}$  and  $\vec{t}^{(2)}$  has an equivalent transmissivity  $\vec{t}^{(s)}$  given by [120]

$$t_\alpha^{(s)} = t_\alpha^{(1)} t_\alpha^{(2)} \quad (\alpha = 0, 1, \dots, q-1) \quad (213)$$

If the array is a *parallel* one, the equivalent transmissivity  $\vec{t}_p$  is given by

$$t_\alpha^{(p)D} = t_\alpha^{(1)D} t_\alpha^{(2)D} \quad (\alpha = 0, 1, \dots, q-1) \quad (214)$$

where (for  $j = 1, 2, p$ )  $\vec{t}^{(j)} \equiv (t_0^{(j)}, t_1^{(j)}, \dots, t_{q-1}^{(j)})$  and its *dual*  $\vec{t}^{(j)D} \equiv (t_0^{(j)D}, t_1^{(j)D}, \dots, t_{q-1}^{(j)D})$

are related through

$$t_\alpha^D = \frac{\sum_{\beta=0}^{q-1} t_\beta \exp(-i2\pi\alpha\beta/q)}{\sum_{\beta=0}^{q-1} t_\beta} \quad (\alpha = 0, 1, \dots, q-1) \quad (215)$$

and

$$t_\beta = \frac{\sum_{\alpha=0}^{q-1} t_\alpha^D \exp(-i2\pi\alpha\beta/q)}{\sum_{\alpha=0}^{q-1} t_\alpha^D} \quad (\beta = 0, 1, \dots, q-1) \quad (216)$$

Let us illustrate the series parallel algorithms with the Z(4) model. In this case we have [125]:

$$t_\alpha^{(s)} = t_\alpha^{(1)} t_\alpha^{(2)} \quad (\alpha = 1, 2) \quad (217)$$

for the series array,

$$t_1^{(p)} = \frac{t_1^{(1)} + t_1^{(2)} + t_1^{(1)} t_2^{(2)} + t_1^{(2)} t_2^{(1)}}{1 + 2t_1^{(1)} t_1^{(2)} + t_2^{(2)} + t_2^{(1)} t_2^{(2)}} \quad (218)$$

and

$$t_2^{(p)} = \frac{t_2^{(1)} + t_2^{(2)} + 2t_1^{(1)} t_1^{(2)}}{1 + 2t_1^{(1)} t_1^{(2)} + t_2^{(1)} t_2^{(2)}} \quad (219)$$

for the parallel array, and finally [121, 125]

$$t_1^D = \frac{1 - t_2}{1 + 2t_1 + t_2} \quad (220)$$

and

$$t_2^D = \frac{1 - 2t_1 + t_2}{1 + 2t_1 + t_2} \quad (221)$$

or equivalently

$$t_1 = \frac{1 - t_2^D}{1 + 2t_1^D + t_2^D} \quad (222)$$

and

$$t_2 = \frac{1 - 2t_1^D + t_2^D}{1 + 2t_1^D + t_2^D} \quad (223)$$

for the dual relations. In eqs. (217-223) the vector transmissivity  $\vec{t} \equiv (1, t_1, t_2, t_3)$  is defined as (see eq. 210):

$$t_1 = t_3 = \frac{1 - e^{-4K_1}}{1 + 2e^{-2(K_1+2K_2)} + e^{-4K_1}} \quad (224.a)$$

$$t_2 = \frac{1 - 2e^{-2(K_1+2K_2)} + e^{-4K_1}}{1 + 2e^{-2(K_1+2K_2)} + e^{-4K_1}} \quad (224.b)$$

Now let us consider the general case corresponding to an arbitrary connected two-rooted graph  $G$  whose edges are associated with  $q$ -dimensional vector transmissivities  $\{\vec{t}_i\}$ . Similarly to the Potts model (see eqs. 109), one can define the *vector transmissivity*  $\vec{T}(1, 2; G) \equiv \{T_\alpha(1, 2; G), \alpha = 0, 1, \dots, q - 1\}$  between the roots 1 and 2 of  $G$  as the transmissivity  $\vec{t}_{eff}$  of a single effective edge  $e_{eff}$  between 1 and 2 having an equivalent Hamiltonian  $\mathcal{H}_{eq}(n_1 - n_2)$  given by [197]:

$$C e^{-\mathcal{H}_{eq}(n_1 - n_2)/k_B T} = Tr' \{ e^{-\mathcal{H}(G)/k_B T} \} \quad (225)$$

where  $C$  is constant and  $Tr'$  denotes the trace over the configurations of only the internal spins (on the unrooted vertices).

It has been proved [197] for any graph  $G$  that:

$$T_\alpha(1, 2; G) = \langle e^{-2\pi i(n_1 - n_2)\alpha/q} \rangle = \frac{N_\alpha(1, 2; G)}{D(G)} \quad (\alpha = 0, 1, \dots, q - 1) \quad (226)$$

where  $\langle \dots \rangle$  stands for a thermal average involving all the spins on the graph  $G$ .

Analogously to the Potts model (see eqs. 111), the denominator  $D(G)$  (which is independent of the roots and of the component  $\alpha$ ) of  $T_\alpha(1, 2; G)$  is related to the partition function  $Z(G)$  through [197, 198]:

$$Z(G) = BD(G) \quad (227.a)$$

with

$$B = q^{N_s - N_b} \prod_{e=1}^{N_b} \left\{ \sum_{\alpha=0}^{q-1} e^{-\mathcal{H}_e(\alpha)/k_B T} \right\} \quad (227.b)$$

where the product is over all the  $N_b$  edges  $\{e\}$  ( $e = 1, 2, \dots, N_b$ ) of the graph  $G$  with  $N_s$  vertices; to each edge  $e$  joining the vertices  $i$  and  $j$  is associated the Hamiltonian  $\mathcal{H}_e(\alpha = n_i - n_j)$  given by eq. (9).

Concerning the numerators  $\{N_\alpha(1, 2; G)\}$  ( $\alpha = 0, 1, \dots, q - 1$ ) they satisfy [197]:

$$N_\alpha(1, 2; G) = N_{q-\alpha}(1, 2; G) \quad (\alpha = 1, 2, \dots, q - 1) \quad (228.a)$$

and

$$N_0(1, 2; G) = D(G) \quad (228.b)$$

from which it follows that the relations (211) and (212) are valid, not only for an edge, but also for an effective edge linking the roots of a graph  $G$ , i.e., for  $T_\alpha(1, 2; G)$ .

In the case of the Potts model, these numerators reduce, for  $\alpha \neq 0$ , to [197]:

$$N_1(1, 2; G) = N_2(1, 2; G) = \cdots = N_{q-1}(1, 2; G) = N_{12}(G) \quad (229)$$

where  $N_{12}(G)$  is the numerator of  $T_{12}(G)$  defined previously (see section 3.2.2). Consequently the Potts model corresponds to the particular case  $T_1(1, 2; G) = T_2(1, 2; G) = \cdots = T_{q-1}(1, 2; G) = T_{12}(G)$ .

Pair correlation functions can normally be written as the thermal average of some function  $f(n_1 - n_2)$  which depends only on the difference, mod- $q$ , of the state variables  $n_1$  and  $n_2$ . It has been shown that the Fourier decomposition of  $\langle f(n_1 - n_2) \rangle$  involves  $T_\alpha(1, 2; G)$  through [197]:

$$\langle f(n_1 - n_2) \rangle = \frac{1}{q} \sum_{\alpha=0}^{q-1} f_{q-\alpha} T_\alpha(1, 2; G) \quad (230)$$

The above relation reduces, for the Potts model, to eq. (110) if one chooses  $f(n_1 - n_2) = [q\delta(n_1 - n_2) - 1]/(q - 1)$ .

The generalizations of the factorization rules (115), (116) and (117) to the  $Z(q)$  model are given, respectively, by [197]:

$$N_\alpha(1, 2; G) = N_\alpha(1, 2; G_1)D(G_2) \quad (231)$$

$$N_\alpha(1, 2; G) = N_\alpha(1, i; G_1)N_\alpha(i, 2; G_2) \quad (232)$$

and

$$N_\alpha(1, 2; G) = T_\alpha(1, 2; G) = 0 \quad (\alpha = 0, 1, \cdots, q - 1) \quad (233)$$

Notice that eq. (232) reduces to eq. (213) for two edges in series.

The extension to the  $Z(q)$  model of the parallel algorithm (eq. 122) for effective edges with vector equivalent transmissivities  $\vec{T}^{(1)} \equiv \{N_\alpha^{(1)}/D^{(1)}, \alpha = 0, 1, \cdots, q - 1\}$  and  $\vec{T}^{(2)} \equiv \{N_\alpha^{(2)}/D^{(2)}, \alpha = 0, 1, \cdots, q - 1\}$  is [197]:

$$\tilde{N}_\alpha^{(p)} = \tilde{N}_\alpha^{(1)} \tilde{N}_\alpha^{(2)} \quad (\alpha = 0, 1, \cdots, q - 1) \quad (234.a)$$



where, for  $j = 1, 2, p$ ,  $\tilde{N}_\alpha$  is the discrete Fourier transform of  $N_\alpha$ :

$$\tilde{N}_\alpha = \sum_{\beta=0}^{q-1} N_\beta \exp(-2\pi i \alpha \beta / q) \quad (\alpha = 0, 1, \dots, q-1) \quad (234.b)$$

Observe that, for an ordinary edge with vector equivalent transmissivity  $\vec{t} \equiv (t_0, t_1, \dots, t_{q-1})$ , the ratio  $\tilde{N}_\alpha / \tilde{N}_0$  equals  $t_\alpha^D$  ( $\alpha = 0, 1, \dots, q-1$ ). Therefore eq. (234a) recovers eq. (214) for two edges in parallel.

With eqs. (231-234) we can calculate pair correlation functions for the  $Z(q)$  model on any two-rooted graph  $G$  reducible in series and/or parallel operations. If the graph is an irreducible one, we should use the following break-collapse equation [197] for  $q \geq 4$ :

$$N_\alpha(1, 2; G) = \left( D^{(j)} + (\bar{q} - 2)N_1^{(j)} - \sum_{\beta=2}^{\bar{q}} N_\beta^{(j)} \right) N_\alpha(1, 2; G_j^{bb \dots b}) + N_{1_{eff}} N_\alpha(1, 2; G_j^{cc \dots c}) + \sum_{\beta=2}^{\bar{q}} (N_\beta^{(j)} - N_1^{(j)}) N_\alpha(1, 2; G_j^{bb \dots c \dots b}) \quad (\alpha = 0, 1, \dots, \bar{q}) \quad (235)$$

with the superscript  $c$  in the last term occupying the  $\beta^{th}$  position.  $N_\alpha(1, 2; G_j^{bb \dots b})$ ,  $N_\alpha(1, 2; G_j^{cc \dots cc})$  and  $N_\alpha(1, 2; G_j^{bb \dots c \dots b})$  are the  $N_\alpha$  of the respective broken ( $bb \dots b, t_1^{(j)} = t_2^{(j)} = \dots = t_{q-1}^{(j)} = 0$ ), collapsed ( $cc \dots c; t_1^{(1)} = t_2^{(j)} = \dots = t_{q-1}^{(j)} = 1$ ) and the  $\beta$ -type precollapsed ( $bb \dots c \dots b; t_\beta^{(j)} = t_{q-\beta}^{(j)} = 1$  and  $t_\gamma^{(j)} = 0$  for  $\gamma \neq \beta, q - \beta, 0$ ) graphs.  $N_\alpha^{(j)}$  ( $\alpha = 1, 2, \dots, q-1$ ) and  $D^{(j)}$  correspond, respectively, to the numerators and denominator of the  $\alpha$ -component of the vector transmissivity  $\vec{t}^{(j)}$  associated with the effective edge  $j$ .

Notice that eq. (235) recovers eqs. (119) for the Potts model (where  $N_1^{(j)} = N_2^{(j)} = \dots = N_{\bar{q}}^{(j)} \equiv N_j$ ). Furthermore the equation reduces, when  $j$  is an ordinary (i.e., non-effective) edge, to the break-collapse equation conjectured by Mariz et al for  $q = 4$  [121] and  $q = 6$  [199]. Let us make it explicit for the  $Z(4)$  model namely:

$$N_\alpha(1, 2; G) = (1 - t_2^{(j)})N_\alpha(1, 2; G_j^{bb}) + t_1^{(j)}N_\alpha(1, 2; G_j^{cc}) + (t_2^{(j)} - t_1^{(j)})N_\alpha(1, 2; G_j^{bc}) \quad (\alpha = 0, 1, 2) \quad (236)$$

See, in Fig. 20, the standard Wheatstone-bridge graph, and its corresponding broken, collapsed and precollapsed graphs where the break-collapsing has been done on the central bond.

The iterative use of Eqs. (217-219) and (236) yields, for the  $Z(4)$  model, the complete answer for  $\vec{T}(1, 2; G)$  if we know the answer for that *same* graph with *all* its bonds being precollapsed (last and unique non trivial element of the iterative chain). It has been proved [197] that such a graph is precollapsed itself with the following attribution:  $t_1 = 0/2^c$  and  $t_2 = 2^c/2^c$ , with the cyclomatic number  $c = N_b - N_s + 1$  for a connected graph  $G$ .

The BCM enabled a relatively easy solution for the graph of Fig. (20.a); the solution is given [200] by  $T_1(1, 2; G) = N_1(1, 2; G)/D(G)$  and  $T_2(1, 2; G) = N_2(1, 2; G)/D(G)$  with

$$\begin{aligned}
 N_1(1, 2; G) &= N_3(1, 2; G) = t_1^{(1)}t_1^{(2)} + t_1^{(3)}t_1^{(4)} + t_1^{(1)}t_1^{(4)}t_1^{(5)} + t_1^{(2)}t_1^{(3)}t_1^{(5)} \\
 &+ t_1^{(1)}t_1^{(2)}t_2^{(3)}t_2^{(4)} + t_1^{(3)}t_1^{(4)}t_2^{(1)}t_2^{(2)} + t_1^{(1)}t_1^{(4)}t_1^{(5)}t_2^{(2)} \\
 &+ t_1^{(1)}t_1^{(4)}t_1^{(5)}t_2^{(3)} + t_1^{(2)}t_1^{(3)}t_1^{(5)}t_2^{(1)} + t_1^{(2)}t_1^{(3)}t_1^{(5)}t_2^{(4)} \\
 &+ t_1^{(1)}t_1^{(2)}t_2^{(3)}t_2^{(5)} + t_1^{(1)}t_1^{(2)}t_2^{(4)}t_2^{(5)} + t_1^{(3)}t_1^{(4)}t_2^{(1)}t_2^{(5)} \\
 &+ t_1^{(3)}t_1^{(4)}t_2^{(2)}t_2^{(5)} + t_1^{(1)}t_1^{(4)}t_1^{(5)}t_2^{(2)}t_2^{(3)} + t_1^{(2)}t_1^{(3)}t_1^{(5)}t_2^{(1)}t_2^{(4)} \quad (237.a)
 \end{aligned}$$

$$\begin{aligned}
 N_2(1, 2; G) &= t_2^{(1)}t_2^{(2)} + t_2^{(3)}t_2^{(4)} + t_2^{(1)}t_2^{(4)}t_2^{(5)} + t_2^{(2)}t_2^{(3)}t_2^{(5)} \\
 &+ 2t_1^{(1)}t_1^{(2)}t_1^{(3)}t_1^{(4)} + 2(t_1^{(1)}t_1^{(3)}t_1^{(5)}t_2^{(2)} + t_1^{(1)}t_1^{(3)}t_1^{(5)}t_2^{(4)} \\
 &+ t_1^{(2)}t_1^{(4)}t_1^{(5)}t_2^{(1)} + t_1^{(2)}t_1^{(4)}t_1^{(5)}t_2^{(3)}) + 2t_1^{(1)}t_1^{(2)}t_1^{(3)}t_1^{(4)}t_2^{(5)} \quad (237.b)
 \end{aligned}$$

and

$$\begin{aligned}
 D(G) &= 1 + t_2^{(1)}t_2^{(3)}t_2^{(5)} + t_2^{(2)}t_2^{(4)}t_2^{(5)} + 2(t_1^{(1)}t_1^{(3)}t_1^{(5)} + \\
 &+ t_1^{(2)}t_1^{(4)}t_1^{(5)}) + t_2^{(1)}t_2^{(2)}t_2^{(3)}t_2^{(4)} + 2t_1^{(1)}t_1^{(2)}t_1^{(3)}t_1^{(4)} + \\
 &+ 2(t_1^{(1)}t_1^{(2)}t_1^{(3)}t_1^{(4)}t_2^{(5)} + t_1^{(1)}t_1^{(3)}t_1^{(5)}t_2^{(2)}t_2^{(4)} + t_1^{(2)}t_1^{(4)}t_1^{(5)}t_2^{(1)}t_2^{(3)}) \quad (237.c)
 \end{aligned}$$

Let us now focus on the  $Z(6)$  model where the equivalent vector transmissivity  $\vec{T}(1, 2; G)$  of an arbitrary two-rooted graph is given by  $T_\alpha(1, 2; G) = N_\alpha(1, 2; G)/(G)$  ( $r = 1, 2, 3$ ). Setting  $q = 6$  in eq. (235) and choosing an ordinary edge  $j$ , one obtains the following break-collapse equation:

$$\begin{aligned}
 N_\alpha(1, 2; G) &= (1 + t_1^{(j)} - t_2^{(j)} - t_3^{(j)})N_\alpha(1, 2; G_j^{bbb}) + t_1^{(j)}N_\alpha(1, 2; G_j^{ccc}) + \\
 &+ (t_2^{(j)} - t_1^{(j)})N_\alpha(1, 2; G_j^{bcb}) + (t_3^{(j)} - t_1^{(j)})N_\alpha(1, 2; G_j^{bbc}) \quad (\alpha = 0, 1, 2, 3) \quad (238)
 \end{aligned}$$

See, in Fig. 21, the standard Wheatstone-bridge graph and its corresponding broken, collapsed and precollapsed graphs, the  $j$ -th bond being the central one.

The iterative use of Eqs. (231-234) and (238) yields the complete answer for  $\vec{T}(1, 2; G)$  if we know the answers for all the associated graphs where *all* of its bonds are precollapsed. An arbitrary graph  $G$  yields in general, for the  $Z(6)$  model,  $2^{N_b}$  such associated terminal graphs (noted  $\{G_{pr}\}$ ) as each one of its bonds can be either of the precollapsed-2 or of the precollapsed-3 type.

In this case there are no simple formulae for the  $T_\alpha(1, 2; G_{pr})$  ( $\alpha = 1, 2, 3$ ) such as those mentioned for  $q = 4$ . Their calculation involves the explicit enumeration of certain mod-6 flows on  $G_{pr}$ . A model- $N$  flow  $\vec{\phi}$  on any graph  $G$  is defined as follows (see ref. [139]). First, consider an arbitrary directing of the  $N_b$  edges  $e_1, e_2, \dots, e_{N_b}$  of  $G$  and then associate to each edge  $e_i$  a value  $\phi_i$  which takes on the  $N$  values  $0, 1, \dots, N - 1$ . Define an incidence matrix  $S$  for each vertex  $j$  and edge  $e$  by:

$$S_{je} = \begin{cases} 1 & \text{if } e \text{ is directed into } j \\ -1 & \text{if } e \text{ is directed out of } j \\ 0 & \text{if } j \text{ is not a vertex of } e \end{cases} \quad (239)$$

We say that  $\vec{\phi} = (\phi_1, \phi_2, \dots, \phi_{N_b})$  is a *mod- $N$  flow* on  $G$  if for each vertex  $j$  there is a conservation condition mod- $N$  given by

$$\partial\phi_j \equiv \sum_{e=1}^{N_b} S_{je}\phi_e = 0 \text{ mod-}N \quad (240)$$

$\vec{\phi}$  is a *rooted mod- $N$   $\alpha$  flow* on  $G$  if (240) applies to all unrooted vertices and if, in addition, there is an external flow  $\alpha$  entering at root 1 and leaving at root 2, in other words:

$$\partial\phi_j = \begin{cases} -\alpha & \text{if } j = 1 \\ +\alpha & \text{if } j = 2 \\ 0 & \text{otherwise} \end{cases} \quad (241)$$

The particular case of  $\alpha = 0$  corresponds to a mod- $N$  flow.

Concerning our problem of calculating  $T_\alpha(1, 2; G_{pr})$ , it has been proved [197] that  $N_\alpha(1, 2; G_{pr})$  ( $\alpha = 1, 2, 3$ ) is the number of rooted mod-6  $\alpha$  flows such that the flow on any precollapsed edge of type 2 must be 0, 2 or 4 and the flow on any precollapsed edge of

type 3 must be 0 or 3.  $D(G_{pr})$  corresponds to the particular case of zero external flow, i.e.,  $D(G_{pr}) = N_0(G_{pr})$ . An example of a terminal graph  $G_{pr}$  with 2 and 3 precollapsed edges of respective types 2 and 3 is shown in Fig. 22. In this example there is only one mod-6  $\alpha$  flow for a fixed external flow  $\alpha$  ( $\alpha = 0, 1, 2, 3$ ) and therefore  $T_\alpha(1, 2, G_{pr}) = (\frac{1}{1}, \frac{1}{1}, \frac{1}{1})$  for this specific terminal graph.

We have presented in Fig. 23 the 14 non equivalent associated  $G_{pr}$  graphs of Fig. 21 (a) with their respective  $T_\alpha(1, 2; G_{pr})$  ( $\alpha = 1, 2, 3$ ). As an illustration of the use of the  $Z(6)$  BCM we present below the result obtained for the graph of Fig. 21 (a) with all transmissivities equal among themselves and given by  $(t_1, t_2, t_3)$ , namely [199]:

$$N_1(1, 2; G) = 2\{t_1^2 + t_1^3 + 3t_1^2t_2^2 + t_2^2t_3^2 + 2t_1^3t_2 + 2t_1t_2^2t_3 + 2t_1t_2t_3^2 + 3t_1^2t_2^2t_3 + 2t_1t_2^3t_3 + t_1t_2^2t_3^2\} \quad (242.a)$$

$$N_2(1, 2; G) = 2t_2^2 + 2t_2^3 + t_1^4 + 5t_2^4 + 2t_1^2t_3^2 + 4t_1^3t_2 + 4t_1t_2t_3^2 + 2t_1^2t_2t_3^2 + 6t_1^2t_2^2t_3 + 4t_1^3t_2t_3 + 4t_1^2t_2t_3 \quad (242.b)$$

$$N_3(1, 2; G) = 2\{t_3^2 + t_3^3 + 2(t_1^2t_2^2 + t_1^3t_2^2 + t_1^2t_2^3)\} + 4(t_1^2t_2t_3 + t_1t_2^2t_3) + 2t_1^2t_2^2t_3 \quad (242.c)$$

and

$$D(G) = 1 + 4t_1^3 + 4t_2^3 + 2t_3^3 + 2t_1^4 + 2t_2^4 + t_3^4 + 2t_1^4t_2 + 4t_1^3t_2^2 + 4t_1^2t_2^2t_3 + 4t_1^2t_2t_3^2 + 4t_1t_2^2t_3^2 + 2t_2^5 \quad (242.d)$$

where  $t_i$  is related to the coupling constants through (see eq. 210):

$$t_1 = t_5 \equiv [1 + e^{-(K_1+3K_2+4K_3)} - e^{-3(K_1+K_2)} - e^{-4(K_1+K_3)}] / D_0 \quad (243.a)$$

$$t_2 = t_4 \equiv [1 - e^{-(K_1+3K_2+4K_3)} - e^{-3(K_1+K_2)} + e^{-4(K_1+K_3)}] / D_0 \quad (243.b)$$

$$t_3 \equiv [1 - 2e^{-(K_1+3K_2+4K_3)} + 2e^{-3(K_1+K_2)} - e^{-4(K_1+K_3)}] / D_0 \quad (243.c)$$

with

$$D_0 = 1 + 2e^{-(K_1+3K_2+4K_3)} + 2e^{-3(K_1+K_2)} + e^{-4(K_1+K_3)} \quad (243.d)$$

For a general fixed value of  $q$  the BCM for the  $Z(q)$  model consists in applying eqs. (231-235) as many times as needed to arrive at terminal graphs  $G_{pr}$  with all edges precollapsed. Such graphs contain, at most,  $(\bar{q} - 1)$  different types of precollapsed edges. The calculation of their corresponding  $N_\alpha(1, 2; G)$  ( $\alpha = 0, 1, \dots, \bar{q}$ ) requires, except for

$q = 4$ , the explicit enumeration of all rooted mod- $q$  flow on  $G_{pr}$  with the constraint that the flow on each precollapsed edge of type  $\beta$  ( $\beta = 2, 3, \dots, \bar{q}$ ) can take only the values 0,  $\beta$  or  $q - \beta$ .

There has been also established [197] a generalization, to the  $Z(q)$  model, of the subgraph break-collapse method for the Potts model [133]. In ref. [197] it is argued that an alternative break-collapse equation, which uses fixed-flow bonds rather than precollapsed ones, leads to an algorithm more efficient than the BCM.

### 3.3.5 The Discrete Cubic Model

As we mentioned in section 1.2.4, the discrete  $N$ -vector model (or the  $N$ -component cubic model) is an interesting particular case of the  $Z(2N)$  model. It contains many important limiting cases (e.g, self-avoiding walks, spin 1/2 Ising model, the Ashkin-Teller model and the Potts model) and it reduces to the Ising and  $Z(4)$  models for  $N = 1$  and 2 respectively. In this subsection we particularize the vector transmissivity and the BCM of the previous section to the case of the discrete cubic model.

Let us recall that the dimensionless pair Hamiltonian can be written as [42]:

$$\frac{\mathcal{H}_{ij}}{k_B T} = -NK \vec{S}_i \cdot \vec{S}_j - NL (\vec{S}_i \cdot \vec{S}_j)^2 \quad (K \equiv J_1/k_B T, L \equiv J_2/k_B T) \quad (244)$$

where the  $N$ -component unit vector  $\vec{S}_i$  can point in one of the  $2N$  directions (positive and negative) of the  $N$ -dimensional orthogonal axes, i.e.

$$\vec{S}_i = (\pm 1, 0, \dots, 0) \text{ or } (0, \pm 1, 0, \dots, 0) \text{ or } \dots (0, 0, 0, \dots, \pm 1) \quad (245)$$

When the pair interaction energies  $\mathcal{H}_{ij}(\alpha \equiv n_i - n_j)$  ( $\alpha = 0, 1, \dots, 2N - 1$ ) of the  $Z(2N)$  model become highly degenerate such that

$$\mathcal{H}_{ij}(1) = \mathcal{H}_{ij}(2) = \dots = \mathcal{H}_{ij}(N - 1) = \mathcal{H}_{ij}(N + 1) = \dots = \mathcal{H}_{ij}(2N - 1) \quad (246)$$

then one recovers (see [47]) the  $N$ -component cubic model with dimensionless coupling constants  $K$  and  $L$  given by:

$$\mathcal{H}_{ij}(N) - \mathcal{H}_{ij}(0) = 2N k_B T \quad (247.a)$$

and

$$\mathcal{H}_{ij}(1) - \mathcal{H}_{ij}(0) = N(K + L)k_B T \quad (247.b)$$

In this case the  $Z(2N)$  spectrum of  $(N + 1)$  levels became reduced to only 3 levels ( $\forall N$ ) :  $\mathcal{H}_{ij}(0)$  and  $\mathcal{H}_{ij}(N)$  having, each one, a degeneracy  $2N$  and the other level (corresponding to the case given by eq. 246) has a degeneracy  $(4N^2 - 4N)$ .

Substituting eqs. (246) and (247) in the definition of  $\vec{t}$  (eq. 210) we obtain that:

$$t_1 = t_3 = \dots = t_{2N-1} = \frac{1 - e^{-2NK}}{1 + 2(N-1)e^{-N(K+L)} + e^{-2NK}} \equiv t_1 \quad (248.a)$$

and

$$t_2 = t_4 = \dots = t_{2N-2} = \frac{1 - 2e^{-N(K+L)} + e^{-2NK}}{1 + 2(N-1)e^{-N(K+L)} + e^{-2NK}} \equiv t_2 \quad (248.b)$$

showing that the  $N$ -component cubic model has a vector transmissivity  $\vec{t} \equiv (t_1, t_2)$  with only 2 different components.

The series and parallel algorithms of 2 edges continue to be given by eqs. (213) and (214) respectively where now the dual vector transmissivity  $\vec{t}^D \equiv (t_1^D, t_2^D)$  is [46, 47]

$$t_1^D = \frac{1 - Nt_1 + (N-1)t_2}{1 + Nt_1 + (N-1)t_2} \quad (249.a)$$

and

$$t_2^D = \frac{1 - t_2}{1 + Nt_1 + (N-1)t_2} \quad (249.b)$$

The parallel algorithm  $\vec{t}^{(p)} \equiv (t_1^{(p)}, t_2^{(p)})$  can be obtained directly through [46, 47]:

$$t_1^{(p)} = \frac{t_1^{(1)} + t_1^{(2)} + (N-1)[t_2^{(1)}t_1^{(2)} + t_1^{(1)}t_2^{(2)}]}{1 + Nt_1^{(1)}t_1^{(2)} + (N-1)t_2^{(1)}t_2^{(2)}} \quad (250.a)$$

and

$$t_2^{(p)} = \frac{t_2^{(1)} + t_2^{(2)} + Nt_1^{(1)}t_1^{(2)} + (N-2)t_2^{(1)}t_2^{(2)}}{1 + Nt_1^{(1)}t_1^{(2)} + (N-1)t_2^{(1)}t_2^{(2)}} \quad (250.b)$$

Using eqs. (226) and (230) one can show that the equivalent vector transmissivity  $\vec{T}(1, 2; G) \equiv \{T_1(1, 2; G), T_2(1, 2; G)\}$  between the roots 1 and 2 of a graph  $G$  is:

$$T_1(1, 2, G) = \frac{N_1(1, 2; G)}{D(G)} = \langle \vec{S} \cdot \vec{S}_2 \rangle \quad (251.a)$$

and

$$T_2(1, 2; G) = \frac{N_2(1, 2; G)}{D(G)} = \frac{\langle N(\vec{S}_1 \cdot \vec{S}_2)^2 - 1 \rangle}{N - 1} \quad (251.b)$$

The factorization rules (eqs. (231-233)) are not modified in the case of the cubic model, while the parallel combination of graphs is given by eq. (234a) where now the discrete Fourier transforms  $\tilde{N}_\alpha$  are [47]:

$$\tilde{D}(G) = \tilde{N}_0(G) = D(G) + NN_1(1, 2; G) + (N - 1)N_2(1, 2; G) \quad (252.a)$$

$$\tilde{N}_N(1, 2; G) = D(G) - NN_1(1, 2; G) + (N - 1)N_2(1, 2; G) \quad (252.b)$$

and

$$\tilde{N}_\alpha(1, 2; G) = D(G) - N_2(1, 2; G) \quad (\forall \alpha \neq 0 \text{ or } N) \quad (252.c)$$

The break-collapse, for the cubic model, (eq. (235)) reduces to [47]:

$$\begin{aligned} N_\alpha(1, 2; G) &= (D^{(j)} - N_2^{(j)})N_\alpha(1, 2; G_j^{bb}) + N_1^{(j)}N_\alpha(1, 2; G_j^{cc}) + \\ &+ (N_2^{(j)} - N_1^{(j)})N_\alpha(1, 2; G_j^{bc}) \quad (\alpha = 0, 1, 2) \end{aligned} \quad (253)$$

where  $G_j^{bb}$ ,  $G_j^{cc}$  and  $G_j^{bc}$  are the broken ( $t_1^{(j)} = t_2^{(j)} = 0$ ), collapsed ( $t_1^{(j)} = t_2^{(j)} = 1$ ) and precollapsed ( $t_1^{(j)} = 0, t_2^{(j)} = 1$ ) graphs and the edge  $j$  has a vector transmissivity  $\vec{t}^j \equiv (t_1^{(j)} = N_1^{(j)}/D^{(j)}, t_2^{(j)} = N_2^{(j)}/D^{(j)})$ .

Notice that, unlike the break-collapse equation for the  $Z(2N)$  model (eq. 235), eq. (253) allows the calculation of  $T_\alpha(1, 2; G)$  as a *function of  $N$*  rather than for a specified value of  $N$ . Furthermore, instead of  $(N - 1)$  precollapsed graphs generated by the application of eq. (235) to the  $Z(2N)$  model, there is *only one precollapsed graph (independent of the value of  $N$ )* generated by eq. (253).

The iterative use of eqs. (231-233), (234a), (252) and (253) (which constitutes the BCM) leads to the calculation of  $\vec{T}(1, 2; G)$  for *any* two-rooted graph  $G$  provided that we know  $\vec{T}(1, 2; G_{pr})$  for that same graph with *all* its bonds being precollapsed. It has been proved [47], similarly to the  $Z(4)$  model, that such a graph is precollapsed itself with the following attribution:

$$T_1(1, 2; G_{pr}) = 0/N^c \text{ and } T_2(1, 2; G_{pr}) = N^c/N^c .$$

The application of the BCM to the graph of Fig. (20a) for the homogeneous case where the vector transmissivities are all equal to  $\vec{t} \equiv (t_1, t_2)$  leads to [47]:

$$\begin{aligned} N_1(1, 2; G) &= 2t_1^2 + 2t_1^3 + 6(N-1)t_1^2t_2^2 + 2(N-1)(N-2)t_1^2t_2^3 + \\ &+ 4(N-1)t_1^3t_2 + 2(N-1)^2t_1^3t_2^2 \end{aligned} \quad (254.a)$$

$$\begin{aligned} N_2(1, 2; G) &= 2t_2^2 + 2t_2^3 + Nt_1^4 + 5(N-2)t_2^4 + 4Nt_1^3t_2 + 2N(N-2)t_1^3t_2^2 \\ &+ N(N-1)t_1^4t_2 + (N-2)(N-3)t_2^5 \end{aligned} \quad (254.b)$$

and

$$\begin{aligned} D(G) &= N_0(1, 2; G) = 1 + 2Nt_1^3 + 2(N-1)t_2^3 + Nt_1^4 + (N-1)t_2^4 + (N-1)(N-2)t_2^5 \\ &+ 2N(N-1)t_1^3t_2^2 + N(N-1)t_1^4t_2 \end{aligned} \quad (254.c)$$

Let us also mention that the modifications of the subgraph break-collapse algorithm of the Potts model necessary for dealing with the cubic model are described in ref. [47].



## 4 REAL-SPACE RENORMALIZATION-GROUP APPROACHES

Since the formulation of the renormalization group formalism by Wilson in 1971 [201] (see also [202]), we have witnessed an explosion of theoretical studies focusing the static (and dynamic) properties associated with critical phenomena occurring in all types of cooperative systems (geometrical, thermal and mixed statistical systems). Two main flows can be distinguished which only differ methodologically, but not in the essence of the formalism. We refer to *reciprocal-space* and *real-space* techniques. The former use Field Theory mathematical tools, which typically substitute the crystalline system by its *continuous* limit (vanishing crystalline parameter), and therefore lose the particular structural information (e.g., no distinction remains between simple cubic, FCC and diamond structures). As a natural consequence, these techniques are normally unable for predicting values for critical points, critical lines, phase diagrams generally speaking. But in compensation they naturally provide analytical, and quite well controlled, asymptotically exact results for the critical exponents ( $\nu, \beta, \gamma$ , etc) which characterize the various universality classes of the equation of states and correlation functions. Typical such results are the  $\varepsilon \rightarrow 0$  expansions ( $d = 4 - \varepsilon, d = 1 + \varepsilon, d = 2 + \varepsilon$ ) for arbitrary  $n$ , and  $n \rightarrow \infty$  expansions for arbitrary  $d$ , for the  $n$ -vector model ( $d$  and  $n$  being respectively the dimensionalities of the space and of the field therein defined); also the  $\varepsilon = 6 - d$  expansion for uncorrelated non-directed percolation. Quite generally speaking, the  $\varepsilon$ -expansions can in principle be done (see e.g. [203–204]) for  $d = d_u - \varepsilon, d = d_\ell + \varepsilon$  and  $d = d_s + \varepsilon$ , where  $d_u$  is the *upper critical dimensionality* above which all (static) critical exponents equal their classical, Landau-like, values, (e.g,  $d_u = 4$  for the  $n$  ferromagnetic model,  $d_u = 6$  for uncorrelated non-directed percolation,  $d_u = 5$  for uncorrelated directed percolation);  $d_\ell$  is the *lower critical dimensionality* below which no critical phenomenon occurs at *finite* values of the relevant external parameter, for instance  $T > 0$  for thermal transitions,  $1 - p > 0$  for percolation,  $p$  being the bond (or site) concentration ( $d_\ell = 1$  for the  $q$ -state Potts ferromagnet,  $d_\ell = 2$  for the Heisenberg ferromagnet); finally,  $d_s = 2s$  is a special dimensionality for which [31] some  $s$ -simplex models are *self-dual* (e.g,  $s = 1$  might be the

bond  $Z(q)$  ferromagnet, which includes the Potts model as a particular case,  $s = 2$  might be the plaquette  $Z(q)$  ferromagnet and so on). The  $n \rightarrow \infty$  (spherical model) asymptotic behaviour as well as the long range interaction case (see, for instance, [206] as well as [207–210]) have been analytically studied, for arbitrary  $d$ , along similar lines.

The other main flow concerns the real-space techniques. Within these techniques, the renormalization is based upon cells which are *finite* along at least one direction, their (linear) size being characterized by  $b$  (in units of the crystalline parameter). The expectation is that the lattice under study can be recovered in the  $b \rightarrow \infty$  limit. The RG recursive relations are established by renormalizing a  $b$ -sized cell into a  $b'$ -sized cell, with  $b' < b$ . The  $b \rightarrow \infty$  extrapolations are typically done with constant  $b'$  or with constant  $b - b'$  (the latter is a procedure which normally presents faster convergence towards the infinite lattice result, as illustrated in [211–213] and Appendix). These techniques are capable of predicting *both* phase diagrams and critical exponents (and even full equations of states and similar thermodynamical functions), the treatment of the small sizes (both  $b$  and  $b'$  comparable to unity) being in general quite simple from the operational stand-point. However the results are in most cases only *approximate*; to achieve precision,  $b \rightarrow \infty$  extrapolations (not always operationally simple) are quite often unavoidable. Furthermore, the estimation of errors is typically quite less controlled than in the reciprocal-space techniques, as the results for finites  $b$  and  $b'$  might strongly depend on the shapes and symmetries chosen for the cells, as well as on the variables retained for the construction of the RG parameter space. For the real-space techniques, much more than for the reciprocal-space ones, applies Wilson’s remark [214] “that achieving a reduction to subproblems of manageable size is a challenge and an art”. To the illustration of *this challenge and this art* we devote the present Section.

Within the statistical equilibrium static properties of a system, two classes can be distinguished, namely *phase diagrams* and *state functions*. A phase diagram is represented in the space of the *external parameters* of the problem (temperature, concentrations, coupling constants, electric and magnetic fields, stress), and appears as a partition of the physically accessible parameter-space into two or more regions corresponding to the equilibrium phases of the system, these regions are separated by *critical frontiers* (e.g., critical

point, line or surface in a one, two-or three-dimensional parameter-space). Within the recursive  $RG$  framework the regions appear as attractive basins, each of which being associated with an *attractor*, typically a fixed point (named *trivial fixed* point), but whose nature might be more complex (see, for instance, [215, 216]); the critical frontiers separating these regions appear as lower dimensionality attractive basins which present at least one unstable direction (in the full parameter-space), and are associated with semi-stable attractors, typically (but not necessarily) fixed points (named *critical* fixed points, each of which determines the universality class of its attractive basin). A critical frontier might present more than one attractive basin, in turn separated by *multicritical frontiers* (even lower dimensionality and more unstable regions); critical frontiers are commonly singular on their multicritical regions, the singularities being characterized by *crossover* critical exponents and amplitudes. Typical phase diagrams and their  $RG$  flows are illustrated on Fig. 24. A state function  $X$  is a statistical equilibrium quantity defined in the parameter-space  $\{Y_r\}$  described above; examples of state functions are the free and internal energies, specific heat, equation of states, susceptibility, surface tension and correlation length. The equation of state contains an important particular case, namely the behaviour of the *spontaneous order parameter*, i.e., the dependence, on its relevant parameters, of the order parameter at vanishing value of its thermodynamically conjugate parameter (e.g., the thermal behaviour of the magnetization at vanishing external magnetic field for a standard ferromagnet). The state functions are *singular* ( $X$  non analytic in  $\{Y_r\}$ ) on the critical frontier, where they typically (but not necessarily) vanish or diverge. The singularity is commonly characterized by its critical exponents and amplitudes as follows:

$$X - X_c \sim \sum_r A_r (Y_r - Y_r^c)^{\alpha_r} \quad (Y_r \rightarrow Y_r^c, \forall r) \quad (255)$$

where  $\{Y_r^c\}$  is a critical point (e.g.,  $M \sim A_M (T_c - T)^\beta$  in the  $T \rightarrow T_c - 0$  limit, and  $\chi \sim A_\chi^\pm |T - T_c|^{-\gamma}$  and  $\xi \sim A_\xi^\pm |T - T_c|^{-\nu}$  in the  $T \rightarrow T_c \pm 0$  limits, for a standard ferromagnet). Within the attractive basin of a critical fixed point,  $\{\alpha_r\}$  do not vary with  $\{Y_r^c\}$  but  $\{A_r\}$  (as well as  $X_c$ ) in general do.

The  $RG$  formalism is essentially based on the fractal structure [217, 218] normally exhibited by the system at its critical frontiers. Consequently, what is commonly done

is to establish a recursive relation which transforms the parameter-space  $\{Y_r\}$  into itself. The  $RG$  flow enables then the determination of the phase diagram (numerically most of the time, but also analytically occasionally), as well as of some critical exponents (typically the correlation length, magnetic field and crossover critical exponents noted  $\nu$ ,  $y_H$  and  $\phi$  respectively) through the linearization of the recursive relation in the neighbourhood of the various semi-stable or fully unstable fixed points. The rest of the critical exponents  $\{\alpha_r\}$  can be determined through scaling and hyperscaling relations (e.g.,  $\alpha + 2\beta + \gamma = 2$ ,  $\gamma = \nu(2 - \eta)$ ,  $2 - \alpha = d\nu$ , etc). However if to the  $\{Y_r\}$   $RG$  equations we add recursive relations for one or more state functions  $(X_1, X_2, \dots)$ , we can *directly* obtain not only the  $\{\alpha_r\}$  but also the  $\{A_r\}$  and  $(X_{1c}, X_{2c}, \dots)$ . Furthermore, if the recurrence scheme for the  $X$ -variables is conveniently constructed, we can obtain their dependence on  $\{Y_r\}$  *for the entire parameter-space*, and not only in the neighbourhood of the critical frontiers (where the fractal structure strictly holds). The results can be quite good approximations, which can be systematically improved. This is not so surprising if one takes into account that very frequently the critical phenomenon, whenever it exists, is of such importance that its effects remain heavy even far away from the critical point (e.g., for  $T \gg T_c$  or  $T \ll T_c$  for thermal phase transitions): this fact can be verified in a variety of theoretical and experimental situations [219–222]. The first treatment of a state function of a Hamiltonian system, for the entire parameter-space, is due to Niemeijer and van Leeuwen [223]. Since then, several alternative procedures (either more direct, or enabling the calculation of subextensive quantities such as the surface tension, or devised for non Hamiltonian systems such as the geometrical ones) have been proposed [224–228], [134].

We discuss the phase diagram (and associated critical exponents) and the state function problems in Section 4.1 and 4.2 respectively; finally, we treat in Section 4.3 the phase diagram problem associated with complex systems, namely those presenting interfaces.

## 4.1 Phase diagram and critical exponents

This subsection might, in some sense, be considered as the central part of the present review as it is here where we apply the exact cluster calculations presented in Section 3 to treat, with  $RG$  techniques, various pure and random Potts-like models. In 4.1.1 we

exhibit in detail how to construct the  $RG$  recurrence in the parameter-space by preserving appropriate correlation functions; in 4.1.2 we summarize similar procedures (the phenomenological, Monte Carlo and mean field  $RG$ 's) which have been applied with success to several problems; finally in 4.1.3 we compare the correlation function preserving and the phenomenological  $RG$ 's.

### 4.1.1 Correlation function preserving RG

#### $q$ -state isotropic Potts ferromagnet on the square lattice

Let us consider the  $q$ -state isotropic Potts ferromagnet on the square lattice described by the dimensionless Hamiltonian (a particular case of eq. (1))

$$-\beta\mathcal{H} = qK \sum_{\langle i,j \rangle} \delta_{\sigma_i, \sigma_j} + \text{constant} \quad (\sigma_i = 1, 2, \dots, q, \forall i) \quad (256)$$

where  $\langle i, j \rangle$  runs over all pairs of first-neighbouring sites of a square lattice and  $K > 0$ . We recall that the corresponding thermal transmissivity associated to each bond is given by

$$t \equiv \frac{1 - e^{-qK}}{1 + (q - 1)e^{-qK}} \quad t \in [0, 1] \quad (257)$$

We choose, for instance, a two-rooted graph  $G_b$  with roots 1 and 2 (we could similarly choose three – or higher-rooted graphs) whose *chemical length* (number of bonds of the shortest path between the roots) is  $b$ , and a smaller two-rooted graph  $G'$  (also noted  $G_{b'}$ ) whose chemical length is  $b' < b$ . We then renormalize one into the other by imposing

$$\text{Tr}_{3,4,\dots,N'_s} e^{-\beta\mathcal{H}_{G'}(K')} = \text{Tr}_{3,4,\dots,N_s} e^{-\beta\mathcal{H}_{G_b}(K)} \quad (258)$$

which implies that the equivalent transmissivity  $T_{12}(t, G_b)$  of the graph  $G_b$  equals the equivalent transmissivity  $T_{12}(t', G_{b'})$  of the graph  $G'$ , hence the two-body correlation function  $\Gamma_{12}$  (see definition 101) between the roots is preserved [139]. In other words, Eq. (258) implies that

$$T_{12}(t', G_{b'}) = T_{12}(t, G_b) \quad (259)$$

Any reasonable choice of the graphs  $G_b$  and  $G'$  will admit  $t = 0$  and  $t = 1$  as trivial (stable) fixed points characterizing the paramagnetic ( $P$ ) and ferromagnetic ( $F$ ) phases

respectively; in between, another fixed point, critical (unstable) this time, will exist at  $t = t' = t_{bb'}^*$ , which will be an approximation of the critical point  $t_c$  we are looking for. The expectation is that

$$t_c^{exact} = \lim_{\substack{b \rightarrow \infty \\ b' < b}} t_{bb'}^* \quad (260)$$

The calculation of the correlation length critical exponent  $\nu$  proceeds as follows. Linearization of Eq. (259) at  $t_{bb'}^*$  yields

$$\left. \frac{dT_{12}(t', G_{b'})}{dt'} \right|_{t_{bb'}^*} (t' - t_{bb'}^*) \sim \left. \frac{dT_{12}(t, G_b)}{dt} \right|_{t_{bb'}^*} (t - t_{bb'}^*) \quad (261)$$

On the other hand, the original and renormalized correlation lengths ( $\xi$  and  $\xi'$  respectively) are approximately given by

$$\xi \sim \frac{A^\pm}{|t - t_{bb'}^*|^{\nu_{bb'}}} \quad (t \rightarrow t_{bb'}^* \pm 0) \quad (262.a)$$

and

$$\xi' \sim \frac{A^\pm}{|t' - t_{bb'}^*|^{\nu_{bb'}}} \quad (t' \rightarrow t_{bb'}^* \pm 0) \quad (262.b)$$

hence

$$\frac{\xi}{\xi'} \sim \left| \frac{t' - t_{bb'}^*}{t - t_{bb'}^*} \right|^{\nu_{bb'}} \sim \left| \frac{dT_{12}(t, G_b)/dt}{dT_{12}(t, G_{b'})/dt} \right|_{t_{bb'}^*}^{\nu_{bb'}} \quad (263)$$

where we have used Eq. (261). Finally, if we take into account that  $\xi/\xi' = b/b'$  we obtain that

$$\left| \frac{dT_{12}(t, G_b)/dt}{dT_{12}(t, G_{b'})/dt} \right|_{t_{bb'}^*}^{\nu_{bb'}} = \frac{b}{b'} \quad (264)$$

hence

$$\nu_{bb'} = \frac{\ln(b/b')}{\ln \left| \frac{dT_{12}(t, G_b)/dt}{dT_{12}(t, G_{b'})/dt} \right|_{t_{bb'}^*}} \quad (265)$$

which is an approximation of the critical exponent we are looking for. The expectation is that

$$\nu^{exact} = \lim_{\substack{b \rightarrow \infty \\ b' < b}} \nu_{bb'} \quad (266)$$

To treat the square lattice we can consider the family of two-rooted graphs presented in Table III. The expectation (over which we will come back later on) is that the square lattice is obtained at the right-lower corner of this table ( $b \rightarrow \infty, N \rightarrow \infty$ ). In the phenomenological *RG* approach (section 4.1.2) the expectation is to achieve that limit through strips ( $b \rightarrow$

$\infty$ ,  $N$  finite). In the present approach we shall work along the  $b = N$  diagonal because its graphs are self-dual and therefore very adapted to the square lattice, self-dual itself. This choice yields, *for all  $b$  and  $b' < b$* , the *exact* critical point, i.e.,  $t_{bb'}^* = t_c = 1/(\sqrt{q} + 1)$ .

One can easily prove this as follows. Consider eq. (259) evaluated at the fixed point  $t = t' = t_{bb'}^*$ , namely

$$T_{12}(t_{bb'}^*, G_{b'}) = T_{12}(t_{bb'}^*, G_b) \quad (267)$$

Applying the duality transformation to both sides *in the case of self-dual graphs* (i.e.,  $G_b^D = G_b$  and  $G_{b'} = G_{b'}^D$ ) and using eq. (131) one obtains that:

$$T_{12}(t_{bb'}^{*D}, G_{b'}) = \frac{1 - T_{12}(t_{bb'}^*, G_b)}{1 + (q - 1)T_{12}(t_{bb'}^*, G_b)} \quad (268)$$

Suposing that there is only one phase transition (and hence  $t_{bb'}^* = t_{bb'}^{*D}$ ), eq. (268) evaluated at the critical point  $t_c$  together with eq. (267) leads to:

$$T_{12}(t_c, G_{b'}) = \frac{1 - T_{12}(t_c, G_{b'})}{1 + (q - 1)T_{12}(t_c, G_{b'})} \quad (269)$$

from which it follows that  $T_{12}(t_c, G_{b'}) = 1/(\sqrt{q} + 1)$ , and in particular for  $b' = 1$  corresponding to a single bond one gets that  $t_c = 1/(\sqrt{q} + 1)$  which coincides with the exact critical point of the Potts model on the square lattice.

The equivalent transmissivities between the roots have been calculated through the (computer-implemented) *BCM*, and are given by

$$T_{12}(t, G_b) = \frac{\sum_{i=b}^{b^2+(b-1)^2} n_i(q)t^i}{1 + \sum_{i=3} d_i(q)t^i} \quad (b = 1, 2, \dots) \quad (270)$$

where the  $\{n_i(q), d_i(q)\}$  are given in Table IV.

The correlation length critical exponent is given by

$$\nu_{bb'} = \frac{\ln(b/b')}{\ln(\lambda_b/\lambda_{b'})} \quad (271)$$

where  $\lambda_b \equiv [dT_{12}(t, G_b)/dt]_{t=1/(\sqrt{q}+1)}$  can be expressed as follows:

$$\lambda_b = \frac{\sum_{i=0}^{\ell_b} a_i q^{i/2}}{\sum_{i=0} m_b b_i q^{i/2}} \quad (272)$$

where  $\ell_b(m_b)$  is the maximum value of the integer  $i$  which appears in the numerator (denominator) of  $\lambda_b$  such that  $a_i$  is non-null;  $\{a_i, b_i\}$  are given in Table V (see [107]). The various approximations for  $\nu(q)$  are presented in Fig. 25 and compared to the exact result [91]. We also present, in Table VI, the numerical results corresponding to  $q = 1, 2, 3$  and 4, as well as the  $q \rightarrow 0$  and  $q \rightarrow \infty$  asymptotic behaviours.

We remark in Fig. 25 that nothing happens in the neighbourhood of  $q = 4$  which could indicate a tendency of the transition to become a first-order one above  $q = 4$ . This is in great contrast with the *exact*  $q$ -dependence of  $\nu$  (see Fig. 25), and can be considered as a very strong suspicion that expectation of Eq. (266) is not verified *for all values of  $q$* . However, our calculations are *exact* for the two-rooted graphs we have been considering: what is it wrong? What happens is that we have implicitly replaced our *Bravais* square-lattice (translationally invariant) by a family of *hierarchical* lattices (scale invariant). For instance, our  $(b, b') = (2, 1)$  *RG* approach is *exact* [64–66] for the hierarchical lattice indicated in Fig. 26, whose intrinsic fractal dimensionality  $d_f = \ln N_b / \ln b$  ( $N_b \equiv$  aggregation number  $\equiv$  number of bonds; see [128, 229]) is given by  $d_f = \ln 5 / \ln 2 \simeq 2.32$  (whereas the dimensionality of our Bravais lattice is  $d = 2$ ). Our result for  $\nu(q)$  implies that, for the hierarchical lattice, the transitions are of the second order for all values of  $q$ . This is a good illustration of the kind of limitation that might appear in real-space techniques. We shall verify (in Section (4.1.2)) the same limitation in the phenomenological *RG*. As a matter of fact, as far as we know, only very recently appeared [230] a real space *RG* (the finite size scaling *RG*), for the *pure* Potts ferromagnet, which recovers the first-order transitions for  $q$  high enough (see [231] for a *RG* approach where this fact can be recovered if a model *larger* than the pure Potts ferromagnet is assumed).

Before closing the discussion of this model (which can be treated along similar lines for cubic and hypercubic lattices [227]) it is worth mentioning (without proof) two interesting properties of hierarchical lattices:

(i) Hyperscaling hopefully holds as follows [229] (at least for the Potts ferromagnet):

$$2 - \alpha = d_f \nu \tag{273}$$

where  $\alpha$  is the specific heat critical exponent [66, 232] and  $d_f \equiv \ln N_b / \ln b$ ,  $N_b$



being the number of bonds ( $N_b = (d - 1)b^{d-2}(b - 1)^2 + b^d$  for the  $d$ -dimensional hypercubic-like hierarchical lattices generated by the two-rooted graphs indicated in Fig. 11; notice that  $\lim_{b \rightarrow \infty} d_f = d$ ). Some arguments which are consistent with Eq. (273) can be found in Refs. [128],[233–236]. Eq. (273) has been numerically verified for the Potts ferromagnet on the  $d = b = 2$  Wheatstone bridge hierarchical lattice (for  $q = 2$  see [229], for a general value of  $q$  see [237]), on diamond-type (Fig. 12f), in the left, contains the simplest one) hierarchical lattices ( $q = 2$  [238], for any  $q$  [237]) and on Sierpinski Gasket-type three-rooted hierarchical lattices ( $q = 2$  [239]). Furthermore, it has been proved analytically [152] for the three-state antiferromagnetic Potts model on a diamond-type hierarchical lattice family.

- (ii) For the Potts ferromagnet on Wheatstone-bridge-like hierarchical lattices we can verify (see note added in Ref. [229]) that

$$\lim_{q \rightarrow \infty} \nu(q) = \frac{1}{d_f} \quad (274)$$

which implies, through Eq. (273),  $\lim_{q \rightarrow \infty} \alpha(q) = 1$  (thermodynamical upper limit). This property is illustrated in all the examples of the type  $\nu_{b1}$  appearing in Table VI. It is however violated for other types of hierarchical lattices (see, for instance, Table VII): the full comprehension of this point is presently missing.

*q-state anisotropic Potts ferromagnet on the square-lattice:*

In this case, the dimensionless Hamiltonian is given by

$$-\beta\mathcal{H} = q \sum_{\langle i,j \rangle} K_{ij} \delta_{\sigma_i, \sigma_j} \quad (\sigma_i = 1, 2, \dots, q, \forall i) \quad (275)$$

where  $K_{ij}$  equals  $K_x(K_y)$  if  $\langle i, j \rangle$  are first-neighbour sites along the  $x$ -axis ( $y$ -axis) of a square lattice, and vanishes otherwise;  $K_x, K_y \geq 0$ . This problem generalizes that presented in Eq.(256); it also contains, as a particular case, the  $d = 1$  case.

To treat this problem, it should be convenient to work with a family of graphs satisfying (i) the *self-duality* of the square lattice (to ensure the exactness of the critical line), and (ii) the *one-dimensional topology* of the linear chain in the special cases  $K_x = 0$  or  $K_y = 0$  (to ensure the correct  $d = 1 \leftrightarrow d = 2$  crossover). Such family does exist (see Fig. 27): it

has been introduced for the isotropic bond percolation in Ref. [240], then extended to the anisotropic bond percolation in Ref. [241] (where it was first noticed that it conveniently reproduces the  $d = 1$  limit), and finally generalized [136] to the anisotropic Potts model. It is this last work the one we follow here. We shall work with transmissivities  $t_x$  and  $t_y$  (respectively related to  $K_x$  and  $K_y$ ). We note  $T_{12}(t_x, t_y, G_b)$  the equivalent transmissivity between the roots 1 and 2 associated with the  $b$ -sized graph of the family indicated in Fig. 27. Then the  $RG_{bb'}$  is constructed through:

$$T_{12}(t'_x, t'_y, G_{b'}) = T_{12}(t_x, t_y, G_b) \quad (276.a)$$

$$T_{12}(t'_y, t'_x, G_{b'}) = T_{12}(t_y, t_x, G_b) \quad (276.b)$$

with  $b = 3, 5, 7, \dots$  and  $b' = 1, 3, \dots, b - 2$ , and where we have used the  $t_x \rightleftharpoons t_y$  invariance of the lattice. The expression of  $T_{12}(t_x, t_y, G_3)$  can be found in eq. (12) of ref. [136]. The  $RG$  flow for all  $(b, b')$  is indicated in Fig. 28, and yields the *exact* critical line  $t_x = (1 - t_y)/[1 + (q - 1)t_y]$  for all  $q$ . The  $RG$  flow is consistent with universality, in the sense that the *anisotropic* Potts ferromagnet on the square-lattice has the same set of critical exponents of the *isotropic* case, presenting a crossover phenomenon at the  $d = 1$  limit  $((t_x, t_y) = (1, 0)$  or  $(0, 1))$ .

The  $\nu$  exponent for the anisotropic case is given by

$$\nu_{bb'} = \frac{\ln(b/b')}{\ln(\lambda_b/\lambda_{b'})} \quad (277)$$

with

$$\lambda_b \equiv \left. \frac{dT_{12}(t, t, G_b)}{dt} \right|_{t=1/(\sqrt{q}+1)} \quad (278)$$

where we have implicitly used the fact that  $t_x = t_y$  is an invariant subspace of the present  $RG$  (i.e.,  $t_x = t_y$  implies  $t'_x = t'_y$ ). The results are presented in Fig. 4 and Table VII.

In the  $d = 1$  limit, say  $t_y = 0$ , Eqs. (276.a) and (276.b) respectively become  $(t'_x)^{b'} = (t_x)^b$  and  $0 = 0$ , hence

$$\nu_{bb'} = \frac{\ln(b/b')}{\ln\left(\frac{dt'_x}{dt_x}\right)_{t_x=1}} = \frac{\ln(b/b')}{\ln(b/b')} = 1 \quad (279)$$

which is the *exact* result.

Before closing the discussion of the present model, let us mention that:

- i) The  $RG_{b1}$  results are exact for the corresponding hierarchical lattice (the  $RG_{31}$  case is illustrated in Fig. 29 for  $t_y \neq t_x$ ). The intrinsic fractal dimensionality of these lattices is given, for  $t_x = t_y$ , by  $d_f = 2, \forall b$ .
- ii) The present  $RG$  framework uses graphs with *odd* value for  $b$  and  $b'$ , and can therefore describe antiferromagnetic situations (negative  $K_x$  and/or  $K_y$ ) considerably well. In particular, for the  $q = 2$  model, it *exactly* preserves the square-lattice equivalence between the  $K_x > 0$  and  $K_y > 0$  ferromagnet and the  $K_x < 0$  and  $K_y < 0$  antiferromagnet (for instance, it is perfectly consistent with the  $T = 0$  fully antiferromagnetic order associated with the  $K_x < 0$  and  $K_y < 0$  model). For arbitrary values of  $q$ , see refs [3, 4, 101] for further information.

*q-state anisotropic Potts ferromagnet on the simple cubic lattice*

The dimensionless Hamiltonian is given by Eq. (275), where  $K_{ij}$  equals now  $K_x, K_y$  or  $K_z$  if  $\langle i, j \rangle$  are first-neighbour sites along the  $x$ -,  $y$ - or  $z$ -axis of a simple cubic lattice, and vanishes otherwise;  $K_x, K_y, K_z \geq 0$ . This problem generalizes the anisotropic square-lattice Potts model just discussed. It is therefore convenient to use graphs which themselves generalize those used for the  $d = 2$  case. This generalization has been achieved in Ref. [104] which we now follow.

We only consider the  $RG_{31}$  framework, the corresponding  $b = 3$  graph being indicated in Fig. 30; its equivalent transmissivity will be noted  $T_{12}(t_x, t_y, t_z, G_3)$  (its numerator and denominator are polynomials with thousands of terms, which have been calculated through computer implementation of the BCM). The  $RG_{31}$  relations are the following ones:

$$t'_x = T_{12}(t_x, t_y, t_z, G_3) \tag{280.a}$$

$$t'_y = T_{12}(t_y, t_z, t_x, G_3) \tag{280.b}$$

$$t'_z = T_{12}(t_z, t_x, t_y, G_3) \tag{280.c}$$

These equations reproduces Eqs. (276) for  $t_z = 0$  (or equivalently  $t_y = 0$ , or  $t_x = 0$ ). Before presenting the results, let us define a convenient variable  $s_\alpha^{(d)}$  introduced in ref. [93] which extends the  $s$ -variable defined for plane graphs in eq. (134) to  $d$ -dimensional

lattices, namely:

$$s_\alpha^{(d)} \equiv s^{(d)}(t_\alpha) \equiv \frac{\ln[1 + (q-1)h(d)t_\alpha]}{\ln[1 + (q-1)h(d)]} \in [0, 1] \quad (\alpha = x, y, z) \quad (281)$$

where the dimensionless number  $h(d)$  depends sensibly on  $d$  and very slightly on the particular  $d$ -dimensional lattice;  $h(2) = 1$  for the square lattice and  $h(3) = 0.377 \pm 0.044$  for the simple cubic lattice [93].

The results for the critical surface are indicated in Figs. 31 and 32 as well as in Table VIII. The table includes the direct  $RG$  results as well as high precision extrapolated ones (the extrapolation method consists essentially in “pushing” the  $RG$  value of the point for the *isotropic* simple cubic lattice Potts model up to the best available value for that particular value of  $q$ ); the quality of the extrapolation can be checked on Fig. 33 where, whenever possible, comparison with other high precision methods is done.

The calculation of the eigenvalues of the Jacobian associated with Eqs. (280) (evaluated on the relevant fixed points) provides various critical exponents. The  $d = 1$  fixed point (e.g.,  $(s_x, s_y, s_z) = (1, 0, 0)$ , where we use for convenience the  $s$ -variable defined in Eq. (134)) yields  $\phi_{12} = \phi_{13} = 1$  ( $\phi_{12}$  and  $\phi_{13}$  are respectively the  $d = 1 \leftrightarrow d = 2$  and  $d = 1 \leftrightarrow d = 3$  crossover exponents), which are the exact results. The  $d = 2$  fixed point (e.g.,  $(s_x^{(2)}, s_y^{(2)}, s_z^{(2)}) = (1/2, 1/2, 0)$ ) yields, besides the previously presented  $d = 2$  value for  $\nu$ , the  $d = 2 \leftrightarrow d = 3$  crossover  $\phi_{23}$  (see Fig. 34b). The  $d = 3$  fixed point  $P_I(s_x, s_y, s_z) = (s_c^{(3)}, s_c^{(3)}, s_c^{(3)})$ , where  $s_c^{(3)}$  is the critical point, expressed in the variable defined in eq. (134), corresponding to a given value of  $q$ , yields the  $d = 3$  critical exponent  $\nu_3 = \ln 3 / \ln \lambda$  ( $\lambda \equiv$  eigenvalue along the  $(1, 1, 1)$  axis): see Fig. 34a.

### Isotropic quenched bond-mixed $q$ -state Potts ferromagnet on the square-lattice

In this case, the dimensionless Hamiltonian is given by eq. (275) where the pair coupling constants  $K_{ij}$  has the following probability distribution:

$$P(K_{ij}) = (1 - p)\delta(K_{ij} - K_1) + p\delta(K_{ij} - K_2) \quad (282)$$

where  $K_1, K_2 \geq 0$ ,  $0 \leq p \leq 1$  and  $\langle i, j \rangle$  run over all pairs of first-neighbour sites on a square-lattice. Eq. (282) can be rewritten in terms of transmissivities as follows:

$$P(t) = (1 - p)\delta(t - t_1) + p\delta(t - t_2) \quad (283)$$

with  $0 \leq t_1, t_2 \leq 1$ .

Particular cases of the present problem (e.g.,  $q = 2$ , *diluted* model, i.e.,  $K_1 = 0$ ) have been treated [242, 157, 159, 160, 135, 243] on their own right. We present here the quite general approach followed in Ref. [107], in which the  $b = 2$  Wheatstone-bridge (Fig. 11(b)) graph is renormalized into a single edge. The transmissivity  $T_{12}(\{r_i\}, G)$  of this graph  $G$  for arbitrary elementary transmissivities  $r_1, r_2, \dots, r_5$  (see Fig. 35) is given [135, 107] by eq. (151). This expression deserves a quick comment before going on: if we take  $r_1 = r_4 = t_x t_y$ ,  $r_2 = r_3 = [t_x + t_y + (q-2)t_x t_y]/[1 + (q-1)t_x t_y]$  and  $r_5 = t_x$ , Eq. (151) reproduces  $T_{12}(t_x, t_y, G_3)$  of Eq. (276a).

Let us continue now. If we associate the 2 delta distributions (283) with each one of the 5 edges of the graph, we obtain the distribution  $P_G(t_1, t_2)$  given by

$$P_G(t_1, t_2) = \sum_{r_1=t_1, t_2} \sum_{r_2=t_1, t_2} \dots \sum_{r_5=t_1, t_2} (1-p)^m p^{5-m} \delta[t - T_{12}(\{r_i\}, G)] \quad (284)$$

where  $m$  equals the number of bonds with transmissivity  $t_1$  which appears in a particular configuration of  $\{r_i\}$  (among the  $2^5$  possible ones) we are considering.  $P_G$  has  $2^5 = 32$  terms; however, some of them being repeated, it finally comes out to be a 14 delta distribution whose explicit form is:

$$P_G(t_1, t_2) = \sum_{\ell=1}^{14} M_\ell (1-p)^{m_\ell} p^{5-m_\ell} \delta(t - t_\ell(t_1, t_2)) \quad (285)$$

where the multiplicity factors  $\{M_\ell\}$ , the exponents  $\{m_\ell\}$  and equivalent transmissivities  $\{t_\ell\}$  are presented in Table I of ref. [107]. If we were to iterate once more, we would obtain a distribution with a number of deltas comparable to  $14^5 = 537824$ . Even followed through computer, the problem quickly becomes untractable. We must therefore make an approximation. Two (at least) different schemes can be followed. The first one (introduced by Young and Stinchcombe [244] for random-resistor problems) consists in replacing the successively renormalized distribution by histograms (with a partition of the interval  $[1, 0]$  for  $t$  in, say, 100 smaller intervals) which are followed through the iterations until they arrive to fixed forms, characterizing the para- and ferro-magnetic phases as well as the critical frontier separating them. The preliminary tests [245] of this procedure for the present problem have been succesful; it has been used [246] to discuss the relevance of randomness, on which we will come back later on.

The second approximative scheme (herein followed) consists in artificially holding the renormalized distribution within its original parameter space. This means, in the present case, a 2 delta distribution  $P'(t)$  given by

$$P'(t) = (1 - p')\delta(t - t'_1) + p'\delta(t - t'_2) \quad (286)$$

where  $(p', t'_1, t'_2)$  are functions of  $(p, t_1, t_2)$  to be determined. A simple and natural way for determining these functions is to impose that the lower momenta (first, second and third momenta in the present case where we have 3 free parameters) of the distribution are preserved. To be more precise, we impose

$$\langle g(t) \rangle_{P'} = \langle g(t) \rangle_{P_G} \quad (287.a)$$

$$\langle [g(t)]^2 \rangle_{P'} = \langle [g(t)]^2 \rangle_{P_G} \quad (287.b)$$

$$\langle [g(t)]^3 \rangle_{P'} = \langle [g(t)]^3 \rangle_{P_G} \quad (287.c)$$

where  $g(t)$  is a function to be chosen quite arbitrarily (thus yielding to different approximations). If  $g(t)$  is conveniently chosen the present scheme can provide high-precision results for the critical surface, while being, on the same foot, computationally much simpler than the first scheme. let us write explicitly Eqs. (287):

$$\begin{aligned} (1 - p')g'_1 + p'g'_2 &= \sum_{r_1=t_1, t_2} \cdots \sum_{r_5=t_1, t_2} (1 - p)^m p^{5-m} g(T_{12}(\{r_i\}, G)) \\ &\equiv F(p, g_1, g_2) \end{aligned} \quad (288.a)$$

$$\begin{aligned} (1 - p')[g'_1]^2 + p'[g'_2]^2 &= \sum_{r_1=t_1, t_2} \cdots \sum_{r_5=t_1, t_2} (1 - p)^m p^{5-m} [g(T_{12}(\{r_i\}, G))]^2 \\ &\equiv G(p, g_1, g_2) \end{aligned} \quad (288.b)$$

$$\begin{aligned} (1 - p')[g'_1]^3 + p'[g'_2]^3 &= \sum_{r_1=t_1, t_2} \cdots \sum_{r_5=t_1, t_2} (1 - p)^m p^{5-m} [g(T_{12}(\{r_i\}, G))]^3 \\ &\equiv H(p, g_1, g_2) \end{aligned} \quad (288.c)$$

where  $g_j \equiv g(t_j) \quad (j = 1, 2)$ .

Note that, for the *pure model* ( $p = 1, \forall t_1$ , or  $p = 0, \forall t_2$ , or  $t_1 = t_2, \forall p$ ) eqs. (288) become one and the same equation, namely

$$t' = T_{12}(t, t, t, t, t, G) \quad (289)$$

where the right hand side of eq. (289) is equal to that of eq. (128), thus conveniently reproducing the  $RG$  recurrence of the pure model. There is another particular case, namely that of *pure percolation* ( $T = 0$ ), in which we would like to recover the corresponding one-parameter case. This can be done by choosing for  $g(t)$  a monotonous function of  $t$  such that  $g(0) = 0$  and  $g(1) = 1$ . Then, the percolation limit (e.g.,  $t_1 = 1$  and  $t_2 = 1$ ) makes Eqs. (288) to become one and the same equation, namely

$$p' = P_{12}(p, G) \quad (290)$$

(where  $P_{12}(p, G)$  is given by eq. (84)), which is the bond percolation  $RG$  recurrence ( $q = 1$  particular case of Eq. (289)).

The solution of Eqs. (288) is given by

$$p' = \frac{L^2}{1 + L^2} \quad (291.a)$$

$$g'_1 = F \pm L\sqrt{K} \quad (291.b)$$

$$g'_2 = F \mp \frac{1}{L} \sqrt{K} \quad (291.c)$$

where

$$K \equiv G - F^2 > 0 \quad (292)$$

and

$$L \equiv \frac{\sqrt{(H - 3FK - F^3)^2 + 4K^3} - (H - 3KF - F^3)}{2K^{3/2}} \quad (293)$$

The upper (lower) signs in Eqs. (291.b) and (291.c) are to be used in the region  $t_1 > t_2$  ( $t_1 < t_2$ ) hence  $J_1 > J_2$  ( $J_1 < J_2$ ). Eqs. (291) are explicit  $RG$  recursive relations, and therefore completely close the operational problem once the function  $g(t)$  is chosen. The simplest choice is  $g(t) = t$ , and already is an extremely satisfactory one (for instance, the estimated error, in the  $t$ -variables, for the critical line of the diluted model is nowhere larger than 0.5%). However, even better results can be obtained with  $g(t) = s(t)$  given by Eq. (134).

The critical surface evolves very slowly with  $q$  if represented in the  $(p, s_1, s_2)$  space (as also happened in ref. [100]); see the  $q = 2$  result in Fig. 36. The present  $RG$  yields the following *exact* results: (i) pure ferromagnet critical point for all  $q$  (Eq. (35)); (ii) pure bond percolation critical point  $p_c = 1/2$  for any  $q$ ; (iii) equal concentration model

( $p = 1/2$ ) critical line for all  $q$  (Eq. (54)); (iv)  $ds/dp$  slope at the  $p_c = 1/2$  limit of the dilute model critical line for all  $q$  easily derivable from Eqs. (53) and (134)); (v) critical surface for  $q = 1$  given by eq. (6) of ref. [107] (i.e., a generalized form of the Kasteleyn and Fortuin theorem [16] is recovered). The  $ds/dp$  slope at the  $p = 1$  limit of the dilute model critical line (whose exact result is derivable from eq. (52)) exhibits an error which increases from 0% to 1.5% while  $q$  varies from  $q = 1$  to  $q = 4$ . For arbitrary points of the (still unknown) critical surface, this  $RG$  yields results whose precision certainly is very high (see Fig. 37 and, for numerical values, Ref. [107]).

The  $RG$  flow presents, for all  $q$ , two equivalent fully unstable fixed points at  $p = 1/2$  ( $(s_1, s_2) = (1, 0)$  and  $(0, 1)$ ) characterizing the *percolation* universality class. The rest of the critical surface belongs to the *pure ferromagnet* universality class if  $q \leq q^*$ , where  $q^*$  is a value which depends on the particular graph under consideration (see Fig. 36 for the  $RG$  flow corresponding to  $q = 2 < q^*$ ). For  $q > q^*$ , a new universality class, namely the *random* one, appears through a pitchfork bifurcation of the  $p = s_1 = s_2 = 1/2$  fixed point which becomes fully unstable while generating two semi-stable fixed points. The two new fixed points are equivalent, remain on the equal concentration critical line ( $p = 1/2$ ), and symmetrically become further and further apart while  $q$  increases above  $q^*$ ; they are located at  $(p, s_1, s_2) = (\frac{1}{2}, s_r, 1 - s_r)$  and  $(\frac{1}{2}, 1 - s_r, s_r)$  (see Fig. 38).

The calculation of the Jacobian  $\partial(p', s'_1, s'_2)/\partial(p, s_1, s_2)$  at the relevant fixed points enables, through its eigenvalues  $\lambda_1, \lambda_2$  and  $\lambda_3$ , the knowledge of various critical exponents. At the pure percolation fixed point one has that  $\lambda_1 = \lambda_2 = \lambda_3 \equiv \lambda_p > 1$  for all values of  $q$ . Consequently, the percolation crossover exponent  $\phi_p = 1$  (*exact* result), and the correlation length critical exponent  $\nu_p = \ln b / \ln \lambda_p$  reproduces the  $q = 1$  values of Table VI. At the  $p = s_1 = s_2 = 1/2$  pure Potts ferromagnet fixed point,  $\lambda_1 \cong 0.5$  for  $q \in [1, 10]$ ;  $\lambda_2 \equiv \lambda_t > 1$  for all  $q$ , consequently  $\nu_t = \ln b / \ln \lambda_t$  (see Fig. 39);  $\lambda_3 \gtrless 1$  if  $q \gtrless q^*$ , consequently we can calculate the pure ferromagnet crossover exponent  $\phi_t = \ln \lambda_3 / \ln \lambda_t$  for  $q \geq q^*$  (see Fig. 40). Finally, at the random fixed point,  $\lambda_1 < 1$  for all  $q > q^*$ ,  $\lambda_2 = 1$  for  $q = q^*$  and decreases for  $q > q^*$ , and  $\lambda_3 \equiv \lambda_r > 1$  for all  $q > q^*$ , which enables the calculation of  $\nu_r = \ln b / \ln \lambda_r$  (see Fig. 39).

Let us now turn our attention into an interesting related problem, namely the Harris



criterion [247], which essentially states that, for a random ferromagnet on a Bravais lattice, randomness is *relevant* (*irrelevant*) in the sense that it determines (does not determine) a new universality class – different from the pure model one – if the pure ferromagnet specific heat critical exponent  $\alpha_t$  is positive (negative). Does this criterion hold for hierarchical lattices? The answer is [248] that *not necessarily*. More explicitly,  $\alpha_t > 0$  implies relevance of the randomness, but relevance of the randomness does not imply  $\alpha_t > 0$ . In what follows we illustrate this point through the quenched bond-random Potts ferromagnet we are interested in. We know [229] that, for an hierarchical lattice,  $2 - \alpha_t(q) = d_f \nu_t(q)$ . We denote by  $q_c$  the value of  $q$  which satisfies  $\alpha_t(q_c) = 0$ , hence

$$\nu_t(q_c) = 2/d_f \tag{294}$$

For the generalized Wheatstone-bridge graphs we are dealing with we obtain  $q_c \simeq 5.911$ , 5.218 and 4.829 for  $b = 2, 3$  and 4 respectively. On the other hand, we recall that  $q^*$  is, by definition, the threshold above which randomness is relevant. The value  $q^*$  satisfies

$$\sum_{i=1}^{N_b} \left[ \frac{\partial T_{12}(t_1, \dots, t_{N_b}, G_b)}{\partial t_i} \right]_{t_1=\dots=t_{N_b}=t_c} = 1 \tag{295}$$

where  $T_{12}(t_1, \dots, t_{N_b}, G_b)$  is the equivalent transmissivity of the graph  $G_b$  (with  $N_b$  bonds) we are working with, and  $t_c$  is the fixed point, i.e.  $t_c = T_{12}(t_c, \dots, t_c, G_b)$ . Eq. (295) follows immediately from condition (7) of Ref. [248]. We obtain  $q^* = 5.3$  and 4.9 for  $b = 2$  and 3 respectively (see Fig. 41). We see that 3 regions can be distinguished, namely  $q < q^*$  ( $\alpha_t < 0$  and randomness is irrelevant),  $q^* < q < q_c$  ( $\alpha_t < 0$  and randomness is relevant) and  $q > q_c$  ( $\alpha_t > 0$  and randomness is relevant). Finally it is worth noting that our binary-approximated *RG* yields the *exact*  $q^*$  as given by Eq. (295) (this is a consequence from the obvious fact that for infinitely small randomness, the error involved in our approximation is infinitely small as well).

### Isotropic Directed bond percolation on the square lattice

We consider a square lattice of *double* opposite-directed bonds, and note  $p(q)$  the independent occupancy probability of the “up”-and “right”-directed (“down”-and “left”-directed) bonds: see Fig. 42. To study its criticality we shall renormalize the graph of

Fig. 17(a) into a single double opposite-directed bond [28]. The RG recursive relations are [28]:

$$p' = P_{12}(p, q, G) \equiv f(p, q) \quad (296.a)$$

and

$$q' = f(q, p) \quad (296.b)$$

where  $P_{12}(p, q, G)$  is given by eq. (195).

The flow diagram is represented in Fig. 43. Four phases are observed, namely the *double-way percolating* ( $P_{+-}$ ), two *single-way percolating* ( $P_+$  and  $P_-$ ) and the *non-percolating* (NP) ones. At  $p = q = 1/2$  we have a multicritical point whose universality class is that of the isotropic bond percolation (with  $\nu = \ln 2 / \ln(13/8) \simeq 1.43$ ); to be more precise, this is correct for all directions *except* along the  $p + q = 1$  direction, for which  $\nu = \ln 2 / \ln(3/2) \simeq 1.71$  (see [28] for further discussion). The rest of the critical lines belong to the universality class of the directed bond percolation (with  $\nu \simeq 1.54$ ); four critical (semi-stable) fixed points are present, namely at  $(p, q) = (p_c, 0), (0, p_c), (1, 1 - p_c)$  and  $(1 - p_c, 1)$  with  $p_c \simeq 0.555$ .

*T = 0 spin-glass on the square lattice:*

We consider a quenched bond-random spin 1/2 Ising model on a square lattice, the probability law for the coupling constant being given by

$$P(J_{ij}) = p\delta(J_{ij} - J) + q\delta(J_{ij} + J) + r\delta(J_{ij}) \quad (297)$$

with  $J > 0$ ,  $0 \leq p, q, r \leq 1$  and  $p + q + r = 1$ . We want to study, through RG, its (still unknown, to the best of our knowledge) phase diagram at vanishing temperature.

It is intuitive that this parameter space (characterized by  $(p, q, r)$ ) is not invariant under renormalization: for instance, the point  $p = q = 1/2$  (hence  $r = 0$ ) clearly will introduce frustration. *This frustration is essentially different from dilution*, and therefore it cannot be taken into account just by allowing for  $r = 1 - p - q \neq 0$ : the renormalization of most points of the  $p + q + r = 1$  space will produce  $p + q + r < 1$ . We shall then work in a larger space, by phenomenologically introducing a *frustration variable*  $\phi$ , allowed to take the values  $\phi = 1$  (fully frustrated bond) and  $\phi = 0$  (non frustrated bond). The

probability law (297) will consistently be enlarged into the following one:

$$\begin{aligned}
 P(J_{ij}, \phi_{ij}) &= p\delta(J_{ij} - J)\delta(\phi_{ij}) + q\delta(J_{ij} + J)\delta(\phi_{ij}) \\
 &+ r\delta(J_{ij})\delta(\phi_{ij}) + s\delta(J_{ij})\delta(\phi_{ij} - 1)
 \end{aligned}
 \tag{298}$$

with  $0 \leq p, q, r, s \leq 1$  and  $p + q + r + s = 1$ . Our final aim is the  $s = 0$  model: it just happens that it is not a RG invariant subspace.

We shall adopt the composition laws described in subsection 3.3.3, and choose the graph of Fig. 19 to be renormalized into a single bond (characterized by  $(p', q', r', s')$ ). This choice, besides its convenient respect of self-duality, exactly preserves the well known isomorphism between pure ferromagnetic and pure antiferromagnetic spin 1/2 Ising model on the square lattice (this isomorphism is violated by the  $b = 2$  Wheatstone bridge graph, as can be immediately seen from a ground state analysis; e.g., see the all-ferromagnetic and the all-antiferromagnetic configurations of Table II). The RG recursive relations are those of Eqs. (209). We present the results [195] on Fig. 44 ( $r = 0$  invariant subspace), Fig. 45 (full  $(p, q, r)$  space) and Fig. 46 ( $s = 0$  cut of Fig. 45, i.e., the  $p + q + r = 1$  plane, non-invariant subspace). The RG presents four trivial (fully stable) fixed points, namely at  $p = 1, q = 1, r = 1$  and  $s = 1$ , (the remaining components being zero in all the 4 points) respectively characterizing the ferromagnetic (F), antiferromagnetic (AF), paramagnetic (P) and spin-glass (SG) phases. In addition to the pure percolation and pure Ising model universality classes, we observe a new one associated with the critical (semi-stable) fixed point on the F-SG frontier (or equivalently on the AF-SG frontier). Finally, we obtain  $p_c \simeq 0.93$  (defined on Figs. 44-46), which compare well with the results yielded by other methods [249, 250].

The present approach could possibly be improved or generalized (to *finite* temperature, for instance) by allowing  $\phi$  to take values between 0 and 1 as well. For example, the rules (208) could be replaced, in the  $E^F = F^{AF}$  case, by less rigid ones, in the sense that  $\phi$  could be a continuous function of  $g^F$  and  $g^{AF}$  such that  $\phi = 1$  if  $g^F = g^{AF}$  and  $\phi \simeq 0$  if  $g^F \gg g^A$  or  $g^F \ll g^{AF}$  (e.g.,  $\phi = 1 - |g^F - g^{AF}|/(g^F + g^{AF})$ , or similar ones). Such attempts, if successful, could enlighten the present view of d-dimensional spin-glass systems.

Isotropic  $Z(4)$  ferromagnet on the square lattice

Let us consider the  $Z(4)$  model with first neighbour interactions on a square lattice. The pair Hamiltonian is given by eq. (67) where  $J_1 \geq 0$  and  $J_1 + 2J_2 \geq 0$  (ferromagnetic case). We shall work with the convenient variables  $t_1$  and  $t_2$  ( $t_\alpha \in [0, 1]$ ;  $\alpha = 1, 2$ ) defined in eqs. (224).

This problem has some interesting particular cases, namely, the 4-state Potts ferromagnet ( $t_1 = t_2$ ) and three equivalent versions of the spin 1/2 Ising ferromagnet ( $t_2 = t_1^2$ ;  $t_1 = 0$  and  $t_2 = 1$ ). We shall treat it within a RG where the  $b = 2$  Wheatstone-bridge graph is renormalized into a single bond [121]. The RG recursive relations are quickly obtained from Eqs. (237) by considering that all five transmissivities are one and the same. Hence

$$t'_1 = \frac{2(1 + t_2^2)t_1^2 + 2(1 + t_2)^2t_1^3 + 4t_1^2t_2^2}{1 + t_2^4 + 2t_1^4 + 4(1 + t_2^2)t_1^3 + 2t_2(t_2^2 + t_1^4)} \quad (299.a)$$

and

$$t'_2 = \frac{2(t_2^2 + t_1^4) + 8t_1^3t_2 + 2t_2(t_2^2 + t_1^4)}{1 + t_2^4 + 2t_1^4 + 4(1 + t_2^2)t_1^3 + 2t_2(t_2^2 + t_1^4)} \quad (299.b)$$

The corresponding phase diagram is presented in Fig. 10 (in both  $t_2$  vs.  $t_1$  and  $k_B T/J_1$  vs.  $(J_1 + 2J_2)/J_1$  representations). Three phases are observed, namely the *paramagnetic* ( $P$ ;  $Z(4)$  symmetry), the *intermediate* ( $I$ ;  $Z(2)$  symmetry) and the *ferromagnetic* ( $F$ ; fully broken symmetry) ones. The Potts ( $\tilde{P}$ ) as well as the three equivalent Ising critical points  $I_\alpha$  ( $\alpha = 1, 2, 3$ ) are exactly located; the same happens with the  $P - F$  critical line (which coincides with eq. (68)). The  $P - I$  critical line (and its dual, the  $F - I$  critical line) is yet unknown: the present RG approximation could well be an excellent approximation. The main asymptotic behaviours in the neighborhood of the respective  $T_2$ ,  $I_3$  and  $\tilde{p}$  points are the following ones:

$$t_2 \sim (\sqrt{2} - 1) - ct_1^3 \quad [(c = 2(3\sqrt{2} - 2)/7 \simeq 0.64)] \quad (300)$$

$$t_2 \sim 1 - d[(\sqrt{2} - 1) - t_1] - e[(\sqrt{2} - 1) - t_1]^3 \quad (301)$$

$$[d = 2/(\sqrt{2} - 1) \simeq 4.83 \quad ; \quad e = c/\sqrt{2} (\sqrt{2} - 1)^4 \simeq 15.4]$$

and

$$t_2 \sim 1 - 2t_1 \pm f(1/3 - t_1)^\phi \quad (302)$$

$$[f \simeq 982; \phi = \ln(27/13)/\ln(17/13) \simeq 2.7245]$$

With respect to the  $t_1^3$  correction in Eq. (300), Zittartz [251] argues it should be, *for the square lattice*, a  $t_1^4$  one. With respect to the thermal critical exponent  $\nu$ , the results are as follows: (i) at all three Ising points  $\nu = \ln 2 / \ln(2\sqrt{2} - 1) \simeq 1.149$  [ $\nu$  (exact) = 1]; (ii) at the Potts point,  $\nu = \ln 2 / \ln(27/13) \simeq 0.948$  [ $\nu$  (exact) = 2/3]; (iii) the  $I - F$  and  $I - P$  lines belong to the Ising universality class as expected; (iv) the  $P - F$  line belongs to the Ising universality class in disagreement with the known result [122] given by eq. (69) (this error could possibly disappear in the increasingly large-cluster limit). It is clear, however, that *all* the present results are exact for the associated hierarchical lattice.

For the present or other  $Z(q)$  systems, various similar RG approaches are available in the literature [252–255], [125, 199]

### Isotropic discrete cubic ferromagnet on the square lattice

We consider the  $N$ -component cubic model with first neighbor interactions on a square lattice. Its dimensionless pair Hamiltonian is given by eq. (244) where  $K > 0$  and  $L \geq -K$  (ferromagnetic case). This model contains some interesting particular cases, namely the  $2N$ -state Potts ferromagnet ( $t_1 = t_2$ ), the  $N$ -state Potts ferromagnet ( $t_1 = 0$ ), the spin  $1/2$  Ising ferromagnet ( $N = 1 \forall t_1, t_2$ ;  $t_2 = 1 \forall N$ ), the  $Z(4)$  ferromagnet ( $N = 2 \forall t_1, t_2$ ) and the self-avoiding walk ( $L = 0$  and  $N \rightarrow 0$ ).

We shall treat this problem in a RG framework where the  $b = 2$  Wheatstone bridge graph is renormalized into a single edge [46]. Associating the vector transmissivity  $\vec{t} \equiv (t_1, t_2)$  defined in eqs. (248) to each edge of this graph  $G$  one obtains the following recursive relations:

$$t'_1 = \frac{N_1(1, 2; G)}{D(G)} \quad (303.a)$$

and

$$t'_2 = \frac{N_2(1, 2; G)}{D(G)} \quad (303.b)$$

where  $N_\alpha(1, 2; G)$  ( $\alpha = 1, 2$ ) and  $D(G)$  are defined in eqs. (254). These equations, when expressed in the variable  $K$  and  $L$ , coincide with the expression (14)-(18) of ref. [46]. The corresponding phase diagrams for typical values of  $N$  are shown in Figs. 47 represented in both  $t_2$  vs.  $t_1$  and  $k_B T / J_1$  vs.  $(J_1 + J_2) / J_1$  variables. Similarly to the  $Z(4)$  model (which corresponds to  $N = 2$  in our model), there are three phases for any given value of

$N$ , namely the *paramagnetic* ( $P$ , characterized by the fully stable fixed point  $t_1 = t_2 = 0$ ), the *ferromagnetic* ( $F$ ; characterized by the attractor  $t_1 = t_2 = 1$ ) and the *intermediate* ( $I$ ; whose attractor is  $(t_1, t_2) = (0, 1)$ ) ones. The appearance of the non physical  $P - I$  critical frontier for  $N = 1$  (Ising model) should be considered as spurious; as expected the physically meaningful critical temperature for  $N = 1$  does not depend on  $J_2/J_1$  (see the “horizontal” line in Fig. 47b). For any fixed value of  $N$ , the Ising, the  $N$ -state and the  $2N$ -state critical points are exactly located. Besides these ones, there is a fourth critical point corresponding to the cubic one ( $(t_1, t_2) = (t_1^c, t_2^c)$ ) whose transmissivities can be seen in Fig. 3a of ref. [46]) which governs the transition  $P - F$  for  $N < N^* \simeq 6.9$  and becomes completely unstable for  $N > N^*$ . At  $N = N^*$  a special multicritical point emerges as the  $2N$ -state Potts and the cubic fixed points collapse; at this value of  $N$  these two fixed points interchange stability (a quite common phenomenon in fact).

Concerning the critical exponents, the thermal one  $\nu_T(N)$  and the crossover exponent  $\phi(N)$  are shown in figs. 48(a) and 48(b) for the  $2N$ -state Potts and cubic ferromagnets respectively. In particular,  $\nu_T(N)$  of Fig. 48(a) reproduces the values  $\nu_{21}$  of Table VI for the Wheatstone-bridge hierarchical lattice Potts model with  $q = 2N$  states.

Although neither the critical frontier nor the critical exponents of the cubic model are known analitically, there have been many approximate calculations (see for example [46], [256] and references therein) indicating that the cubic phase transition ( $P - F$ ) becomes a first order one above a certain value  $N_c$  of  $N$  (for example, Nienhuis et al [44] found  $N_c = 2$  using variational renormalization group techniques). As the present RG led to only continuous transitions, we expect that the present results are good approximations, for  $N \leq 2$ , for the square lattice and are, surely, exact for the Wheatstone-bridge hierarchical lattice.

Similar RG techniques have been used [257, 48, 258, 50] for the discrete cubic model in more general situations.

#### 4.1.2 Other real space RG approaches

Several other real space RG approaches are available in the literature, e.g, the Monte Carlo RG (MCRG), the Mean Field RG (MFRG), the Effective Field RG (EFRG), the

Finite Size Scaling RG (FSSRG) and the phenomenological RG.

The MCRG combines Monte Carlo computer simulations with RG techniques. Since the first suggestion of Ma [259] in 1976 for combining these two methods, different approaches to the MCRG have been developed and applied with success to a variety of systems. For discussion and illustration of these approaches the reader is referred to the excellent review by Swendsen [260], as well as the subsequent references [261–264]. The MFRG combines the standard Mean Field Approximation with RG techniques. The results obtained up to now are frequently not very accurate and it does not fully satisfactorily describe crossovers from one universality class to another. But on the other hand, the procedure is operationally simple, and can therefore be useful for a first analysis of complex systems. For a critical discussion of this method and list of references before 1987, the reader is referred to [265], see also [266–276] for more recent applications. The EFRG [277–280] consists on a further improvement along the same line. Finally, the use of now standard ideas on finite size scaling has enabled recently the formulation of an interesting real space RG, the FSSRG, which presents various advantages (see [281] for details) and that has been tested on a variety of models [282–284], [230].

We address now with some detail the phenomenological RG ([285] and references therein). It enables high accuracy calculations of critical points, exponents (also equations of states) of a variety of  $d = 2$  physical systems. It can be also used for  $d > 2$ , but, similarly to any other real space RG, the precision decreases when  $d$  increases.

The system to be considered is a long strip in  $d = 2$  (a long bar in  $d = 3$ ) whose length equals that of  $L$  unitary cells and whose width equals that of  $N$  unitary cells. (typical values are  $L \simeq 100 - 10000$  and  $N$  up to  $10 - 20$ ). Several boundary conditions can be used, the periodic ones being the most usual. The partition function  $Z = \sum_{\text{configurations}} e^{-\beta\mathcal{H}}$  of such system can be written ([30] and references therein) as follows

$$Z = \sum_{\text{conf.}} \prod_{i=1}^{L-1} \langle \phi_i | T | \phi_{i+1} \rangle \quad (304)$$

where  $i$  refers to the  $i - th$  column ( $i - th$  plane in  $d = 3$ ),  $|\phi_i\rangle$  denotes its configuration, and  $T$  is the *transfer-matrix* given by  $T = e^{-\beta\mathcal{H}_i}$  where  $\mathcal{H}_i$  is the Hamiltonian which contains all the bonds of the  $i - th$  column as well as those which connect the  $i - th$  and

$(i + 1) - th$  columns. Using the property

$$\sum_{config.i} |\phi_i\rangle\langle\phi_i| = \mathbf{1} \quad (305)$$

we obtain

$$Z = \langle\phi_1|T^{L-1}|\phi_L\rangle \quad (306)$$

In what follows let us assume periodic boundary conditions, hence

$$Z = Tr T^L \quad (307)$$

For the Potts model  $T$  is a  $q^N \times q^N$  matrix whose structure can be considerably simplified by using various symmetry properties. We note  $\lambda_1$  and  $\lambda_2$  the largest and the second largest eigenvalue of  $T$ . Then, in the  $L \rightarrow \infty$  limit, it can be shown that

$$Z = \lambda_1^L \quad (308)$$

and

$$\xi_N = \frac{1}{\ln(\lambda_1/\lambda_2)} \quad (309)$$

$\xi_N$  being the correlation length characterizing the spin-spin correlation function at long distances within the strip with width  $N$ . Within the finite size scaling picture [286] it is assumed, for sufficiently large  $N$ , that at  $T_c$

$$\xi_N \propto N \quad (310)$$

hence, by using two different widths,

$$\frac{\xi_N(T_c)}{\xi_{N'}(T_c)} = \frac{N}{N'} \quad (311)$$

This equation determines an approximate value for  $T_c$ . The corresponding approximation for  $\nu$  is given by

$$\nu^{-1} = \frac{\ln[(d\xi_N/dT)_{T_c}/(d\xi_{N'}/dt)_{T_c}]}{\ln(N/N')} - 1 \quad (312)$$

Many alternative phenomenological procedures have been devised (see [287–294] and references therein) but they all follow along the lines of what has been exposed herein. Also, in general,  $N \gg 1$  extrapolations enable refined accuracy. We present in Fig. 49 the



result obtained [295, 296] for the square lattice Potts ferromagnet. We notice that the results for the  $q$ -evolution of  $\nu$  are very precise for  $q < 4$ ; however, nothing is detected which could reveal that the phase transition becomes of the first-order for  $q > 4$ . This is to be attributed to the loss of validity, for such transitions, of Eq. (310).

### 4.1.3 Connection between the correlation function preserving RG and the phenomenological one

As stressed in the previous sections, the correlation function preserving RG is exact for hierarchical lattices, while it is expected to be a more or less performant approximation for systems on Bravais lattices. Here we reproduce recent arguments [46] which clarify the nature of this approximation by making explicit the connection between the correlation function preserving RG and the phenomenological one.

To avoid unnecessary complications, let us focus on the particular case of the  $d = 2$  Ising model. We can omit vector notations and represent simply by  $S_i = \pm 1$  the spin at site  $i$ .

Successive clusters of the Wheatstone-bridge family are reported in Figs. 11(a)-(d) (the corresponding  $b = 1, 2$  and  $5$  clusters on the square lattice are shown in Fig. 50). On each of these clusters (with  $b(b - 1)$  internal spins), the summation procedure leading to the renormalized coupling constant  $K'$  can be interpreted as the calculation of an *interface* free energy for blocks of the type indicated in Fig. 50. The spins on the upper and bottom horizontal sides of the block are left out of the summation. Indeed, if we indicate by  $\{S\}$  the configurations of the internal spins of the cluster (i.e., other than  $S_1$  and  $S_2$ ) we have:

$$e^{K'S_1S_2+g} = \text{Tr}_{\{S\}} e^{-\beta\mathcal{H}(\{S\};S_1,S_2)} \equiv Z_{S_1S_2}(K) \quad (313)$$

where  $g$  is an appropriate spin-independent term. From Eq. (313) we obtain that

$$K' \equiv K'(K, b) = \frac{1}{2}[\ln Z_{++} - \ln Z_{+-}] \quad (314)$$

This means that  $K'$  is nothing but the dimensionless excess free energy produced by fixing the horizontal sides to (+) and (−), compared to the case in which both sides are fixed, say, to (+). By definition of the (dimensionless) surface tension  $\sigma$ , we thus have

$$K'(K, b) = (b - 1)\sigma(K, b) \quad (315)$$

where  $\sigma(K, b)$  is expected to become independent of  $b$  in the  $b \rightarrow \infty$  (thermodynamic limit).

From finite size scaling [286, 297] we expect, for  $K \sim K_c$  and  $b \rightarrow \infty$ ,

$$\sigma(K, b) \sim b^{-1} \sigma_0(b/\xi_\infty(K)) \sim 1/\xi(K, b) \quad (316)$$

where  $\xi_\infty(K)$  is the correlation length of the infinite system,  $\sigma_0$  is a scaling function with  $\sigma_0(0) \neq 0$ , and  $\xi(K, b)$  is the correlation length in the finite block.

If we now define, as often done [68], [135–138], [141–147], [159–167], a renormalized coupling constant  $K_{ren}$  corresponding to a linear rescaling factor  $b/b'$  ( $b' < b$ ), through the following cell recurrence relation

$$K'(K_{ren}, b') = K'(K, b) \quad (317)$$

it follows, from Eqs. (315) and (316) and for large  $b$  and  $b'$ , that

$$\xi(K_{ren}, b') = \frac{b'}{b} \xi(K, b) , \quad (318)$$

This is nothing but the definition of renormalized coupling constant in a phenomenological approach [285]. It is clear that various choices can be done for cells to be used. In particular, the standard choice in the phenomenological approach is finite  $\times$  infinite strips, whereas here we are using finite  $\times$  finite self-dual clusters. In view of the nice convergence of results generally obtained with phenomenological renormalization methods, the preceding arguments justify the usual strategy of improvement of the results herein obtained (as well as in similar treatments) as that of considering cell to cell transformations  $K \rightarrow K_{ren}$ , like in Eq. (317), with both  $b$  and  $b'$  becoming increasingly large (as is usually done in the phenomenological RG).

The above derivation can of course be generalized to the case of dimensionality  $d \neq 2$ , and to models different from the Ising one.

Summarizing, we see that the procedure we have used here should not be interpreted as another type of decimation RG approximation. Indeed, although we impose the correlation function to be preserved, we do so between the roots of the graphs, which corresponds to imposing the surface free energy to be preserved in the Bravais blocks, whereas

in the decimation procedures what is imposed is the preservation of the correlation function between two sites of the Bravais lattice. This makes a substantial difference since the decimation procedures, unless conveniently handled, bring along intrinsic difficulties related to the spin rescaling [223]. These difficulties do not exist in the present approach.

The present analysis makes clear that the well known limitations of the Migdal-Kadanoff-like approaches are not due to the fact that correlation functions are preserved, but rather to the fact that diamond (or tress) choices for the graphs lead, even for large clusters, to topologies which are not at all those of the Bravais lattices which are supposed to be approached.

## 4.2 Equation of states and other thermodynamical quantities

We address here the RG calculation of quantities which are defined on the space of the external parameters of the problem. Niemeijer and van Leeuwen [223] have shown how quantities like specific heat, order parameter and susceptibility can be calculated with success in Bravais lattices. However, within their procedure, proliferation of coupling constants is normally observed, which in turn implies in a certain degree of arbitrariness on the choice of those to be taken into account. We shall discuss here RG procedures which frequently avoid this difficulty, but which on the other hand describe hierarchical lattices rather than the Bravais lattices we might be interested in. In practice, we shall see that this restriction is often unimportant, as both types of lattices behave very similarly in many respects. Also, the lower-order approximations of the RG procedures which we intend to describe here are, operationally speaking, as simple as Mean Field calculations, though yielding results which are, both qualitatively and quantitatively, largely superior.

To illustrate this type of approach we shall calculate, for the Potts ferromagnet at *all temperatures*, the free and internal energies, specific heat, spontaneous magnetization, longitudinal surface tension and correlation length. In all cases, to the RG recursive relations in the parameter space (obtained, for instance, through the correlation function preserving procedures), we add recursive equation (s) corresponding to the quantity (ies) we want to calculate.

### 4.2.1 Free energy, internal energy and specific heat

We follow along the lines of Res. [298, 229], where more details can be found than given here. The dimensionless free energy per site of the  $d$ -dimensional Bravais lattice scales, within the RG, as follows:

$$f(K) = b^{-d}f(K') + g(K) \quad (319)$$

where  $K$  and  $K'$  are, respectively, the original and renormalized dimensionless coupling constant of the model, and  $g(K)$  is the standard background term (see [223, 227, 298] and references therein). On the other, at the graph level, the preservation of the correlation function imposes (see Eq. (258))

$$e^{\mathcal{H}_{12}(K') + K'_0} = \text{Tr}_{3, \dots, N_s} e^{\mathcal{H}_{12 \dots N_s}(K)} \quad (320)$$

where by the  $\mathcal{H}_{12}$  and  $\mathcal{H}_{12 \dots N_s}$  we respectively denote here the dimensionless Hamiltonians of a single bond and that of the two-rooted graph that has been chosen to approximate the Bravais lattice.  $K'$  is the additive term that has to be included in order to allow for the zero-energy renormalization. This equation completely determines  $K' = K'(K)$  and  $K'_0 = K'_0(K)$ . We introduce now a proportionality factor  $D(K)$  (to be determined) through the relation

$$g(K) = D(K)K'_0(K) \quad (321)$$

If we shift the zero-energy point by adding an arbitrary value  $\lambda K$  to the (dimensionless) energy associated with each bond ( $\lambda$  is an arbitrary constant),  $f$  transforms according to  $f(K) \rightarrow f(K) + \lambda K d$  and consequently the preservation of equation (319) implies

$$g(K) \rightarrow g(K) + \lambda d [K - b^{-d}K'(K)] \quad (322)$$

At the graph level, the preservation of Eq. (320) implies

$$K'_0(K) \rightarrow K'_0(K) + \lambda [b^{d_f}K - K'(K)] \quad (323)$$

If we impose now that Eq. (321) remains form-invariant under uniform translation of the energy scale (i.e.,  $D(K)$  does not change with  $\lambda$ ) in a similar manner to the Maxwell equations which are form-invariant under the Lorentz transformation, it immediately

follows that

$$D(K) = \frac{d[b^d K - K'(K)]}{b^d[d^{d_f} K - K'(K)]} \quad (324)$$

This equation formally closes the operational procedure as (together with Eq. (321)) it provides  $g(K)$ , which (combined with Eq. (319)) enables us to calculate the free energy and consequently the internal energy and specific heat.

If we are studying the hierarchical lattice generated by the chosen two-rooted graph, then  $d$  is replaced by  $d_f$  (see [229] for a detailed discussion of this point), hence  $D = d_f b^{-d_f}$  becomes a purely topological number, thus yielding

$$f(K) = b^{-d_f} [f(K') + d_f K'_0(K)] \quad (325)$$

Note that  $d_f$  plays in this expression the same role that  $d$  (which is equal to the number of bonds per site) plays in the standard recursive relation associated with a  $d$ -dimensional Bravais lattice (see also Refs. [65, 66]).

If we are interested instead in a hopefully closer approximation to the  $d$ -dimensional Bravais lattice, then  $D(K)$  contains both topological and thermal information; typically  $D(K)$  smoothly and monotonously varies from  $D(0) = db^{-d_f}$  to  $D(\infty) = db^{-d_f}(1 - 1/b)/(1 - b^{-1+d-d_f})$  when  $K$  increases from zero to infinity [298]. If the family of hierarchical lattices is appropriately chosen, one should expect  $\lim_{b \rightarrow \infty} d_f = d$ , hence  $D(K) \sim db^{-d}$  for all values of  $K$  in the  $b \rightarrow \infty$  limit.

The consequences of the apparently innocuous form-invariance hypothesis for Eq. (321) are quite interesting. Indeed, specific heats which present (within RG frameworks that are similar but that do not allow for proper dependence of  $D$  on  $K$ ) negative values for large regions of  $K$  become automatically (without introducing any adjustable parameter) positive for *all* finite temperatures when recalculated within the present scheme.

The Potts ferromagnet has been studied [298, 229, 221] with the generalized Wheatstone-bridge graphs. The results obtained are indicated in Figs. 51-53. In particular, Fig. 53 has been obtained by performing  $C/k_B(q-1) = C_p$  in the  $q \rightarrow 1$  limit (see Kasteleyn and Fortuin results [16]).

The analytic discussion of the present equations shows that the high-temperature expansion for the specific heat recovers, for increasing  $b$ , more and more terms of the expansion which is exact for the corresponding Bravais lattice.

### 4.2.2 Equations of states

We calculate here the magnetization as a function of temperature at vanishing external field (the extension to arbitrary values of the field is feasible along the same lines [299]). The present procedure follows along the lines of [228] and enables the calculation of the magnetization directly, without going through that of the Gibbs energy.

We consider a  $d$ -dimensional hypercubic lattice of linear size  $L$  with Potts interaction between first-neighbouring sites. In the  $L \rightarrow \infty$  limit, the order parameter  $M$  can be defined as  $M = N_L(K)/L^d$ , where  $N_L(K)$  is the thermal canonical average number of sites whose spin is pointing along the easy magnetization direction (say, the  $\sigma_i = 0$  axis, arbitrarily chosen among the  $q$  equivalent states along which the symmetry is to be broken) minus the number of sites whose spins are pointing in any other direction (i.e.  $\sigma_i \neq 0$ ). Furthermore, we associated an elementary dimensionless magneton  $\mu$  with each site of the lattice; we could in principle chose  $\mu = 1$ , but we will instead leave it as a variable since it will change under renormalization. Within a Kadanoff philosophy, we divide the system of  $L^d$  sites into a system of  $L'^d$  cells of linear size  $B \equiv L/L' > 1$ . We then associate with each cell the renormalized variable  $K'$  and  $\mu'$  which will depend on  $K$  and  $\mu$ . The total magnetic momentum (extensive quantity) is to be preserved through renormalization, i.e.,

$$N_{L'}(K')\mu' = N_L(K)\mu \quad (326)$$

Dividing both terms by  $L'^d$  we obtain

$$M(K')\mu' = M(K)\mu B^d \quad (327)$$

with  $M(K') = N_{L'}(K')/L'^d$ . If we start with  $K$  and  $\mu^{(0)}$  and perform  $n$  iterations in Eq. (327) we obtain

$$M(K^{(n)})\mu^{(n)} = B^{nd}M(K)\mu^{(0)} \quad (328)$$

Hence

$$M(K) = \lim_{b \rightarrow \infty} \frac{M(K^{(\infty)})\mu^{(n)}}{B^{nd}\mu^{(0)}} \quad (329)$$

By arbitrarily choosing  $\mu^{(0)} = 1$  we obtain

$$M(K) = \lim_{n \rightarrow \infty} M(K^{(\infty)})\mu^{(n)}/B^{nd} \quad (330)$$

This formula, together with the RG equation for  $K$ , enables the calculation which are looking for. If  $K < K_c$  ( $K_c \equiv$  critical fixed point) then  $K^{(\infty)} = 0$ , hence  $M(K^{(\infty)}) = 0$  which implies (through Eq. (330)) that  $M(K) = 0$  as expected. If  $K > K_c$  then  $K^{(\infty)} = \infty$ , hence  $M(K^{(\infty)}) = 1$  (conventional value for  $T = 0$ ), which yields (through Eq. (330)).

$$M(K) = \lim_{n \rightarrow \infty} \mu^{(n)} / B^{nd} \quad (331)$$

This is the formula which provides the thermal dependence of the order parameter in the entire non trivial region, i.e., for  $T < T_c$ .

To close the procedure we have to specify how the RG recursive relations for  $K$  and  $\mu$  are determined. For  $K$  we use the recurrence provided by the correlation function procedure (Section (4.1.1)). With respect to  $\mu$ , let us anticipate that its RG equation will be of the form

$$\mu' = a(K)\mu \quad (332)$$

$a(K)$  being a function to be determined which satisfies  $a(\infty) = B^d > a(K_c) > a(0) > 0$  (see [228] for more details). The particular form Eq. (332) comes from the fact that it has to be form invariant if we expand the  $\mu$  scale (i.e., if we make  $\mu \rightarrow \lambda\mu$  and  $\mu' \rightarrow \lambda\mu'$  with arbitrary  $\lambda$ ). To determine  $a(K)$  we proceed as follows. In order to break the symmetry we *impose* the spin of, say, root 1 (of both small and large graphs) to be in the  $\sigma = 0$  state, the rest of the spins (that on root 2 included) being free to take all possible orientations ( $q$  configurations for each spin). Each graph configuration (there will be  $q^{N_s-1}$  of them) will be weighed with the corresponding Boltzmann factor, and will be associated with a value for the cluster magnetic momentum  $m$  where *each spin contributes proportionally to its coordination number* (see [238, 300] for further discussion of this point). We then impose

$$\langle m \rangle_{G'} = \langle m \rangle_G \quad (333)$$

where  $\langle \dots \rangle$  denotes thermal canonical average, and  $G'$  and  $G$  respectively denote the small and large graphs. The whole procedure is indicate in Table IX for the  $b = 2$  planar Wheatstone bridge graph renormalized into a single edge  $b' = 1$  (in this case  $B^d = 5$ ). We obtain, for Eq. (332),

$$\frac{2e^{qK'} + (q-2)}{e^{qK'} + (q-1)} \mu' = [10e^{5qK} + 10(q-2)e^{3qK} + 8(3q-5)e^{2qK} + \dots] \mu \quad (334.a)$$

$$+ (16q^2 - 68q + 90)e^{qK} + (2q^3 - 16q^2 + 44q - 40)]\mu/D_\mu$$

where

$$\begin{aligned} D_\mu &= e^{5qK} + 2(q-1)e^{3qK} + 4(q-1)e^{2qK} + \\ &+ (q-1)(5q-9)e^{qK} + (q-1)(q-2)^2 \end{aligned} \quad (334.b)$$

The results obtained for successive approximations for the magnetization on the square-lattice are indicated in Figs. 54 and 55. In the  $T \rightarrow T_c - 0$  limit, we may define the following asymptotic behaviour

$$M \sim A(1 - T/T_c)^\beta \quad (335)$$

The present RG's recover, for all  $q$ , the exact  $T_c$  of the square lattice. The respective  $q$ -evolutions of  $\beta$  (the exact result for the square lattice is given by eq. (37) [92]) and  $A$  (the exact result for the square-lattice is not available, excepting for  $q = 2$ ) is indicated in Figs. 5 and 56. It is interesting to compare the present results with the recently obtained [237] *exact* ones for hierarchical lattices: both procedures yield the same value  $\beta = 0.180$  for the  $q = 2$  standard Wheatstone-bridge lattice, but present discrepancies (typically below 15%) for  $q \neq 2$ .

### 4.2.3 Surface tension

We address here the thermal dependence of the longitudinal surface tension  $\gamma$  of a  $d$ -dimensional hypercubic lattice (see [301]). The procedure follows along the lines of Ref. [226, 161]: the RG equation for  $\gamma$  is given by

$$(b')^{d-1} K' \gamma' = b^{d-1} K \gamma \quad (336)$$

This equation, together with the RG equation for  $K$ , enables the calculation which we are looking for. We present in Fig. 57 the  $q = 2$  results obtained for the square lattice by using the generalized Wheatstone-bridge graphs. Within the  $RG_{bb'}$  framework we obtain

$$\frac{\gamma(T)}{\gamma(0)} \sim 1 - \frac{\ln(b/b')}{2(b-b')} \frac{k_B T}{J} - \left(\frac{b-1}{b}\right)^2 \frac{k_B T}{J} e^{-2J/k_B T} \quad (T/T_c \rightarrow 0) \quad (337)$$

which, in the  $b \rightarrow \infty$  limit, yields [161]:

$$\frac{\gamma(T)}{\gamma(0)} \sim 1 - \frac{k_B T}{J} e^{-2J/k_B T} \quad (T/T_c \rightarrow 0) \quad (338)$$



which is the *exact* result for the surface tension on the square lattice [6].

We also obtain

$$\frac{\gamma(T)}{\gamma(0)} \sim A_{bb'} \left(1 - \frac{T}{T_c}\right)^{\nu_{bb'}} \quad (T \rightarrow T_c - 0) \quad (339)$$

where  $T_c$  is exactly recovered for all  $(b, b')$ ,  $\nu_{bb'}$  is given in Table VI, and  $A_{bb'}$  is represented in Fig. 58.

The present calculation can be straightforwardly extended to arbitrary values of  $q$  and  $d$ .

#### 4.2.4 Correlation length

We address here the thermal dependence of the correlation length  $\xi$  of a  $d$ -dimensional hypercubic lattice. The procedure is completely similar to that used for the surface tension, and follows along the lines of Ref. [302, 195]. Eq. (336) is replaced by

$$\frac{\xi'}{b'} = \frac{\xi}{b} \quad (340)$$

and the rest of the procedure remains exactly the same. The results obtained [302] for the square lattice are represented in Figs. 59 and 60. Also

$$\xi^{-1} \sim -\frac{\ln(b/b')}{b-b'} + \ln\left(\frac{k_B T}{J}\right) - \left[\frac{q-2}{2} + 2\left(\frac{b-1}{b}\right)^2\right] \frac{J}{k_B T} \quad \left(\frac{k_B T}{J} \rightarrow \infty\right) \quad (341)$$

and

$$\xi^{-1} \sim \frac{a(q)J}{k_B T} \left[1 - \frac{\ln(b/b')}{b-b'} \frac{k_B T}{qJ} - 2\left(\frac{b-1}{b}\right)^2 \frac{k_B T}{qJ} e^{-qJ/k_B T}\right] \quad \left(\frac{k_B T}{J} \rightarrow 0\right) \quad (342)$$

where  $a(q)$  cannot be calculated within the present RG framework. In the  $b \rightarrow \infty$  ( $b' < b$ ) these respective expressions yield

$$\xi^{-1} \sim \ln\left(\frac{k_B T}{J}\right) - \left(\frac{q+2}{2}\right) \frac{J}{k_B T} \quad \left(\frac{k_B T}{J} \rightarrow \infty\right) \quad (343)$$

and

$$\xi^{-1} \sim a(q) \frac{J}{k_B T} \left[1 - \frac{2k_B T}{qJ} e^{-qJ/k_B T}\right] \quad \left(\frac{k_B T}{J} \rightarrow 0\right) \quad (344)$$

These expressions recover (with  $a(2) = 2$ ) the *exact* results [6, 303, 5] for  $q = 2$ , namely

$$\xi^{-1} = \ln \coth\left(\frac{J}{k_B T}\right) - \frac{2J}{k_B T} \quad (T > T_c) \quad (345)$$

$$\sim \ln\left(\frac{k_B T}{J}\right) - \frac{2J}{k_B T} \quad \left(\frac{k_B T}{J} \rightarrow \infty\right) \quad (346)$$

and

$$\xi^{-1} = \frac{2J}{k_B T} - \ln \coth \left( \frac{J}{k_B T} \right) \quad (T < T_c) \quad (347)$$

$$\sim \frac{2J}{k_B T} \left[ 1 - \frac{k_B T}{J} e^{-2J/k_B T} \right] \quad \left( \frac{k_B T}{J} \rightarrow 0 \right) \quad (348)$$

Eqs. (343) and (344) might well be exact for all  $q$  (possibly with  $a(q) = q$ ).

For  $d > 2$ , the following asymptotic behaviours are obtained in the  $b \rightarrow \infty$  limit ( $b' < b$ ):

$$\xi^{-1} \sim \ln \left( \frac{k_B T}{J} \right) - \left[ \frac{q-2}{2} + 2(d-1) \right] \frac{J}{k_B T} \quad \left( \frac{k_B T}{J} \rightarrow \infty \right) \quad (349)$$

$$\xi^{-1} \sim a(q, d) \left( \frac{J}{k_B T} \right)^{\frac{1}{d-1}} \left\{ 1 - \frac{q^{2(d-1)}}{d-1} \left( \frac{k_B T}{qJ} \right) e^{-2q(d-1)J/k_B T} \right\} \quad \left( \frac{k_B T}{J} \rightarrow 0 \right) \quad (350)$$

where  $a(q, d)$  cannot be calculated within the present framework. For  $q = 2$  and  $d = 3$  Eq. (349) *exactly* recovers the asymptotic behaviour for the simple cubic lattice [303]. Eqs. (349) and (350) might well be exact for all  $q$  and all  $d > 2$ . It is interesting to notice that the  $d = 2$  and the  $d = 2 + 0$   $T \rightarrow 0$  results do not coincide (see [144]).

### 4.3 Interface effects

Many interesting critical phenomena occur in magnetic systems which are not fully translationally invariant because along at least one direction (say the  $z$ -axis) the system is not homogeneous. A typical such system is a  $d = 3$  semi-infinite bulk (*surface* problem); another typical situation (which in fact generalizes the previous one) is a  $d = 3$  system which is translationally invariant within the  $xy$  plane but which along the  $z$ -axis changes at  $z = 0$  in the sense that two different semi-infinite homogeneous bulks join there (*interface* problem). For a general introduction on both theoretical and experimental aspects of this problem, the reader can refer to the reviews by Binder [297] and Kaneyoshi [304]; reciprocal-space and real space RG approaches have been respectively reviewed by Diehl [305] and one of us [306] (see also [307], [308]). The references appearing in these reviews practically cover the present status of the subject, and will not be reproduced herein.

Our aim in this Subsection is to illustrate how the correlation function preserving RG techniques can be used to study the criticality associated with surface magnetism.

This type of approach has been systematically used by the Rio de Janeiro/CBPF group and collaborators [138, 141, 142, 166, 167, 146, 147] [309–315]. As a prototype system we shall study here the semi-infinite simple cubic ferromagnetic Potts bulk: the first-neighbour coupling constant  $J_{ij}$  equals  $J_S (J_S \geq 0)$  if both  $i$  and  $j$  sites belong to the  $(0, 0, 1)$  surface ( $z = 0$  plane), equals  $J_B (J_B \geq 0)$  if at least one of the sites belongs to the bulk ( $z < 0$ ), and vanishes otherwise ( $z > 0$ ). A typical phase diagram is shown in Fig. 61 ( $q = 2$ ). It is convenient to introduce the variable

$$\Delta \equiv \frac{J_S}{J_B} - 1 = \frac{\ln\{[1 + (q-1)t_S]/(1-t_S)\}}{\ln\{[1 + (q-1)t_B]/(1-t_B)\}} - 1 \quad (351)$$

where we have introduced the transmissivities  $t_S$  and  $t_B$  respectively associated with  $J_S$  and  $J_B$ . We note  $\Delta_c$  the value of  $\Delta$  where all three critical lines of Fig. 61 join. The *surface-ferromagnetic* phase (SF; finite surface magnetic order in the absence of bulk magnetic order) only exists for  $\Delta > \Delta_c$ . The *paramagnetic* (P; vanishing surface and bulk orders) and *bulk-ferromagnetic* (BF; both surface and bulk orders are non-null) phases exist for varying values of  $\Delta$ . At  $\Delta = \Delta_c$  a special transition occurs which corresponds to a multicritical point (with its own universality class).

The RG recursive relations for this problem can be written as follows [138].

$$t'_B = f(t_B) \quad (352)$$

and

$$t'_S = g(t_S, t_B) \quad (353)$$

where  $f(t_B)$  is the equivalent transmissivity associated with the two-rooted graph of Fig. 30b (Fig. 62);  $f(t_B)$  equals  $T_{12}(t_B, t_B, t_B, G_3)$  of Eq. (280).  $g(t_S, t_B)$  is the equivalent transmissivity of the two-rooted graph obtained from the free-surface RG cell shown in Fig. 62 by collapsing the entry nodes (forming one root) and the exit nodes (generating the other root). These equations yield, for all values of  $q$ , the type of RG flow diagram indicated in Fig. 63. We present in Fig. 64 the  $q$ -dependence of  $\Delta_c$  obtained within the present RG as well as within an extrapolated version of it (see [138] for details). In the neighbourhood of the multicritical point we may introduce the following asymptotic behaviour

$$\frac{T_c^{surface}(\Delta)}{T_c^{surface}(\Delta_c)} - 1 \sim A \left( \frac{\Delta}{\Delta_c} - 1 \right)^{1/\phi} \quad (354)$$

We have presented in Fig. 65 the  $q$ -dependences of  $A$  (as well as its extrapolated value  $A^*$  [138]) and  $\phi$ . See finally Fig. 66 for the  $q$ -evolution of the entire phase diagram. For the discussion of the various universality classes present in this problem see [138] as well as the reviews previously mentioned [297, 305, 306].

## 5 FINAL REMARKS

We have seen that the Potts model and a great number of related systems can be studied, quite satisfactorily in some cases and only roughly in others, with real space renormalization group techniques. Let us present here some open problems whose study would be natural extensions of the content of this review.

- (i) No RG techniques (nor any other, as far as we know) have been used to study the general  $q$ -state classical model described by the interaction matrix (10a) without restriction (10b). In particular, it may be possible to devise a BCM for such a model.
- (ii) Continuously varying critical exponents (e.g., the para-ferromagnetic critical line of the  $Z(4)$  ferromagnet on the square-lattice) and transitions like the Kosterlitz-Thouless one remain hard problems within real space RG techniques. Although hard, these problems cannot be considered unsolvable. Indeed, lines of fixed points have already been exhibited in the literature [168, 316] within RG frameworks like the ones discussed herein.
- (iii) The analysis of systems presenting commensurate/incommensurate modulated structures (e.g., the chiral Potts model and frustrated systems like the ANNNI one) is, with very few exceptions, to be done.
- (iv) Some of the approaches presented herein are exact for hierarchical lattices. They could further enlighten the criticality and the scaling laws of fractals as compared to translationally invariant systems. For example: what are the topological ingredients which determine  $\lim_{q \rightarrow \infty} \nu_q$  and for what classes of hierarchical lattices we have that  $\lim_{q \rightarrow \infty} \alpha_q = 1$ ?
- (v) The establishment of a BCM for dealing with probability laws as those presented in Subsection 3.2.4 (quenched-bond random Potts model) would be very elegant and useful.
- (iv) Very recently [317], the correlation function preserving procedures described in this

review have been satisfactorily applied to construct RG's for approaching the classical n-vector model. This fact opens an area to be explored.

## Acknowledgments

We are deeply grateful and indebted to E.M.F. Curado and G. Schwaccheim for uncountable and highly helpful contributions. It is with pleasure that we acknowledge encouragement by R. Ferreira. We have also benefited from many useful discussions with C.G. Bollini, A.O. Caride, A. Chame, A. Coniglio, U.M.S. Costa, J.W. Essam, P.R. Hauser, H.J. Herrmann, S.V.F. Levy, A.M. Mariz, P.M.C. Oliveira, E.F. Sarmiento, B. Shapiro, S.R.A. Salinas, E.P. Silva, L.R. da Silva, H.E. Stanley, A.L. Stella, R.B. Stinchcombe, F.Y. Wu, I.P. Fittipaldi, J.A. Plascak and S. Coutinho. Warm hospitality received at the Universidade Federal do Rio Grande do Norte (Natal), the Universidade Federal de Alagoas (Maceió), and the Centre des Recherches sur les Très Basses Températures/CNRS (Grenoble), where parts of this work were done, is sincerely acknowledged as well. We also thank the financial support from Conselho Nacional de Desenvolvimento Científico e Tecnológico, CNPq (Brazilian agency).

## APPENDIX

### Potts ferromagnet on Migdal-Kadanoff-like hierarchical lattices

Among the simplest available real space RG's we have those which follow along the lines of Migdal and Kadanoff [318] approaches (differential RG's, bond moving procedures, etc; see [319] for an analysis and review of these approaches). Their general tendency, when compared to available results for d-dimensional Bravais lattices, is to be qualitatively correct though quantitatively quite rough (although non trivial): later on we shall illustrate this point. In any case, *all* the results are exact for the associated hierarchical lattices, namely the d-dimensional generalized *diamond*-like and *tress*-like ones: see Fig. 67. In the former case, the generators are equal to the two-rooted graphs resulting from the Migdal-Kadanoff approximations for the considered model on d-dimensional hypercubic lattices. The above hierarchical lattices are completely determined by the dimensionality  $d$  and the linear expansion factor  $b$ . The diamond (tress) generator graph is a parallel (series) array of  $b^{d-1}(b)$  branches, each of which is constituted by  $b(b^{d-1})$  bonds in series (parallel). Two topological properties can be verified: (i) For all  $b$  and  $d$ , and for both diamond and tress types, the intrinsic fractal dimensionality is given by  $d_f = \ln b^d / \ln b = d$ ; (ii) For arbitrary fixed  $b$  and  $d = 2$ , and only then, the diamond and tress hierarchical lattices are dual of each other.

The aim of the present Appendix is to study [143, 145] the q-state Potts ferromagnet on these d-dimensional hierarchical lattices and to follow their behaviour in both  $b \rightarrow \infty$  and  $b \rightarrow 1$  limits. Associating with each elementary bond a thermal transmissivity  $t$ , we have (through the algorithms (102) and (108)) for the equivalent transmissivities between the roots 1 and 2 for the diamond-like ( $D$ ) and tress-like ( $T$ ) graphs:

$$T_{12}(t, D; b, d, q, ) = \frac{1 - \left[ \frac{1-t^b}{1+(q-1)t^b} \right]^{b^{d-1}}}{1 + (q-1) \left[ \frac{1-t^b}{1+(q-1)t^b} \right]^{b^{d-1}}} \quad (\text{diamond}) \quad (\text{A.1})$$

and

$$T_{12}(t, T; b, d, q, ) = \left\{ \frac{1 - \left[ \frac{1-t}{1+(q-1)t} \right]^{b^{d-1}}}{1 + (q-1) \left[ \frac{1-t}{1+(q-1)t} \right]^{b^{d-1}}} \right\}^b \quad (\text{tress}) \quad (\text{A.2})$$

Let us now focus the diamond case (the tress case is strictly analogous). The  $RG_{bb'}$  recursive relation is given by

$$T_{12}(t', D; b', d, q) = T_{12}(t, D; b, d, q) \quad (\text{A.3})$$

This equation admits, for all  $(b, b', d, q)$ , two trivial (stable) fixed points, namely  $t = 0$  (paramagnetic phase; P) and  $t = 1$  (ferromagnetic phase; F), as well as a critical (unstable) fixed point noted  $t_{bb'}^*$  which satisfies:

$$T_{12}(t_{bb'}^*, D; b', d, q) = T_{12}(t_{bb'}^*, D; b, d, q) \quad (\text{A.4})$$

The corresponding thermal critical exponent  $\nu_{bb'}$  is given by

$$\nu_{bb'} = \frac{\ln(b/b')}{\ln(\lambda_b/\lambda_{b'})} \quad (\text{A.5})$$

with

$$\lambda_b \equiv \left. \frac{dT_{12}(t, D; b, d, q)}{dt} \right|_{t=t_{bb'}^*} \quad (\forall b) \quad (\text{A.6})$$

The results obtained for  $d \geq 1, q \geq 0, b \geq 2, b' < b$ , and for both diamond and tress cases, are indicated in Figs. 68-70 (the  $b' = 1$  results correspond to the associated hierarchical lattices). It is worth noticing that, for all  $(q, d)$ , both diamond and tress cases and both  $t_{bb'}^*$  and  $\nu_{bb'}$ , the  $b \rightarrow \infty$  limit is approached through a *power law* ( $1/b$  corrections). This is in contrast with the behaviour expected for lattices with *finite* critical temperature (i.e.,  $0 < \lim_{\substack{b \rightarrow \infty \\ b' < b}} t_{bb'}^* < 1$ ): in such cases, finite size scaling arguments [286] usually suggest, in the  $b \rightarrow \infty$  limit, a *power law* approach for fixed  $(b - b')$ , and a *logarithmic* approach for fixed  $b'$ . It is also worth noting that in *no case* first-order phase transitions appear. This is in contrast with the case of d-dimensional Bravais lattices ( $d > 1$ ): for them, the phase transitions *always* become of the first order for  $q$  large enough. We recall however that the results obtained herein illustrate the common expectation that, for a great variety of models, the para-ferromagnetic transitions are of the continuous type for *all* hierarchical lattices.

Let us now turn our attention onto a different type of limit, namely the differential one (i.e.,  $b' = 1$  and  $b = 1 + \mu$  with  $\mu \rightarrow 0+$ ). We generalize here [143] Shapiro's treatment [320] of the bond percolation case ( $q = 1$ ). We first notice that if we consider the hierarchical



lattices generated by the  $d$ -dimensional generalized Wheatstone-bridge graphs (see Fig. 11) with equivalent transmissivity between the roots 1 and 2 noted  $T_{12}(W)$ , we have, for all  $(t; b, d, q)$ ,

$$T_{12}(t, D; b, d, q) \leq T_{12}(t, W; b, d, q) \leq T_{12}(t, T; b, d, q) \quad (\text{A.7})$$

This is a trivial consequence of the fact that the equivalent transmissivity of *any* graph is a monotonous function of the elementary transmissivity of any of its edges, together with the fact that the breaking (collapsing) of all the “transverse” edges of the Wheatstone-bridge graph precisely yields the diamond (tress) graph (see Fig. 71). It is then straightforward to verify that, in the  $b \rightarrow 1$  limit, the  $RG_{b1}$  recursive relation is *one and the same* for *both* diamond and tress cases (and *consequently for the Wheatstone-bridge case as well*, since it is squeezed between them), namely

$$t' \sim t + \mu \left\{ t \ln t - (d-1) \frac{(1-t)[1+(q-1)t]}{q} \ln \left( \frac{1-t}{1+(q-1)t} \right) \right\} \quad (\text{A.8})$$

The corresponding critical fixed point  $t^*$  satisfies

$$t^* \ln t^* = (d-1) \frac{(1-t^*)[1+(q-1)t^*]}{q} \ln \left[ \frac{1-t^*}{1+(q-1)t^*} \right] \quad (\text{A.9})$$

This equation yields the results presented in Fig. 72 as well as the following ones:

$$t^* \sim 1 - qe^{-\frac{1}{d-1}} \quad (d \rightarrow 1 + 0 ; q > 1) \quad (\text{A.10})$$

which recovers the asymptotically *exact* result for the  $d$ -dimensional hypercubic lattice [25] (see eq. 33);

$$t^* = \frac{1}{\sqrt{q} + 1} \quad (d = 2) \quad (\text{A.11})$$

which is the *exact* result for the square lattice; and

$$t^* \sim e^{-(d-1)} \quad (d \rightarrow \infty) \quad (\text{A.12})$$

which differs from the exact result for  $d$ -dimensional hypercubic lattice.

The fact that the  $d \rightarrow 1$  result is asymptotically exact comes from the fact that the linear chain has an unique topological property, namely to be scale invariant (hierarchical lattice) and translationally invariant (Bravais lattice) simultaneously. The fact that the  $d = 2$  result exactly recovers that of the square lattice comes from the confluence of

the diamond and tress equivalent transmissivities into the *self-dual* Wheatstone-bridge equivalent transmissivity. This is a nice manner for understanding why the *differential* Migdal-Kadanoff approach preserves self-duality.

From Eq. (A.8) we also obtain the thermal critical exponent:

$$\nu^{-1} = 1 + \ln t^* - \frac{d-1}{q} \left\{ [q-2 - 2(q-1)t^*] \ln \left( \frac{1-t^*}{1+(q-1)t^*} \right) - q \right\} \quad (\text{A.13})$$

This equation yields the results shown in Fig. 73 as well as the following ones:

$$\nu \sim \frac{1}{d-1} \quad (d \rightarrow 1+0) \quad (\text{A.14})$$

which recovers the *exact* result for d-dimensional hypercubic lattice (see eq. 34) [25]; and

$$\nu^{-1} = 2 \left( 1 - \frac{1}{\sqrt{q}} \ln(\sqrt{q} + 1) \right) \quad (d = 2) \quad (\text{A.15})$$

and

$$\nu \rightarrow 1 \quad (d \rightarrow \infty) \quad (\text{A.16})$$

which do not coincide with the exact results for the hypercubic lattice [91, 321].

## FIGURE CAPTIONS

**Fig. 1** - Typical phase diagrams of the site-bond percolation ( $S \cap B$ ) and site-or-bond percolation ( $SUB$ ) on  $d$ -dimensional lattices ( $d > 1$ ).  $P$  and  $NP$  respectively denote the percolating and non-percolating regions;  $p_c$  (bond) ( $p_c$  (site)) corresponds to the critical probability of the standard bond (site) percolation.

**Fig. 2** - Two-site spin configurations and its corresponding energy spectrum for the  $Z(4)$  interaction (assuming that  $0 < J_2 < J_1/2$ ) and the  $Z(5)$  one (supposing that  $0 < J_2 < J_1$ ). The spin state  $n_i$  ( $n_i = 0, 1, 2, \dots, q - 1$ ) is represented by a vector pointing into a direction which makes an angle  $2\pi n_i/q$  with the direction shown on the left (which corresponds to  $n_i = 0$ ). For each pair configuration, the heavy line corresponds to its energy while the dashed ones refer to the remaining energy levels of the considered spectrum.

**Fig. 3** - Schematic phase diagram for a quenched bond-and-site diluted ferromagnet on  $d$ -dimensional lattices ( $d > 1$ ).  $P$  and  $F$  respectively denote the paramagnetic and ferromagnetic phases.

**Fig. 4** -  $q$ -dependence of the correlation length critical exponent  $\nu$  for the Potts ferromagnet on the square lattice. The lower curve corresponds to the exact result (given by eq. 36) while the others were obtained through the correlation function preserving  $RG_{bb'}$  using the cells shown in Fig. 27.

**Fig. 5** -  $q$ -dependence of the critical exponent  $\beta$  for the Potts ferromagnet on the square lattice. The exact result (given by eq. 37) is represented by the lower curve (“square lattice”); the remaining curves [228] correspond to successive  $RG_{bb'}$  approximations using the cells shown in Figs. 11(a) – (d). The broken lines are indicative and have been used when the calculation was available only for integer values of  $q$ .

**Fig. 6** - Schematic variation of the main features concerning phase transitions for the  $q$ -state Potts ferromagnet on  $d$ -dimensional Bravais lattices. The transition is of first order above the full line, otherwise it is continuous whenever it exists ( $d > 1$ ).

The broken line at  $d = 6$  for  $q < 2$  separates the region where the critical exponents are classical (mean-field ones) from that with non-trivial ones (notice that for  $q = 2$  this occurs at  $d = 4$ ).

**Fig. 7** - Exact critical temperature (eq. 38) as a function of  $J_y/J_x$  for different values of  $q$  for the anisotropic Potts ferromagnet on the square lattice.  $F$  and  $P$  represents the ferromagnetic and paramagnetic phases respectively.

**Fig. 8** - Exact critical temperature as a function of  $q$  for the ferromagnetic ( $J > 0$ ) and antiferromagnetic ( $J < 0$ ) isotropic Potts model on the square lattice (respectively given by eqs. (38) and (43) at  $J_x = J_y$ ).

**Fig. 9** - Critical temperature as a function of  $J_2$ -concentration  $p$  for different values of  $J_1/J_2$  (numbers parametrizing the curves) for the quenched bond mixed Ising ferromagnet on the square lattice. These curves were obtained [107] through the correlation function preserving  $RG_{21}$  using the cells shown in Fig. 11(a) and (b).  $P$  and  $F$  denotes the paramagnetic and ferromagnetic phases respectively.

**Fig. 10** - (a) Phase diagram of the  $Z(4)$  ferromagnet on the square lattice in the  $(t_1, t_2)$  space (defined in eq. 224) obtained through the  $RG_{21}$  approximation [121] with the cells shown in Figs. 11(a) and (b).  $\tilde{P}$  is the  $q = 4$  Potts fixed point;  $I_1$ ,  $I_2$  and  $I_3$  are the Ising fixed points.  $\blacksquare$  denotes the attractors of the paramagnetic (P), ferromagnetic (F) and intermediate (I) phases. The shaded region is nonphysical. The  $t_2 = t_1$  and  $t_2 = t_1^2$  dashed lines represent Potts and Ising invariant subspaces respectively. (b) Same phase diagram in the  $(k_B T/J_1, (J_1 + 2J_2)/J_1)$  space. The dashed lines are asymptotes.

**Fig. 11** -  $d$ -dimensional two-rooted graphs of the Wheatstone bridge type with chemical length  $b$ . The roots 1 and 2 (internal vertices) are represented by open (full) small circles. The fractal dimensions  $d_f$  are also indicated.

**Fig. 12** - Pairs of two-rooted dual graphs. To each edge is associated an occupancy probability  $p_i$ ;  $p_i^D$  refers to its corresponding dual (eq. 77).

**Fig. 13** - Two-rooted graphs which contain at least one irrelevant edge. Open (full) small circles denote roots (internal vertices).

**Fig. 14** - Multi-rooted graphs.  $G^c$  and  $G^b$  are the respective collapsed and broken graphs obtained from  $G$  by contracting (i.e., collapsing after deleting) and deleting one of its edges. The polynomials in figs. (d), (e) and (f) represent the multi-connectedness function (i.e., the probability of connection of all the roots).

**Fig. 15** - Series (a) and parallel (b) array of two edges. To each vertex  $i$  is associated the Potts variable  $\sigma_i = 1, 2, \dots, q$ . The coupling constants are denoted by  $J_\ell (\ell = 1, 2, s, p)$ .

**Fig. 16** - Two-rooted oriented graphs.  $p_\ell$  denotes the occupancy probability of the oriented edge  $\ell$ . The arrows near the roots 1 and 2 indicate the sense (from 1 to 2) on which the graph should be traversed. The graphs obtained in (b) and (c) are, respectively, the 1-broken and the 1-precollapsed oriented graphs obtained from the one in (a). The 2 graphs in (b) are equivalent.

**Fig. 17** - A two-rooted oriented graph  $G$  (Fig. a) and the following graphs obtained through operating on the horizontal edges: (b) the broken  $G^{bb}$ , (c) the collapsed  $G^{cc}$ , (d) the precollapsed  $G^{bc}$  and (e) the precollapsed  $G^{cb}$  graphs. The arrows near the roots 1 and 2 indicate the sense (from 1 to 2) on which the graph should be traversed.

**Fig. 18** - The two-rooted Wheatstone bridge graph whose edges are associated with the vectors  $(p_i, q_i, r_i, s_i)$  ( $i = 1, 2, \dots, 5$ ) whose components respectively represent the probabilities of the edge being ferromagnetic, antiferromagnetic, absent and frustrated.

**Fig. 19** - Two-rooted graph whose edges are all associated with the vector  $(p, q, r, s)$  whose components represent the respective probabilities of the edge being ferromagnetic, antiferromagnetic, absent and frustrated.

**Fig. 20** - (a) The two-rooted Wheatstone-bridge graph whose edges are associated with the transmissivities  $(t_1^{(\ell)}, t_2^{(\ell)})$  ( $\ell = 1, 2, \dots, 5$ ) defined in eqs. (224) for the  $Z(4)$

model. The graphs obtained from (a) by operating on the edge 5 are: (b) the broken, (c) the collapsed and (d) the precollapsed graphs.

**Fig. 21** - (a) The two-rooted Wheatstone-bridge graph whose edges are associated with the vector transmissivities  $(t_1^{(\ell)}, t_2^{(\ell)}, t_3^{(\ell)})$  ( $\ell = 1, 2, \dots, 5$ ) defined in eqs. (243) for the  $Z(6)$  model. Operating on the edge 5 we obtain the following graphs: (b) the broken, (c) the collapsed, (d) the precollapsed  $G^{bcb}$  and (e) the precollapsed  $G^{bbc}$  one.

**Fig. 22** - Rooted mod-6  $\alpha$  flows for a fixed external flow  $\alpha$  ( $\alpha = 0(a)$ ,  $\alpha = 1(b)$ ,  $\alpha = 2(c)$  and  $\alpha = 3(d)$ ) on a terminal graph  $G_{pr}$  with 2 precollapsed edges of type 2 (represented by broken lines) and 3 precollapsed edges of type 3 (represented by dotted lines). The number on each edge represents the flow component along the considered edge.

**Fig. 23** - The non-equivalent terminal graphs  $G_{pr}$  associated with the graph  $G$  shown in Fig. 21a. The broken (dotted) line stands for a precollapsed edge of type 2 (type 3) whose vector transmissivity is  $(0, 1, 0)$  ( $(0, 0, 1)$ ). The equivalent vector transmissivity  $(T_1, T_2, T_3)$  associated with each graph is shown below it.

**Fig. 24** - Typical phase diagrams (full lines) and RG flows (dashed lines) in the  $(Y_1, Y_2)$  parameter space.  $\square$ ,  $\bullet$  and  $\circ$  respectively denote trivial (fully stable), critical (semi-stable) and multicritical (fully unstable) fixed points; A, B and C denote statistical equilibrium phases. (a) The critical line presents 3 universality classes (two critical and one multicritical), the  $Y_2 = 0$  point of the critical line is simultaneously a critical point and a fixed point, and can be determined by treating the  $Y_2 = 0$  particular case of the system because the  $Y_2 = 0$  axis is an *invariant subspace* under RG; the  $Y_1 = 0$  point of the critical line is a critical point but not a fixed point consequently its determination demands the treatment of the general  $(Y_1, Y_2)$  problem. (b) The critical lines present 4 universality classes (three critical and one multicritical); one of the critical fixed points is at infinity (“run away” fixed point), and consequently the B-C critical line might be a first-order one.

**Fig. 25** - The correlation length critical exponent  $\nu$  as a function of  $q$  for the  $q$ -state Potts ferromagnet on the square lattice. The  $RG_{bb'}$  curves were obtained through the correlation function preserving RG using cells from the  $d = 2$  Wheatstone-bridge graph family (see Figs. 11(a) – (d)). The exact result (eq. 36) is also plotted for comparison.

**Fig. 26** - The initial steps ( $n = 0, 1, 2$ ) of construction of the Wheatstone-bridge hierarchical lattice. The replacement of each bond by the generator ( $n = 1$ ) in the  $n^{\text{th}}$  step leads to the next step of construction. The hierarchical lattice corresponds to the  $n \rightarrow \infty$  limit whose fractal dimension is  $d_f = \ln 5 / \ln 2$ .

**Fig. 27** -  $b$ -sized cells and their two-rooted self-dual graph representations; all the entrances, and all the exits of the cell, indicated by arrows, are to be respectively collapsed in order to generate the two roots 1 and 2 (noted by empty small circles) of the associated graph; the internal sites of the cell become, without any modification, the internal vertices (noted by full small circles) of the graph. The full (dashed) line is associated with a transmissivity  $t_x(t_y)$  for the anisotropic Potts model.

**Fig. 28** - (a)  $RG_{31}$  flow diagram and critical frontier in the transmissivity space  $(t_x, t_y)$  for the anisotropic Ising ( $q = 2$ ) ferromagnet on the square lattice using the cells shown in Figs. 27(a) and (b). The critical line coincides with the exact one  $t_x = t_y^D$ .  $P$  and  $F$  denote the respective paramagnetic and ferromagnetic phases. The fully stable and unstable fixed points are represented by  $\square$  and  $\bullet$ . (b) Critical flow lines associated with various values of  $q$  and any value of  $b$ -sized cell shown in Fig. 27 (they coincide with the exact ones for the anisotropic Potts ferromagnet on the square lattice). The  $q \rightarrow 0$  limit corresponds to tree-like percolation; the  $q$ - and  $q^{-1}$ -frontiers are, for all values of  $q$ , symmetric with respect to the straight line  $t_x + t_y = 1$ .

**Fig. 29** - The initial steps ( $n = 0, 1, 2$ ) of construction of the inhomogeneous hierarchical lattice corresponding to the  $RG_{31}$  approximation using the cells of Fig. 27.

**Fig. 30** - (a)  $d = 3$  extension of the  $b = 3$  sized cell (disregarding the irrelevant bonds)

of Fig. 27b; (b) the two-rooted graph representation of the cell shown in Fig. 30(a).  $t_x$ ,  $t_y$  and  $t_z$  are the Potts transmissivities along the three crystal axes of the simple cubic lattice represented by full, dotted and dashed lines.

**Fig. 31** -  $RG_{31}$  flow diagram and critical surface [104] for the anisotropic Potts ferromagnet on the simple cubic lattice in the  $(s_x^{(2)}, s_y^{(2)}, s_z^{(2)})$  space (whose coordinates are defined in eq. (281) taking  $h = 1$ ). The attractors of the paramagnetic (P) and ferromagnetic (F) phases are denoted by  $\square$ , while the respective  $d = 1$ ,  $d = 2$  and  $d = 3$  critical fixed points are represented by  $\blacksquare$ ,  $\circ$  and  $\bullet$ .

**Fig. 32** -  $q$ -dependence [104] of the  $RG$  critical point (see point  $P_I$  of Fig. 31) corresponding to the isotropic  $d = 3$  Potts ferromagnet (notice the ordinate scale). The dots are series results:  $q = 1$  [322],  $q = 2$  [323],  $q = 3$  [324].

**Fig. 33** - Extrapolated results [104] (represented by full lines) for the critical point corresponding to the particular anisotropic  $d = 3$  Potts ferromagnet where two coupling constants are assumed equal ( $\equiv J_{\perp}$ ) and the third one ( $\equiv J_{//}$ ) possibly different. The isotropic  $d = 1$ ,  $d = 2$  and  $d = 3$  cases are on the ordinate, abscissa and bisectrix respectively. (a)  $q = 1$  (the dots correspond to series results [325]); (b)  $q = 2$  (both dots [326] and circles [327] are series results).

**Fig. 34** -  $q$ -dependence of critical exponents (full lines) obtained through the  $RG_{31}$  approximation [104] for the anisotropic cubic lattice Potts ferromagnet. (a)  $d = 3$  correlation length critical exponent  $\nu_3$  (the dots are series results:  $q = 1$  [328] and  $q = 2$  [329]); (b)  $d = 2 \leftrightarrow d = 3$  crossover exponent  $\phi_{23}$  (the  $q = 1$  dot is a series result [325] while the  $q = 2$  dot is an exact one [330, 331]).

**Fig. 35** - The two-rooted Wheatstone-bridge graph whose edges are associated with the Potts transmissivities  $r_{\ell} (\ell = 1, 2, \dots, 4, 5)$ .

**Fig. 36** - RG flow diagram and critical surface of the quenched bond-mixed  $q$ -state Potts ferromagnet on the square lattice [107] in the  $(p, s_1, s_2)$  space for  $q = 2$ . The attractors of the paramagnetic (P) and ferromagnetic (F) phases are represented by  $\circ$ . The fully unstable and semi-stable fixed points are denoted by  $\bullet$  and  $\blacksquare$ .



respectively. The critical surface is invariant under the  $(p, s_1, s_2) \rightarrow (1 - p, s_2, s_1) \rightarrow (p, 1 - s_1, 1 - s_2)$  transformations and depends very slightly on  $q$  (let us say for  $q \geq 1$ ) and on the  $RG$  linear scaling factor  $b$ . The twisted H-like region determined by  $(s_1 = s_2 = \frac{1}{2} \forall p)$ ,  $(s_1 = \frac{1}{2}, p = 0, \forall s_2)$  and  $(s_2 = \frac{1}{2}, p = 1, \forall s_1)$  corresponds to the pure ferromagnet; the  $p = \frac{1}{2}$  line constitutes an invariant subspace corresponding to the equal concentration model.

**Fig. 37** -  $RG_{21}$  critical temperature of the quenched bond-mixed  $q$ -state Potts ferromagnet on the square lattice [107] as a function of  $J_2$ -concentration  $p$  for typical values of  $q$  and  $J_1/J_2$  (numbers parametrizing curves).

**Fig. 38** - Position of the fixed points which attract almost every point of the critical surface as a function of  $q$  for the quenched bond mixed Potts ferromagnet on the square lattice [107] using the  $RG_{21}$  ( $b = 2$ ) and  $RG_{31}$  ( $b = 3$ ) approximations.

**Fig. 39** -  $q$ -dependence of the  $RG_{21}$  ( $b = 2$ ) pure (full line) and random (dot-dashed line) critical exponents  $\nu_t$  and  $\nu_r$  for the quenched bond mixed Potts ferromagnet on the square lattice [107].  $q^*$  denotes the bifurcation value of  $q$  (see Fig 38); for  $b = 2$ ,  $q^* \simeq 5.3$ . The dashed line represents the exact result for the pure ferromagnet (see eq. (36)) where it was assumed that  $q^* = 2$ .

**Fig. 40** -  $q$ -dependence of the  $RG_{b1}$  ( $b = 2$  and  $3$ ) approximation for the pure to random crossover critical exponent  $\phi_t$  for the quenched bond mixed Potts ferromagnet on the square lattice [107].  $q^*$  denotes the bifurcation value of  $q$ .

**Fig. 41** - Variations of the bifurcation value  $q^*$  and of the value  $q_c$  of  $q$  for which  $\alpha_t = 0$  as functions of the inverse of the  $RG$  linear scaling factor  $b$  for the quenched mixed Potts ferromagnet on the generalized Wheatstone-bridge hierarchical lattices. The dashed lines are speculative ones assuming the Harris criterion to be recovered (i.e.,  $q^* = q_c = 2$ ) in the  $b \rightarrow \infty$  limit.

**Fig. 42** - Portion of a square lattice of double opposite-directed bonds which have independent occupancy probabilities  $p$  (“up” and “right”-directed) and  $q$  (“down” and “left”-directed).

**Fig. 43** -  $RG_{21}$  approximation for the flow diagram and critical frontier of the double opposite-directed bond percolation on the square lattice [28]. The attractors of the double-way percolating ( $P_{+-}$ ), two single-way percolating (up-and right- directed  $P_+$ ; down-and left-directed  $P_-$ ) and non-percolating (NP) phases are represented by ■. The semi-stable and the fully unstable fixed points are denoted by ● and ○ respectively. The arrows indicated the direction of flow under renormalization.

**Fig. 44** -  $RG_{21}$  approximation for the flow diagram and critical frontier at  $T = 0^0K$  for the frustrated Ising model (without dilution) on a square lattice [195]. ■ denote the attractors of the ferromagnetic (F), antiferromagnetic (AF) and spin-glass (SG) phases. The semi-stable and the fully unstable fixed points are represented by ● and ○ respectively. The arrows indicate the direction of flow under renormalization. The flows are symmetric under the transformation  $p \longleftrightarrow q$ .

**Fig. 45** -  $RG_{21}$  approximation for the phase diagram at  $T = 0^0K$  for the quenched bond-random frustrated Ising model on a square lattice [195]. ■ denote the attractors of the ferromagnetic (F), antiferromagnetic (AF), paramagnetic (P) and spin-glass (SG) phases. The semi-stable and fully unstable fixed points are represented by ● and ○ respectively.

**Fig. 46** - The  $s = 0$  cut of Fig. 45 which corresponds to its non-invariant subspace  $p + q + r = 1$ .

**Fig. 47** -  $RG_{21}$  approximation for the flow and phase diagrams for the isotropic  $N$ -component cubic ferromagnet on the square lattice for different values of  $N$  [46]. P, F and I denote the paramagnetic, ferromagnetic and intermediate phases respectively. (a) Flow and phase diagram in the transmissivity  $(t_1, t_2)$  space (defined in eq. (248)). The arrows indicate the  $RG$  flow; the full squares and the full circles respectively indicate stable and unstable fixed points. The line  $t_1 = t_2$  corresponds to the  $2N$ -state Potts model. (b) Phase diagram in the  $(k_B T/J_1, (J_1 + J_2)/J_1)$  space. The dashed lines are asymptotes.

**Fig. 48** -  $N$ -dependences of the thermal correlation length critical exponent  $\nu_T$  and of

the crossover exponent  $\phi$  within the  $RG_{21}$  approximation [46] for the: (a) 2N-state Potts ferromagnet on the square lattice; (b) N-component cubic ferromagnet on the square lattice. In the  $N \rightarrow 0$  limit, which corresponds to the self-avoiding walk (SAW), it was found that  $\nu_T(0) = \ln 2 / \ln(4 - \sqrt{3}) \simeq 0.85$ .

**Fig. 49** -  $q$ -dependences of the thermal (a)  $y_T(y_T = \nu_T^{-1})$  and magnetic (b)  $y_h(y_h = (d+2-\eta)/2)$  anomalous dimensions for the  $q$ -state Potts ferromagnet on the square lattice within the phenomenological  $RG$  approximation [295, 296]. The error bars refer to  $q = 4$  only. The full lines represent the exact results for  $y_T$  [91] and  $y_h$  [92]. The scales on the right refer to the critical exponents  $\alpha = 2(1 - y_T^{-1})$  (a) and  $\delta = y_h/(2 - y_h)$  (b).

**Fig. 50** -  $b = 1, 2$  and  $5$  clusters of spins on the square lattice corresponding to graphs from the Wheatstone-bridge family with chemical length  $b$  (see Fig. 11 (a)-(d)).

**Fig. 51** -  $RG_{b1}$  approximations [298] ( $b = 2$  (a),  $b = 5$  (b)) for the specific heat as a function of the inverse reduced temperature  $K$  for the  $d = 2$  Ising ferromagnet ( $q = 2$ ). The arrows and the dotted curves indicate the exact critical point  $K_c$  and the exact result [6] respectively.

**Fig. 52** -  $RG_{b1}$  approximations [298] for the specific heat as a function of the inverse reduced temperature  $K$  for the  $d = 2$   $q$ -state Potts ferromagnet (dotted curve:  $b = 2$  and  $q = 1.4$ ; full curve:  $b = 5, 4$  and  $3$  if  $q = 2, 3$  and  $4$  respectively). The arrows indicate the exact critical points; the downwards arrow indicates the critical point associated with the  $q \rightarrow 1$  limit ( $C$  vanishes for all  $K$  in this limit).

**Fig. 53** - The  $d = b = 2$  RG percolation ‘specific heat’  $C_p \equiv k_B^{-1}(\partial C / \partial q)|_{q=1}$  [298] as a function of the bond occupancy probability  $p \equiv 1 - e^{-K}$ . The arrow indicates the exact critical point.

**Fig. 54** - Successive  $RG_{bb'}$  approximations [228] for the thermal behavior of the magnetization for the Ising ( $q = 2$ ) ferromagnet on the square lattice. For comparison the exact result [332] is also shown.

**Fig. 55** -  $RG_{21}$  approximation [228] for the thermal behavior of the magnetization for the  $q$ -state Potts ferromagnet on the square lattice for typical values of  $q$ .

**Fig. 56** - Amplitude  $A$  (defined in eq. (335)) of the critical behavior of the magnetization for the Potts ferromagnet on the square lattice as functions of  $q$  within successive  $RG_{bb'}$  approximations [228]. The broken lines are indicative and have been used when the calculation was available only for integer values of  $q$ . For comparison, the exact result [332] for  $A$  in the Ising case ( $q = 2$ ) is also shown.

**Fig. 57** -  $RG_{b1}$  approximations [161] for the thermal behavior of the longitudinal reduced surface tension  $\gamma \equiv \gamma(T)/\gamma(0)$  for the Ising ( $q = 2$ ) ferromagnet on the square lattice. The dashed line corresponds to the exact result [6]. The curves are out of scale (in fact, they are all much closer to the exact result).

**Fig. 58** - Cluster size dependence of the  $RG_{b1}$  coefficients  $A_{b1}$  (defined in eq. (339)) of the critical behavior of the longitudinal reduced surface tension for the Ising ferromagnet on the square lattice [161]. The arrow points to the exact result  $A = 2$  [6].

**Fig. 59** -  $RG_{b1}$  approximations [302] for the thermal behavior of the inverse of correlation length  $\xi^{-1}$  for the Ising ( $q = 2$ ) ferromagnet on the square lattice. For comparison, the exact result [6, 303, 5] is also shown (dashed line).

**Fig. 60** -  $RG_{41}$  approximations ( $b = 4$ ) [302] for the thermal behavior of the inverse of correlation length  $\xi^{-1}$  for the  $q$ -state Potts ferromagnet on the square lattice for typical values of  $q$ .

**Fig. 61** - A typical phase diagram of a semi-infinite ferromagnet with respective bulk and surface coupling constants  $J_B$  and  $J_S$ .  $BF$ ,  $SF$  and  $P$  denote the bulk ferromagnetic, surface ferromagnetic and paramagnetic phases respectively. All three phases join at the surface-bulk multicritical point (special transition). The non-vertical dashed line corresponds to the limiting case where the surface is completely disconnected from the bulk volume.

**Fig. 62** - Free surface  $RG$  cell; the respective dashed and full lines are bonds associated with the surface  $J_S$  and bulk  $J_B$  coupling constants. The arrows are located at the entry and exit nodes (which will generate the two roots of the associated graph).

**Fig. 63** - Flow and phase diagrams for the semi-infinite Ising ( $q = 2$ ) ferromagnet on the simple cubic lattice in the transmissivities space  $(t_S, t_B)$  within the extrapolated  $RG$  approximation of ref. [138].  $BF$ ,  $SF$  and  $P$  refer to the bulk ferromagnetic, surface ferromagnetic and paramagnetic phases respectively.  $\blacksquare$ ,  $\circ$  and  $\bullet$  denote trivial (fully stable), multicritical (unstable) and critical (semi-stable) fixed points respectively. The broken lines are indicative.

**Fig. 64** -  $q$ -dependences of  $\Delta_c$  and its extrapolated value  $\Delta_c^*$  within the  $RG$  approximation of ref. [138].  $\blacksquare$ ,  $\circ$ ,  $\blacklozenge$  and  $\square$  represent the  $q = 2$  respective results obtained by mean field approximation (see [297] and references therein), and in refs. [333], [334] and [335].

**Fig. 65** -  $q$ -dependences of  $A$  (defined in eq. (354)), its extrapolated value  $A^*$  and the crossover exponent  $\phi$  (defined in eq. (354)) within the  $RG$  approximation of ref. [138].  $\bullet$  and  $\circ$  represent the respective results of [336] and [334].

**Fig. 66** - Phase diagrams of a semi-infinite cubic-lattice  $q$ -state Potts ferromagnet in the  $(T_c(q)/T_c(2), \Delta)$  space for different values of  $q$  within the extrapolated  $RG$  approximation of ref. [138].  $BF$ ,  $SF$  and  $P$  denote the respective bulk ferromagnetic, surface and paramagnetic phases.

**Fig. 67** - The initial steps of construction of different  $b$ -sized  $d$ -dimensional generalized diamond-like and tress-like hierarchical lattices. The roots (1 and 2) and internal sites are represented by empty and full dots respectively.

**Fig. 68** - Critical fixed points  $t_{bb'}^*$  (a) and critical exponent  $\nu$  (b) as functions of the linear size  $b$  for fixed  $b' = 1$  and  $b' = b - 1$  for the Ising ferromagnet on the  $d = 2$  diamond-like and tress-like hierarchical lattices within the  $RG_{bb'}$  approach [143]. The dot-dashed line corresponds to the exact result for the Ising ferromagnet on the square lattice.

**Fig. 69** - Dependences of the critical fixed point  $t^*$  on  $q$  and  $d$  within the  $RG_{21}$  approach [143] for the  $q$ -state Potts ferromagnet on  $d$ -dimensional diamond-like ((a), (b)) and tress-like ((c), (d)) hierarchical lattices. The dot-dashed curves ((a), (c)) refer to the exact results for the Potts ferromagnet on the square lattice. In (b) and (d) the results corresponding to the Ising ferromagnet on the  $d$ -dimensional hypercubic lattice have been included for comparison, the dashed line being a guide to the eye.

**Fig. 70** - Dependence of the critical exponents  $\nu$  on  $q$  and  $d$  within the  $RG_{21}$  approach [143] for the  $q$ -state Potts ferromagnet on  $d$ -dimensional diamond-like and tress-like hierarchical lattices (one and the same for both diamond and tress types). (a)  $\nu$  against  $q$  for typical values of  $d$ ; the dot-dashed curve refers to the exact result for the square lattice. (b)  $\nu$  against  $d$  for typical values of  $q$ ; the results corresponding to the Ising ferromagnet on the  $d$ -dimensional hypercubic lattice have been included for comparison, the dashed line being a guide to the eye.

**Fig. 71** - Illustration, for the linear size  $b = 2$ , of the inequalities among the Potts equivalent transmissivities between the roots 1 and 2 of the  $d$ -dimensional ( $d = 2, 3$ ) generalized Wheatstone-bridge, diamond-like and tress-like graphs.

**Fig. 72** - Dependence of the critical point  $t^*$  on  $q$  and  $d$  within the differential RG approach ( $b = 1$  and  $b \rightarrow 1$ ) [143] for the  $q$ -state Potts ferromagnet on  $d$ -dimensional generalized diamond-like, tress-like and Wheatstone-bridge hierarchical lattices (one and the same for all of these hierarchical lattices). (a)  $t^*$  as function of  $q$  for different values of  $d$  (the  $d = 2$  curve coincides with the exact one for the square lattice). (b)  $t^*$  against  $d$  for various values of  $q$ ; the results corresponding to the Ising ferromagnet on  $d$ -dimensional hypercubic lattices have been included for comparison, the dashed line being a guide to the eye.

**Fig. 73** - Dependence of the critical exponent  $\nu$  on  $q$  and  $d$  within the differential RG approach ( $b = 1$  and  $b \rightarrow 1$ ) [143] for the  $q$ -state Potts ferromagnet on  $d$ -dimensional generalized diamond-like, tress-like and Wheatstone-bridge hierarchical lattices (one and the same for all of these hierarchical lattices). (a)  $\nu$  as function of  $q$  for various values of  $d$  (the exact result for the square lattice is represented by a dot-dashed

line). (b)  $\nu$  against  $d$  for different values of  $q$ ; the results corresponding to the Ising ferromagnet on  $d$ -dimensional hypercubic lattices have been included for comparison, the broken line being a guide to the eye.

## TABLE CAPTIONS

**TABLE I** - Exact values [111] for the  $p = 1$  slopes of the bond-dilute  $q$ -state Potts ferromagnet on the triangular and honeycomb lattices for different values of  $q$ .

**TABLE II** - All non-equivalent configurations of the  $d = b = 2$  Wheatstone-bridge graph (where each bond is either a ferro-precollapsed (dotted line) or an antiferro-precollapsed (dashed line) one) and their corresponding ground-state energies  $E^{(\ell)}/|J|$  and degeneracies  $g^\ell$  ( $\ell = F, AF$ ) when the rooted spins are in the same state (F configuration) or in different states (AF configuration). The resulting equivalent bond according to rule (208) is also given (the wavy line corresponding to a frustrated bond). The open (full) dots correspond to the roots (internal vertices).

**TABLE III** - Family of two-rooted graphs with finite chemical length  $b$  and  $N$  incident edges on each root used to treat spin models on the square lattice. The  $b \rightarrow \infty$  limit corresponds to infinite strips with width  $N$ , very common in the phenomenological  $RG$  approach.

**TABLE IV** - The non-vanishing  $\{n_i(q), d_i(q)\}$  coefficients which appear in the equivalent transmissivities (see eq. 270)) between the roots 1 and 2 of the  $q$ -state Potts model on the generalized  $d = 2$   $b$ -sized Wheatstone-bridge graphs (shown in Figs. 11(a)-(d)) whose iterations lead to hierarchical lattices with fractal dimensions  $d_f = \ln[b^2 + (b - 1)^2]/\ln b$  for different values of  $b$ . They satisfy, according to Eq. (124),  $\sum_i n_i(q) = 1 + \sum_i d_i(q) = q^c$  where  $c = b(b - 1)$ .

**TABLE V** - The  $\{a_i, b_i\}$  coefficients [107] which appear in the expression of  $\lambda_b \equiv \left[ \frac{dT_{12}(t, G_b)}{dt} \right]_{t=1/(\sqrt{q}+1)}$  (see eq. (272)) as function of  $q$  in the  $q$ -state Potts model, using as cells the generalized  $d = 2$   $b$ -sized Wheatstone-bridge graphs, for different values of  $b$ .

**TABLE VI** -  $RG_{bb'}$  approximations  $\nu_{bb'}$  for the critical exponent  $\nu$  of the  $q$ -state Potts model on the square lattice, using as cells the generalized  $d = 2$   $b$ -sized Wheatstone-bridge graphs, for different values of  $b$ ,  $b'$  and  $q$  ( $q = 1, 2, 3, 4$ ). The asymptotic be-



haviors for  $q \rightarrow 0$  and  $q \rightarrow \infty$  (the latter one being equal to  $\ln(b/b')/\ln\{[b^2 + (b-1)^2]/[b'^2 + (b'-1)^2]\}$ ) are also included.

**TABLE VII** -  $RG_{bb'}$  approximations  $\nu_{bb'}$  for the critical exponent  $\nu$  of the  $q$ -state Potts model on the square lattice, using as cells those shown in Fig. 27, for different values of  $b$ ,  $b'$  and  $q$  ( $q = 1, 2, 3, 4$ ). The asymptotic behaviors for  $q \rightarrow 0$  and  $q \rightarrow \infty$  are also included.

**TABLE VIII** - Critical points ( $k_B T_c/qJ_x$ ) for the  $q$ -state anisotropic Potts ferromagnet on the simple cubic lattice [104] for  $q = 1$  (a), 2 (b) and 3(c):  $RG$  (top) and extrapolated (bottom) values. \* indicates exact results (see, for example, [3]) for the isotropic  $d = 2$  case; § [322], & [323] and §§ [324] are series results for the isotropic  $d = 3$  case.

**TABLE IX** - Non-equivalent configurations of the  $q$ -state Potts ferromagnet on the graphs  $G'$  (a single edge) and  $G$  (Wheatstone-bridge) with their corresponding total degeneracies (where the multiplying factor 2 accounts for the equivalent symmetric configuration), Boltzmann weights and cluster magnetic momenta  $m$  (where each spin contributes proportionally to its coordination number) necessary to calculate eq. (333). The spin at the root 1 (at the top) is fixed in the state  $\sigma = 0$  (noted  $\uparrow$ ).  $\blacksquare$  represents the  $(q-1)$  configurations different from  $\uparrow$ ;  $\bullet$  denotes the  $(q-2)$  configurations different from  $\uparrow$  and  $\blacksquare$ , while  $\blacktriangle$  represents the  $(q-3)$  configurations different from  $\uparrow$ ,  $\blacksquare$  and  $\bullet$ .

## References

- [1] R.B. Potts, PhD Thesis (1951) University of Oxford; Proc. Camb. Phil. Soc. **48**, 106 (1952).
- [2] C. Domb, J. Phys. **A7**, 1335 (1974).
- [3] F.Y. Wu, Rev. Mod. Phys. **54**, 235 (1982).
- [4] F.Y. Wu, J. Appl. Phys. **55**, 2421 (1984).
- [5] R.J. Baxter, “Exactly solved models in Statistical Mechanics” (Academic Press, 1982).
- [6] L. Onsager, Phys. Rev. **65**, 117 (1944).
- [7] J.W. Essam, in “Phase Transitions and Critical Phenomena”, eds. C. Domb and M.S. Green, Vol. 2, 197 (1972).
- [8] S. Kirkpatrick, Rev. Mod. Phys. **45**, 574 (1973).
- [9] D. Stauffer, Phys. Rep. **54**, 1 (1979).
- [10] J.W. Essam, Rep. Progr. Phys. **43**, 833 (1980).
- [11] A. Coniglio, Phys. Rev. Lett. **46**, 250 (1981).
- [12] D. Stauffer, A. Coniglio and M. Adam, Adv. Polymer Sc. **44**, 103 (1982).
- [13] C.-K. Hu, Chinese J. Phys. **22**, 1 (1984) and Phys. Rev. **29**, 5109 (1984).
- [14] D. Stauffer and A. Aharony, “Introduction to Percolation Theory” (Taylor and Francis, London, revised 2nd edition 1994).
- [15] M. Sahimi, “Applications of Percolation Theory” (Taylor and Francis, London, 1994).
- [16] P. Kasteleyn and C. Fortuin, J. Phys. Soc. Jap. (suppl.) **26**, 11 (1969).
- [17] M.J. Stephen, Phys. Rev. **15**, 5674 (1977).

- [18] F.W. Wu, *J. Stat. Phys.* **18**, 115 (1978).
- [19] M.R. Giri, M.J. Stephen and G.S. Grest, *Phys. Rev.* **B16**, 4971 (1977).
- [20] H. Kunz and F.Y. Wu, *J. Phys.* **C11**, L1 (1978).
- [21] H.N.V. Temperley and S.E. Ashley, *J. Phys.* **A15**, 215 (1982).
- [22] D.K. Arrowsmith and J.W. Essam, *Phys. Rev. Lett.* **65**, 3068 (1990).
- [23] L. Turban, *J. Phys.* **A16**, L15 (1983).
- [24] F. Sevšek, J.M. Debierre and L. Turban, *J. Phys.* **A16**, 801 (1983).
- [25] M.J. Stephen, *Phys. Lett.* **56 A**, 149 (1976).
- [26] G. Deutscher, *Lecture Notes in Physics* **149**, eds. C. Castellani, C. Di Castro and L. Peliti (Berlin, Springer, 1981) p. 26.
- [27] S. Redner, *J. Phys.* **A14**, L349 (1981).
- [28] C. Tsallis and S. Redner, *Phys. Rev.* **B28**, 6603 (1983).
- [29] F. Y. Wu and Y.K. Wang, *J. Math. Phys.* **17**, 439 (1976).
- [30] J.B. Kogut, *Rev. Mod. Phys.* **51**, 659 (1979).
- [31] R. Savit, *Rev. Mod. Phys.* **52**, 453 (1980).
- [32] F.C. Alcaraz and R. Köberle, *J. Phys.* **A13**, L153 (1980).
- [33] F.C. Alcaraz and R. Köberle, *J. Phys.* **A14**, 1169 (1981).
- [34] H. Moraal, “Classical, Discrete Spin Models: Symmetry, Duality and Renormalization”, *Lectures Notes in Physics* **214** (Springer-Verlag, 1984).
- [35] H. Au-Yang and J.H.H. Perk, *J. Stat. Phys.* **78**, 17 (1995).
- [36] J. Yeomans, *Solid State Physics* **41**, 151 (Academic, New York, 1990).
- [37] A.N. Berker, S. Ostlund and F.A. Putnam, *Phys. Rev.* **B17**, 3650 (1978).

- [38] F.Y. Wu and H.E. Stanley, *J. Phys.* **A16**, L751 (1983).
- [39] D. Prato, C. Tsallis and H.E. Stanley, *Physica* **A164**, 28 (1990).
- [40] H.E. Stanley, in “Phase Transitions and Critical Phenomena”, eds. C. Domb and J.L. Lebowitz, Vol. 3, 486 (Academic, London, 1974).
- [41] D. Kim, P.M. Levy and L.F. Uffer, *Phys. Rev.* **B12**, 989 (1975).
- [42] A. Aharony, *J. Phys.* **A10**, 389 (1977).
- [43] H.J. Hilhorst, *Phys. Rev.* **B16**, 1253 (1977).
- [44] B. Nienhuis, E.K. Riedel and M. Schick, *Phys. Rev.* **B27**, 5625 (1983).
- [45] R. Badke, P. Reinicke and V. Rittenberg, *J. Phys.* **A18**, 653 (1985).
- [46] C. Tsallis, A.M. Mariz, A. Stella and L.R. da Silva, *J. Phys.* **A23**, 329 (1990).
- [47] A.C.N. de Magalhães and J.W. Essam, *J. Stat. Phys.* **58**, 1059 (1990).
- [48] E.P. da Silva, A.M. Mariz and C. Tsallis, *J. Phys.* **A24**, 2835 (1991).
- [49] H.R. da Cruz, U.M.S. Costa and C. Tsallis, *Physica* **A181**, 406 (1992).
- [50] A.M.C. de Souza, C. Tsallis and A.M. Mariz, *Phys. Rev.* **B47**, 11940 (1993).
- [51] E. Domany and E.K. Riedel, *Phys. Rev.* **B19**, 5817 (1979).
- [52] P.G. de Gennes, *Phys. Lett.* **38 A**, 339 (1972).
- [53] A. Coniglio, H.E. Stanley and W. Klein, *Phys. Rev. Lett.* **42**, 518 (1979).
- [54] I. Syozi, in “Phase Transitions and Critical Phenomena”, eds. C. Domb and M.S. Green, Vol. 1, 270 (1972).
- [55] R.B. Stinchcombe, in “Phase Transitions and Critical Phenomena”, eds. C. Domb and J.L. Lebowitz, Vol. 7, 151 (1983).
- [56] H.N.V. Temperley, in “Phase Transitions and Critical Phenomena”, eds. C. Domb and M.S. Green, Vol. 1, 227 (1972).

- [57] S.R. Salinas and J.F. Nagle, Phys. Rev. **B9**, 4920 (1974).
- [58] K. Binder and A.P. Young, Rev. Mod. Phys. **58**, 801 (1986).
- [59] M. Blume, Phys. Rev. **141**, 517 (1966).
- [60] H.W. Capel, Physica **32**, 966 (1966), **33**, 295 (1967) and **37**, 423 (1967).
- [61] M. Blume, V.J. Emery and R.B. Griffiths, Phys. Rev. **A4**, 1071 (1971).
- [62] S.R. Broadbent and J.M. Hammersley, Proc. Camb. Phil. Soc. **53**, 629 (1957).
- [63] M. Aizenman, H. Kesten and C.M. Newman, Commun. Math. Phys. **111**, 505 (1987).
- [64] A.N. Berker and S. Ostlund, J. Phys. **C12**, 4961 (1979).
- [65] M. Kaufman and R.B. Griffiths, Phys. Rev. **B24**, 496 (1981).
- [66] R.B. Griffiths and M. Kaufman, Phys. Rev. **B26**, 5022 (1982).
- [67] H. Nakanishi and P.J. Reynolds, Phys. Lett. **71 A**, 252 (1979).
- [68] C. Tsallis and S.V.F. Levy, Phys. Rev. Lett. **47**, 950 (1981).
- [69] W. Kinzel, in “Percolation structure and processes” eds. G. Deutscher, R. Zallen and J. Adler, Annals of the Israel Phys. Soc. 5 (Hilger, Bristol, 1983).
- [70] S.P. Obukhov, Physica **A101**, 145 (1980).
- [71] J.L. Cardy and R.L. Sugar, J. Phys. **A13**, L423 (1980).
- [72] E. Domany and W. Kinzel, Phys. Rev. Lett. **47**, 5 (1981).
- [73] D. Dhar, M. Barma and M.K. Phani, Phys. Rev. Lett. **47**, 1238 (1981).
- [74] S. Redner, Phys. Rev. **B24**, 3242 (1982).
- [75] S. Redner, Phys. Rev. **B24**, 5646 (1982).
- [76] R. Durrett, Annals of Probability **12**, 999 (1984).

- [77] J.W. Essam, A.J. Guttman and K. De'Bell, *J. Phys.* **A21**, 3815 (1988).
- [78] C. Tsallis, *J. Stat. Phys.* **52**, 479 (1988).
- [79] E.M.F. Curado and C. Tsallis, *J. Phys.* **A24**, L69 (1991); Corrigenda: *J. Phys.* **A24**, 3187 (1991) and **25**, 1019 (1992).
- [80] E.P. da Silva, C. Tsallis and E.M.F. Curado, *Physica* **A199**, 137 (1993); Erratum: **203**, 160 (1994).
- [81] J. Ashkin and E. Teller, *Phys. Rev.* **64**, 178 (1943).
- [82] H. Au-Yang, B.M. McCoy, J.H.H. Perk and M.L. Yan, *Phys. Lett.* **123A**, 219 (1987).
- [83] M.L. Martins and C. Tsallis, *J. Phys.* **A23**, 3043 (1990).
- [84] Y.K. Wang and F.Y. Wu, *J. Phys.* **A9**, 593 (1976); F.Y. Wu and Y.K. Wang, *J. Math. Phys.* **17**, 439 (1976).
- [85] J.M. Maillard, F.Y. Wu and C.-K. Hu, *J. Phys.* **A25**, 2521 (1992).
- [86] R.B. Griffiths and J.L. Lebowitz, *J. Math. Phys* **9**, 1284 (1968).
- [87] T.K. Bergstresser, *J. Phys.* **C10**, 3831 (1977).
- [88] S. Goulart Rosa Jr., *Phys. Lett.* **78 A**, 468 (1980) and **80 A**, 185 (1980); *J. Phys.* **A15**, L51 (1982).
- [89] S. Sarbach and F.Y. Wu, *Z. Phys.* **B44**, 309 (1981).
- [90] T. Horiguchi, *Phys. Lett.* **86A**, 437 (1981).
- [91] J.L.Black and V.J. Emery, *Phys. Rev.* **B23**, 429 (1981); M.P.M. den Nijs, *J. Phys.* **A12**, 1857 (1979).
- [92] M.P.M. den Nijs, *Phys. Rev.* **B27**, 1674 (1983).
- [93] A.C.N. de Magalhães and C. Tsallis, *J. Physique* **42**, 1515 (1981).
- [94] B. Nienhuis, E.K. Riedel and M. Schick, *Phys. Rev.* **B23**, 6055 (1981).

- [95] E.K. Riedel, *Physica* **A106**, 110 (1981).
- [96] A. Aharony and E. Pytte, *Phys. Rev.* **B23**, 362 (1981).
- [97] D. Andelman and A.N. Berker, *J. Phys.* **A14**, L91 (1981).
- [98] R.J. Baxter, H.N.V. Temperley and S.E. Ashley, *Proc. Roy. Soc. London, Ser.* **A358**, 535 (1978).
- [99] T.W. Burkhardt and B.W. Southern, *J. Phys.* **A11**, L247 (1978).
- [100] C. Tsallis and A.C.N. de Magalhães, *J. Physique Lett.* **42**, L227 (1981).
- [101] R.J. Baxter, *Proc. R. Soc. London Ser.* **A383**, 43 (1982).
- [102] H.W.J. Blöte and R.H. Swendsen, *Phys. Rev. Lett.* **43**, 799 (1979); S.J.K. Jensen and O.G. Mouritsen, *Phys. Rev. Lett.* **43**, 1736 (1979).
- [103] M. Kolesik and M. Suzuki, *Physica* **A215**, 138 (1995).
- [104] L.R. da Silva, C. Tsallis and G. Schwachheim, *J. Phys.* **A17**, 3209 (1984).
- [105] J.W. Essam and K.M. Gwilym, *J. Phys.* **C4**, L228 (1971).
- [106] F. Peruggi, F. di Liberto and G. Monroy, *J. Phys.* **A16**, 811 (1983) and *Physica* **141A**, 151 (1987).
- [107] U.M.S. Costa and C. Tsallis, *Physica* **128A**, 207 (1984).
- [108] C. Tsallis and R.J.V. dos Santos, *J. Phys.* **A16**, 3601 (1983).
- [109] C. Tsallis, *J. Phys.* **C14**, L85 (1981).
- [110] R.Fisch, *J. Stat. Phys.* **18**, 111 (1987).
- [111] B.W. Southern and M.F. Thorpe, *J. Phys.* **C12**, 5351 (1979).
- [112] W. Kinzel and E. Domany, *Phys. Rev.* **B23**, 3421 (1981).
- [113] S. Sarbach and F.Y. Wu, *Z. Phys.* **B44**, 309 (1981).

- [114] J.P. Straley, Phys. Rev. **B15**, 5733 (1977).
- [115] J. Bernasconi, Phys. Rev. **B18**, 2185 (1978).
- [116] J.M. Luck, J. Phys. **A18**, 2061 (1985).
- [117] R. Fogelholm, J. Phys. **C13**, L571 (1980).
- [118] U.M.S. Costa, C. Tsallis and G. Schwachheim, Phys. Rev. **B33**, 510 (1986).
- [119] J.P. Straley, Phys. Rev. **B15**, 5733 (1977).
- [120] F.C. Alcaraz and C. Tsallis, J. Phys. **A15**, 587 (1982).
- [121] A.M. Mariz, C. Tsallis and P. Fulco, Phys. Rev. **B32**, 6055 (1985).
- [122] M. Kohmoto, M. den Nijs and L. Kadanoff, Phys. Rev. **B24**, 5229 (1981).
- [123] H.A. Kramers and G.H. Wannier, Phys. Rev. **60**, 252 (1941).
- [124] J.L. Cardy, J. Phys. **A13**, 1507 (1980).
- [125] C. Tsallis and J. Souletie, J. Phys. **A19**, 1715 (1986).
- [126] M.F. Sykes and J.W. Essam, Phys. Rev. Lett. **10**, 3 (1963) and J. Math. Phys. **5**, 1117 (1964).
- [127] C. Tsallis, Kinam/Revista de Física (Mexico) **3**, 79 (1981).
- [128] J.R. Melrose, J. Phys. **A16**, L407 and 3077 (1983).
- [129] A.C.N. de Magalhães, J.W. Essam and F.Y. Wu, J. Phys. **A23**, 2651 (1990).
- [130] G.H. Wannier, Rev. Mod. Phys. **17**, 50 (1950).
- [131] J.W. Essam and M.E. Fisher, Rev. Mod. Phys. **42**, 272 (1970).
- [132] J.W. Essam, J. Math. **12**, 874 (1971).
- [133] A.C.N. de Magalhães and J.W. Essam, J. Phys. **A21**, 473 (1988).



- [134] P.J. Reynolds, W. Klein and H.E. Stanley, *J. Phys.* **C10**, L167 (1977).
- [135] J.M. Yeomans and R.B. Stinchcombe, *J. Phys.* **C13**, L239 (1980).
- [136] P.M.C. de Oliveira and C. Tsallis, *J. Phys.* **A15**, 2865 (1982).
- [137] P.M. Oliveira, C. Tsallis and G. Schwachheim, *Phys. Rev.* **B29**, 2755 (1984).
- [138] U.M.S. Costa, C. Tsallis and E.F. Sarmiento, *J. Phys.* **C18**, 5749 (1985) and 6199 (1985).
- [139] J.W. Essam and C. Tsallis, *J. Phys.* **A19**, 409 (1986).
- [140] A.C.N. de Magalhães and J.W. Essam, *J. Phys.* **A19**, 1655 (1986).
- [141] S.B. Cavalcanti and C. Tsallis, *J. Phys.* **C19**, 6799 (1986).
- [142] E.F. Sarmiento and C. Tsallis, *J. Physique* **47**, 1115 (1986).
- [143] L.R. da Silva and C. Tsallis, *J. Phys.* **A20**, 6013 (1987).
- [144] U.M.S. Costa, I. Roditi and E.M.F. Curado, *J. Phys.* **A20**, 6001 (1987).
- [145] P.R. Hauser and E.M.F. Curado, *J. Stat. Phys.* **52**, 517 (1988).
- [146] L.R. da Silva, C. Tsallis and E.F. Sarmiento, *Phys. Rev.* **B37**, 7832 (1988).
- [147] E.L. Albuquerque, E.F. Sarmiento and C. Tsallis, *Physica* **B155**, 372 (1989).
- [148] F.S. Aguiar and S. Goulart Rosa, Jr., *Phys. Lett.* **A143**, 186 (1990); F.S. de Aguiar, F.A. Bosco, A.S. Martinez and S. Goulart Rosa, Jr., *J. Stat. Phys.* **58**, 1231 (1990).
- [149] A. Chame and U.M.S. Costa, *J. Phys.* **A23**, L1127 (1990).
- [150] R.R. dos Santos, N.S. Branco and S.L.A. de Queiroz, *Europhys. Lett.* **13**, 647 (1990).
- [151] F.S. de Menezes and A.C.N. de Magalhães, *Phys. Rev.* **B46**, 11642 (1992).
- [152] J.A. Redinz, A.C.N. de Magalhães and E.M.F. Curado, *Phys. Rev.* **B49**, 6689 (1994).

- [153] J.M.R. dos Santos and P.L. Christiano, *Phys. Lett.* **A195**, 198 (1994).
- [154] C. Domb, in “Phase Transitions and Critical Phenomena”, eds. C. Domb and M.S. Green, vol. 3, 357 (1974).
- [155] D.R. Nelson and M.E. Fisher, *Ann. of Phys.* **91**, 226 (1975).
- [156] J.M. Yeomans and R.B. Stinchcombe, *J. Phys.* **C11**, L525 (1978).
- [157] J.M. Yeomans and R.B. Stinchcombe, *J. Phys.* **C12**, 347 (1979).
- [158] C. Tsallis, *J. Magn. Magnetic Materials* **15**, 243 (1980).
- [159] C. Tsallis and S.V.F. Levy, *J. Phys.* **C13**, 465 (1980).
- [160] S.V.F. Levy, C. Tsallis and E.M.F. Curado, *Phys.* **B21**, 2991 (1980).
- [161] E.M.F. Curado, C. Tsallis, S.V.F. Levy and M.J. de Oliveira, *Phys. Rev.* **B23**, 1419 (1981).
- [162] N-C. Chao, G. Schwachheim and C. Tsallis, *Z. Phys.* **B43**, 305 (1981).
- [163] N-C. Chao, *J. Phys.* **C14**, L 473 (1981) and L1093 (1981).
- [164] A.C.N. de Magalhães, G. Schwachheim and C. Tsallis, *J. Phys.* **C15**, 6791 (1982).
- [165] P.M. Lam and Z.Q. Zhang, *Z. Phys.* **B52**, 315 (1983); errata: *Z. Phys.* **B5**, 371 (1984).
- [166] R.J.V. dos Santos, E.F. Sarmiento, C. Tsallis and U.M.S. Costa, *Phys. Rev.* **B33**, 1741 (1986); erratum: **34**, 2008 (1986).
- [167] C. Tsallis, E.F. Sarmiento and E.L. Albuquerque, *J. Magn. Magn. Mater.* **54**, 667 (1986).
- [168] P.M.C. de Oliveira, *J. Physique* **47**, 1107 (1986).
- [169] N.S. Branco, R.R. dos Santos and S.L.A. de Queiroz, *J. Phys.* **C20**, L103 (1987).
- [170] N.S. Branco, S.L.A. de Queiroz and R.R. dos Santos, *J. Phys.* **C21**, 2463 (1988).

- [171] N.S. Branco, S.L.A. de Queiroz and R.R. dos Santos, *Phys. Rev.* **B38**, 946 (1988).
- [172] S.M. Oliveira, P.M.C. de Oliveira and M.A. Continentino, *Physica* **A152**, 477 (1988).
- [173] K. Kotowski and M. Suffczynski, *Physica Scripta* **37**, 332 (1988).
- [174] L.R. da Silva, C. Tsallis and E.F. Sarmiento, *Phys. Rev.* **B37**, 7832 (1988).
- [175] S.L.A. de Queiroz and R.R. dos Santos, *J. Phys.* **C21**, 1995 (1988).
- [176] W.A. Morgado, S. Coutinho and E.M.F. Curado, *J. Stat. Phys.* **61**, 913 (1990).
- [177] N.S. Branco, S.L.A. de Queiroz and R.R. dos Santos, *Phys. Rev.* **B42**, 458 (1990).
- [178] P.M.C. de Oliveira, “Computing Boolean Statistical Models” (World Scientific, Singapore, 1991), chapter 7, pg. 77.
- [179] S. Coutinho, O.D. Neto, J.R.L. de Almeida, E.M.F. Curado and W.A.M. Morgado, *Physica* **A185**, 271 (1992).
- [180] N.S. Branco and A. Chame, *Phys.* **A198**, 11 (1993).
- [181] A. Hintermann, H. Kunz and F.Y. Wu, *J. Stat. Phys.* **19**, 623 (1978).
- [182] M. Suzuki and H. Takano, *Phys. Lett.* **69A**, 426 (1979).
- [183] C. Castelani, C. Di Castro and J. Ranninger, *Nucl. Phys.* **B200**, 45 (1982).
- [184] A.O. Caride, C. Tsallis and S.I. Zanette, *Phys. Rev. Lett.* **51**, 145 and 616 (1983).
- [185] M. Kaufman and M. Kardar, *Phys. Rev. Lett.* **52**, 483 (1984).
- [186] A.M. Mariz, R.M.Z. dos Santos, C. Tsallis and R.R. dos Santos, *Phys. Lett.* **108A**, 95 (1985).
- [187] A.M. Mariz, C. Tsallis and A.O. Caride, *J. Phys.* **C18**, 4189 (1985).
- [188] R.M.Z. dos Santos, A.M. Mariz, R.R. dos Santos and C. Tsallis, *J. Phys.* **C18**, 5475 (1985).

- [189] A.M. Mariz and C. Tsallis, Phys. Rev. **B31**, 7491 (1985).
- [190] A.M.C. de Souza, Phys. Rev. **B48**, 3744 (1993).
- [191] J. Chalupa, P.L. Leath and G.R. Reich, J. Phys. **C12**, L31 (1979).
- [192] L. Turban, J. Phys. **C12**, 5009 (1979).
- [193] H.E. Stanley, J. Phys. **A12**, L329 (1979).
- [194] C. Tsallis, A. Coniglio and S. Redner, J. Phys. C **16**, 4339 (1983).
- [195] E.M.F. Curado, PhD thesis (1983), Centro Brasileiro de Pesquisas Físicas (CBPF/CNPq) – Rio de Janeiro (Brazil).
- [196] G. Toulouse, Comm. Phys. **2**, 115 (1977).
- [197] A.C.N. de Magalhães and J.W. Essam, J. Phys. **A22**, 2549 (1989).
- [198] N. Biggs, Math. Proc. Camb. Phil. Soc. **80**, 429 (1976) and “Interaction Models” (Cambridge University Press, Cambridge, 1977).
- [199] A.M. Mariz, A.C.N. de Magalhães, L.R. da Silva and C. Tsallis, Physica **A162**, 161 (1990).
- [200] A.M. Mariz, PhD thesis (1985), Centro Brasileiro de Pesquisas Físicas (CBPF/CNPq) – Rio de Janeiro (Brazil).
- [201] K.G. Wilson, Phys. Rev. **B4**, 3174 and 3184 (1971).
- [202] K.G. Wilson and M.E. Fisher, Phys. Rev. Lett. **28**, 240 (1972).
- [203] D.J. Wallace, in “Phase Transitions and Critical Phenomena”, ed. C. Domb and M.S. Green, vol. 6, 294 (1976); D.J. Wallace and R.K.P. Zia, Rep. on Progress in Physics **41**, 1 (1978).
- [204] K.G. Wilson, Rev. Mod. Phys. **55**, 583 (1983).
- [205] C.S.O. Yokoi, M.D. Coutinho-Filho and S.R. Salinas, Phys. Rev. **B31**, 4502 (1985).

- [206] W.K. Theumann and M.A. Gusmão, *Phys. Rev.* **B31**, 379 (1985).
- [207] B.J. Hiley and G.S. Joyce, *Proc. Phys. Soc.* **85**, 493 (1965).
- [208] N. Boccara, “Symétries Brisées” (Hermann, Paris, 1976).
- [209] F.D. Nobre and C. Tsallis, *Physica* **A213**, 337 (1995).
- [210] S.A. Cannas, *Phys. Rev. B* in press.
- [211] B. Derrida and J. Vannimenus, in “Colloque sur les méthodes de calcul pour l’étude de phénomènes critiques de Carry le Rouet,” (Springer, Berlin, 1980).
- [212] B. Derrida, L. de Seze and J. Vannimenus, *Disordered Systems and Localization* (Conference Rome 1981), *Lecture Notes in Physics* **149**, 46 eds. C. Castellani, C. di Castro and L. Peliti (Berlin, Springer Verlag, 1982).
- [213] C. Tsallis, *J. Physique Lett.* **43**, L 471 (1982).
- [214] K.G. Wilson, in “Phase Transitions and Critical Phenomena”, eds. C. Domb and M.S. Green, vol. 6, 1 (1976).
- [215] B. Hu, *Phys. Rep.* **91**, 233 (1982).
- [216] S.R. McKay and A.N. Berker, *J. Appl. Phys.* **55**, 1646 (1984).
- [217] B. Mandelbrot, “Les Objects Fractals (Flammarion, Paris, 1975). (English versions: “Fractals: Form, Chance and Dimension”, W.H. Freeman, San Francisco, 1977; “The Geometry of Nature”, Ibid., (1982).
- [218] H.E. Stanley and A. Coniglio, in *Annals of the Israel Physical Soc.*, vol. 5, “Percolation Structures and Processes”, eds. G. Deutscher, R. Zallen and J. Adler (Israel Phys. Soc.), 101 (1983).
- [219] J. Souletie and J.L. Tholence, *Solid St. Commun.* **48**, 407 (1983).
- [220] M. Fahnle and J. Souletie, *J. Phys.* **C17**, L469 (1984) and *Phys. Rev.* **B32**, 3328 (1985).

- [221] J. Souletie, H. Martín and C. Tsallis, *Europhys. Lett.* **2**, 863 (1986).
- [222] E. Carre, J.P. Renard and J. Souletie, *J. Magn. Magn. Mater.*, **54-57**, 697 (1986).
- [223] Th. Niemeijer and J.M.J. van Leeuwen, in “Phase Transitions and Critical Phenomena”, eds. C. Domb and M.S. Green, vol. 6, 425 (1976).
- [224] A.P. Young and R.B. Stinchcombe, *J. Phys.* **C8**, L535 (1975).
- [225] R.B. Stinchcombe and B.P. Watson, *J. Phys.* **C9**, 3221 (1976).
- [226] M.J. de Oliveira, D. Furman and R.B. Griffiths, *Phys. Rev. Lett.* **40**, 977 (1978).
- [227] H.O. Martín and C. Tsallis, *J. Phys.* **C14**, 5645 (1981) and *Z. Phys.* **B44**, 325 (1981).
- [228] A.O. Caride and C. Tsallis, *J. Phys.* **A20**, L665 (1987).
- [229] C. Tsallis, *J. Phys.* **C18**, 6581 (1985).
- [230] P.M.C. de Oliveira, S.M.M. de Oliveira, C.E. Cordeiro and D. Stauffer, to appear in *J. Stat. Phys.* (1995).
- [231] B. Nienhuis, A.N. Berker, E.K. Riedel and M. Schick, *Phys. Rev. Lett.* **43**, 737 (1979); B. Nienhuis, E.K. Riedel and M. Schick, *J. Phys.* **A13**, L31 (1980).
- [232] M. Kaufman and R.B. Griffiths, *Phys. Rev.* **B28**, 3864 (1983).
- [233] J.R. Melrose, *J. Phys.* **A16**, 1041 (1983).
- [234] M. Kaufman and K. Mon, *Phys. Rev.* **B29**, 1451 (1984).
- [235] B. Hu, *Phys. Rev. Lett.* **55**, 2316 (1985); Comments by J.R. Melrose, *Phys. Rev. Lett.* **57**, 2601 (1986); Response by B. Hu, *Phys. Rev. Lett.* **57**, 2602 (1986).
- [236] J.R. Melrose, *J. Phys.* **A19**, 2395 (1986).
- [237] L. da Silva, MSc. thesis (1992), Centro Brasileiro de Pesquisas Físicas (CBPF/CNPq) – Rio de Janeiro (Brazil).

- [238] S. Coutinho, O.D. Neto, J.R.L. de Almeida, E.M.F. Curado and W.A.M. Morgado, *Physica* **A185**, 271 (1992).
- [239] J.A. Redinz and A.C.N. de Magalhães, *Phys. Rev.* **B51**, (1995).
- [240] A.C.N. de Magalhães, C. Tsallis and G. Schwachheim, *J. Phys.* **C14**, 1393 (1981).
- [241] P.M.C. de Oliveira, *Phys. Rev.* **B25**, 2034 (1982).
- [242] C. Jayaprakash, E.K. Riedel and M. Wortis, *Phys. Rev.* **B18**, 2244 (1978).
- [243] B.W. Southern, *J. Phys.* **C13**, L285 (1980).
- [244] A.P. Young and R.B. Stinchcombe, *J. Phys.* **C9**, 4419 (1976).
- [245] P. Beale, C. Tsallis and R.B. Stinchcombe, unpublished
- [246] H.R. da Cruz and R.B. Stinchcombe, *J. Phys.* **C19**, 3555 (1986).
- [247] A.B. Harris, *J. Phys.* **C7**, 1671 (1974).
- [248] B. Derrida, H. Dickinson and J. Yeomans, *J. Phys.* **A18**, L53 (1985).
- [249] I. Morgenstern and K. Binder, *Phys. Rev.* **B22**, 288 (1980); F. Barahona, R. Maynard, R. Rammal and J.P. Uhry, *J. Phys.* **A15**, 673 (1982).
- [250] J.M. Carlson, J.T. Chayes, L. Chayes, J.P. Sethna and D.J. Thouless, *J. Stat. Phys.* **61**, 987 (1990); J.M. Carlson, J.T. Chayes, J.P. Sethna and D.J. Thouless, *J. Stat. Phys.* **61**, 1069 (1990).
- [251] H. Zittartz, private communication
- [252] P. Ruján, G.O. Williams, H.L. Frisch and G. Forgács, *Phys. Rev.* **B23**, 1362 (1981).
- [253] V.L.V. Baltar, G.M. Carneiro, M.E. Pol and N. Zagury, *J. Phys.* **17A**, 2119 (1984); *Rev. Bras. Fis.* **14**, 48 (1984).
- [254] E.S. de Souza, MSc. thesis (1988), Universidade Federal do Rio Grande do Norte (UFRN)-Natal (Brazil).

- [255] A.M. Mariz, F.D. Nobre and E.S. de Souza, *Physica* **A178**, 364 (1991).
- [256] R. Badke, *Phys. Lett.* **119 A**, 365 (1987).
- [257] A. Chame and C. Tsallis, *Physica* **A165**, 41 (1990).
- [258] E.P. da Silva and C. Tsallis, *Nuovo Cimento* **D15**, 615 (1993).
- [259] S.K. Ma, *Phys. Rev. Lett.* **37**, 461 (1976).
- [260] R.H. Swendsen, in “Real-Space Renormalization”, *Topics in Current Physics* **30**, eds. T.W. Burkhardt and J.M.J. van Leeuwen, (Springer-Verlag, Berlin, Heidelberg, New York), pg. 57 (1982).
- [261] K. Binder, *Z. Phys.* **B43**, 119 (1981) and *Phys. Rev. Lett.* **47**, 693 (1981).
- [262] D.P. Landau and R.H. Swendsen, *Phys. Rev. Lett.* **46**, 1437 (1981).
- [263] M. Kikuchi and Y. Okabe, *Prog. Theor. Phys.* **75**, 192 (1986) and **78**, 540 (1987); *Phys. Rev.* **B35**, 5382 (1987).
- [264] M. Kikuchi, *Prog. Theor. Phys. Suppl.* **101**, 557 (1990).
- [265] J.O. Indekeu, A. Maritan and A.L. Stella, *Phys. Rev.* **B35**, 305 (1987).
- [266] E.C. Valadares and J.A. Plascak, *J. Phys.* **A20**, 4967 (1987).
- [267] J.A. Plascak and W. Figueiredo, *Phys. Lett.* **A 123**, 135 (1987).
- [268] H.F.V. de Resende, F.C.S. Barreto and J.A. Plascak, *Physica* **A 149**, 606 (1988).
- [269] M.C. Marques, *J. Phys.* **A21**, 1297 (1988).
- [270] M.L. Lyra and S. Coutinho, *Physica* **A155**, 232 (1989).
- [271] P.M.C. de Oliveira and F.C. Sá Barreto, *J. Stat. Phys.* **57**, 53 (1989).
- [272] J.A. Plascak, *Physica* **A183**, 563 (1992).
- [273] A. da Neves, J.K.L. da Silva and J.A. Plascak, *Physica* **A189**, 367 (1992).



- [274] K. Croes and J.O. Indekeu, *Mod. Phys. Lett.* **B7**, 699 (1993).
- [275] L.A. Serkov and V.O. Shvaley, *Phys. Solid. St.* **36**, 98 (1994).
- [276] J.K.L. da Silva, R.A. Nogueira, J.A. Plascak and M. Droz, *J. Phys.* **A27**, 1495 (1994).
- [277] Z.Y. Li and C.Z. Yang, *Phys. Rev.* **B37**, 5744 (1988).
- [278] I.P. Fittipaldi and D.F. de Albuquerque, *J. Magn. & Magn. Mater.* **104-107**, 236 (1992); I.P. Fittipaldi, *J. Magn. Magn. Mater.* **131**, 43 (1994).
- [279] J.R. de Souza and I.P. Fittipaldi, *J. Appl. Phys.* **75**, 5835 (1994).
- [280] D.F. de Albuquerque and I.P. Fittipaldi, *J. Appl. Phys.* **75**, 5832 (1994).
- [281] P.M.C. de Oliveira, *Europhys. Lett.* **20**, 621 (1992).
- [282] J.M.F. Neto, S.M.M. de Oliveira and P.M.C. de Oliveira, *Physica* **A206**, 463 (1994).
- [283] P.M.C. de Oliveira, *Physica* **A205**, 101 (1994).
- [284] S.M.M. de Oliveira, P.M.C. de Oliveira and F.C. Sá Barreto, *J. Stat. Phys.* **78**, 1619 (1995).
- [285] P. Nightingale, *J. Appl. Phys.* **53**, 7927 (1982); in “Finite-size Scaling and Numerical Simulations of Statistical Systems”, ed. V. Privman (Singapore, World Scientific, 1990).
- [286] N.N. Barber, in “Phase Transitions and Critical Phenomena”, eds. C. Domb and J.L. Lebowitz, Vol. 8, 145 (1983).
- [287] B. Derrida, D. Stauffer, H.J. Herrmann and J. Vannimenus, *J. Physique Lettr.* **44**, L701 (1983); B. Derrida and J. Vannimenus, *J. Phys.* **A15**, L557 (1982); B. Derrida and L. de Seze, *J. Physique* **43**, 475 (1982); B. Derrida and H.J. Herrmann, *J. Physique* **44**, 365 (1983).
- [288] J.G. Zabolitzky, *Phys. Rev.* **B30**, 4076 (1984).

- [289] D.C. Hong, S. Havlin, H.J. Herrmann and H.E. Stanley, *Phys. Rev.* **B30**, 4083 (1984).
- [290] C.J. Lobb and D.J. Frank, *Phys. Rev.* **B30**, 4090 (1984).
- [291] S.L.A. de Queiroz and J.M. Yeomans, *J. Phys.* **A24**, 1867 and L933 (1991).
- [292] S.L.A. de Queiroz and R.B. Stinchcombe, *Phys. Rev.* **B46**, R6635 (1992); *Phys. Rev.* **B50**, 9976 (1994).
- [293] P. Serra and J.F. Stilck, *Europhys. Lett.* **17**, 423 (1992), *Phys. Rev.* **E49**, 1336 (1994).
- [294] J.F. Stilck, *Macromol. Symp.* **81**, 321 (1994).
- [295] H.W.J. Blöte, M.P. Nightingale and B. Derrida, *J. Phys.* **A14**, L45 (1981).
- [296] H.W.J. Blöte and M.P. Nightingale, *Physica* **112A**, 405 (1982).
- [297] K. Binder, in “Phase Transitions and Critical Phenomena”, eds. C. Domb and J.L. Lebowitz, vol. 8 (New York: Academic), 1 (1983).
- [298] H.O. Martín and C. Tsallis, *J. Phys.* **C16**, 2787 (1983).
- [299] E.P. da Silva and C. Tsallis, *Physica* **A167**, 347 (1990).
- [300] A. Chame, C. Tsallis and U.M.S. Costa, *Phys. Rev.* **B37**, 7549 (1988).
- [301] B. Widom, in “Phase Transitions and Critical Phenomena”, vol. 2, Eds. C. Domb and M.S. Green (1972).
- [302] P.R. Hauser and E.M.F. Curado, *Notas de Física – Centro Brasileiro de Pesquisas Físicas (CBPF)-029/84* (1984).
- [303] M.E. Fisher and R.J. Burford, *Phys. Rev.* **156**, 583 (1967).
- [304] T. Kaneyoshi, “Introduction to Surface Magnetism” (CRC press, Boca Raton, 1990).

- [305] H.W. Diehl, in “Phase Transitions and Critical Phenomena”, eds. C. Domb and J.L. Lebowitz, vol. 10, 76 (1986).
- [306] C. Tsallis, in “Magnetic Properties of Low-dimensional Systems”, eds. L.M. Falicov and J.L. Moran-Lopez (Springer-Verlag), 98 (1986).
- [307] C. Tsallis and A. Chame, in “Thin Films and Small Particles”, eds. M. Cadorna and J. Giraldo (World Scientific), 49 (1989).
- [308] C. Tsallis, in “Magnetism, Magnetic Materials and Their Applications”, eds. F. Lecabue and J.L. Sanchez Llamazares (The Institute of Physics), 89 (1992).
- [309] U.M.S. Costa, A.M. Mariz and C. Tsallis, *J. Physique Lettr.* **46**, L851 (1985).
- [310] L.R. da Silva, U.M.S. Costa and C. Tsallis, *J. Phys.* **C18**, 6199 (1985).
- [311] C. Tsallis and E.F. Sarmiento, *J. Phys.* **C18**, 2777 (1985).
- [312] A.M. Mariz, U.M.S. Costa and C. Tsallis, *Europhys. Lett.* **3**, 27 (1987).
- [313] E.F. Sarmiento, E.L. Albuquerque and C. Tsallis, *Revista Brasileira de Física* **18**, 384 (1988).
- [314] C. Tsallis and A. Chame, *J. Physique* **49**, (Colloque C8), 1619 (1988); see also T.W. Burkhardt and H.W. Diehl, *Phys. Rev.* **B50**, 3894 (1994).
- [315] A. Chame and C. Tsallis, *J. Phys.: Condens. Mat.* **1**, 10129 (1989).
- [316] M.L. Martins and C. Tsallis, *J. Phys.* **A23**, 3043 (1990).
- [317] C. Tsallis, T.A. Kaplan and S.V.F. Levy, “Critical temperature of the classical n-vector ferromagnet in d-dimensional hierarchical lattices for real d and n”, preprint (1995).
- [318] A.A. Migdal, *Zh. Eksp. Fiz.* **69**, 810 and 1457 (1975) (*Sov. Phys. - JETP* **42**, 743 (1976)); L.P. Kadanoff, *Ann. Phys., NY* **100**, 359 (1976); V.J. Emery and R.H. Swendsen, *Phys. Lett.* **64A**, 325 (1977).

- [319] T.W. Burkhardt, in “Real-Space Renormalization”, Topics in Current Physics **30**, eds. T.W. Burkhardt and J.M.J. van Leeuwen (Springer-Verlag, Berlin, Heidelberg, New York), pg. 33 (1982).
- [320] B. Shapiro, J. Phys. **C13**, 3387 (1980).
- [321] K.G. Wilson and M.E. Fisher, Phys. Rev. Lett. **28**, 24 (1972).
- [322] D.S. Gaunt and M. Ruskin, J. Phys. **A11**, 1369 (1978).
- [323] J. Zinn-Justin, J. Physique **40**, 969 (1979).
- [324] S.J.K. Jensen and O.G. Mouritsen, Phys. Rev. Lett. **43**, 1736 (1979).
- [325] S. Redner and H.E. Stanley, J. Phys. **A12**, 1267 (1979).
- [326] J. Oitmaa and G.I. Enting, Phys. Lett. **36A**, 91 (1971).
- [327] G. Paul and H.E. Stanley, Phys. Rev. **B5**, 2578 (1972).
- [328] D.W. Heerman and D. Stauffer, Z. Phys. **B44**, 339 (1981).
- [329] J.C. Le Guillou and J. Zinn-Justin, Phys. Rev. **B21**, 3976 (1980).
- [330] L.L. Liu and H.E. Stanley, Phys. Rev. Lett. **29**, 927 (1972) and Phys. Rev. **B8**, 2279 (1973).
- [331] C.A. Citteur and P.W. Kasteleyn, Phys. Lett. **42A**, 143 (1972) and Physica **68**, 491 (1973).
- [332] C.N. Yang, Phys. Rev. **85**, 808 (1952).
- [333] K. Binder and P.C. Hohenberg, Phys. Rev. **B9**, 2194 (1974).
- [334] K. Binder and D.P. Landau, Phys. Rev. Lett. **52**, 318 (1984).
- [335] E.F. Sarmiento, I. Ramura and T. Kaneyoshi, Z. Phys. **B54**, 241 (1984).
- [336] H.W. Diehl and S. Dietrich, Phys. Lett. **80A**, 408 (1980).

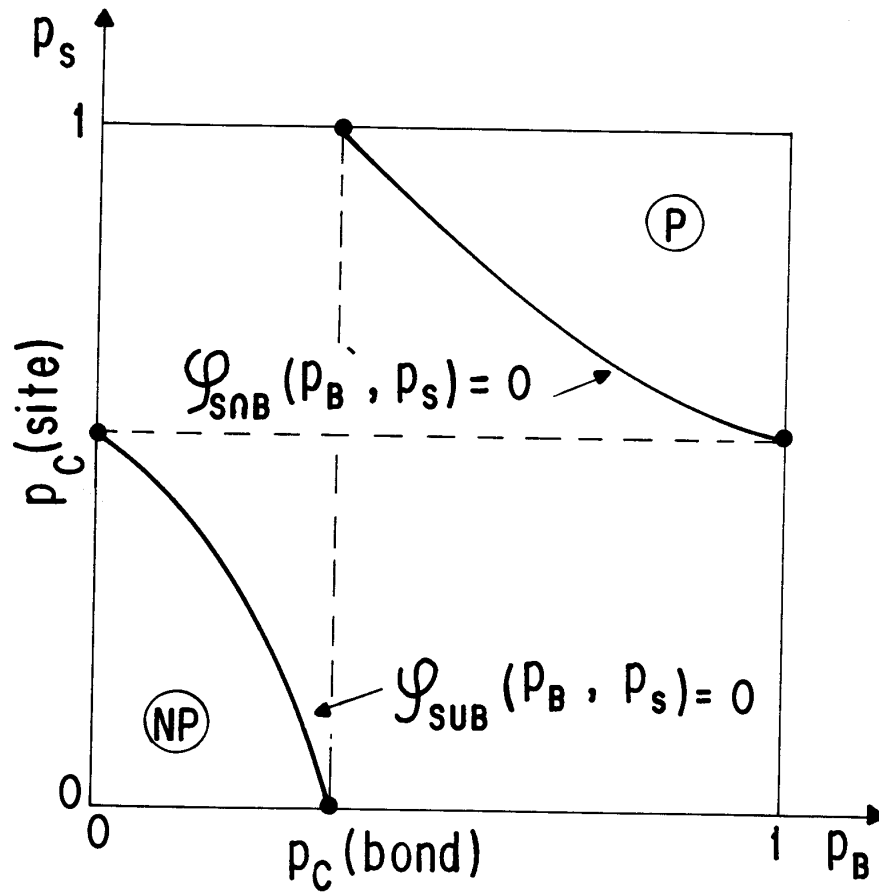


FIG. 1

Z(4) interaction		Z(5) interaction	
configurations	spectrum	configurations	spectrum
	$\begin{array}{c} \text{---} 3J_1 - 2J_2 \text{---} \\ \text{---} J_1 + 2J_2 \text{---} \\ \text{---} J_1 - 2J_2 \text{---} \end{array}$		$\begin{array}{c} [J_1(3 + \sqrt{5}) - J_2(\sqrt{5} - 1)]/2 \\ [J_1(3 - \sqrt{5}) + J_2(\sqrt{5} + 1)]/2 \\ \text{---} J_1 - 2J_2 \text{---} \end{array}$

FIG. 2

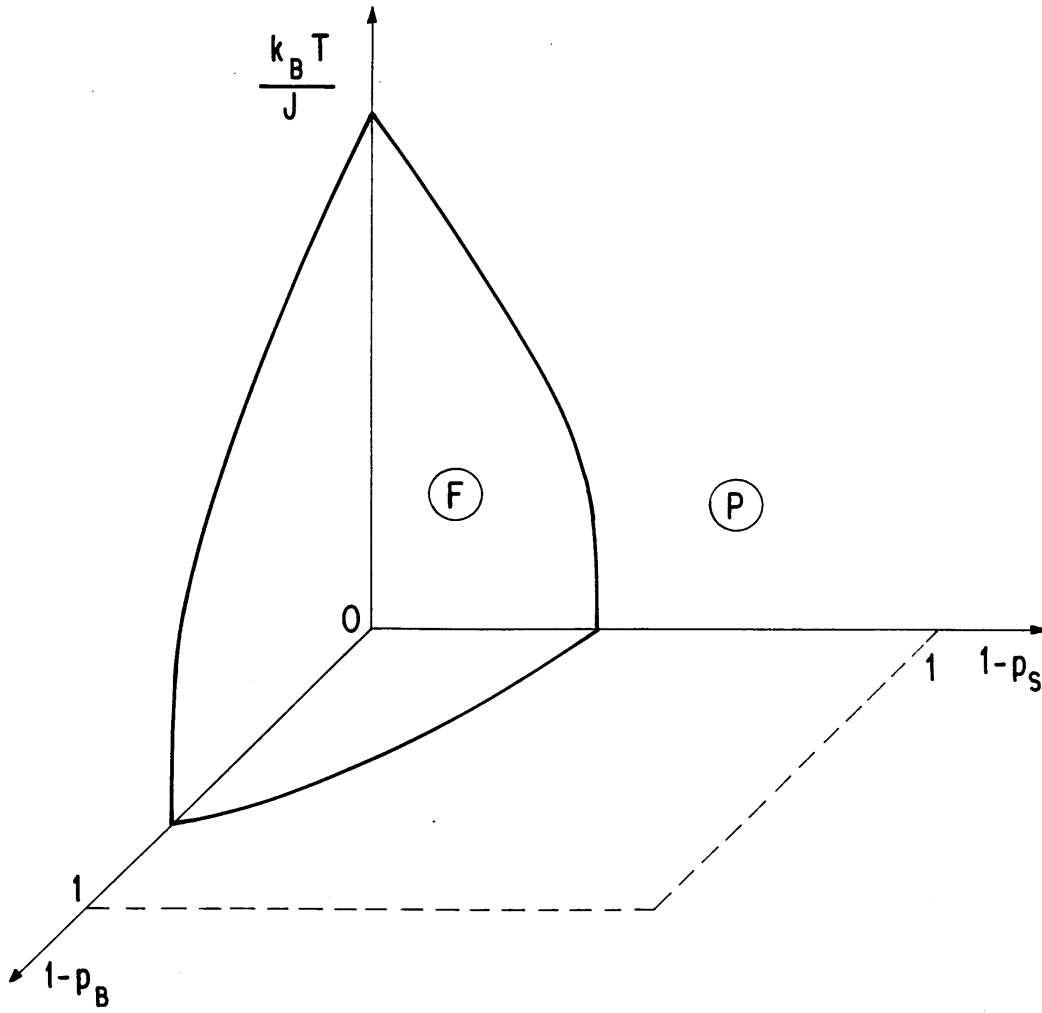


FIG. 3

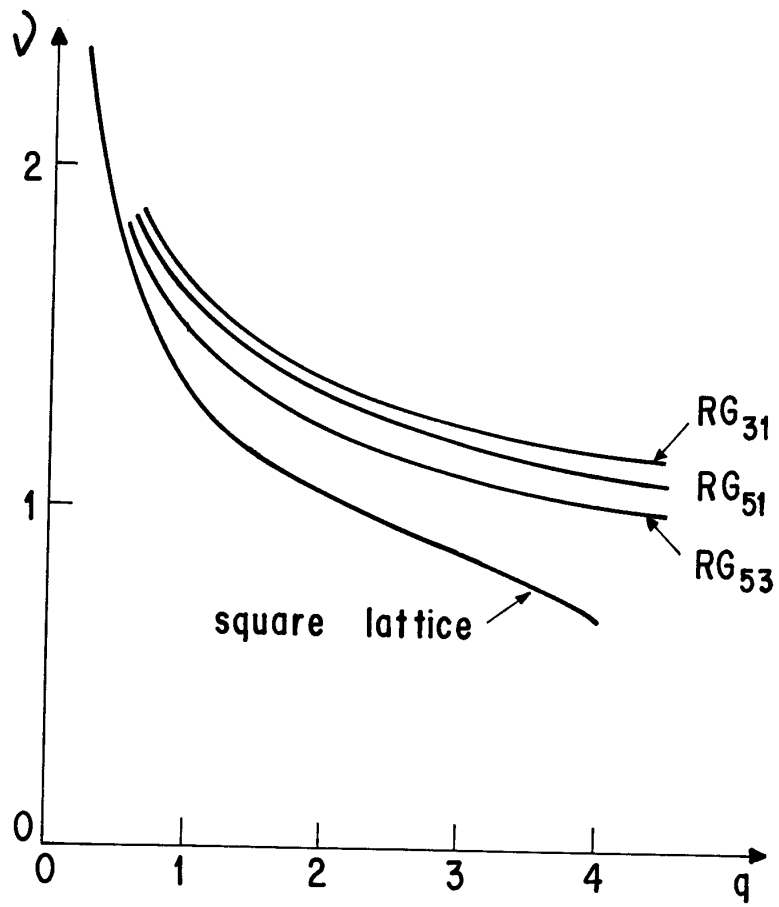


FIG. 4



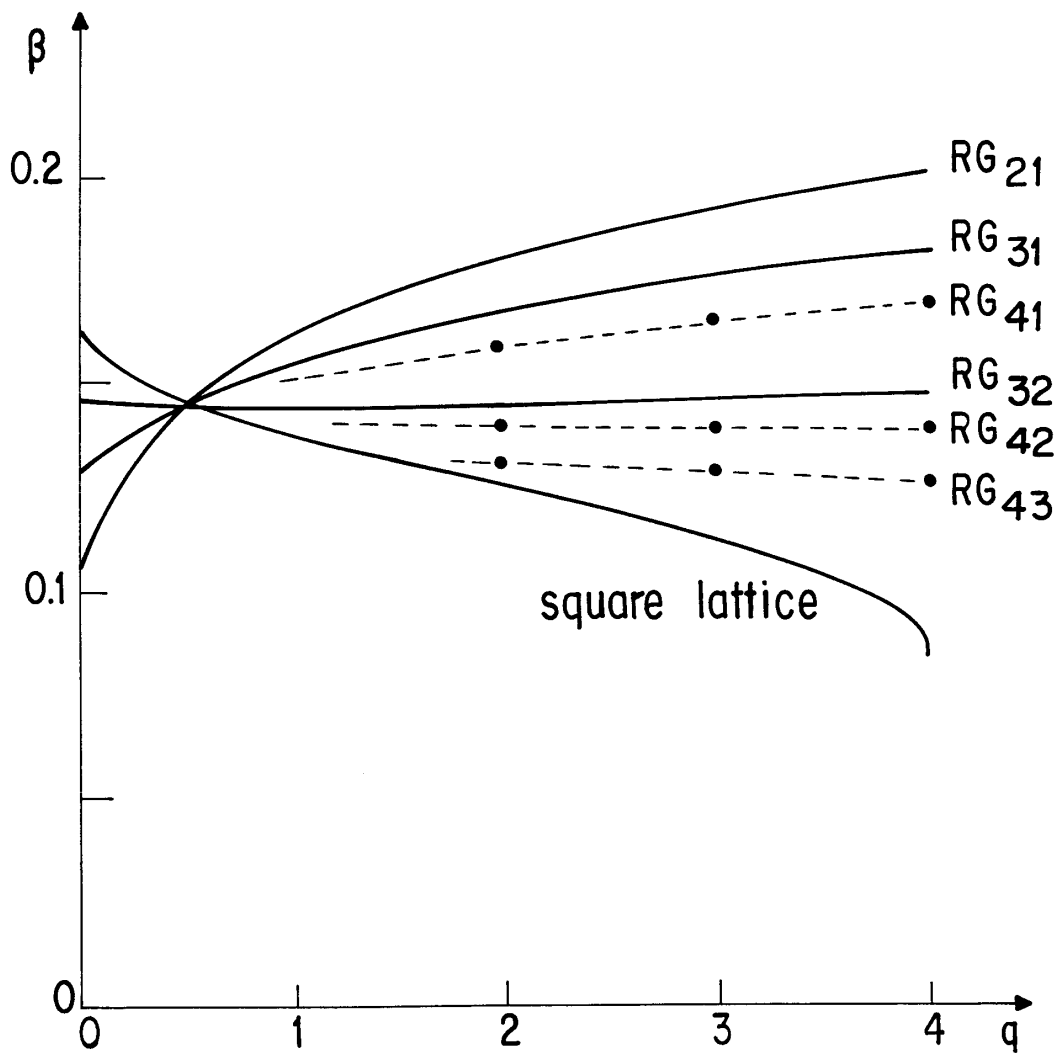


FIG.5

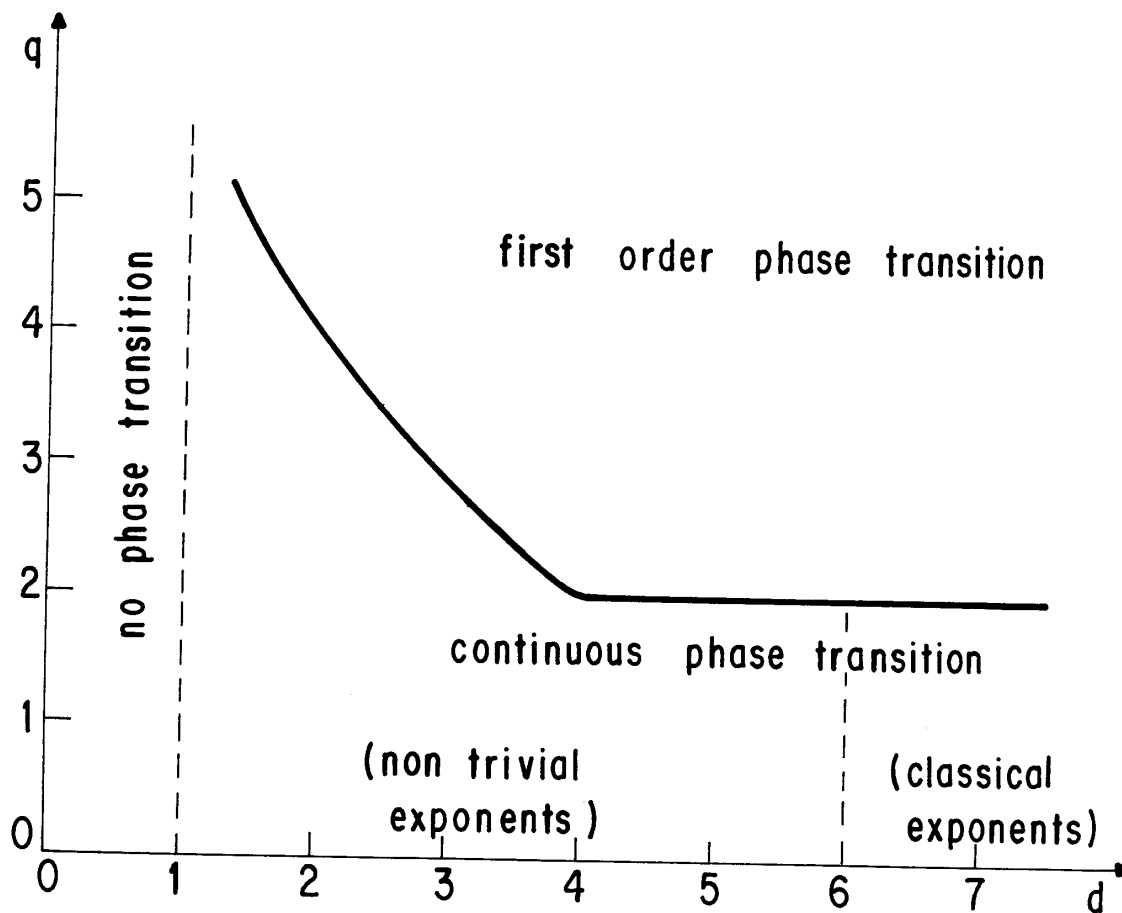


FIG. 6

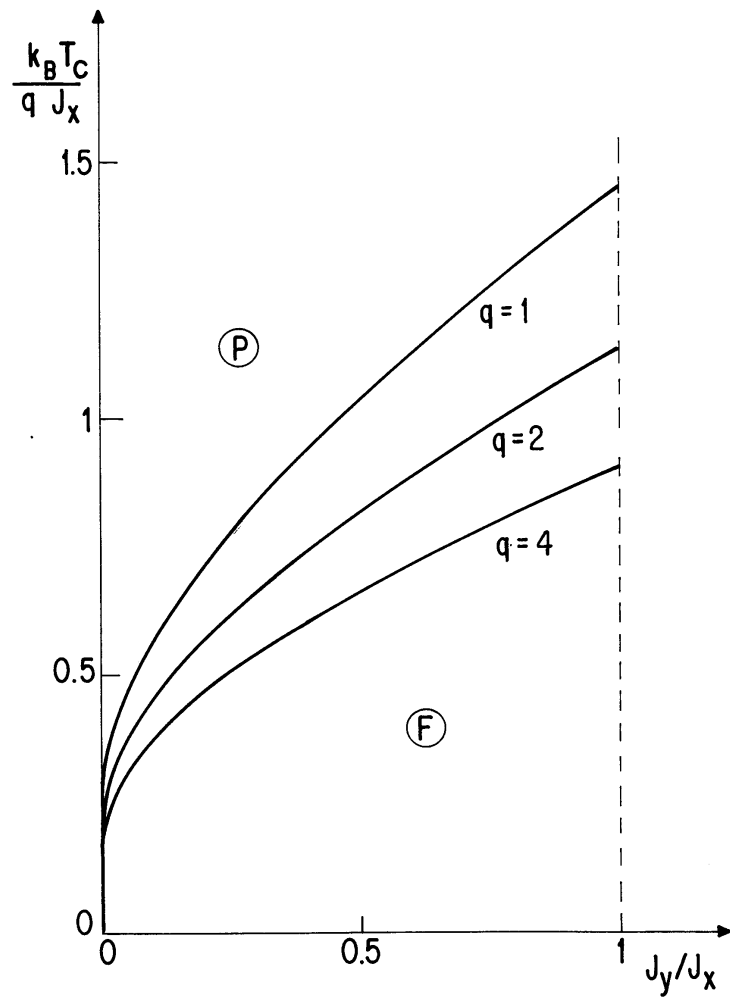


FIG. 7

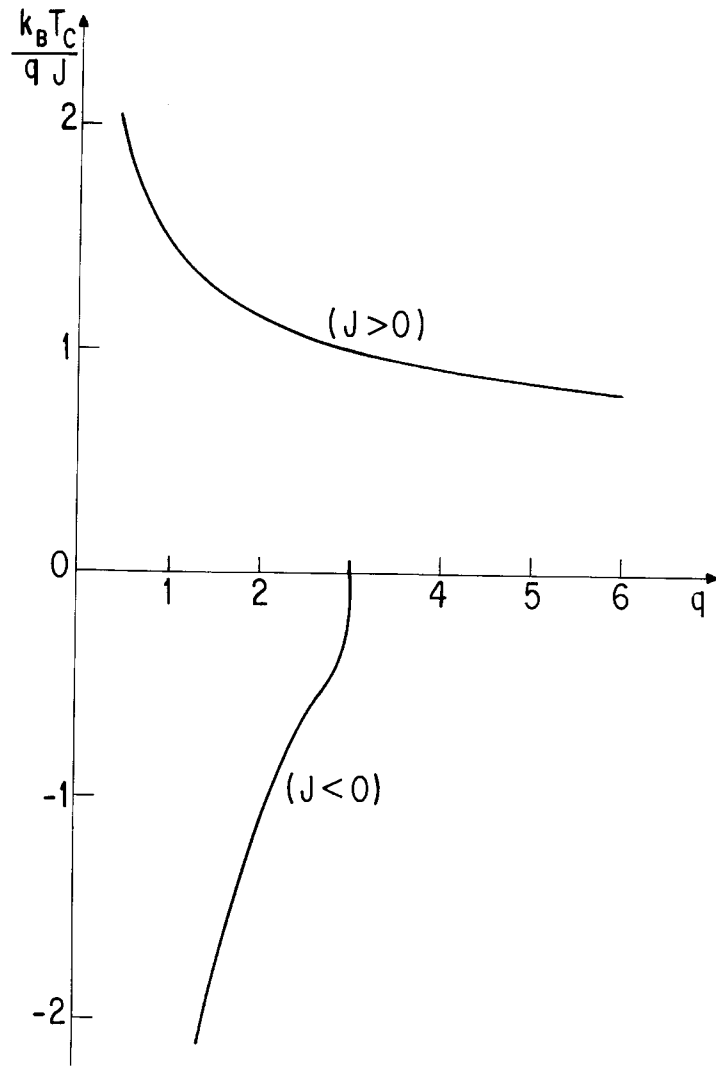


FIG. 8

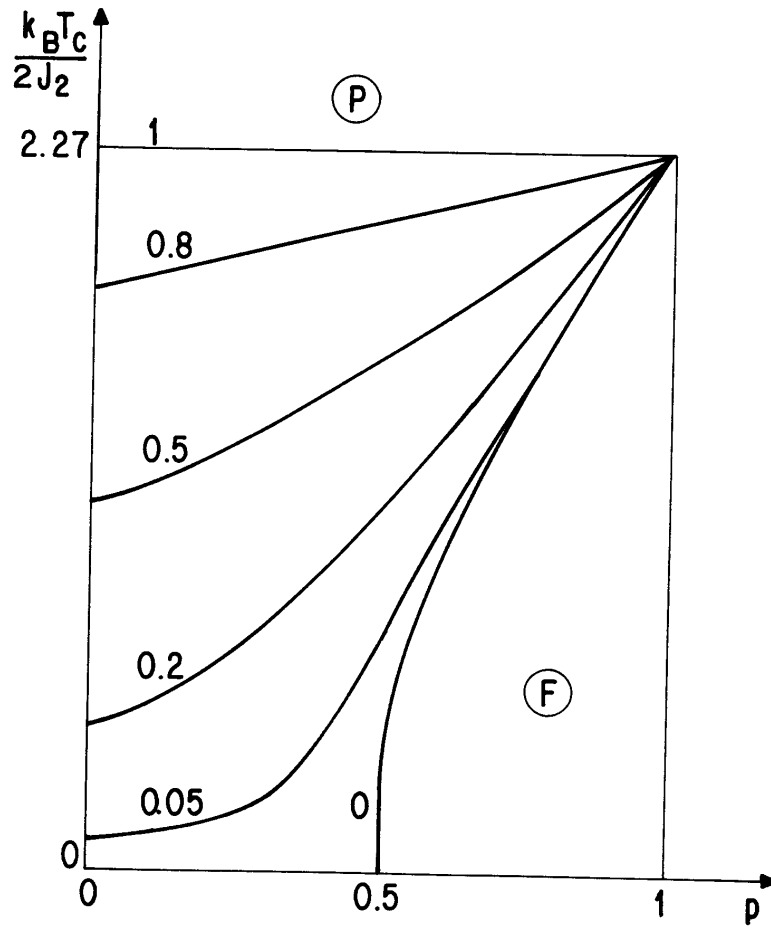


FIG. 9

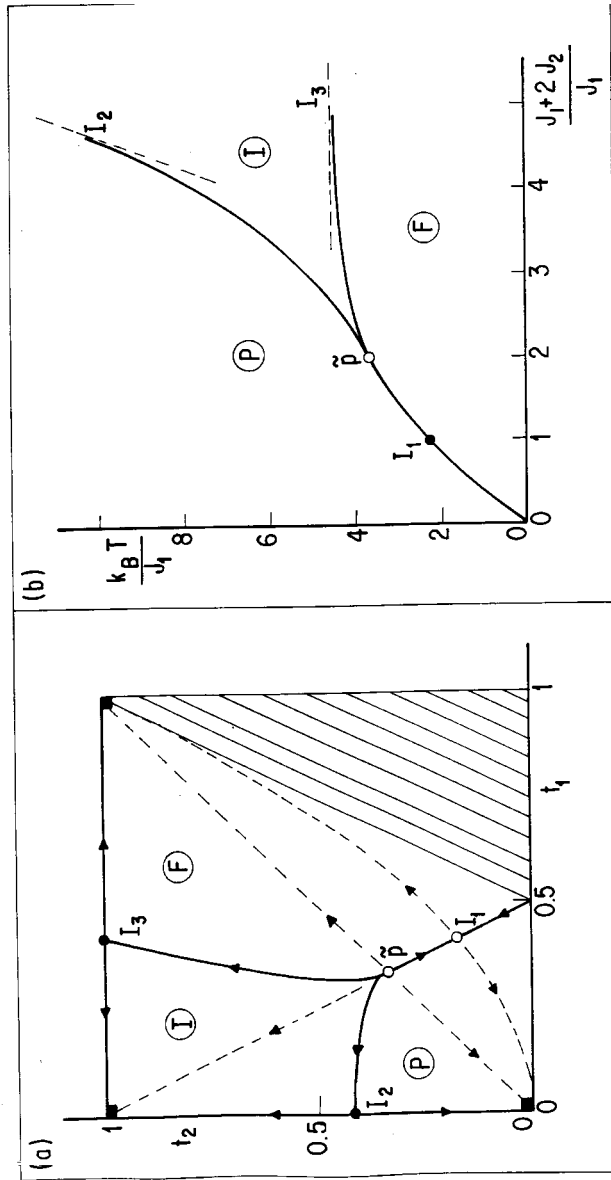


FIG. 10

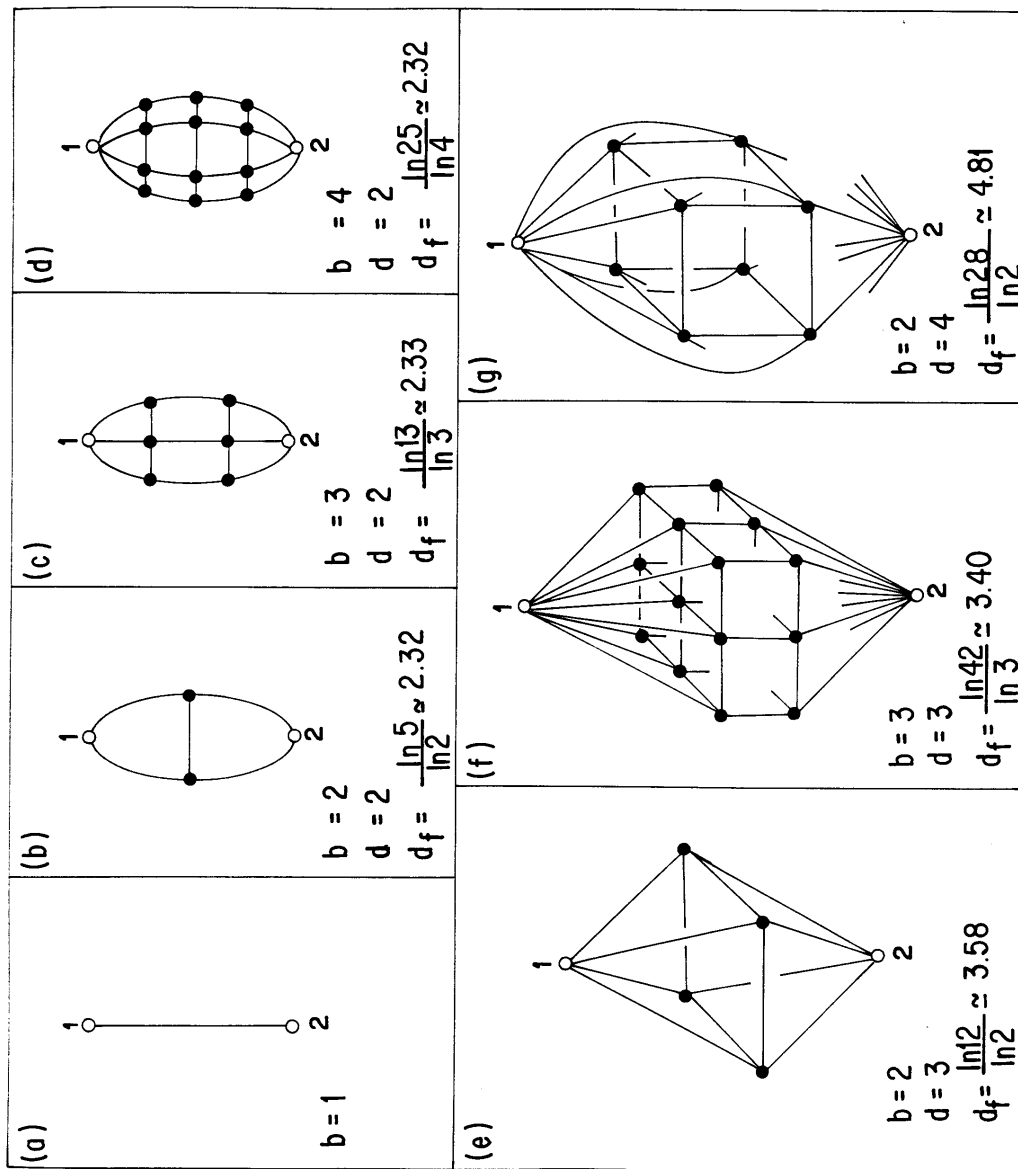


FIG. 11

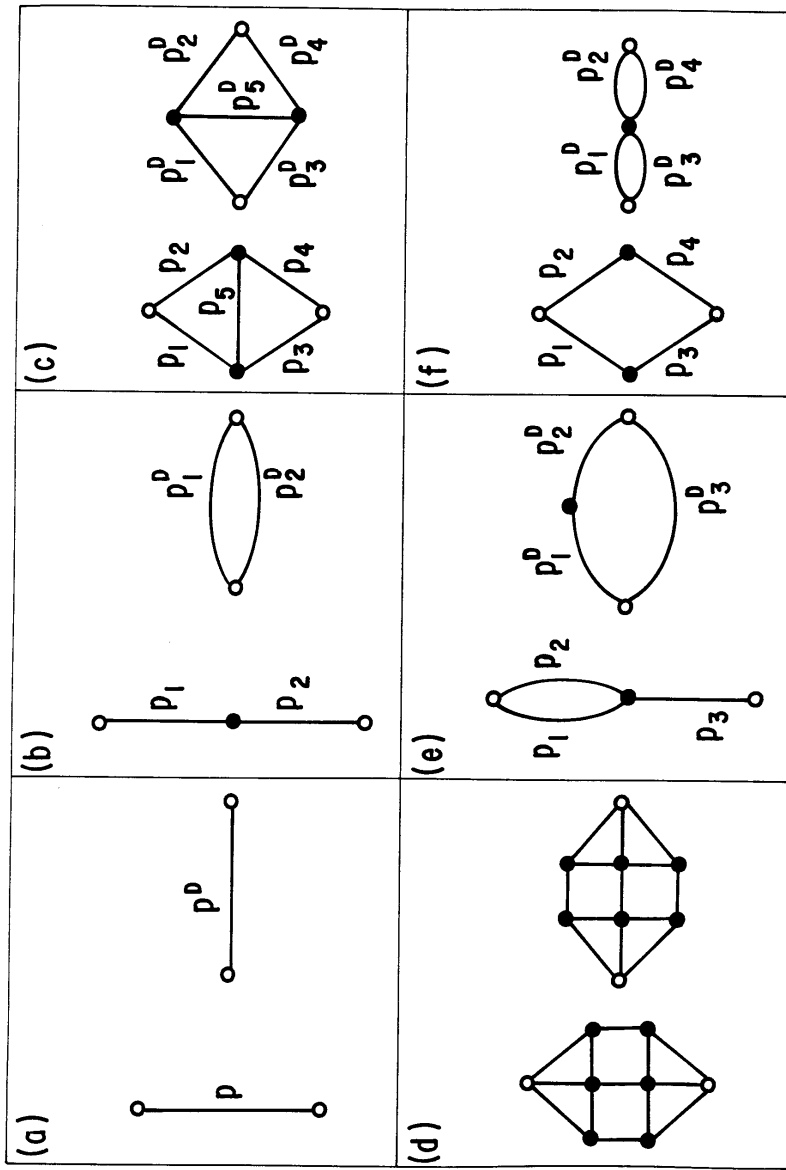


FIG. 12



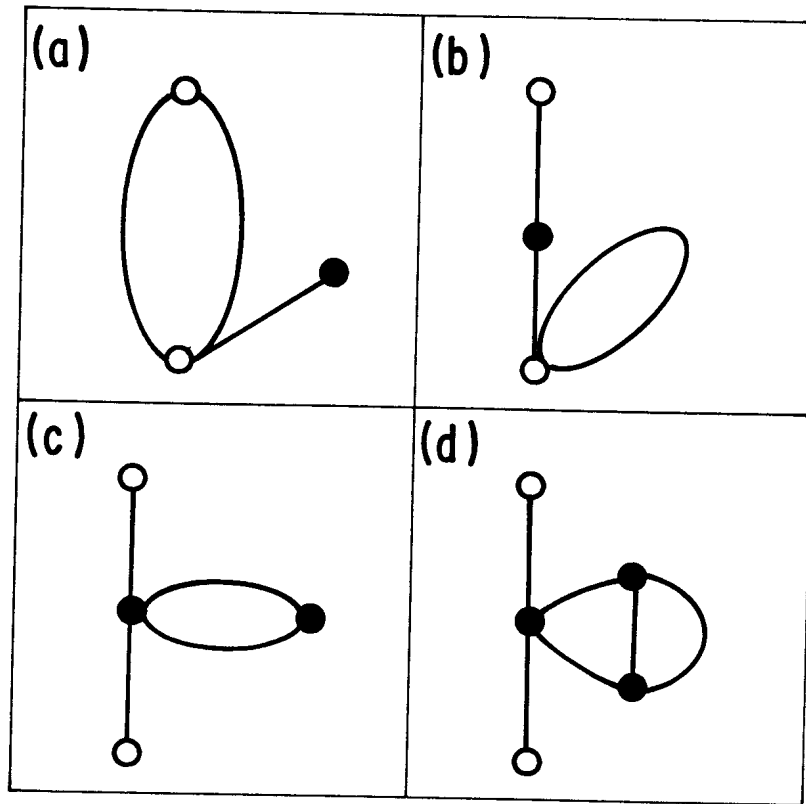


FIG. 13

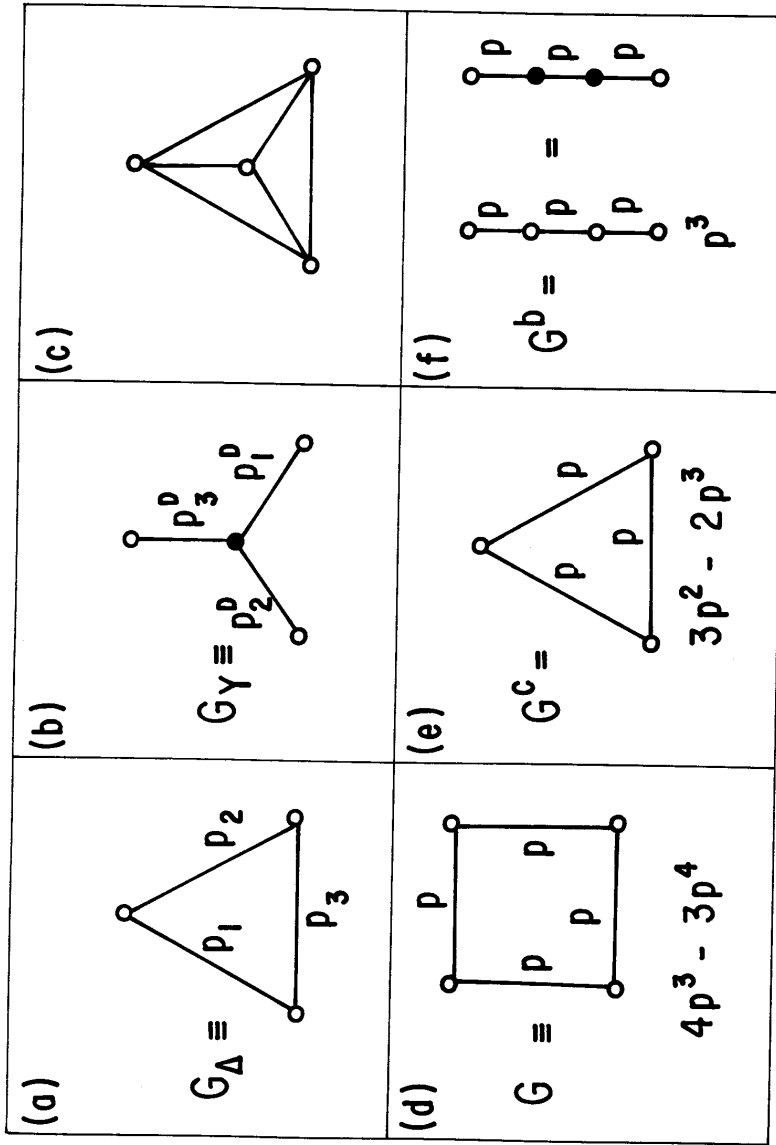


FIG. 14

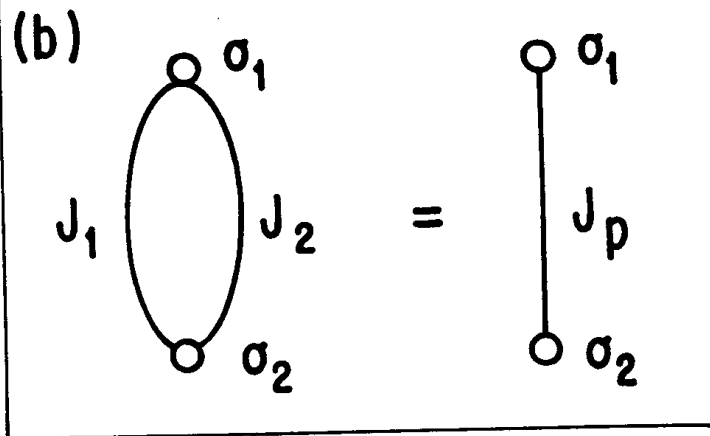
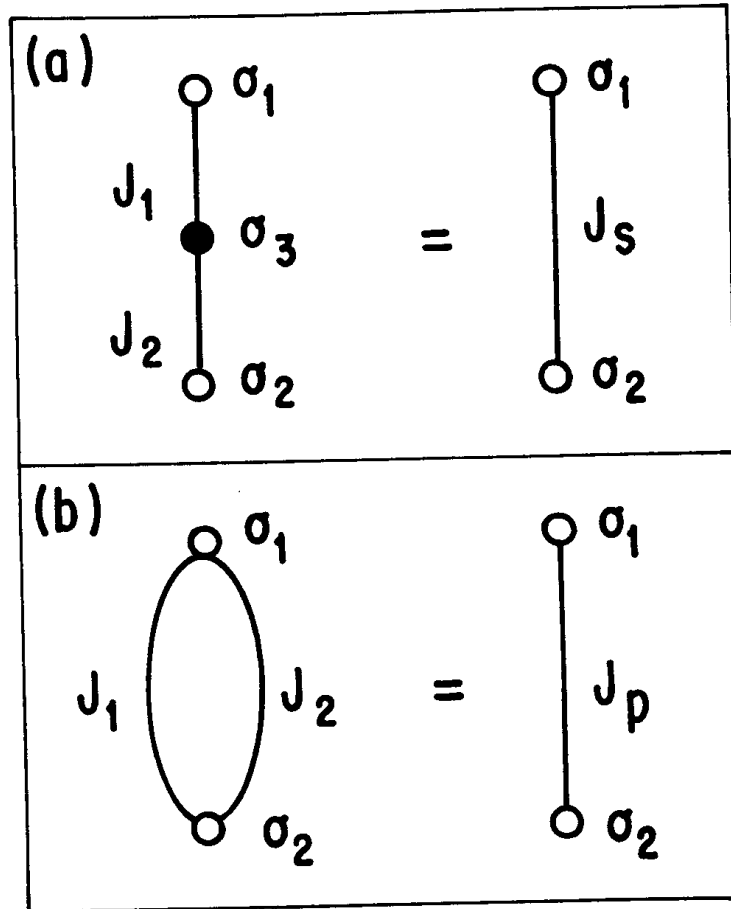


FIG. 15

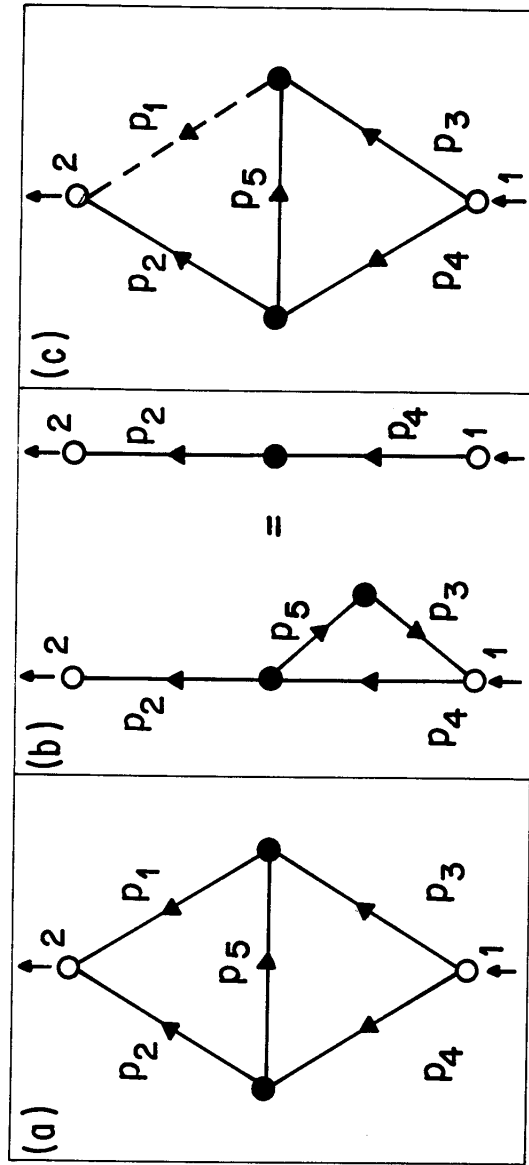


FIG. 16

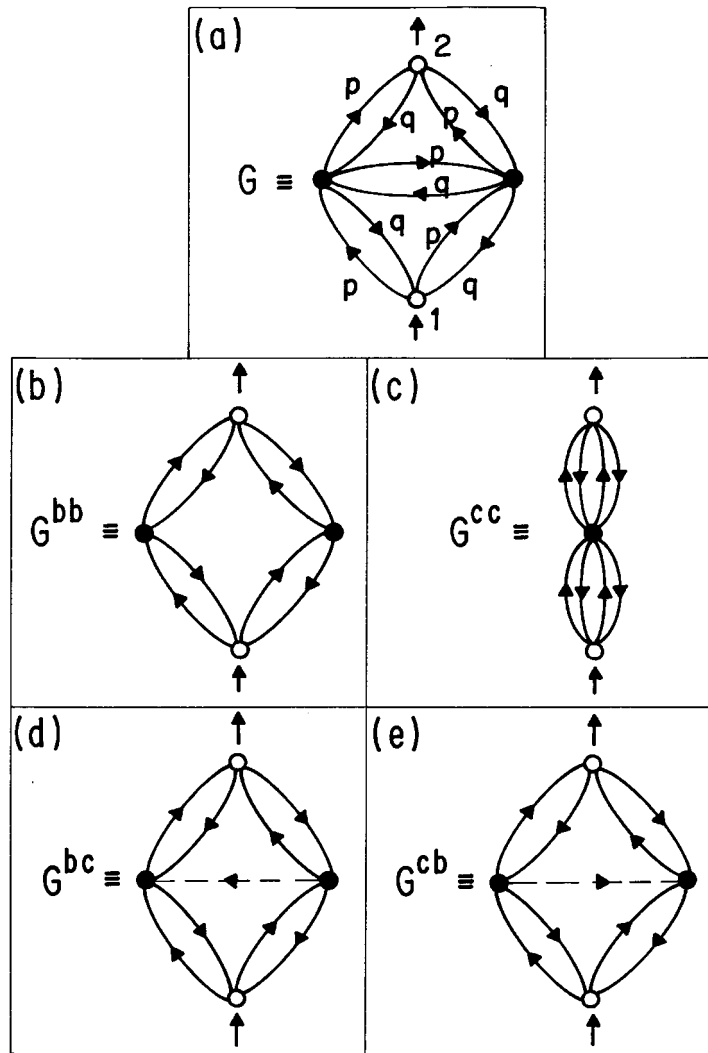


FIG. 17

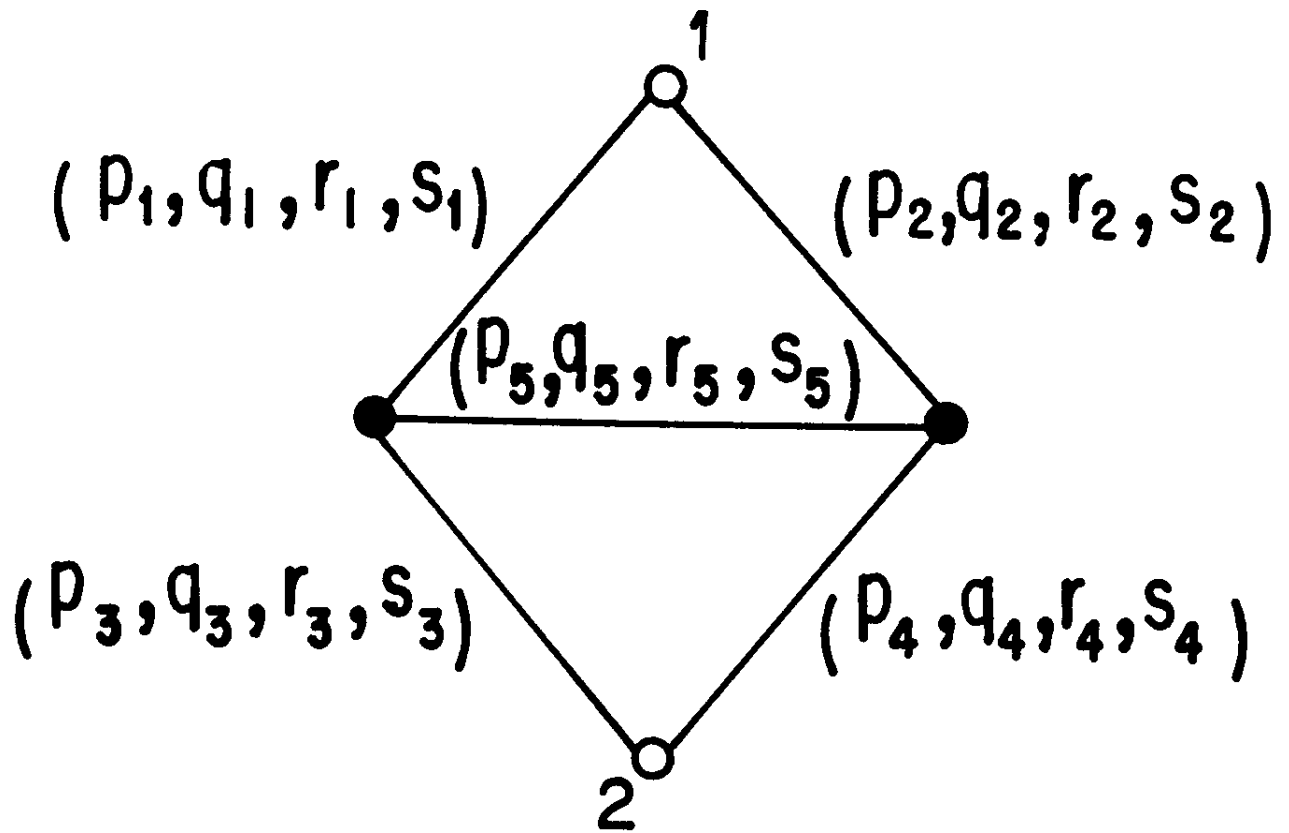


FIG. 18

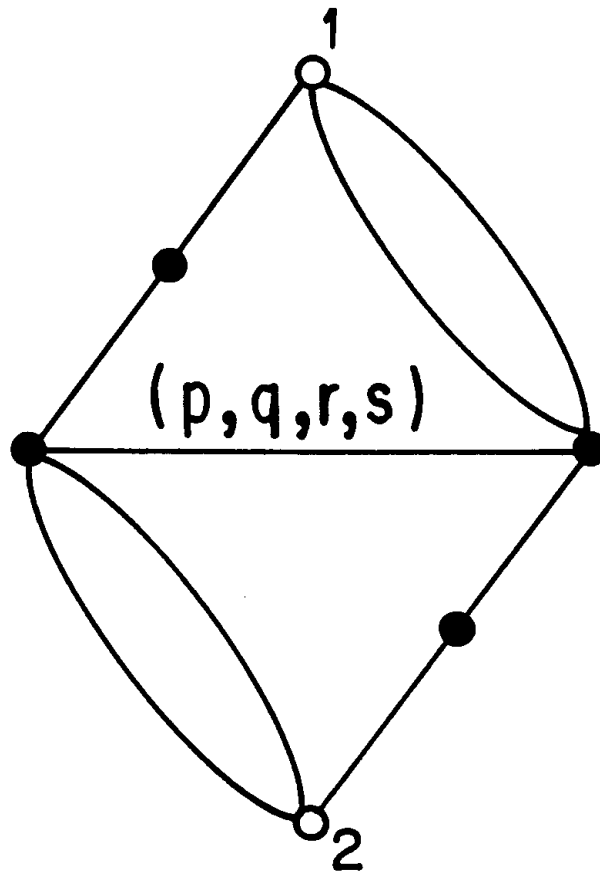


FIG. 19

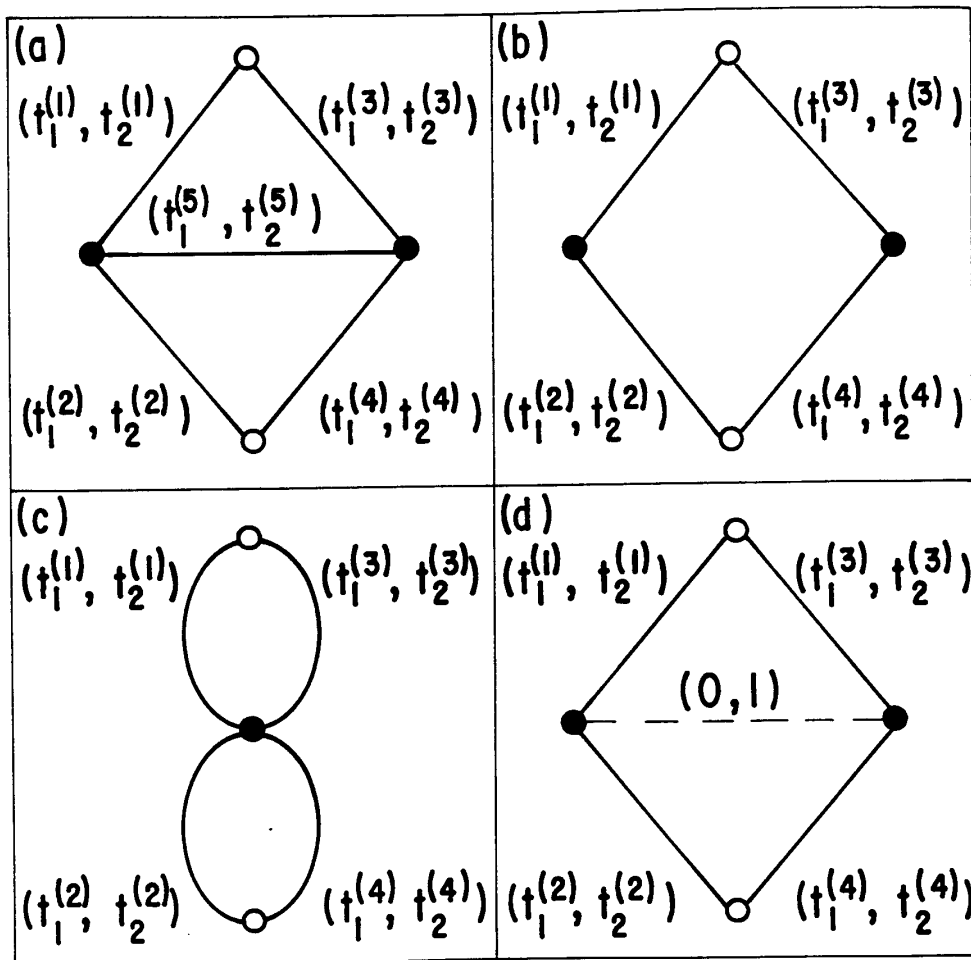


FIG. 20



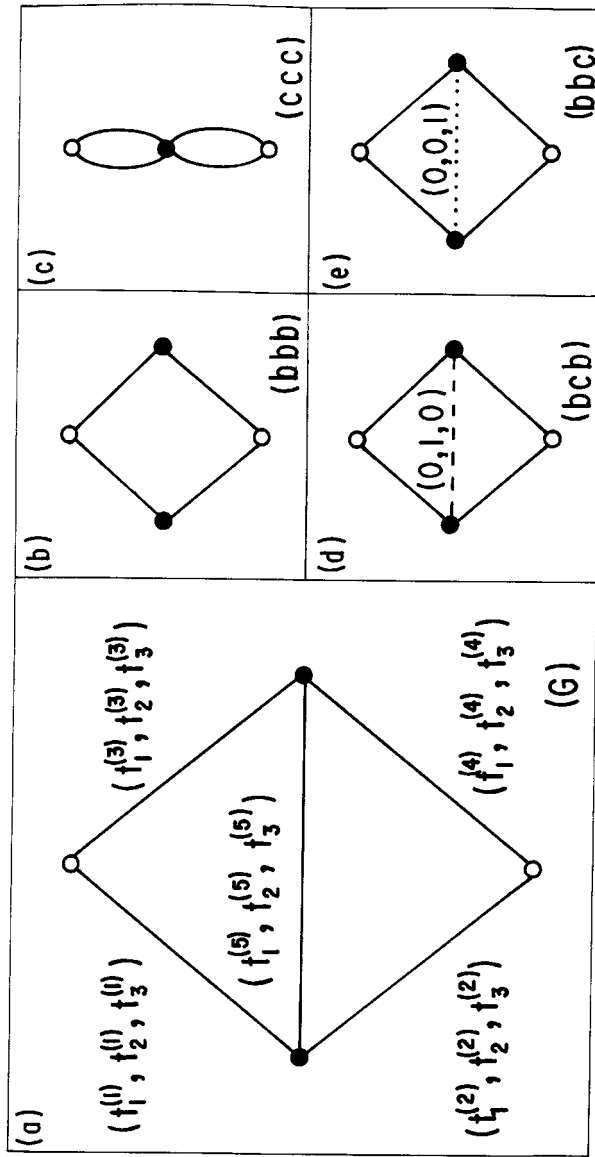


FIG. 21

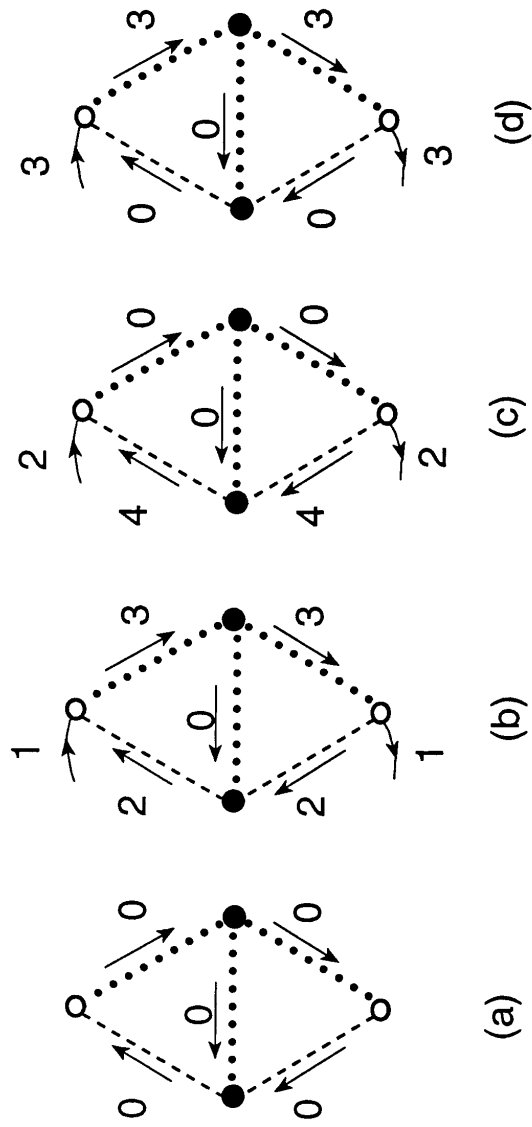


FIG. 22

-171-

CBPF-NF-046/95

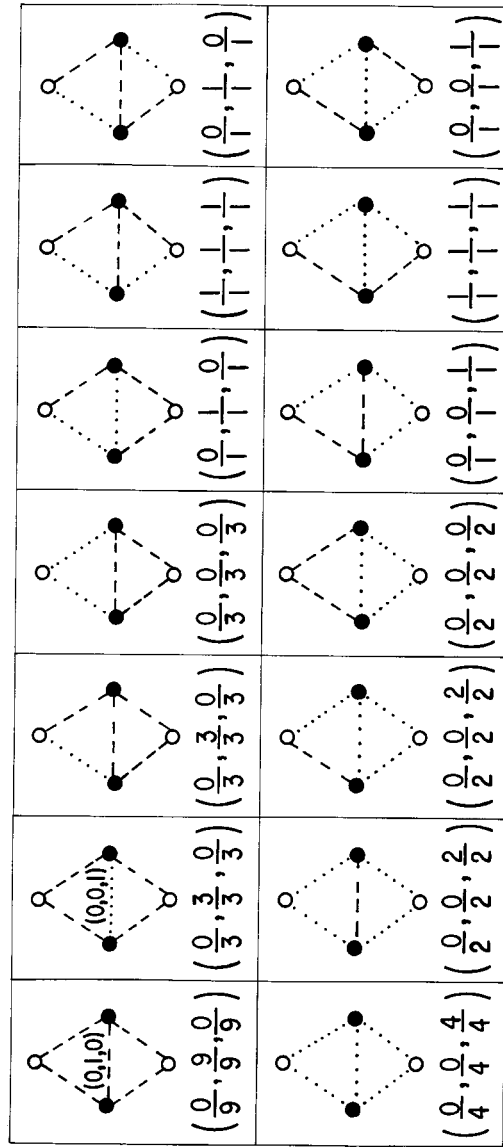


FIG. 23

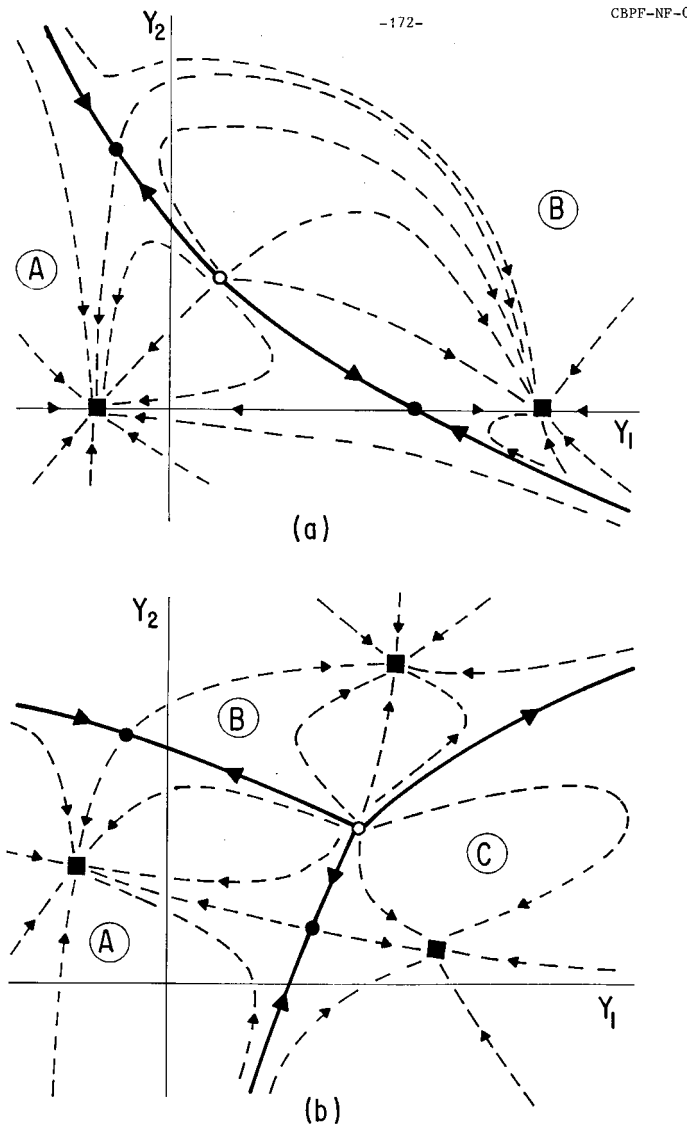


FIG. 24

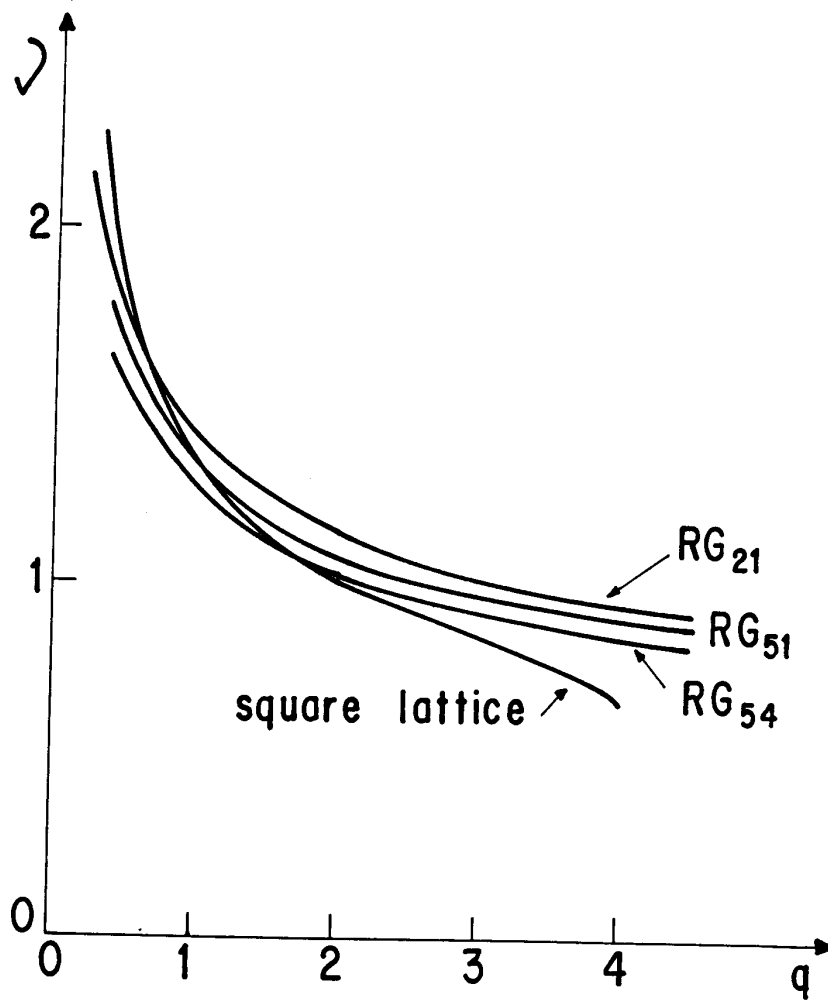


FIG. 25

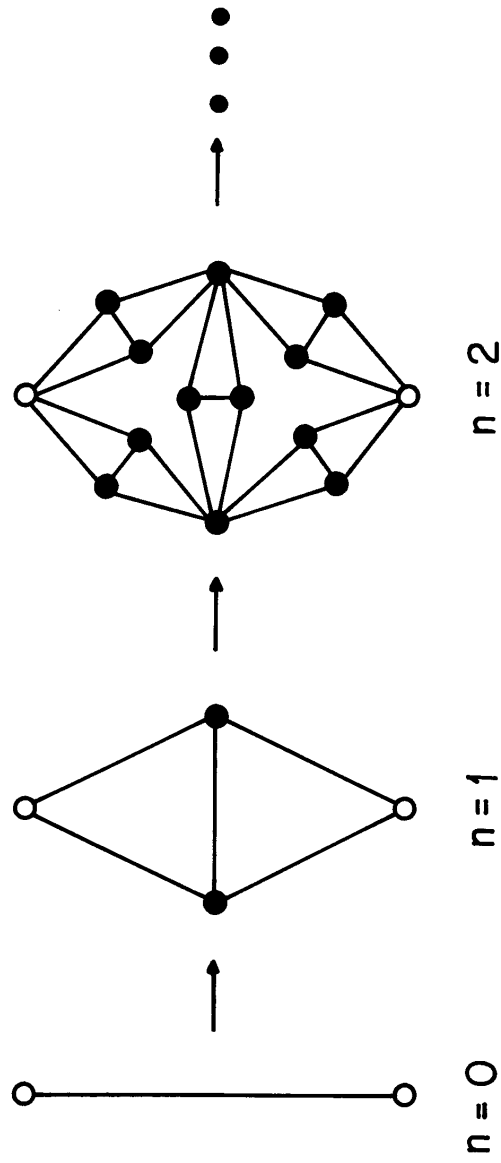


FIG. 26

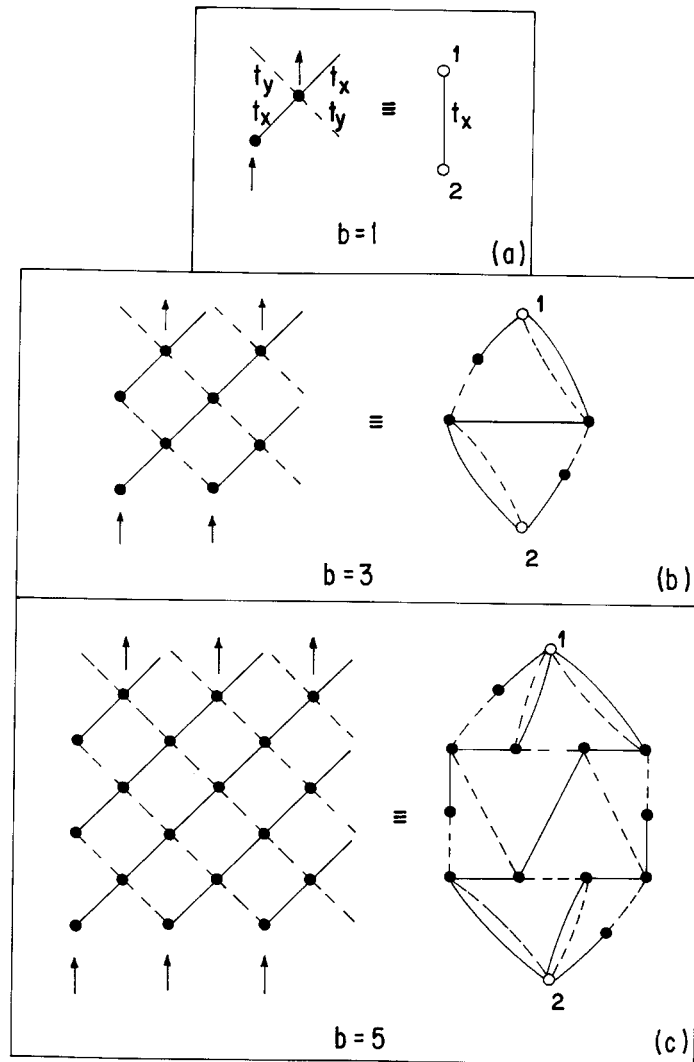


FIG. 27

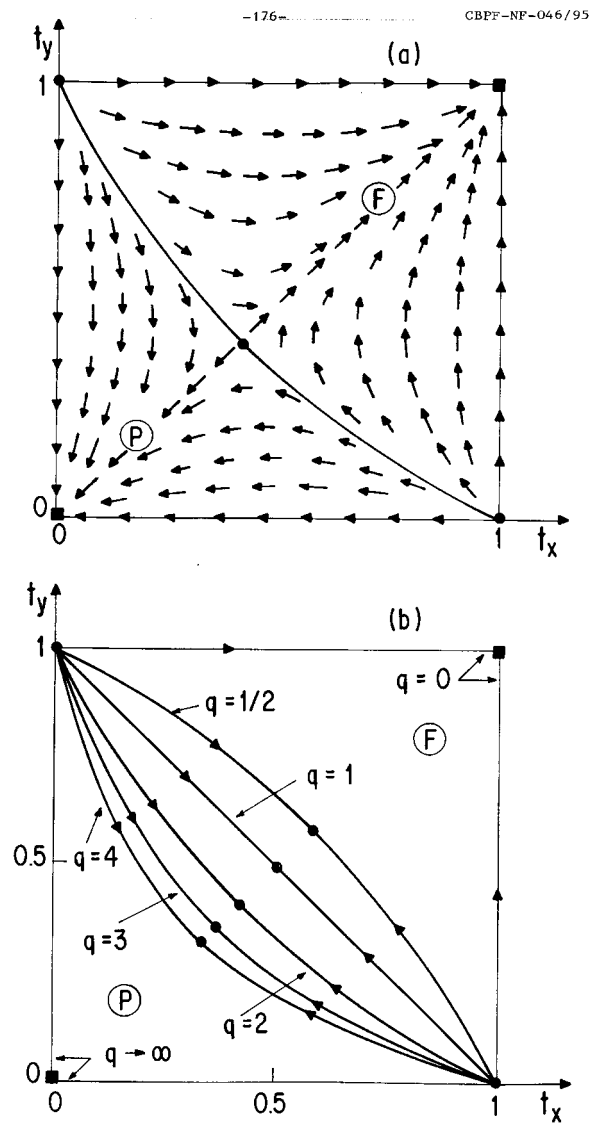


FIG. 28



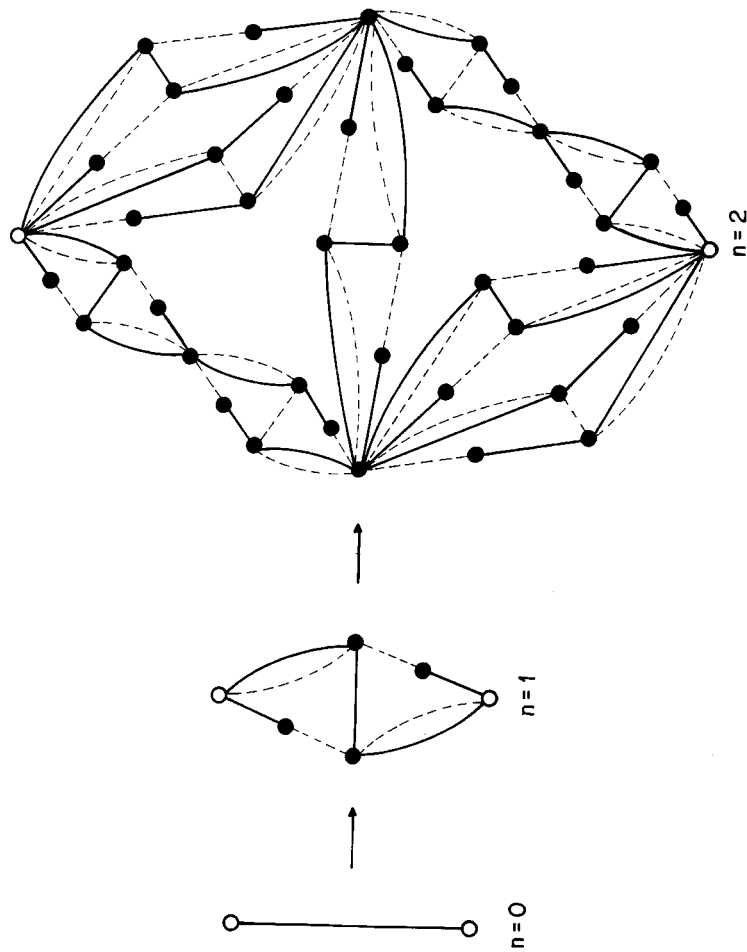


FIG. 29

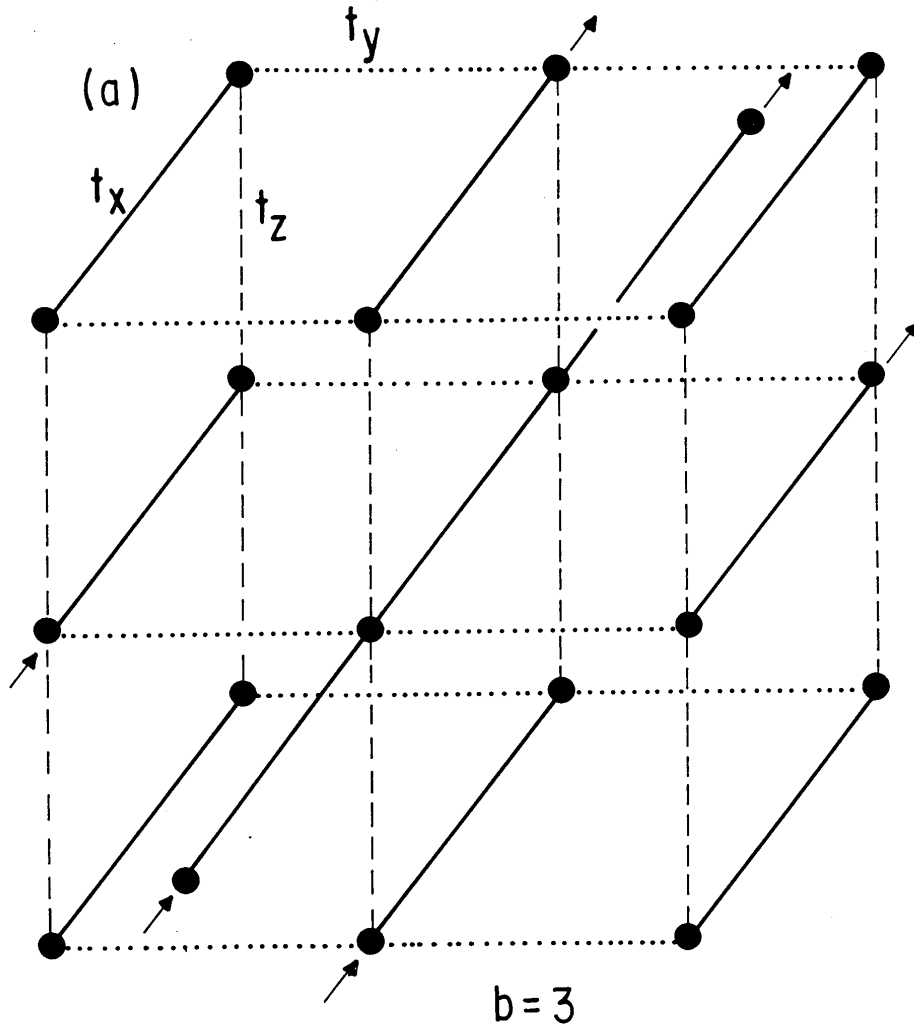


FIG. 30

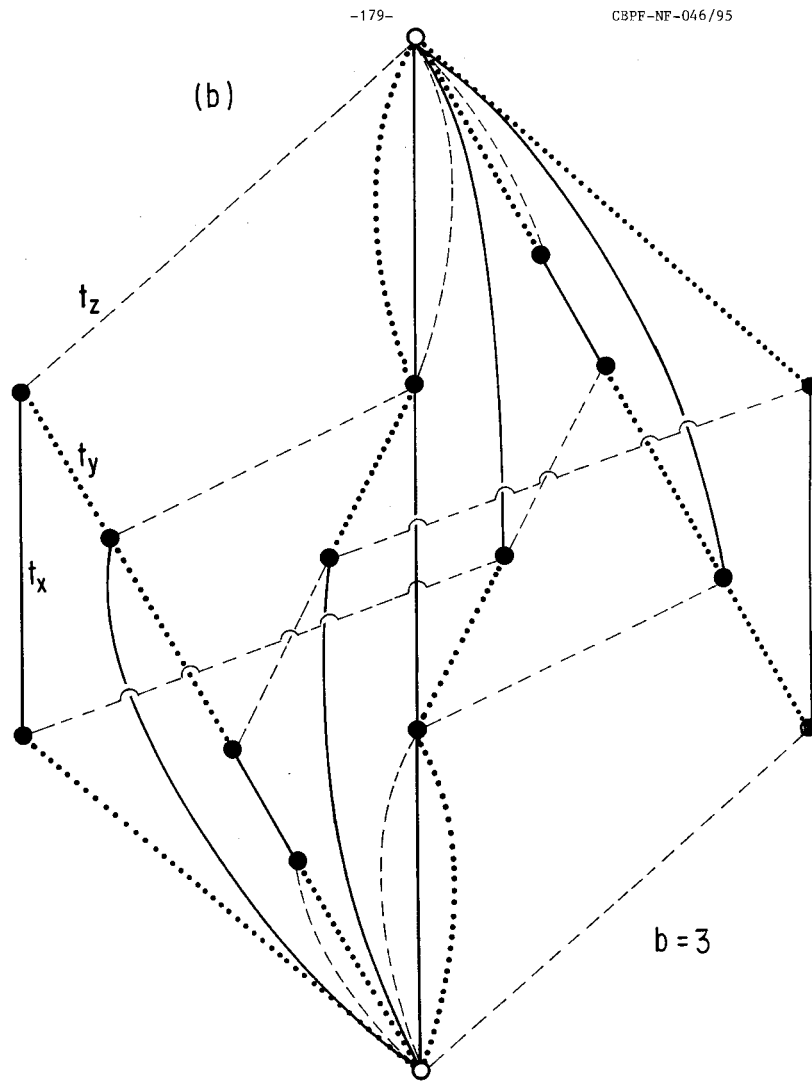


FIG. 30

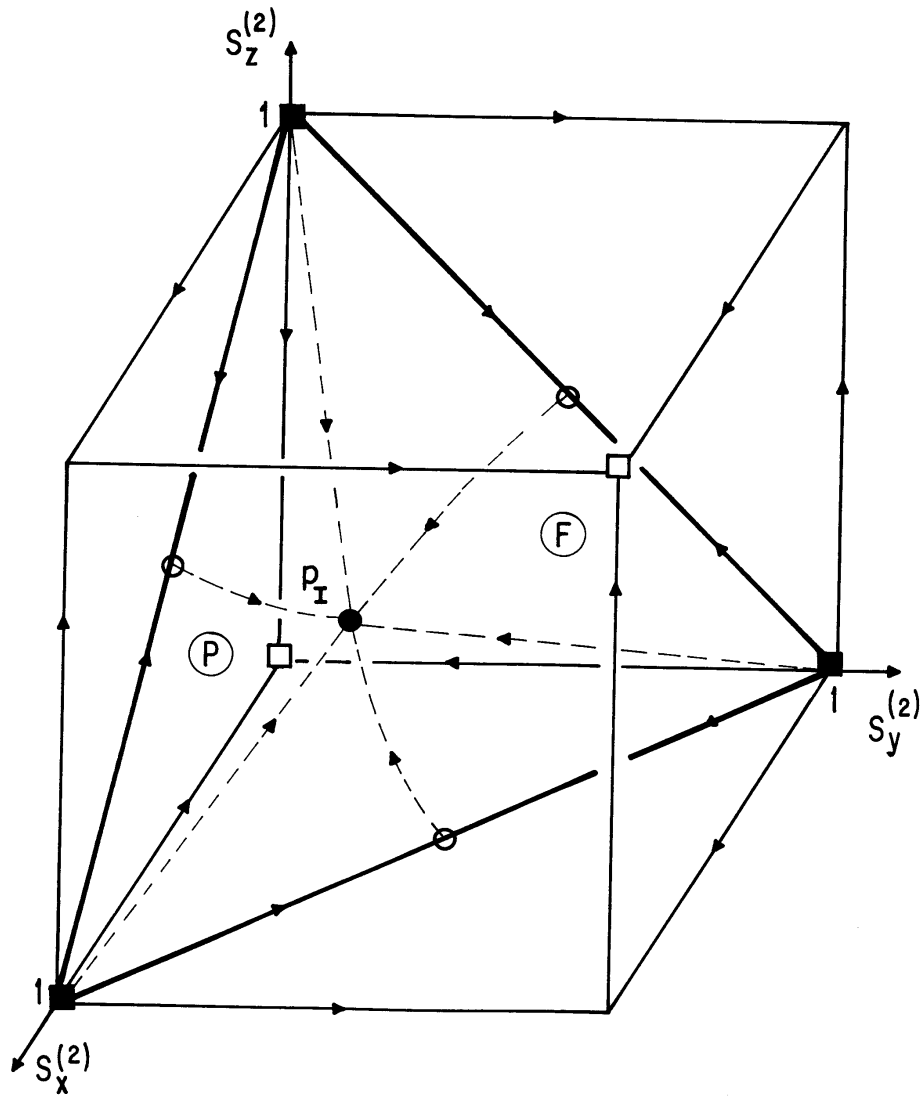


FIG. 31

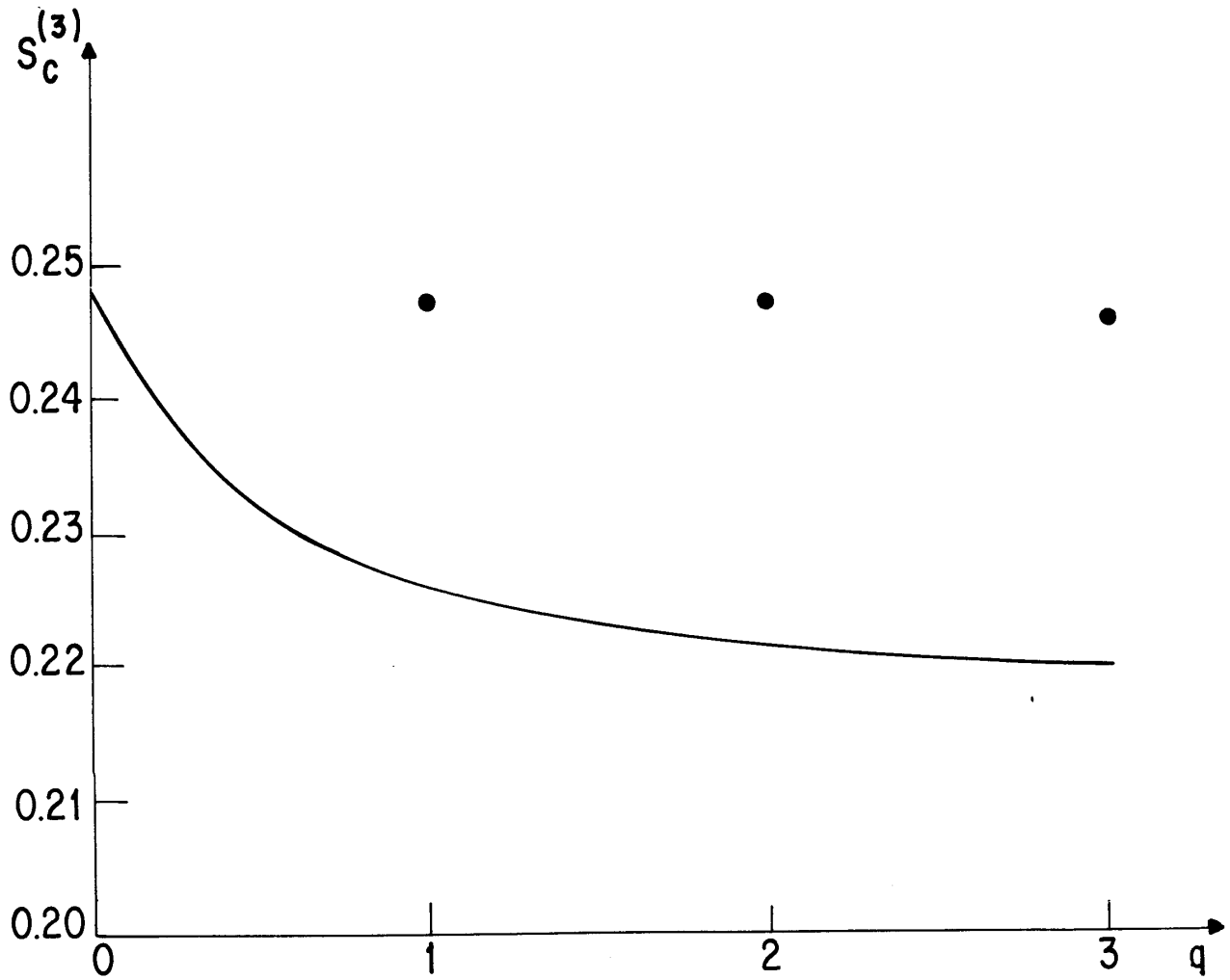


FIG. 32

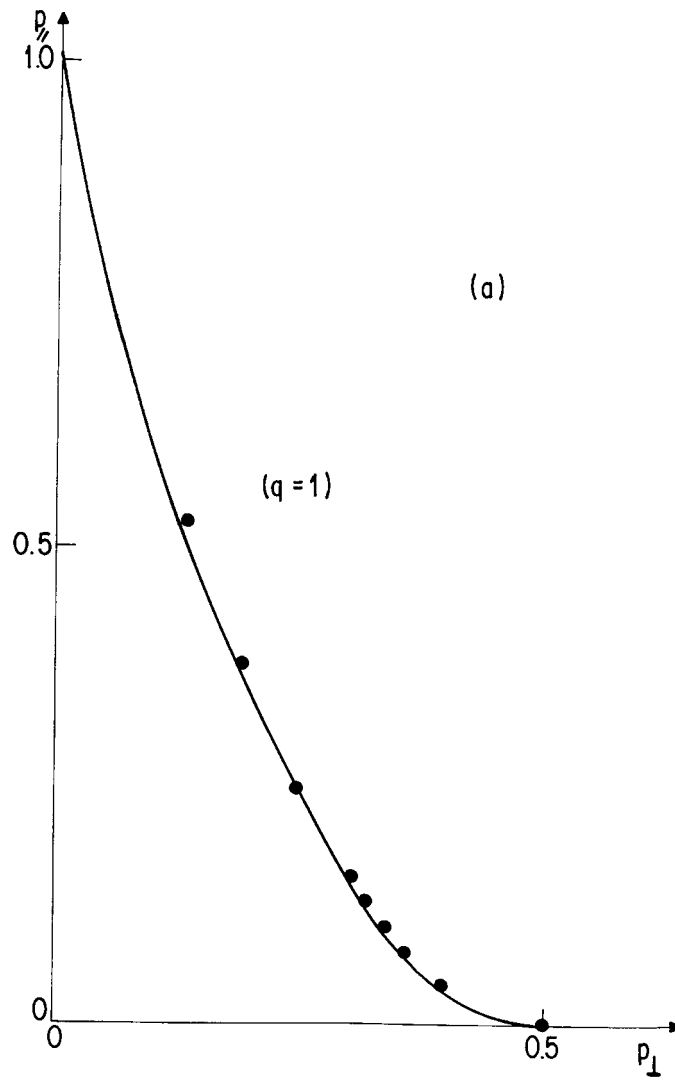


FIG. 33

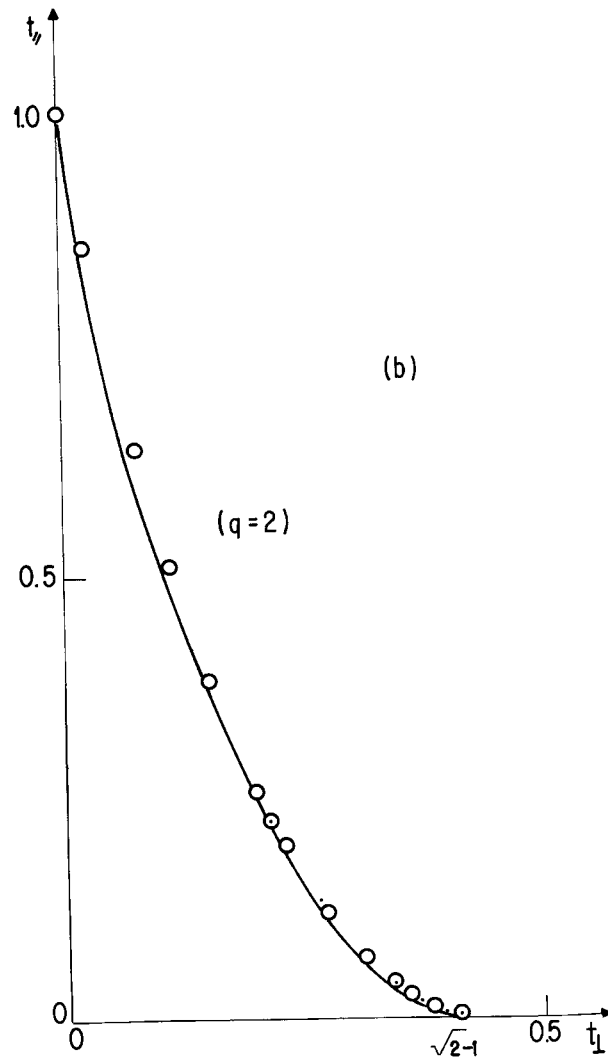


FIG. 33

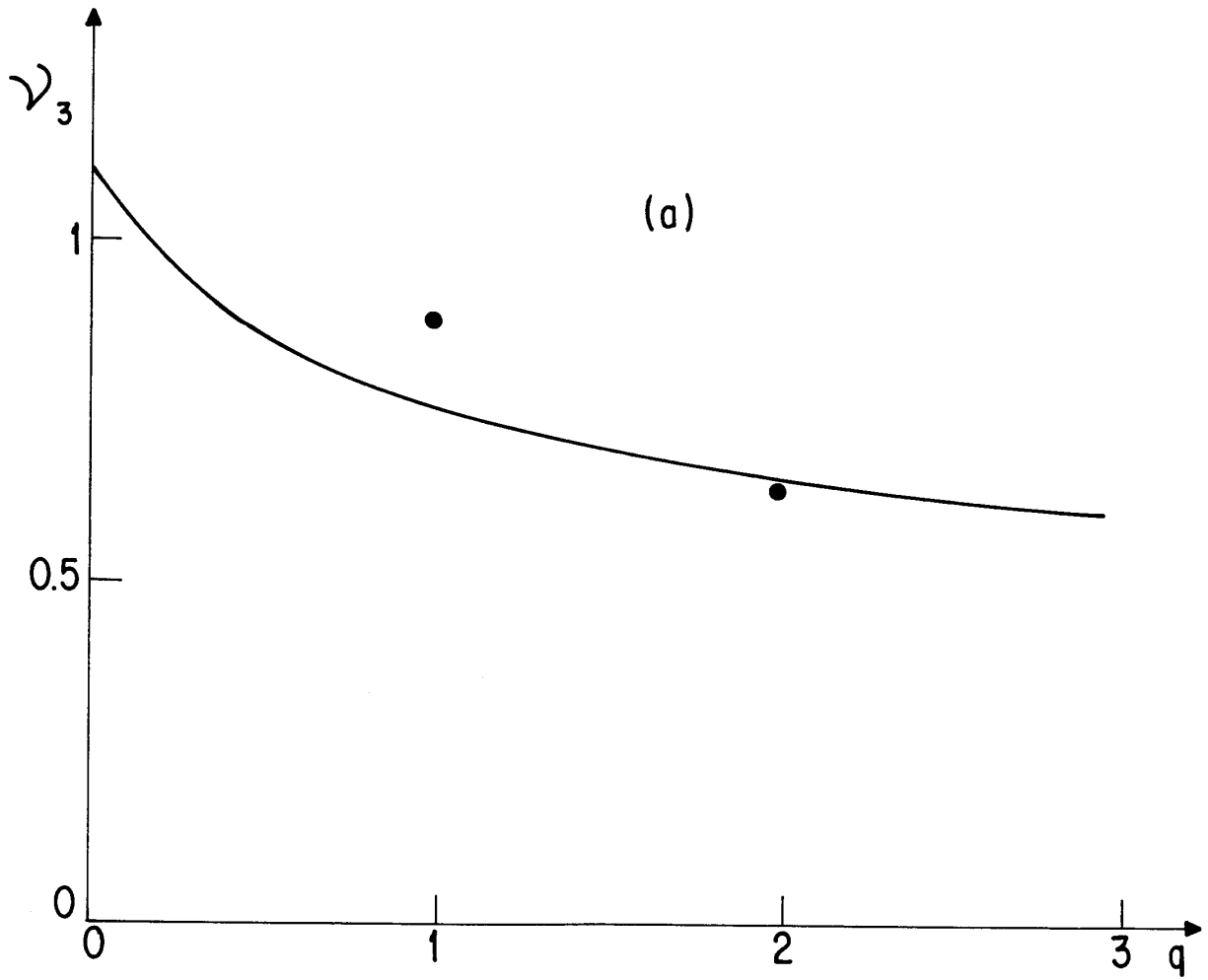


FIG. 34



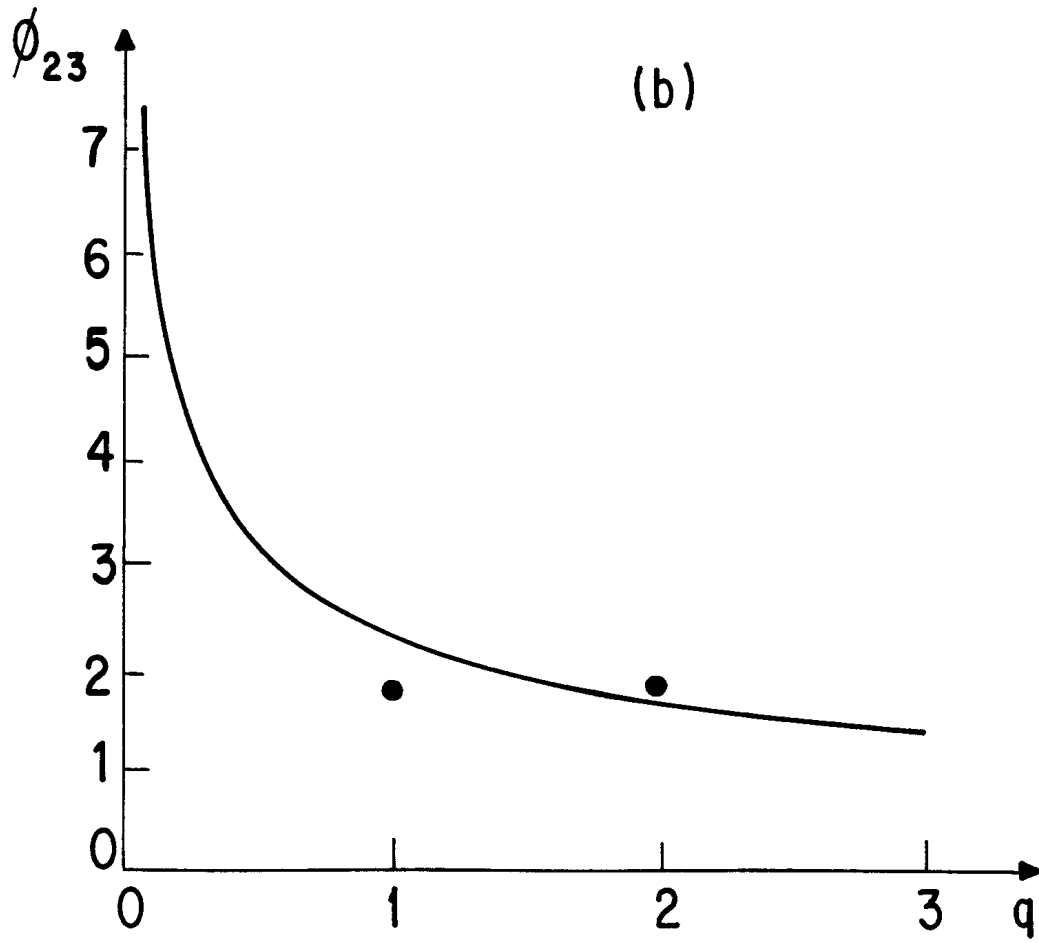


FIG. 34

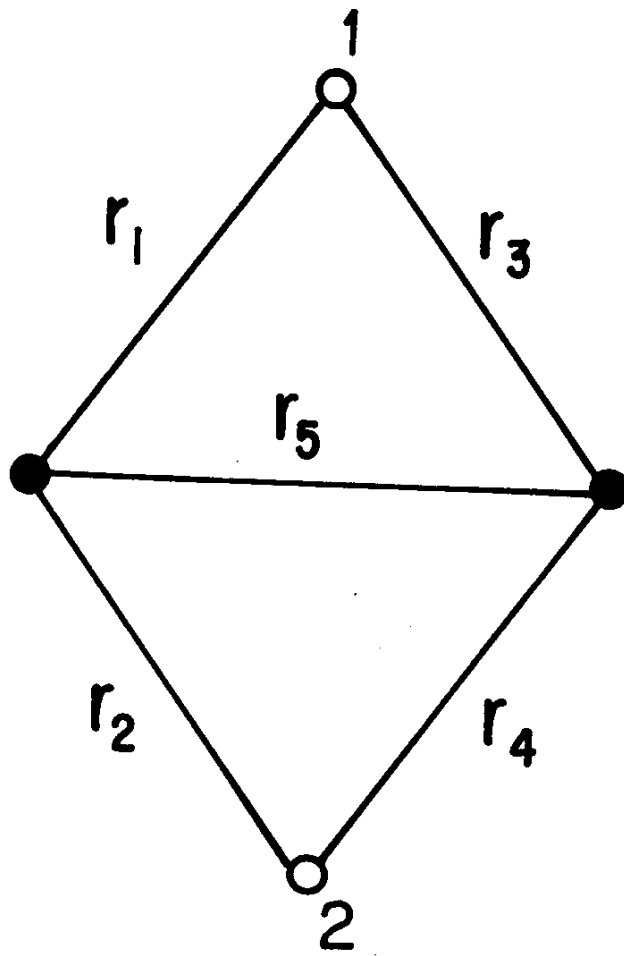


FIG. 35

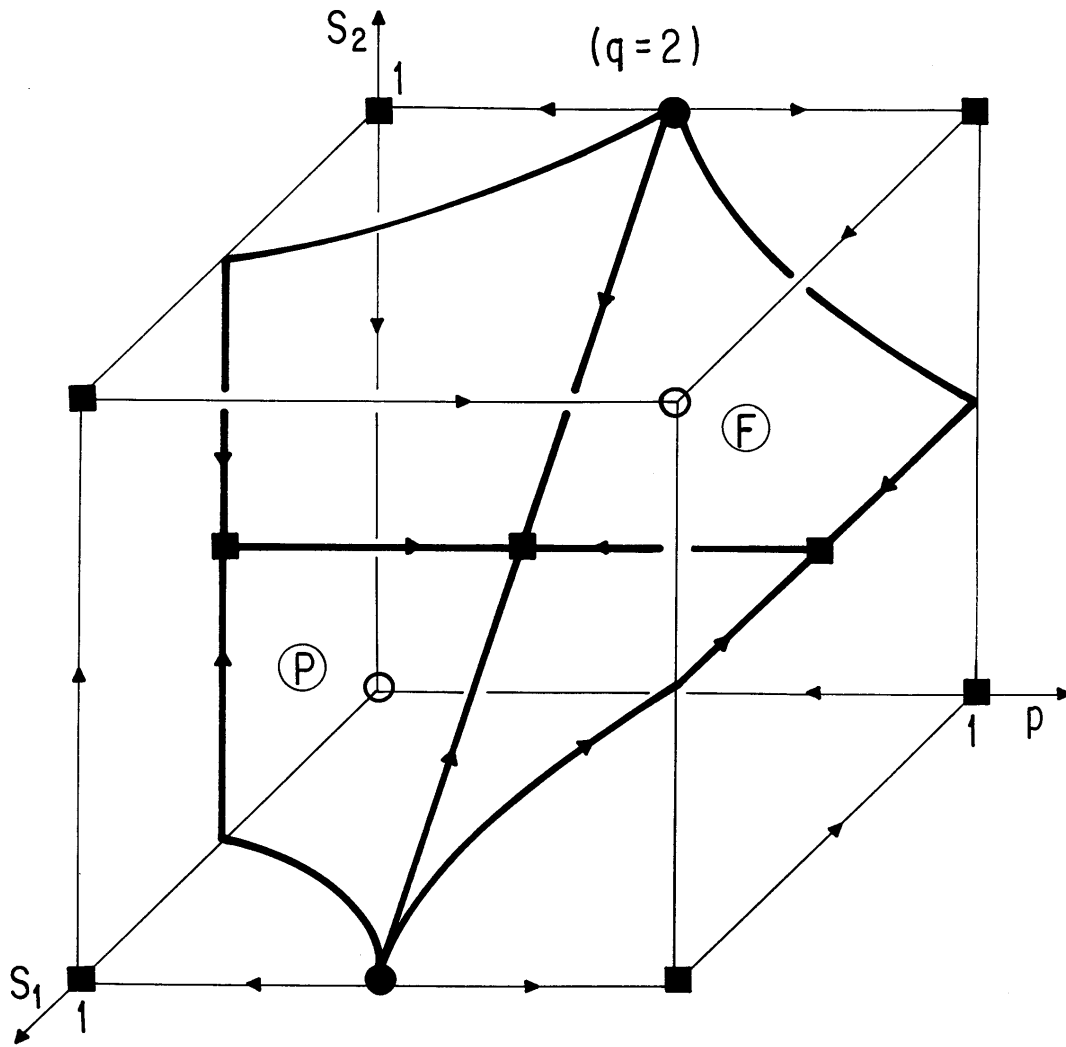


FIG. 36

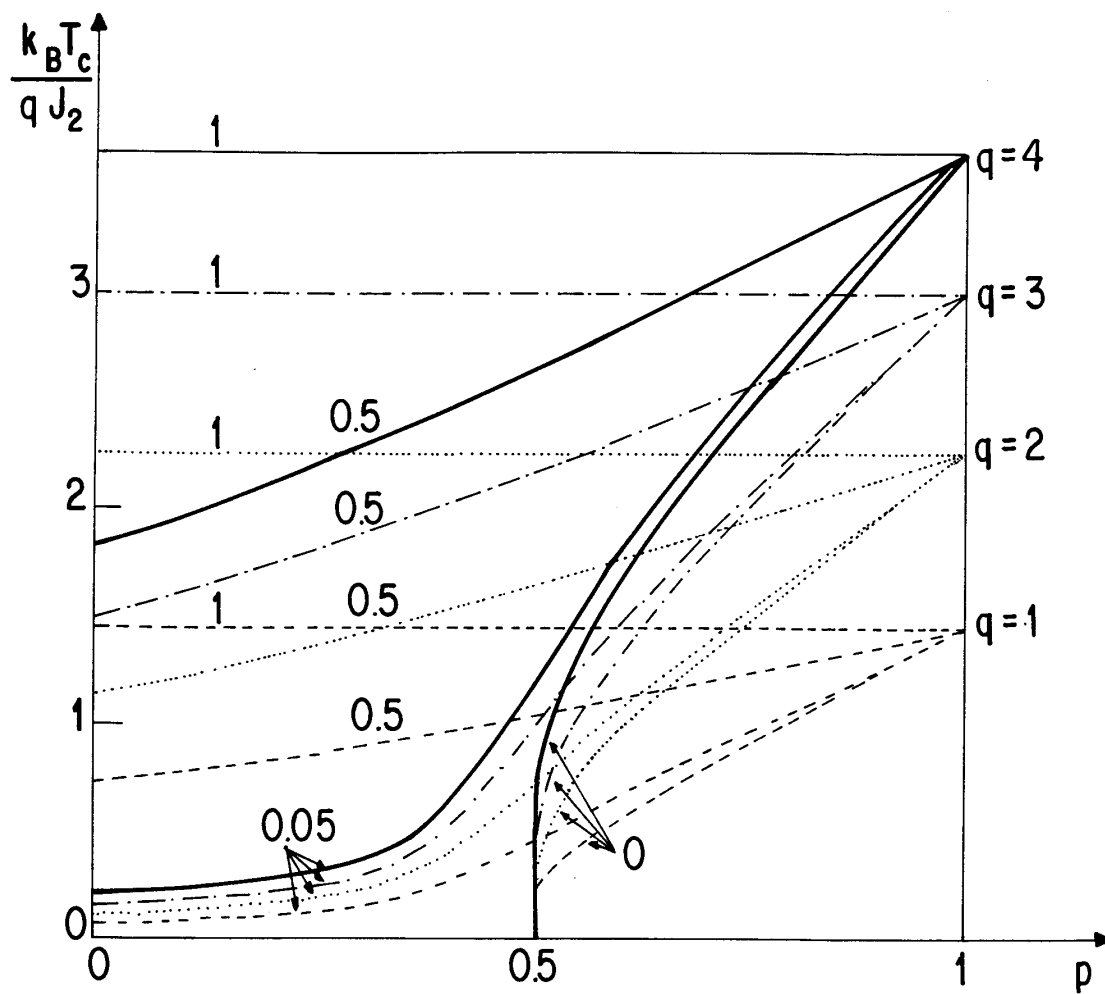


FIG. 37

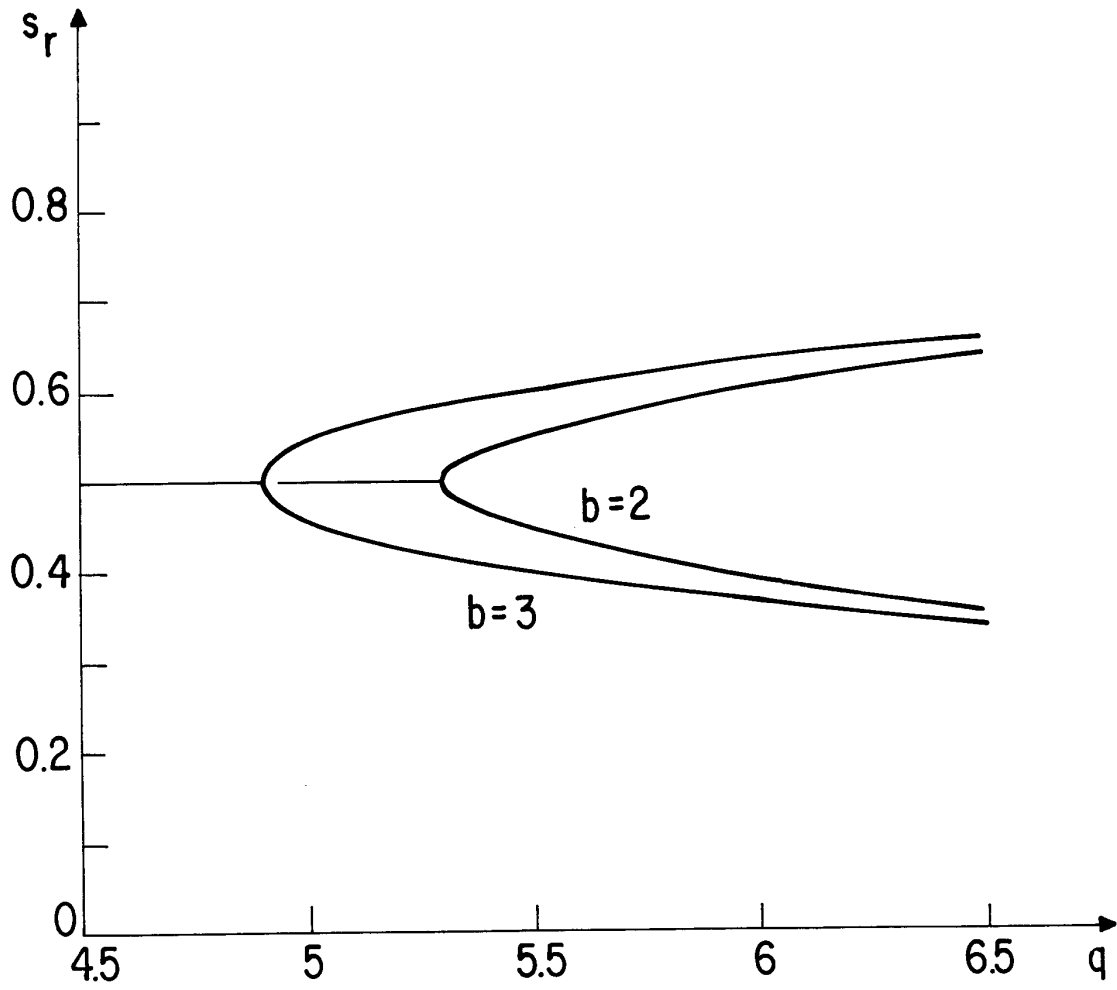


FIG. 38

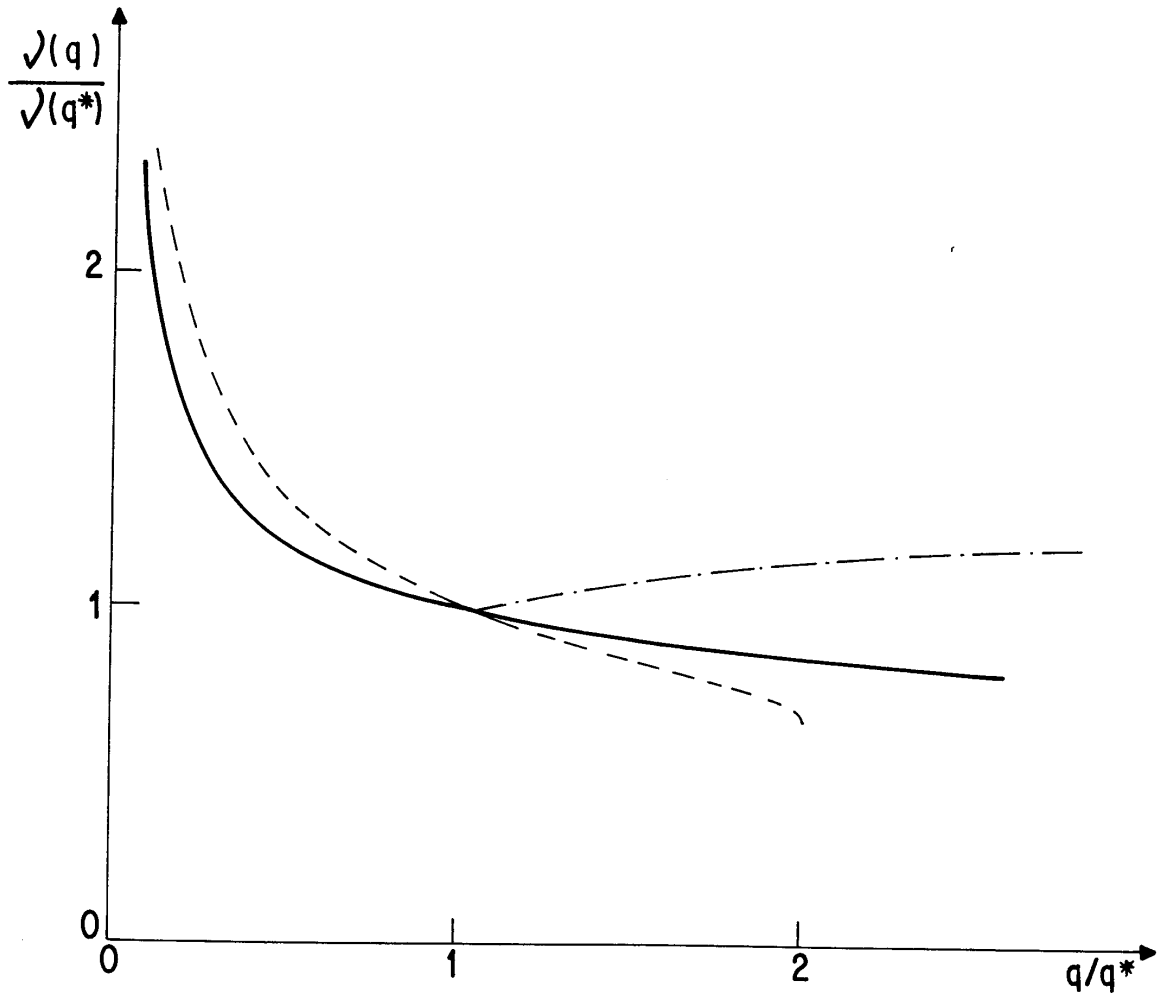


FIG. 39

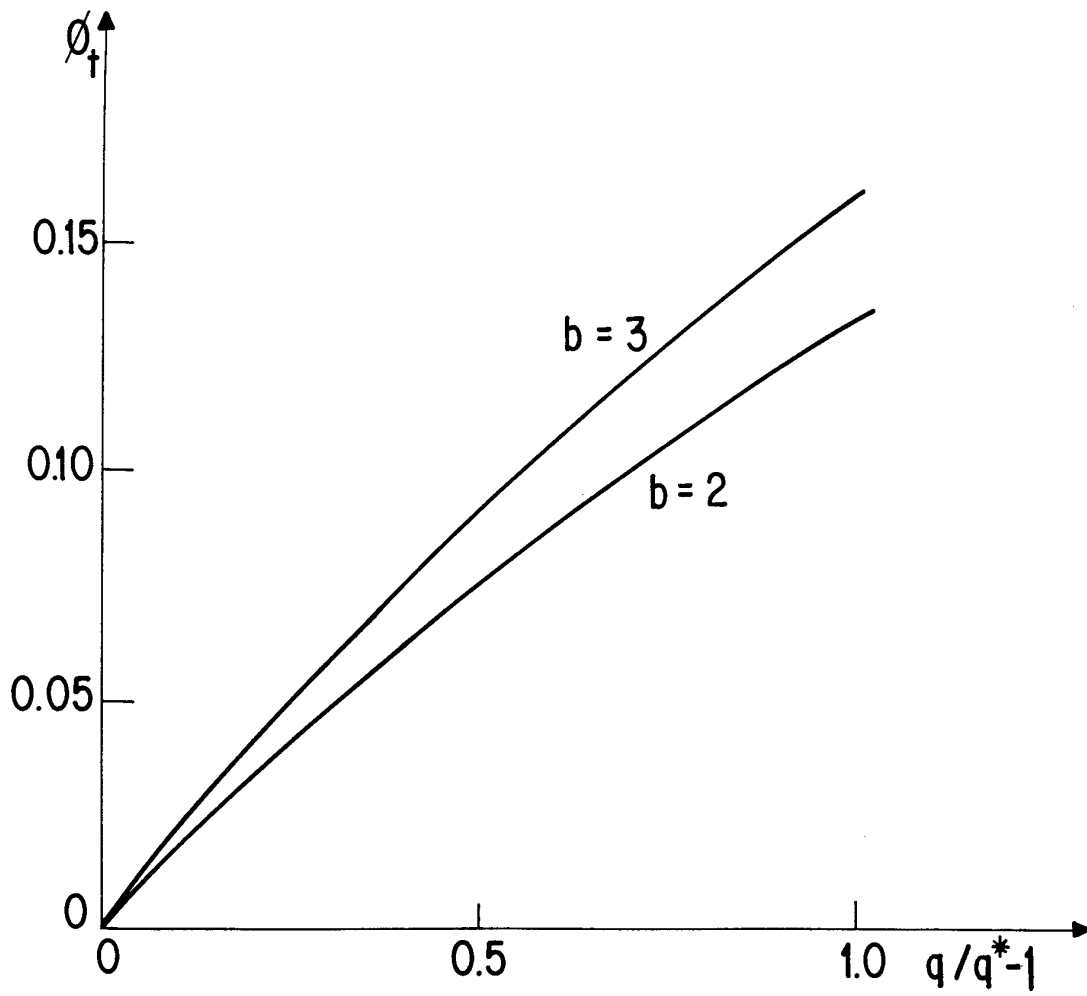


FIG. 40

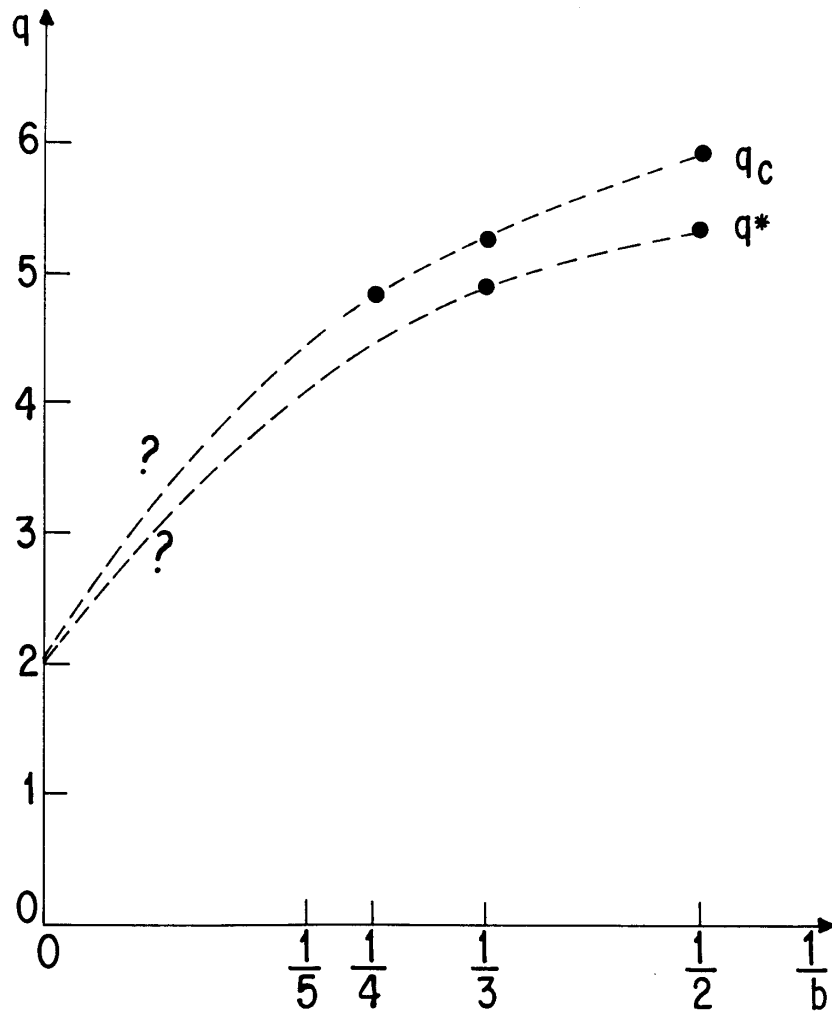


FIG. 41



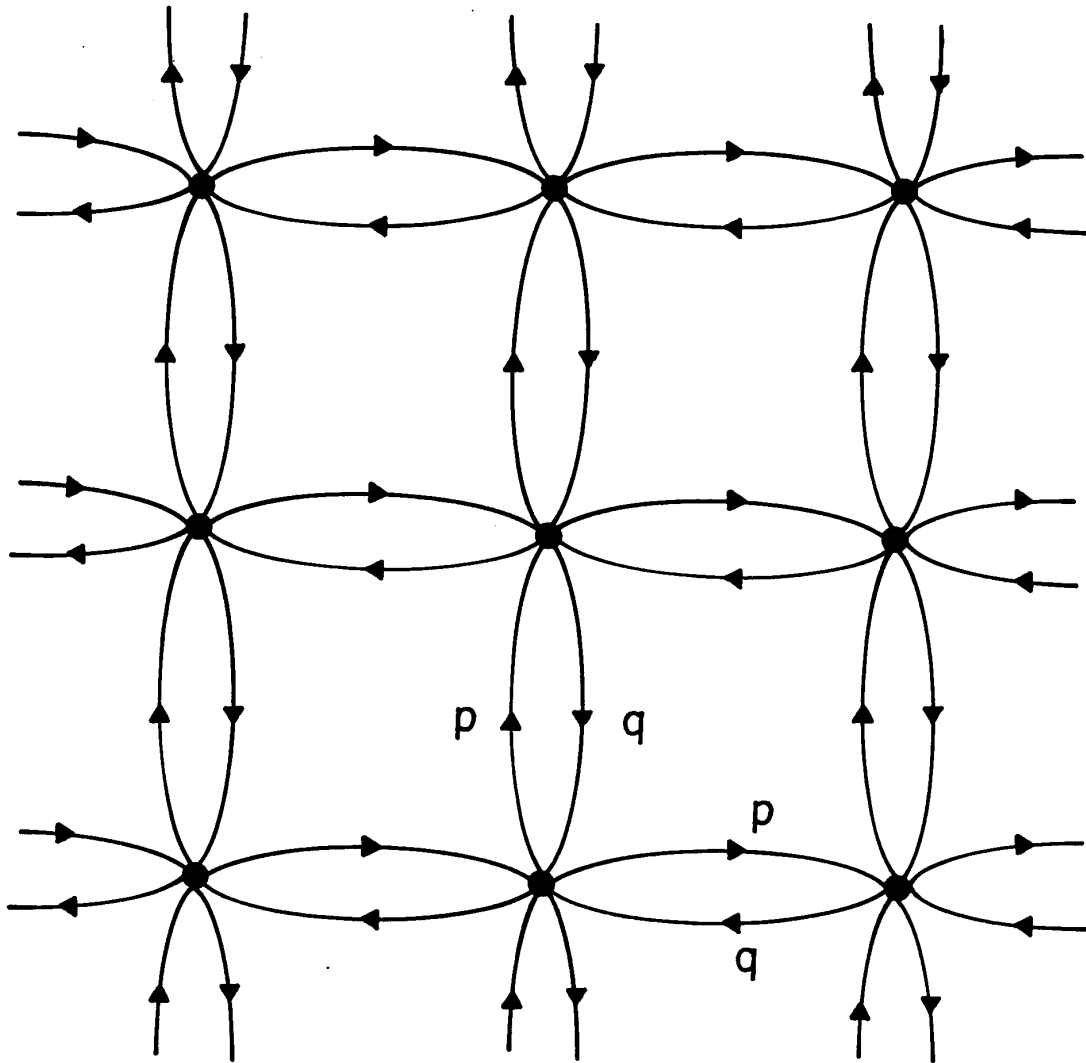


FIG. 42

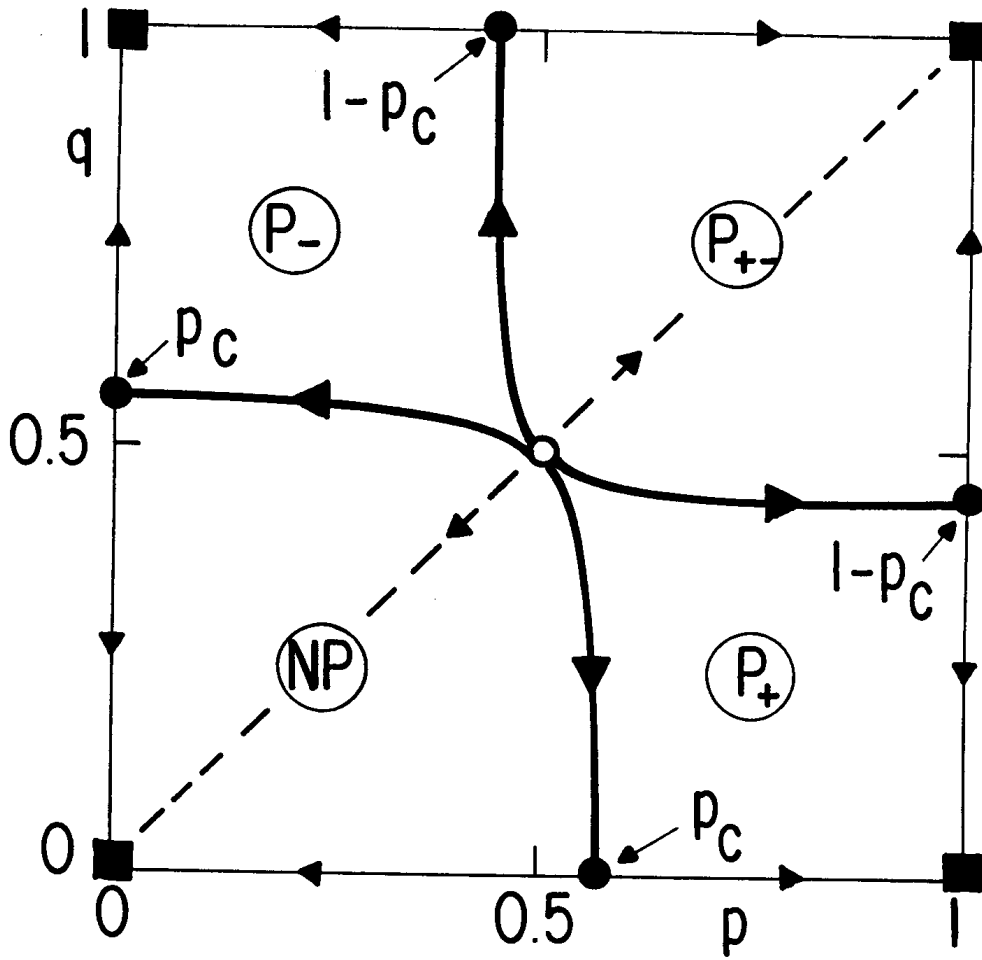


FIG. 43



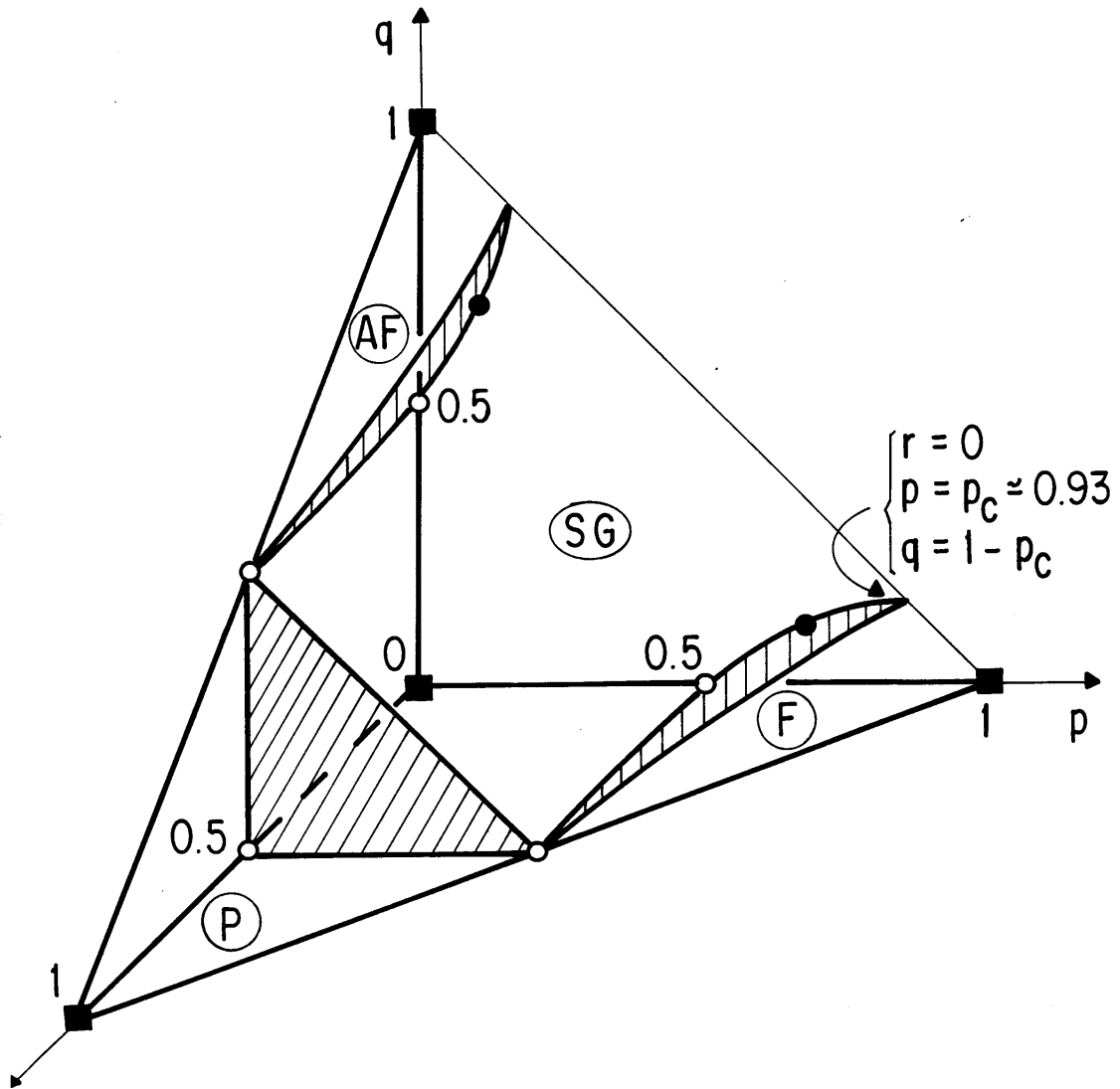


FIG. 45

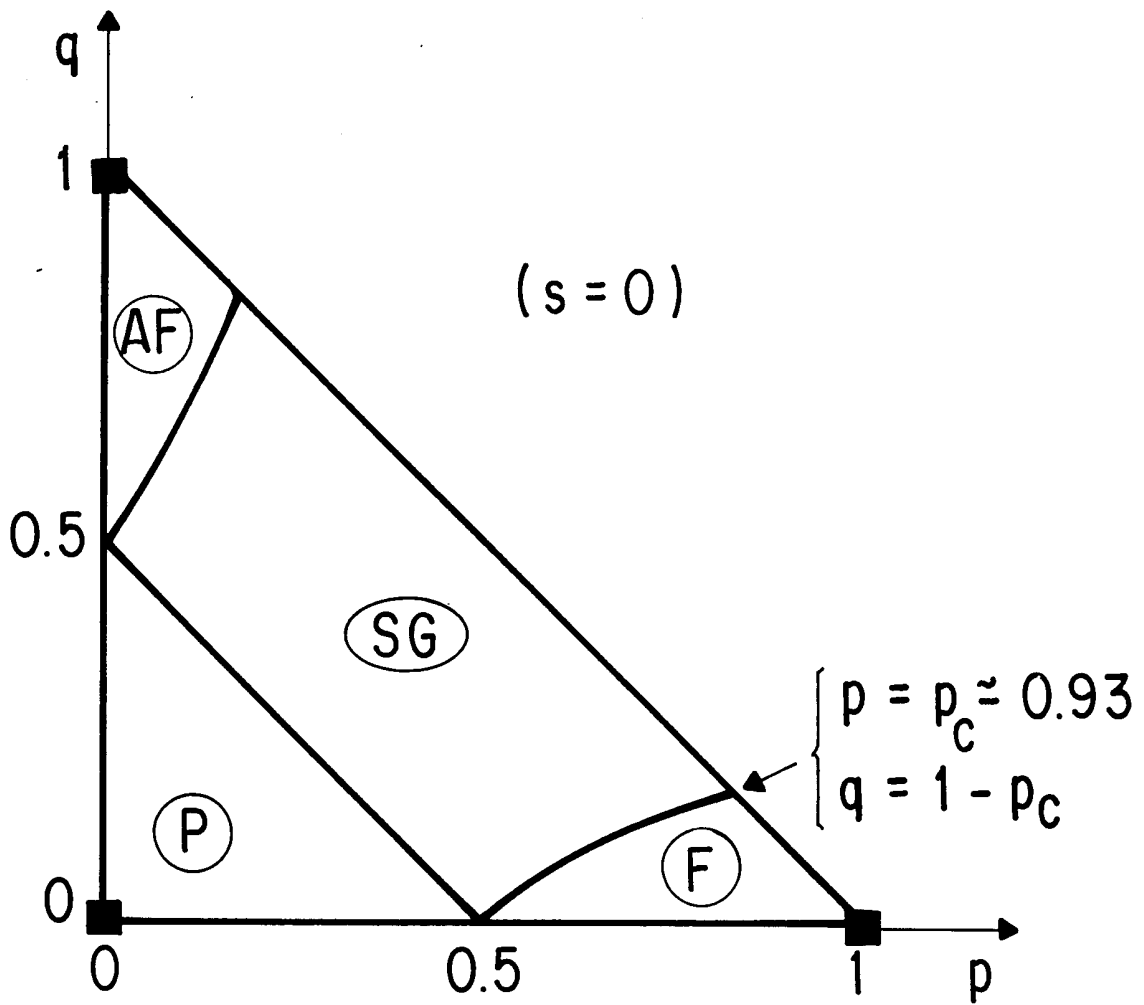


FIG. 46

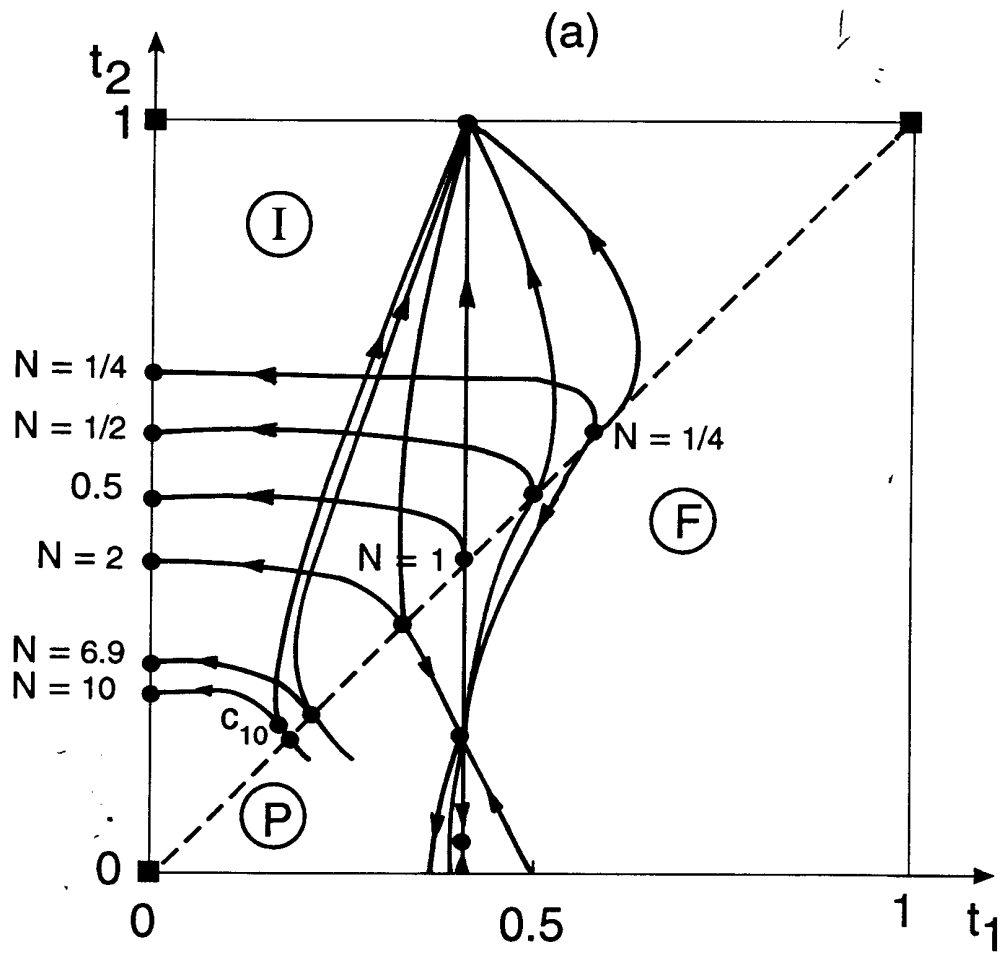


FIG. 47

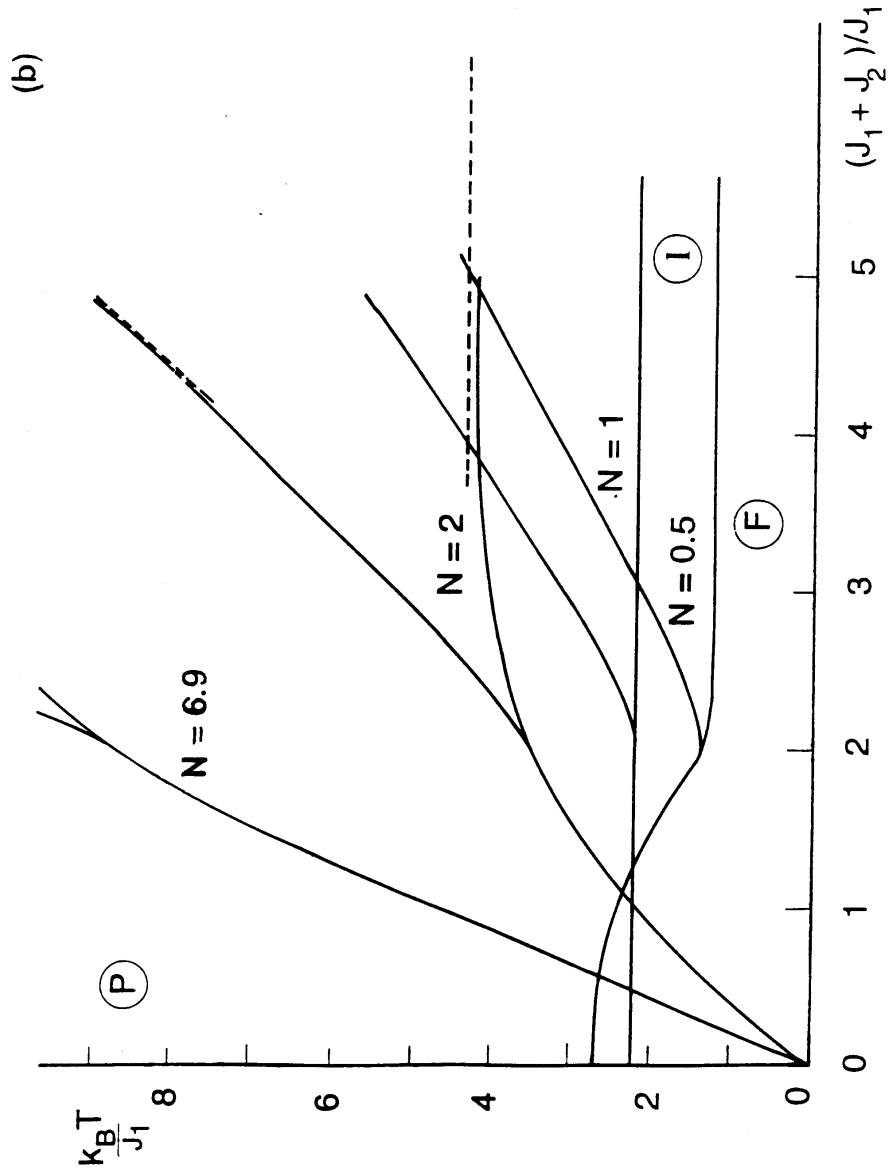


FIG. 47

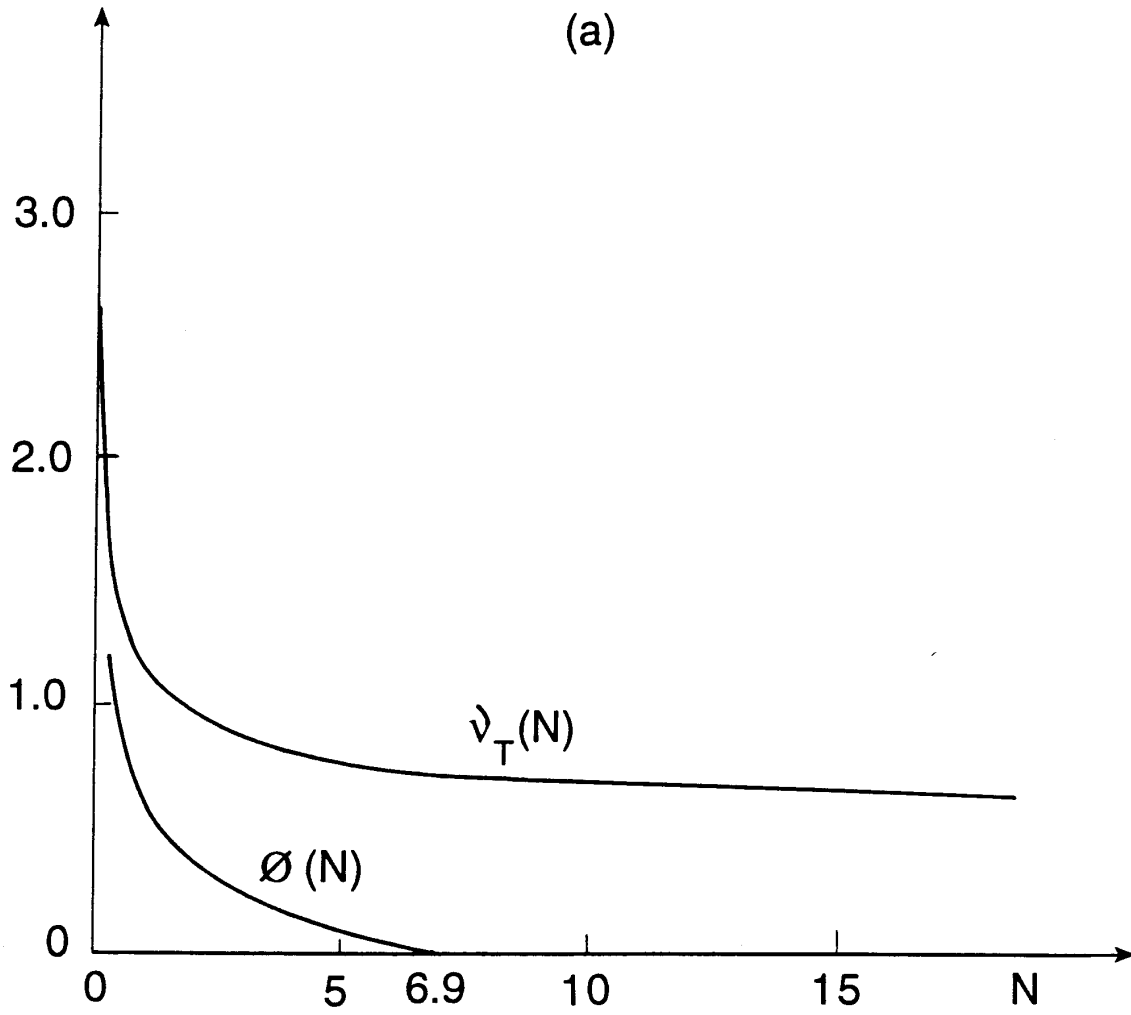


Fig. 48



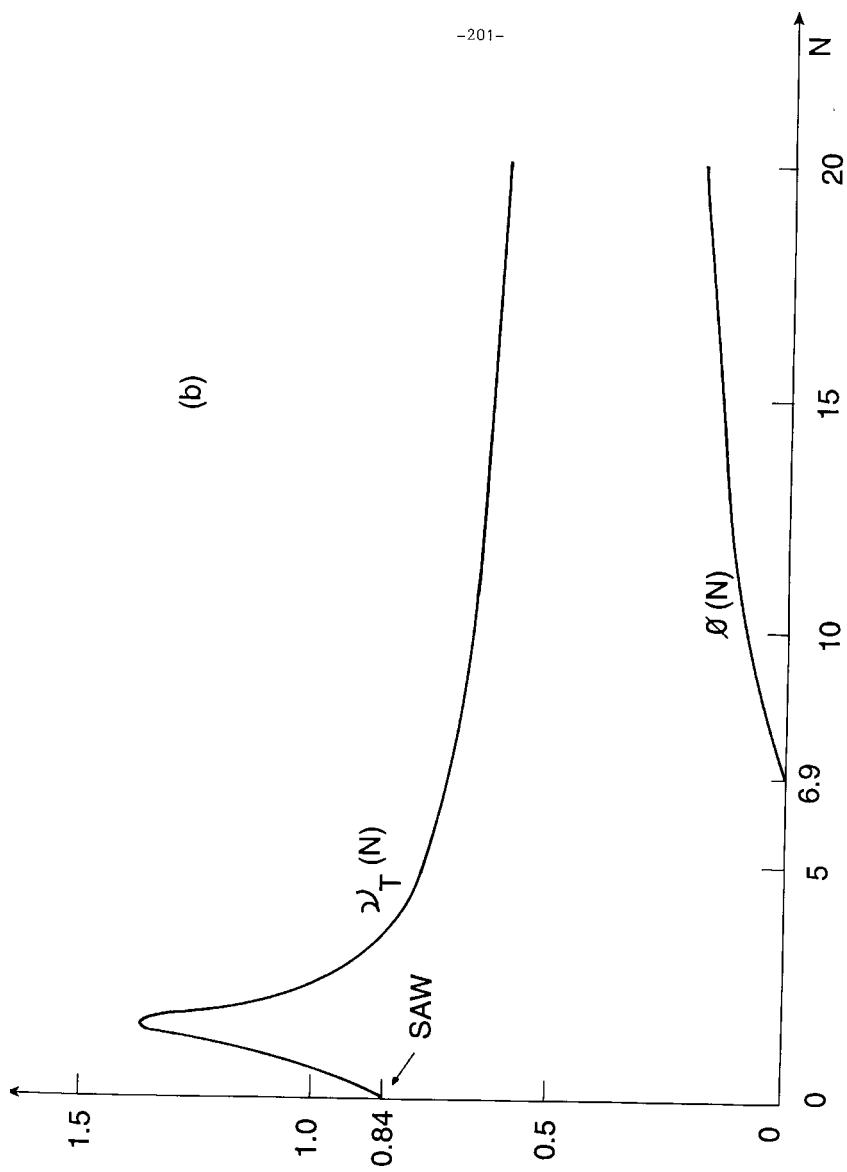


FIG. 48

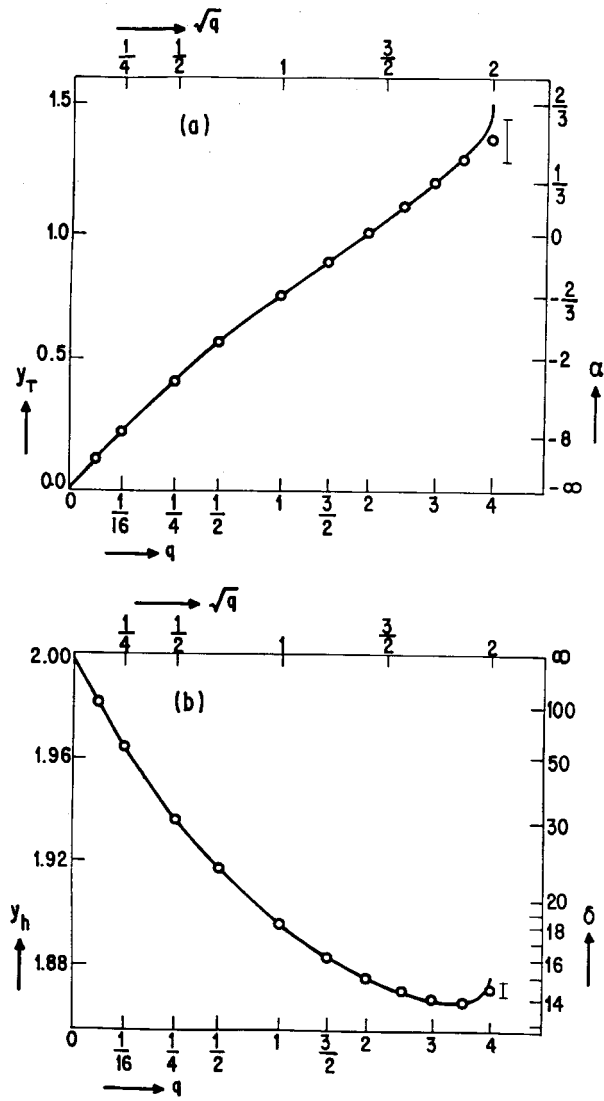


FIG. 49

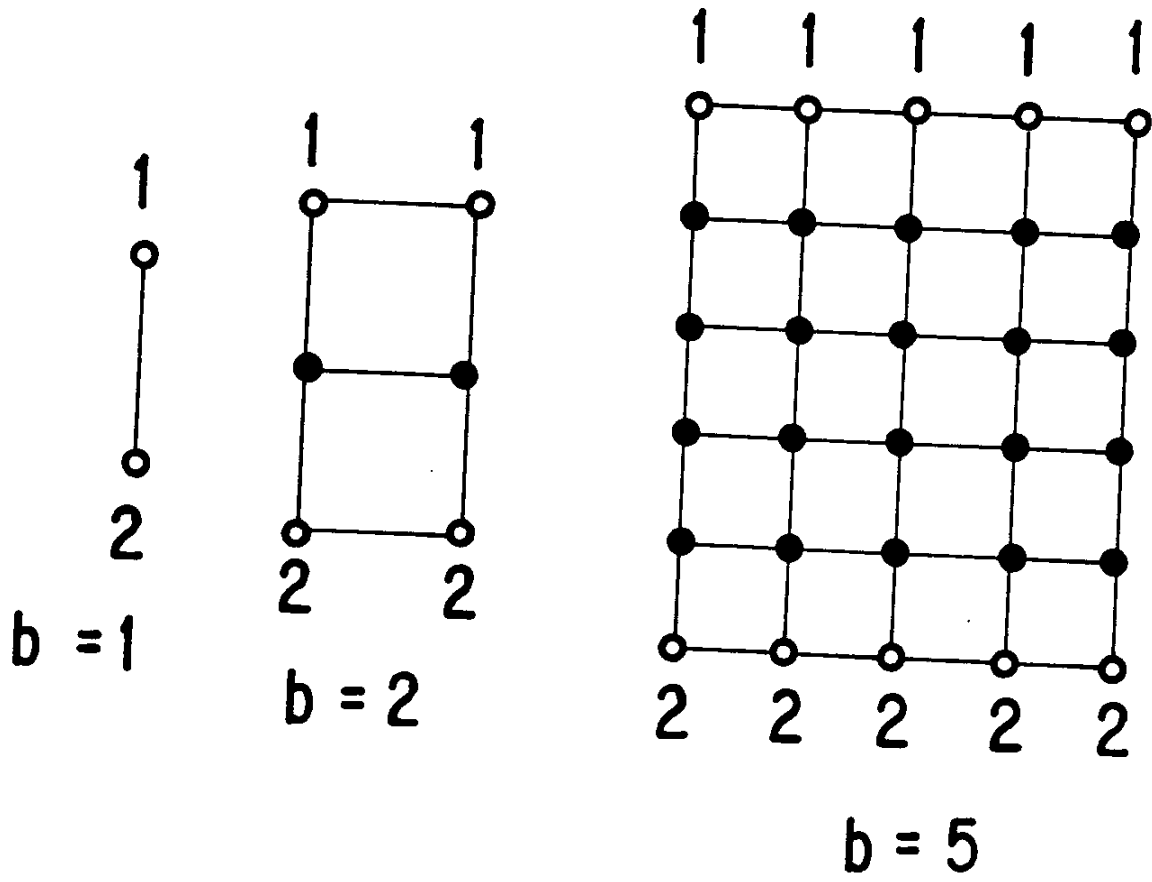


FIG. 50

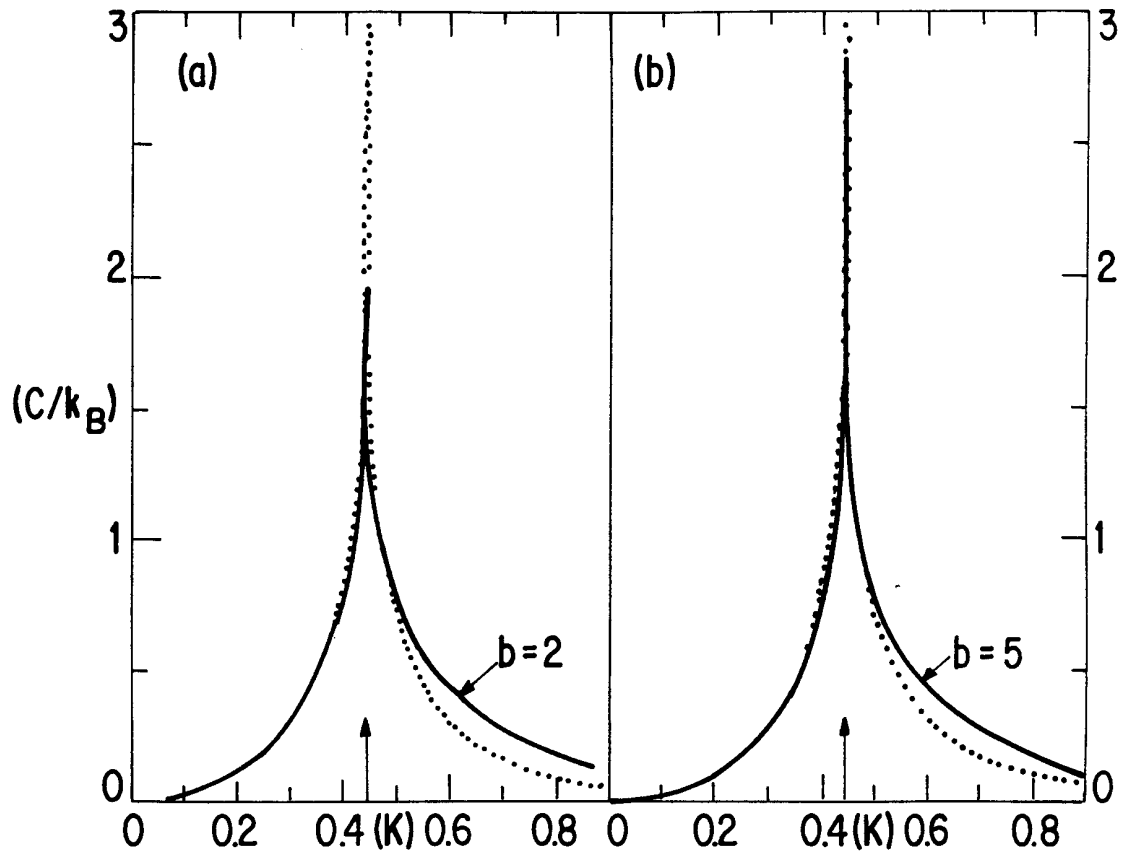


FIG. 51

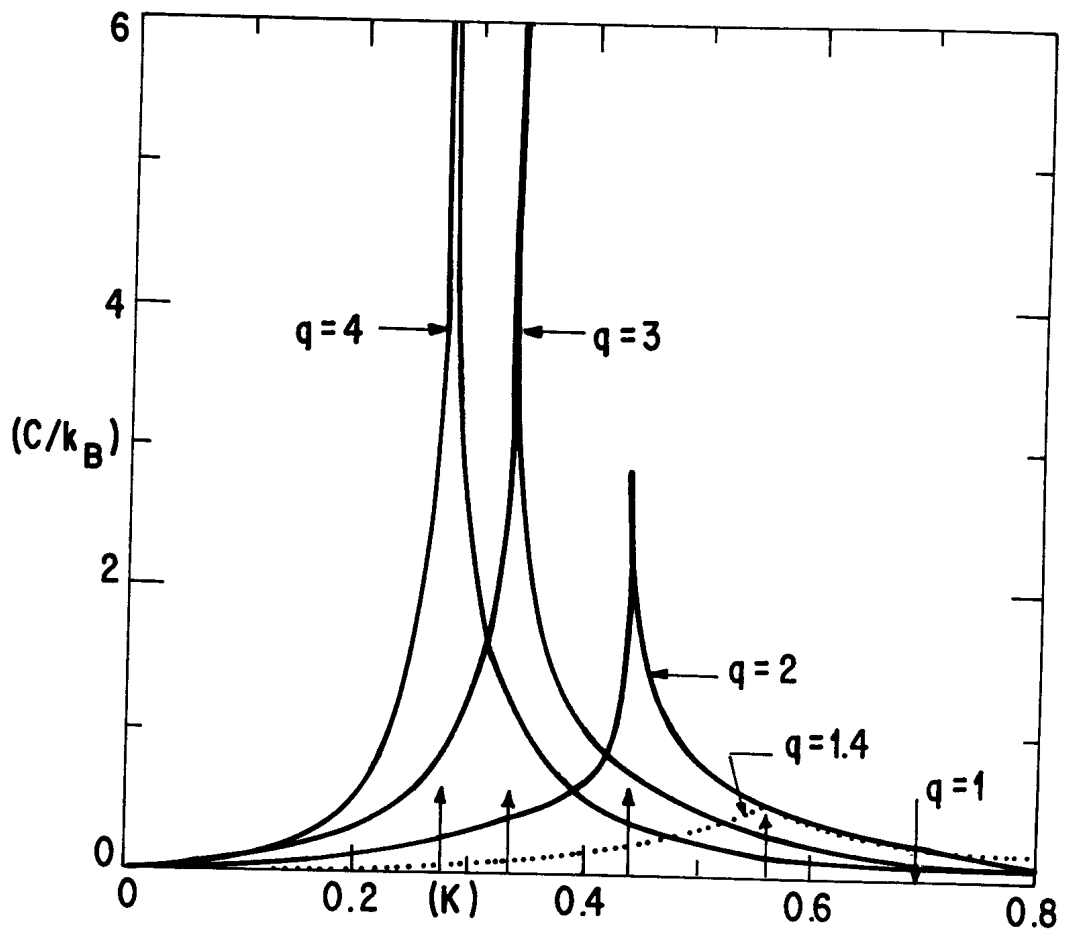


FIG. 52

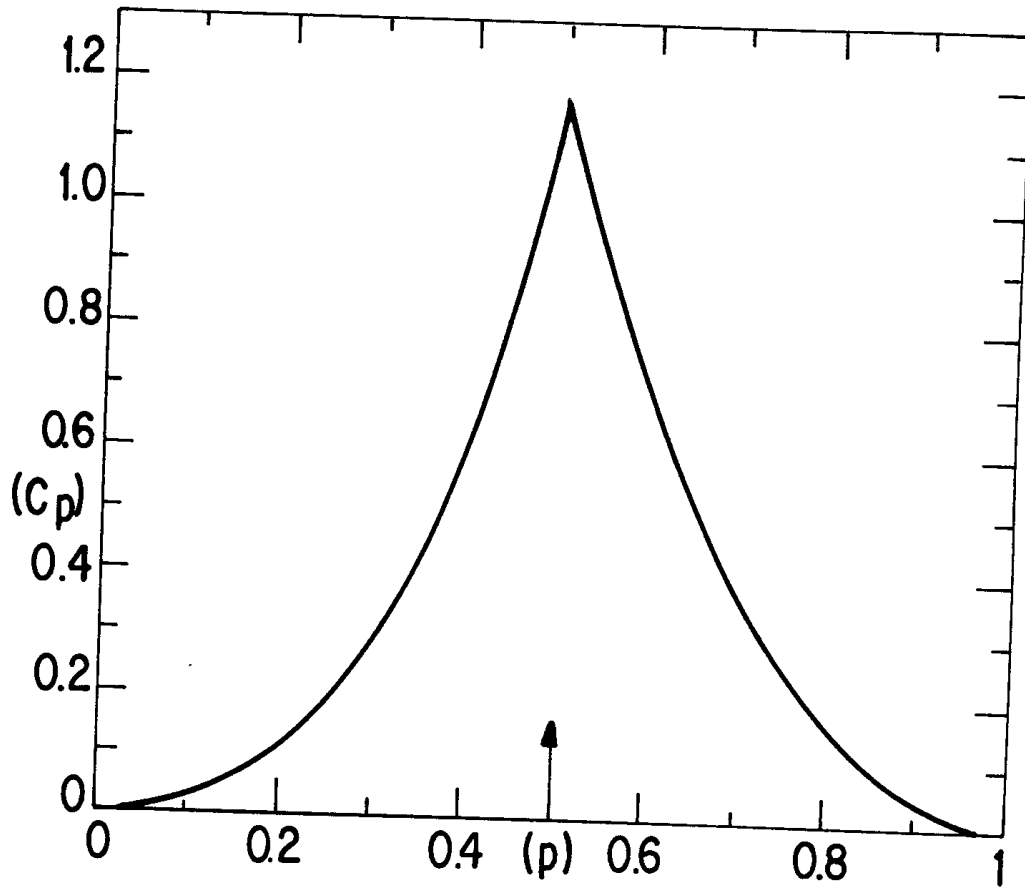


FIG. 53

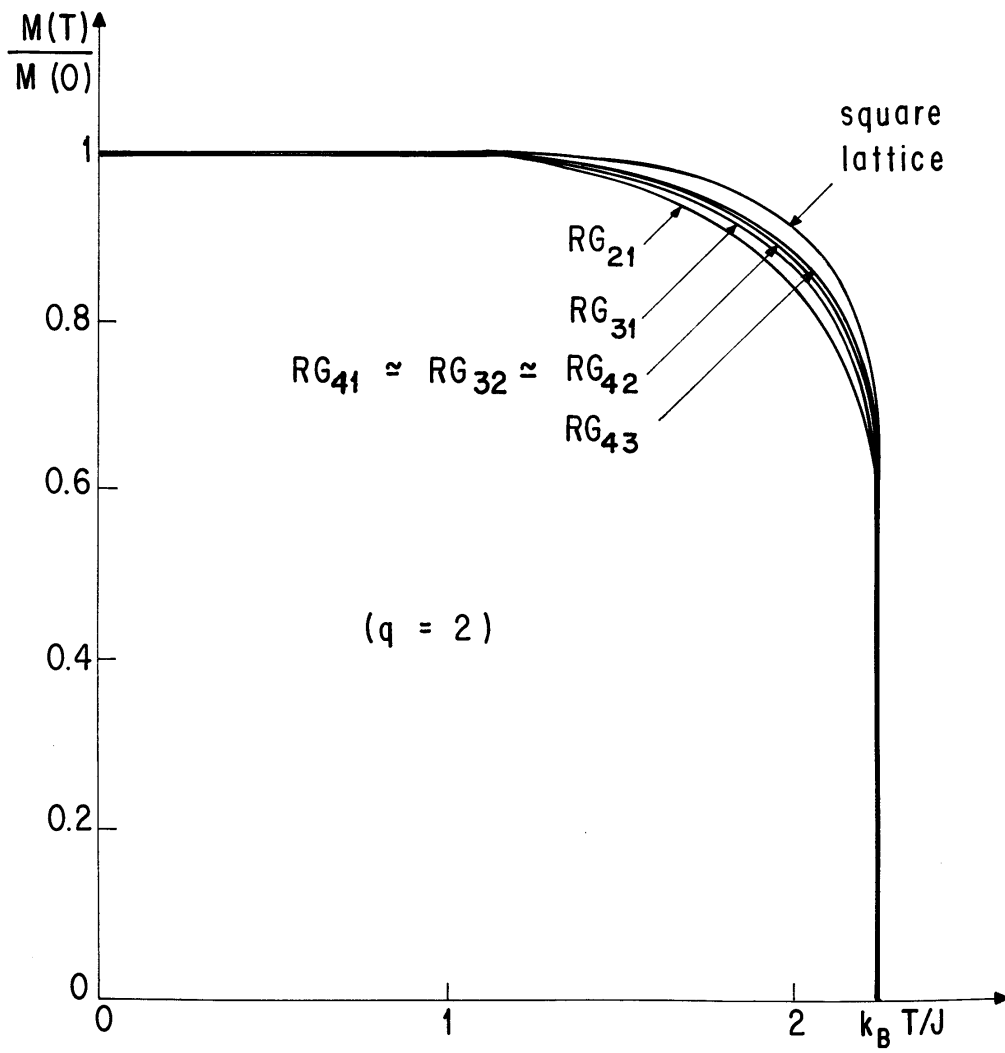


FIG. 54

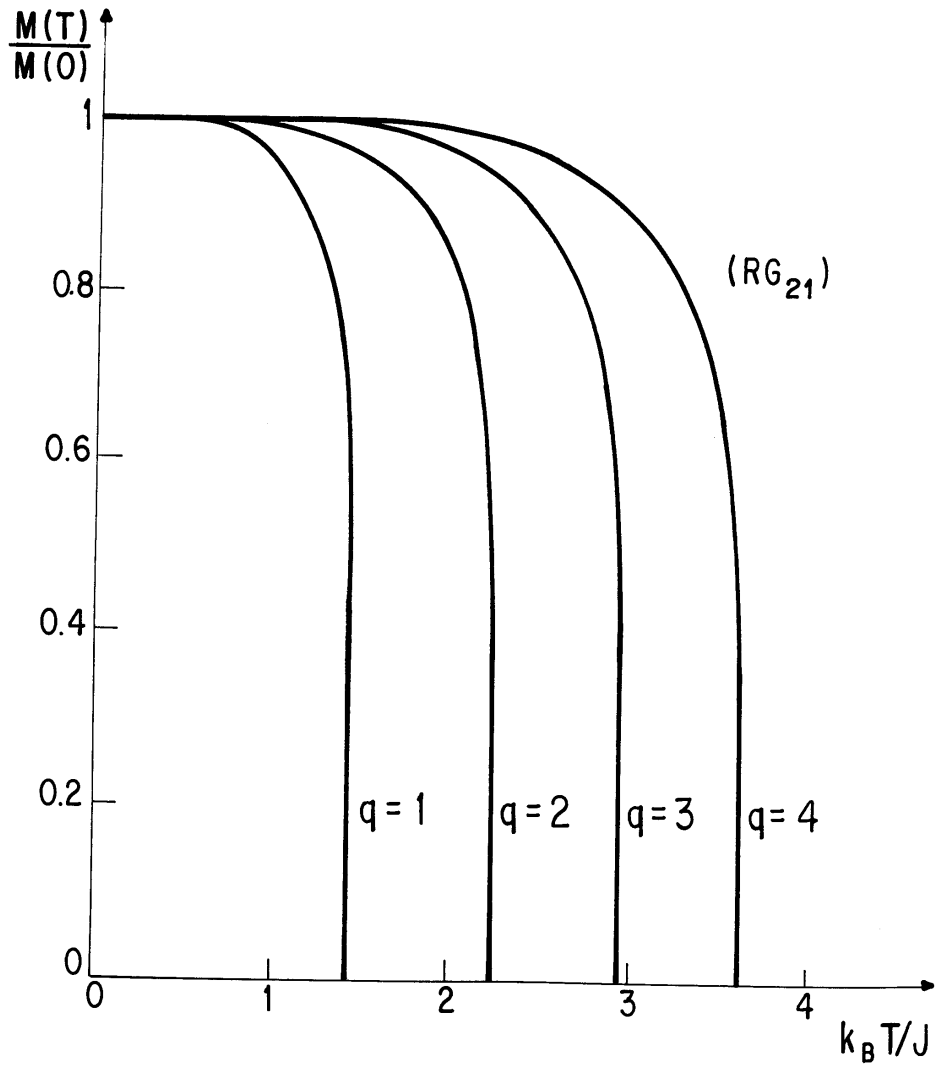


FIG. 55



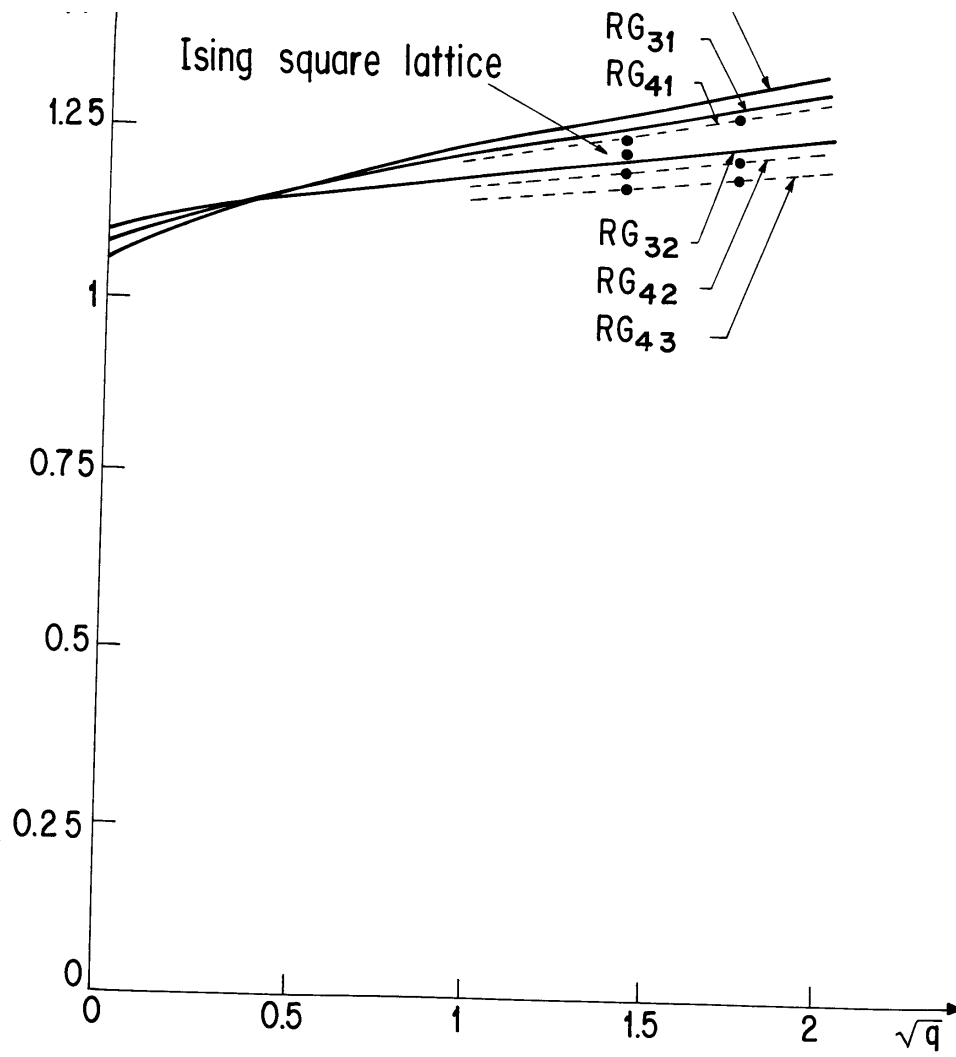


FIG. 56

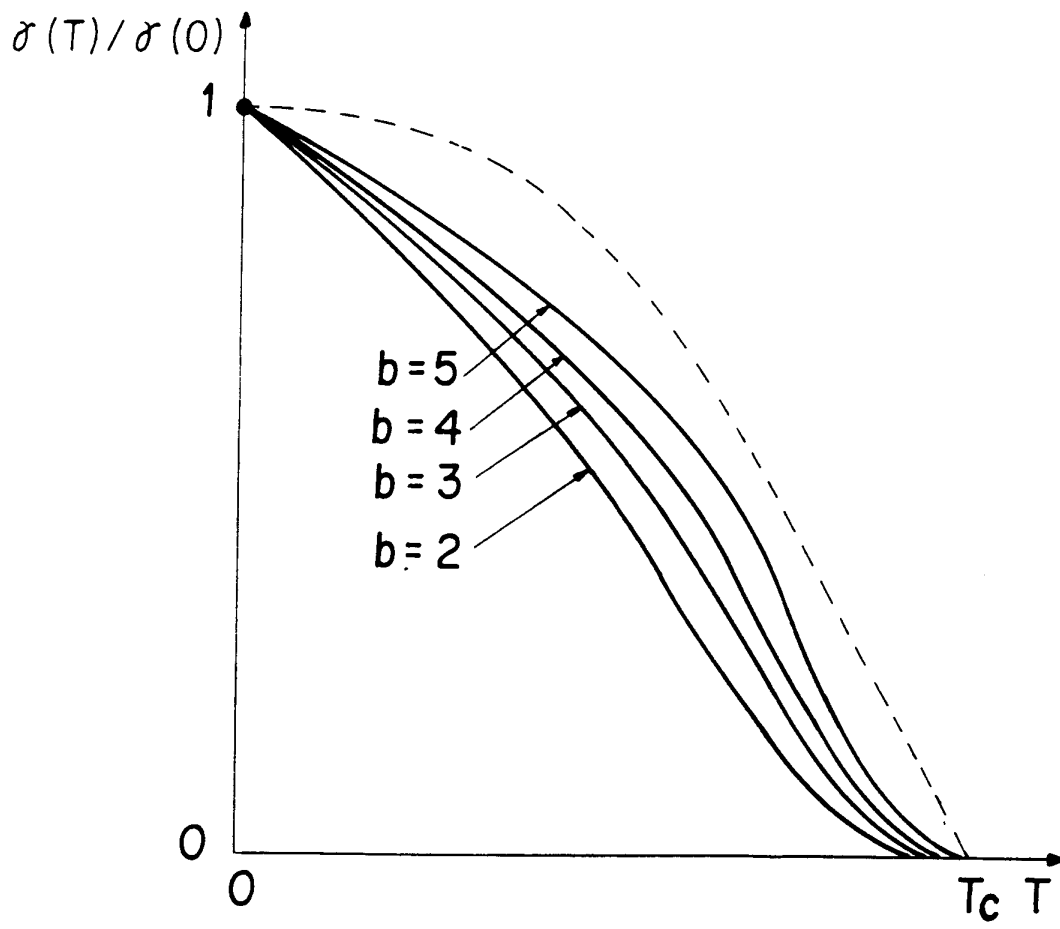


FIG. 57

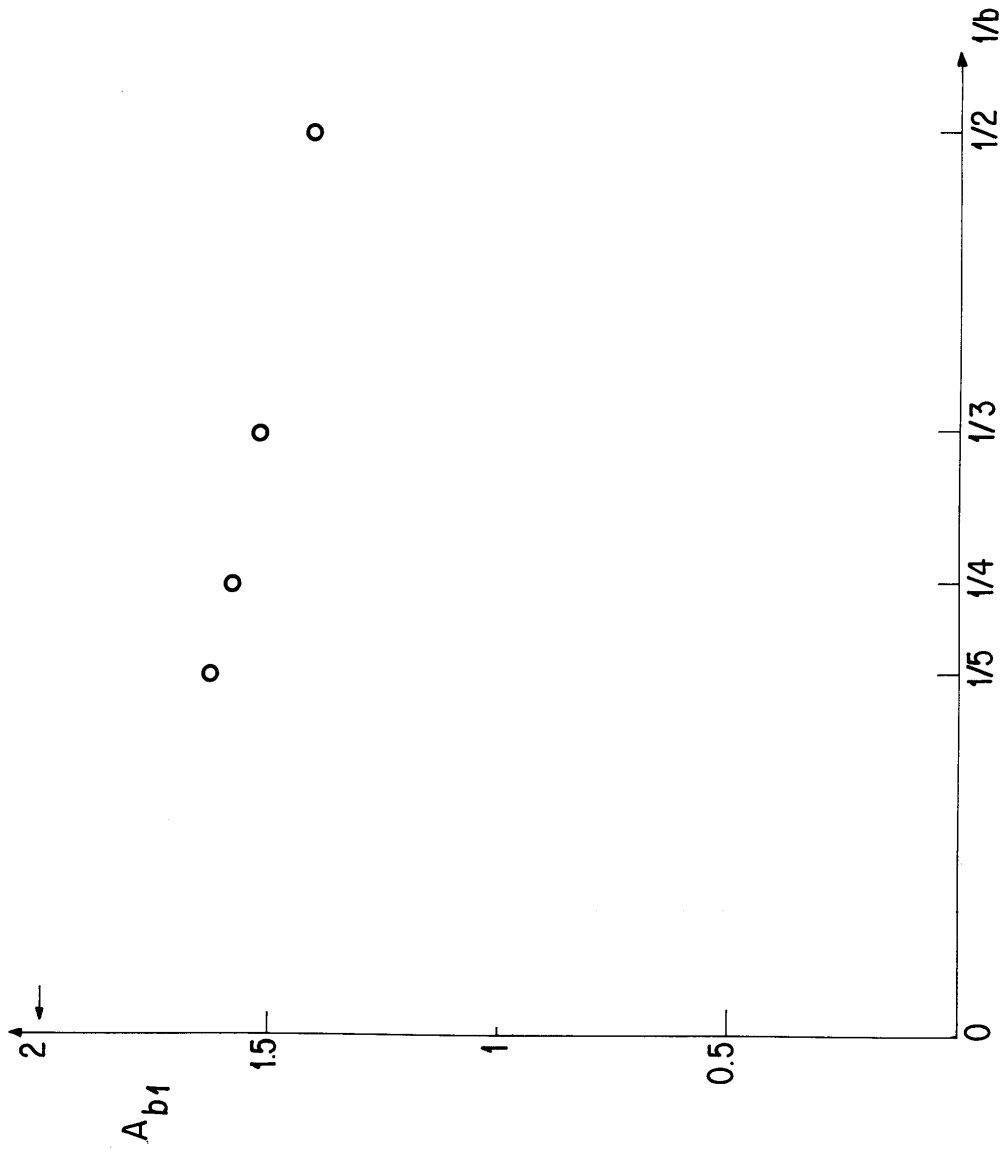


FIG. 58

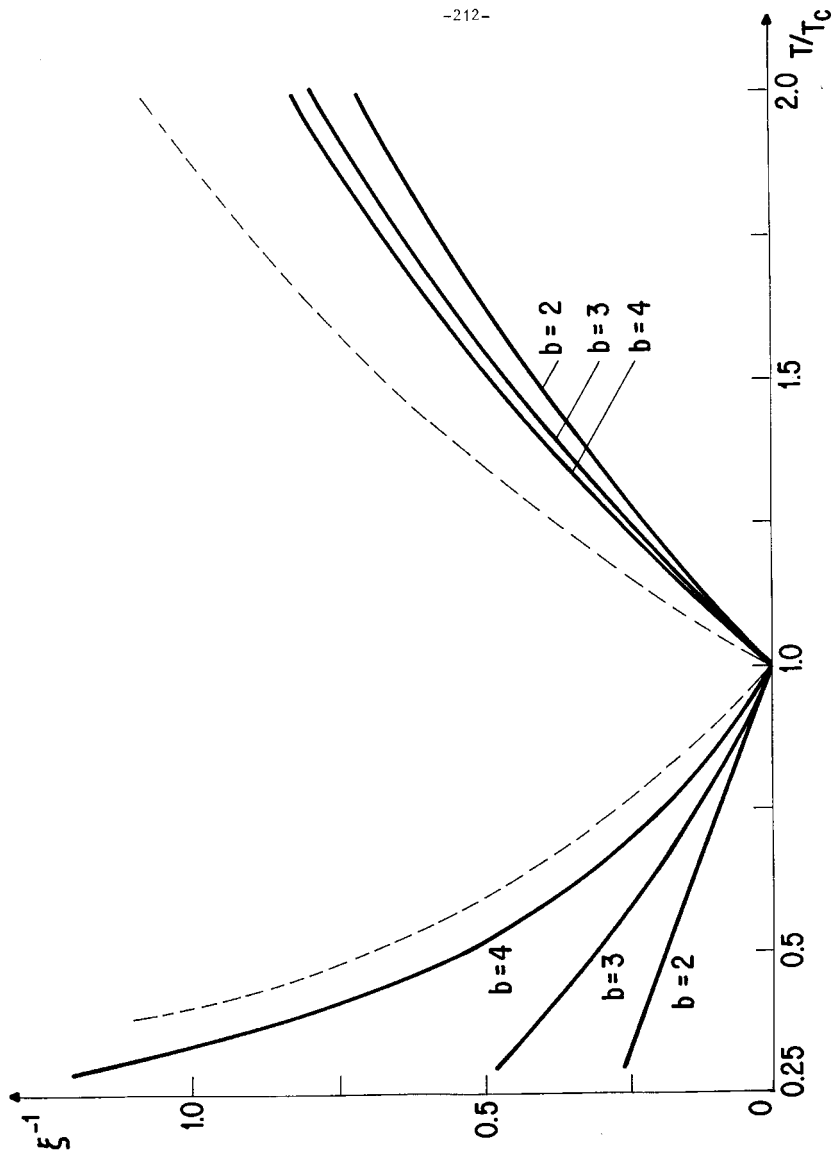


FIG. 59

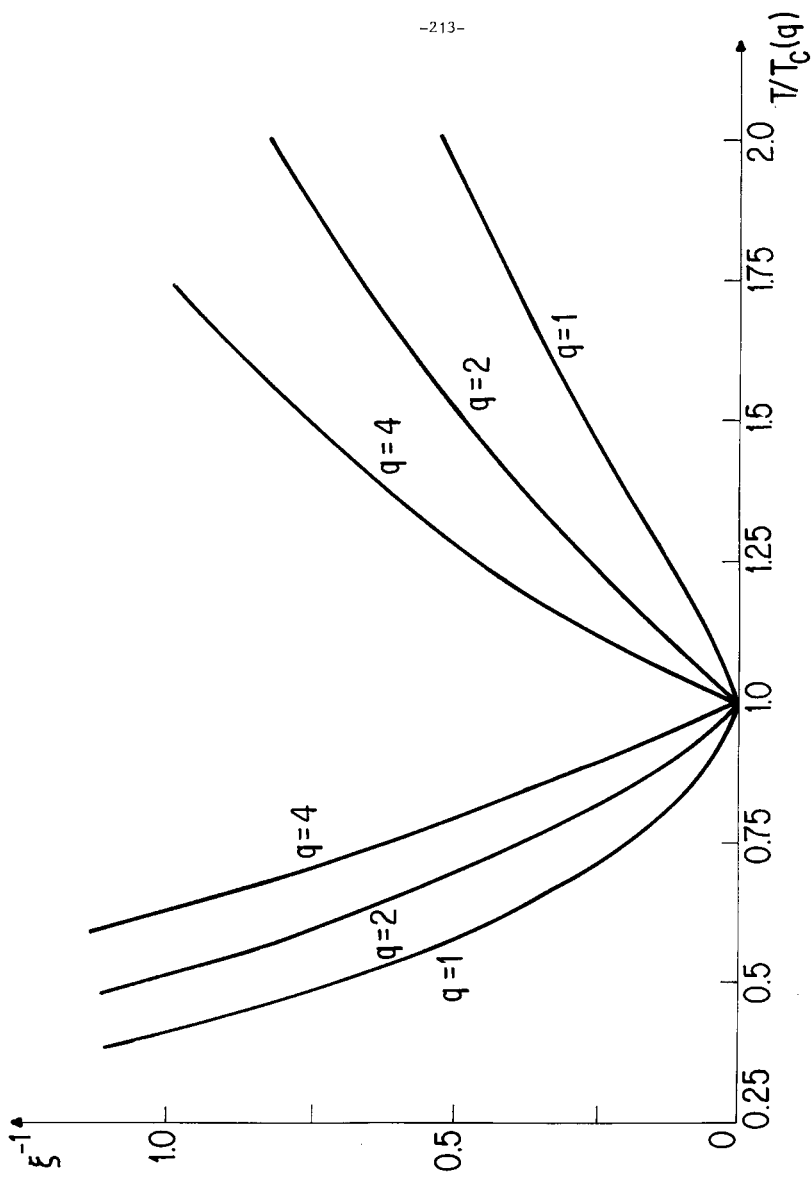


FIG. 60

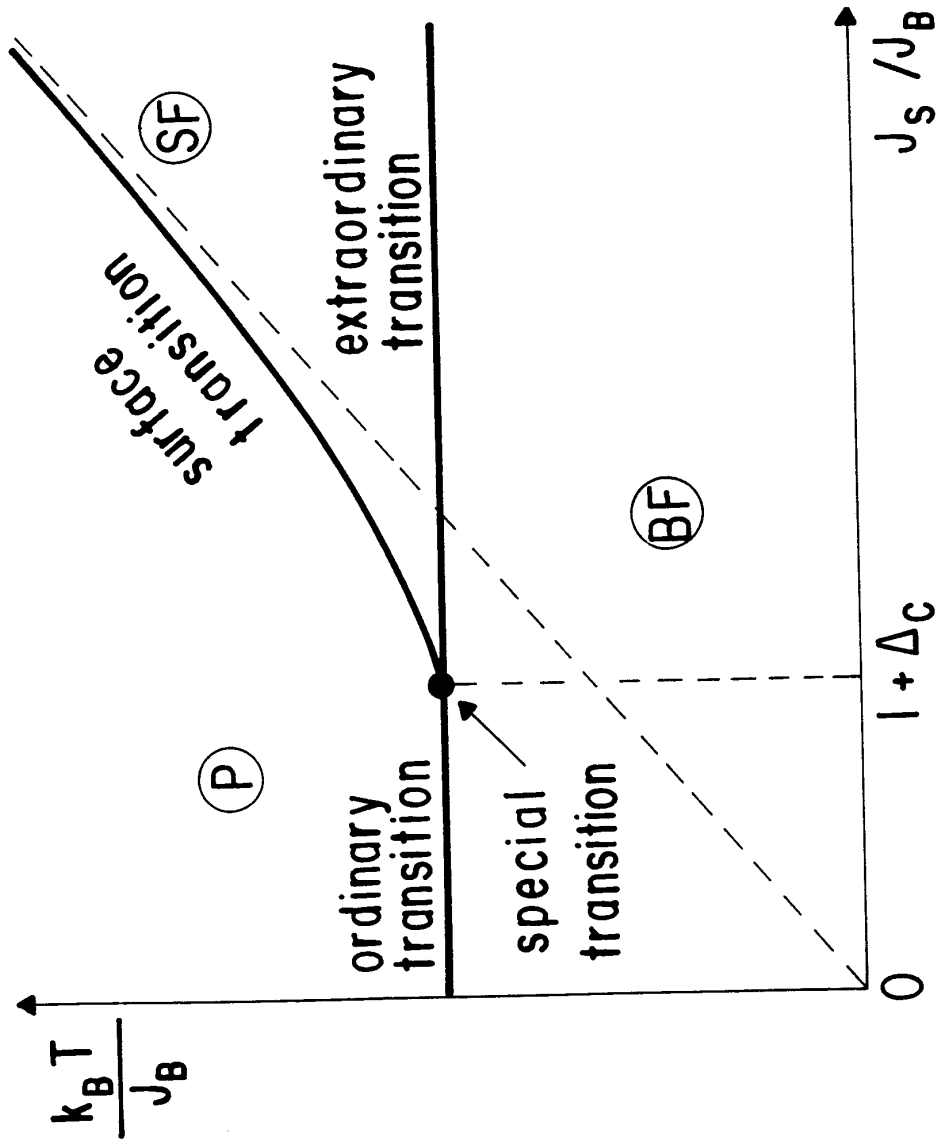


FIG. 61

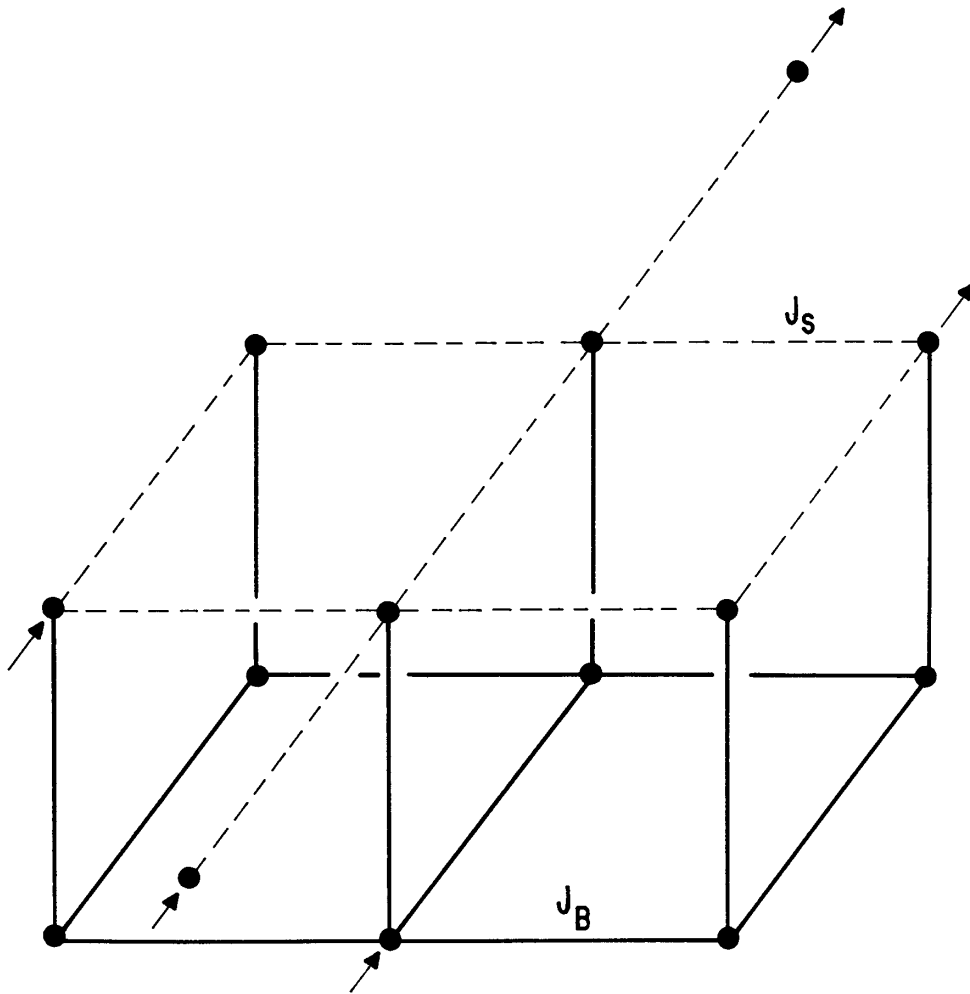


FIG. 62

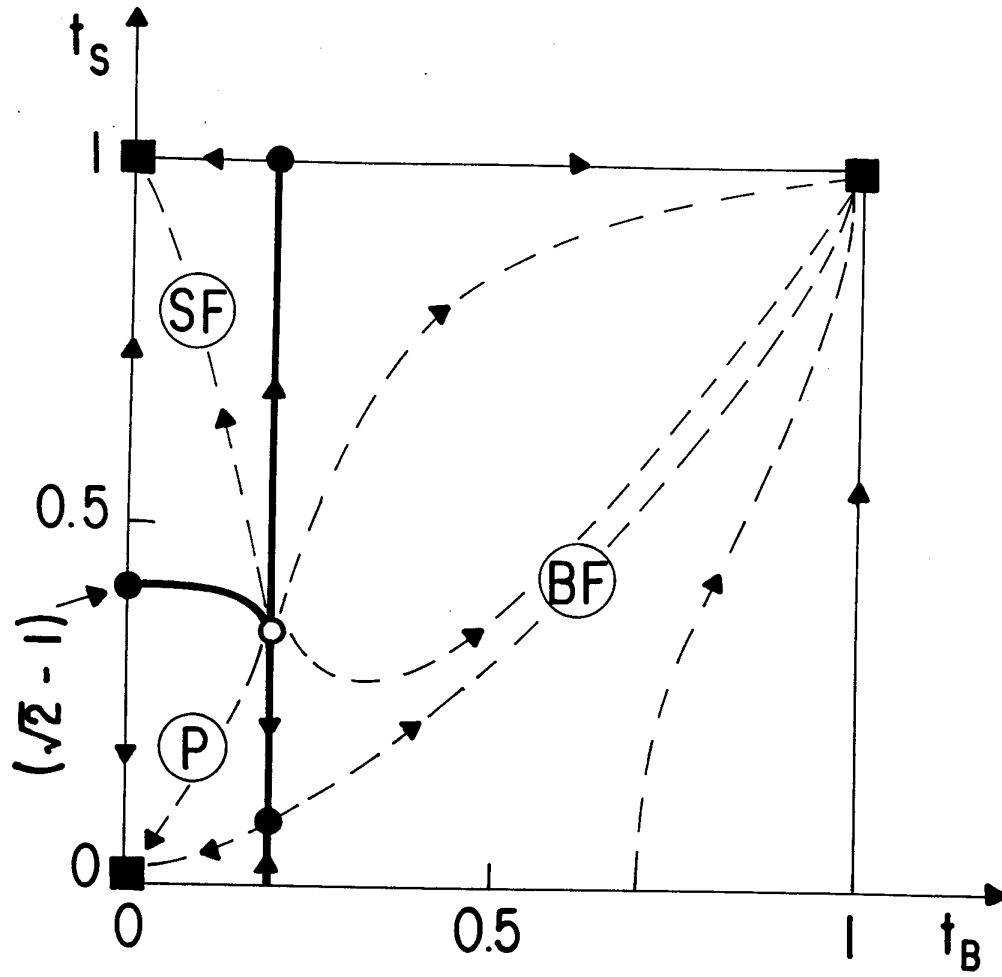


FIG. 63



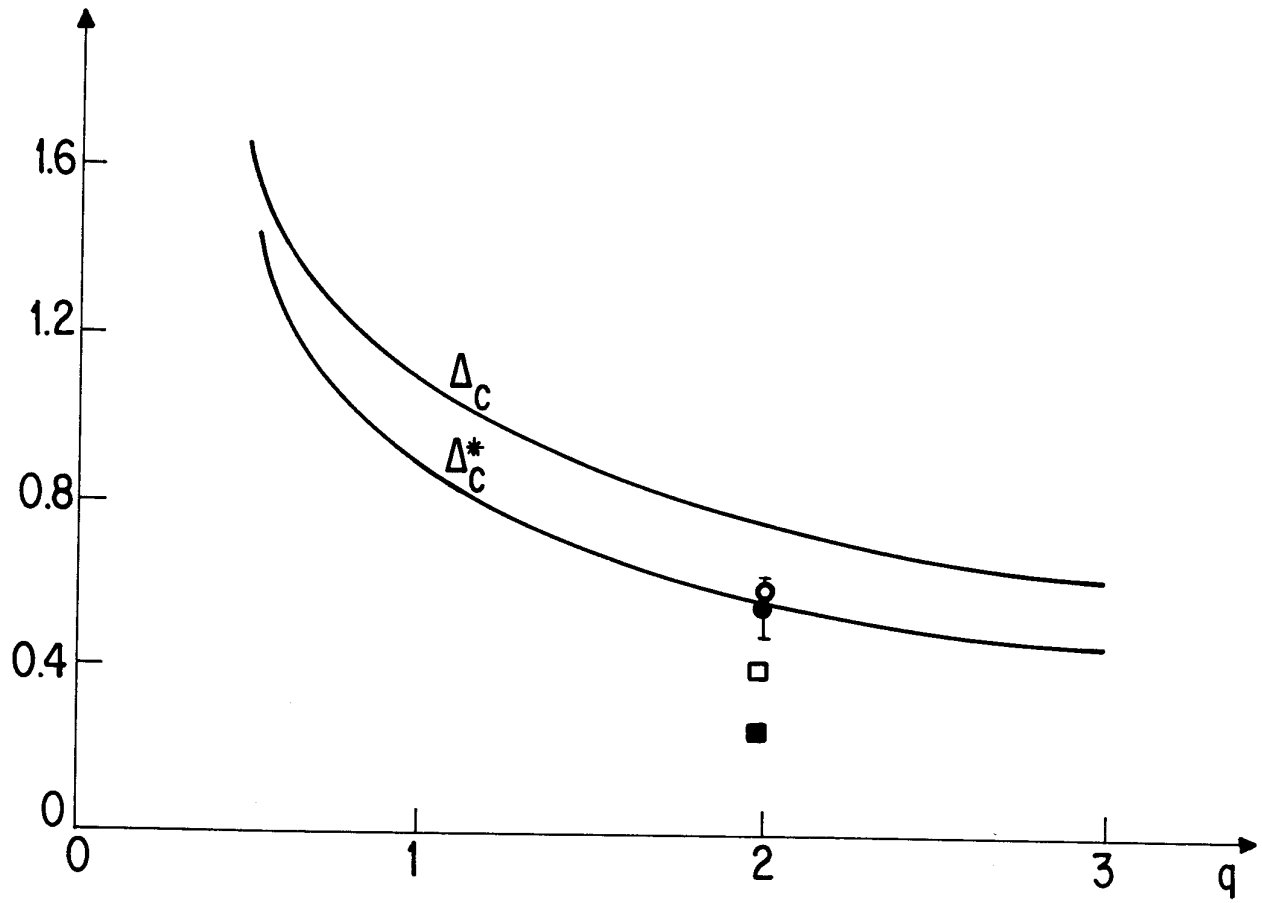


FIG. 64

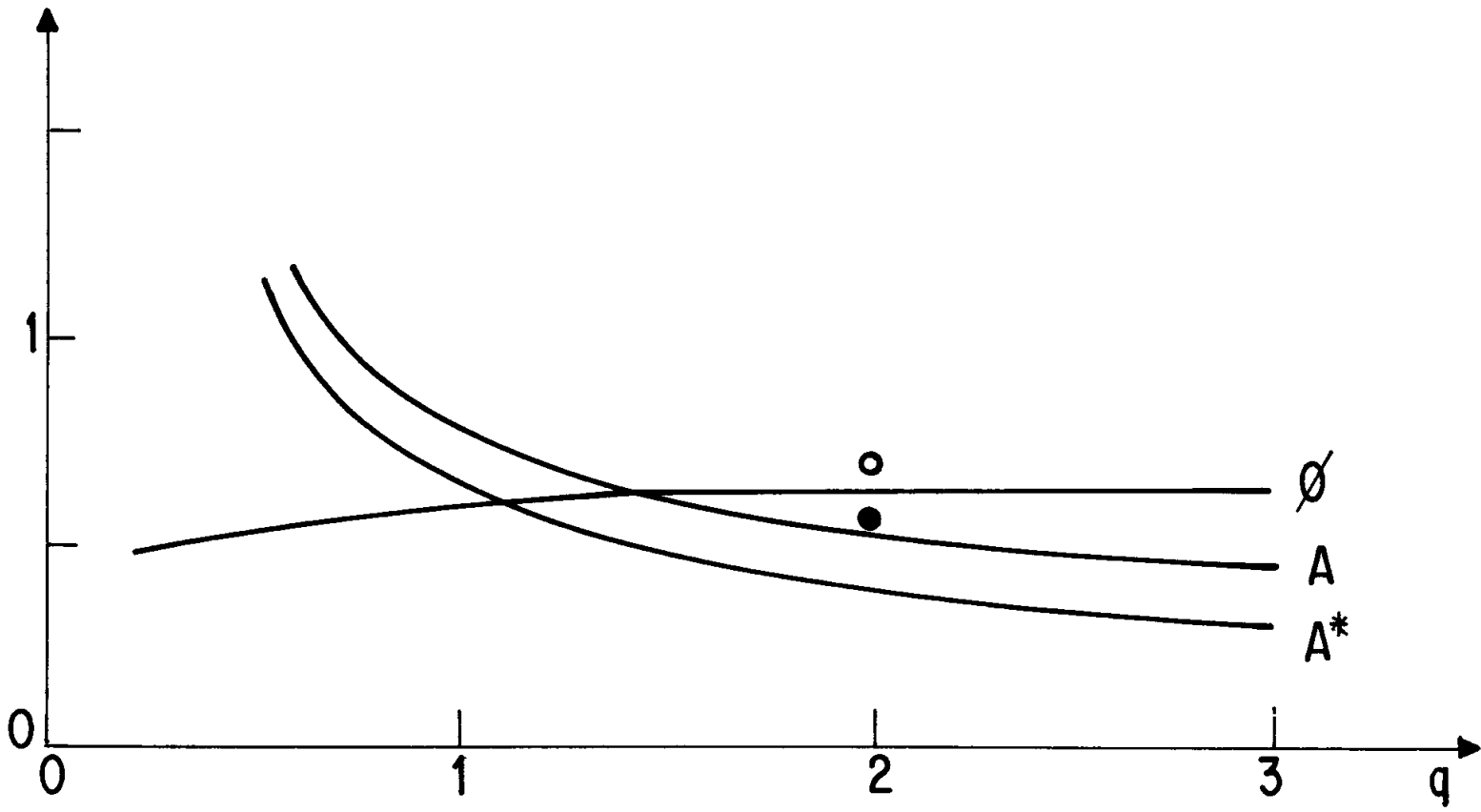


FIG. 65

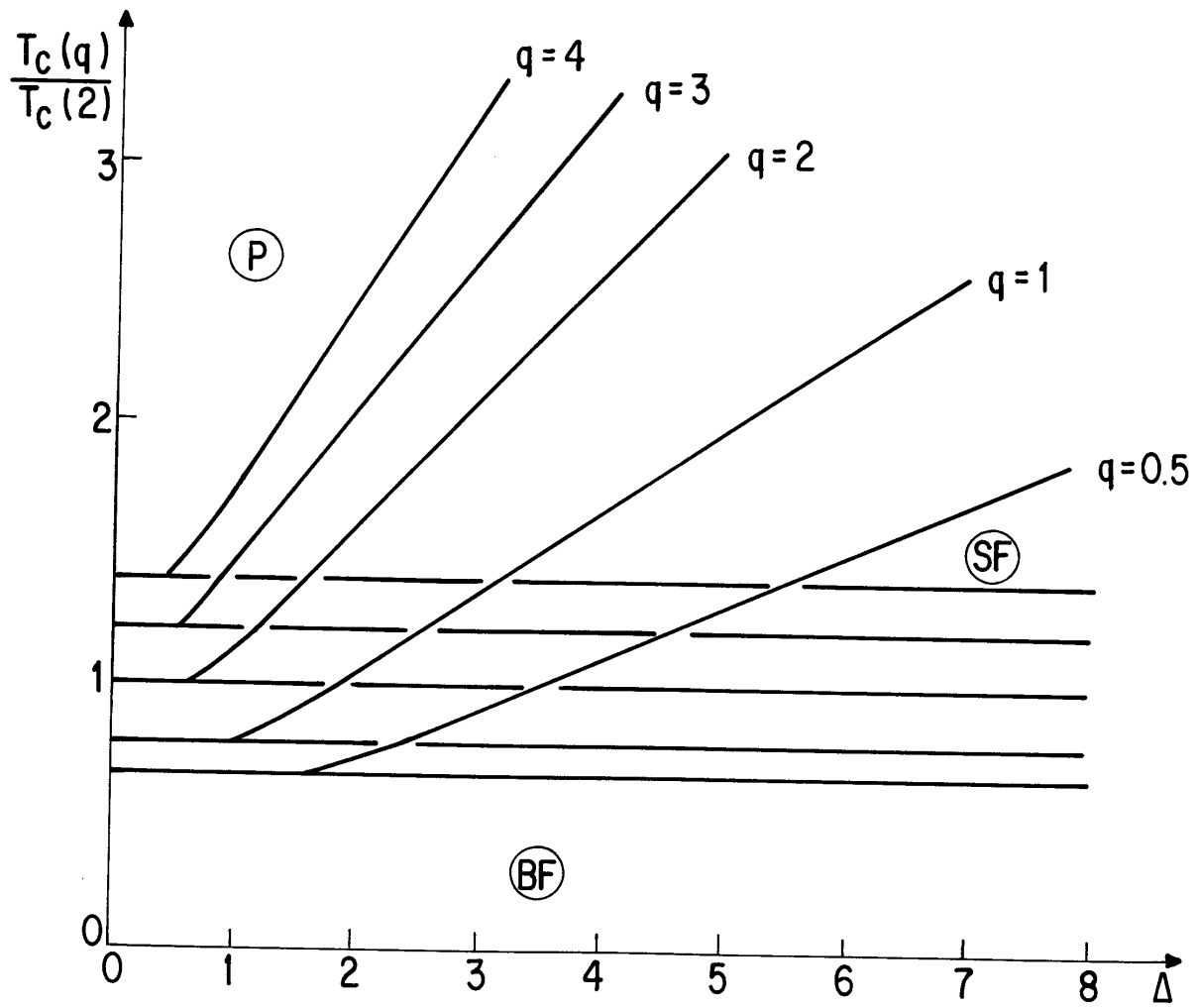


FIG. 66

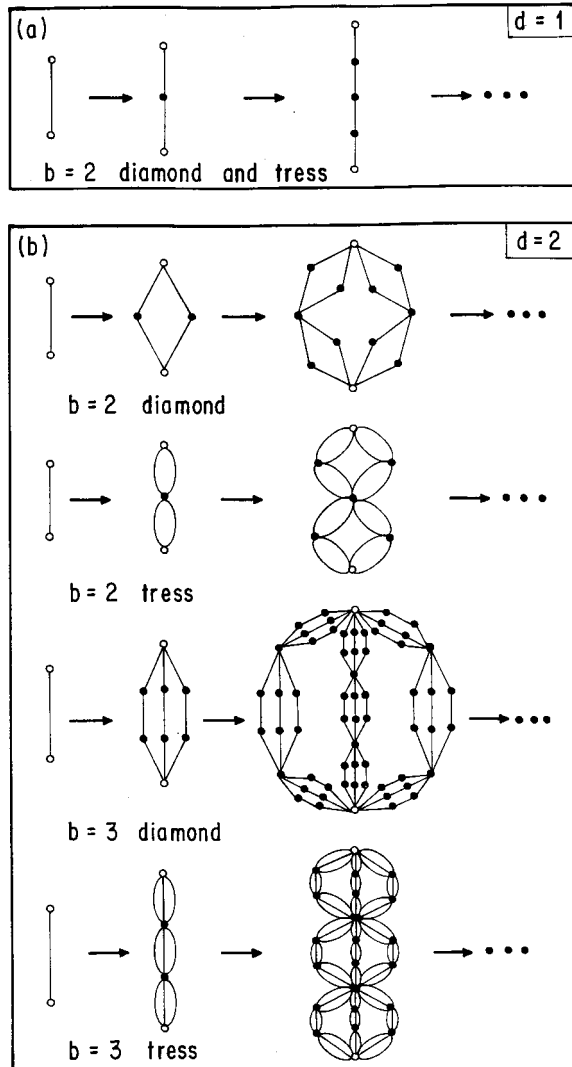


FIG. 67

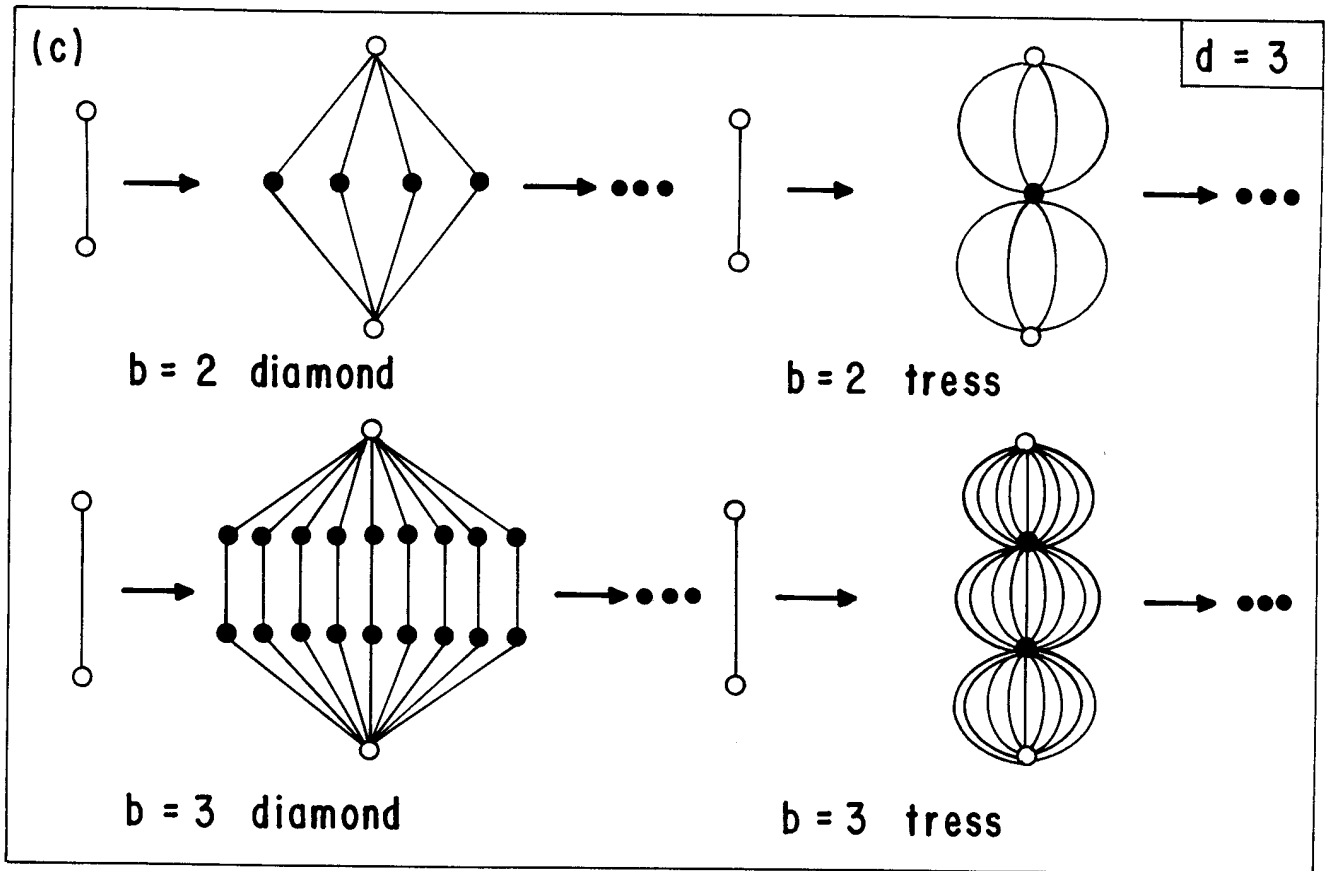


FIG. 67

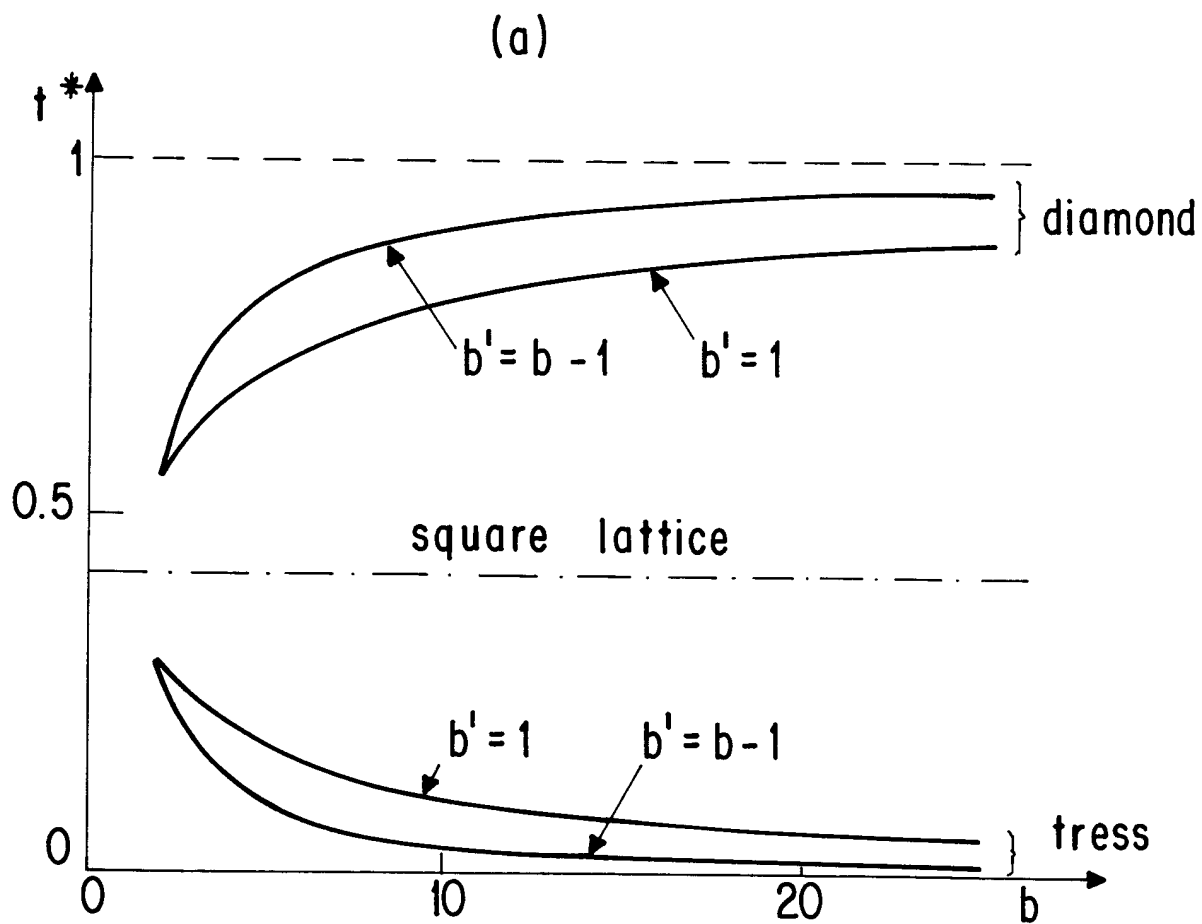


FIG. 68

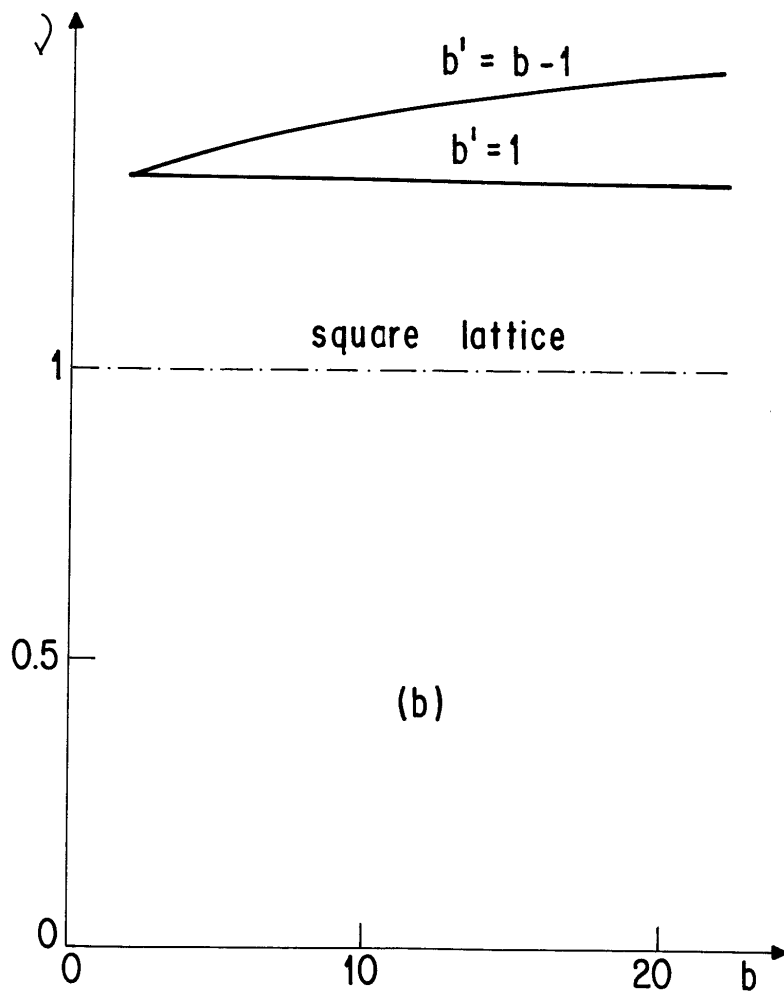


FIG. 68

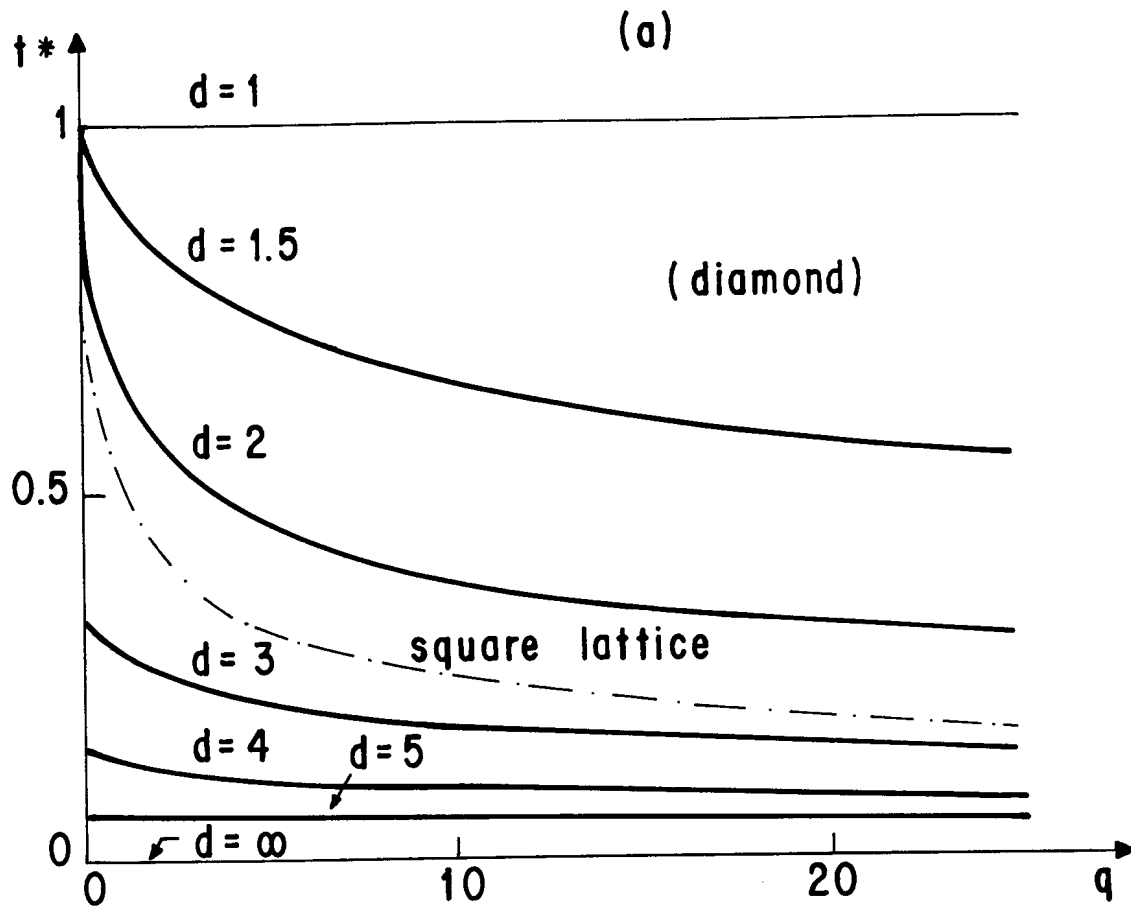


FIG. 69



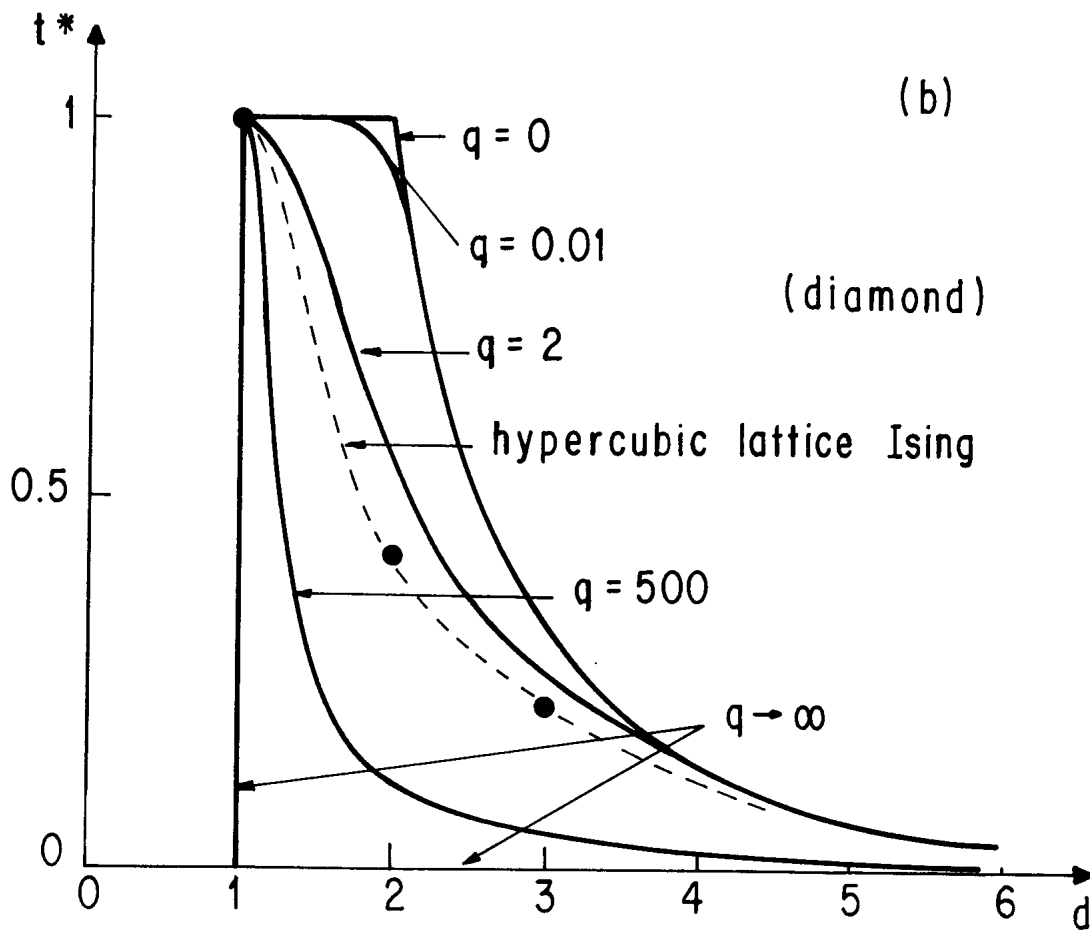


FIG. 69

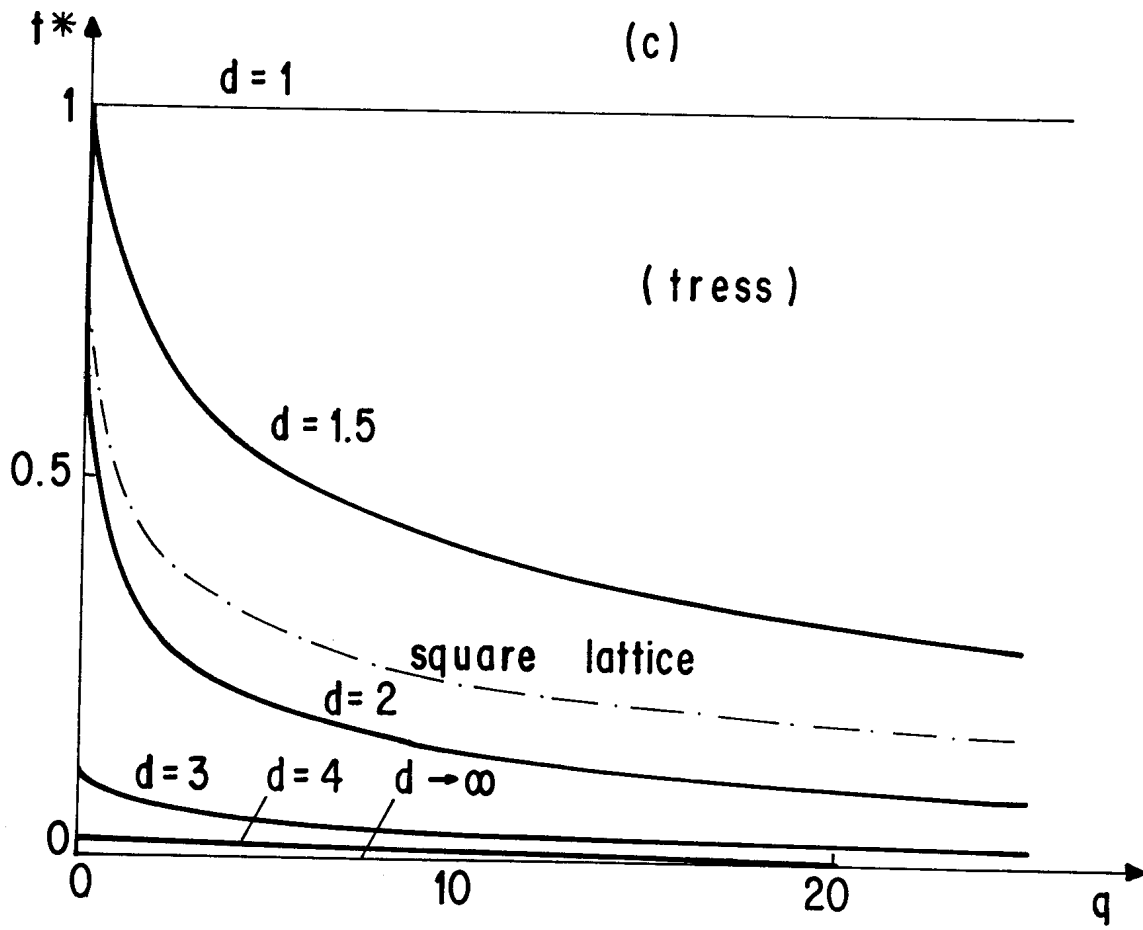


FIG. 69

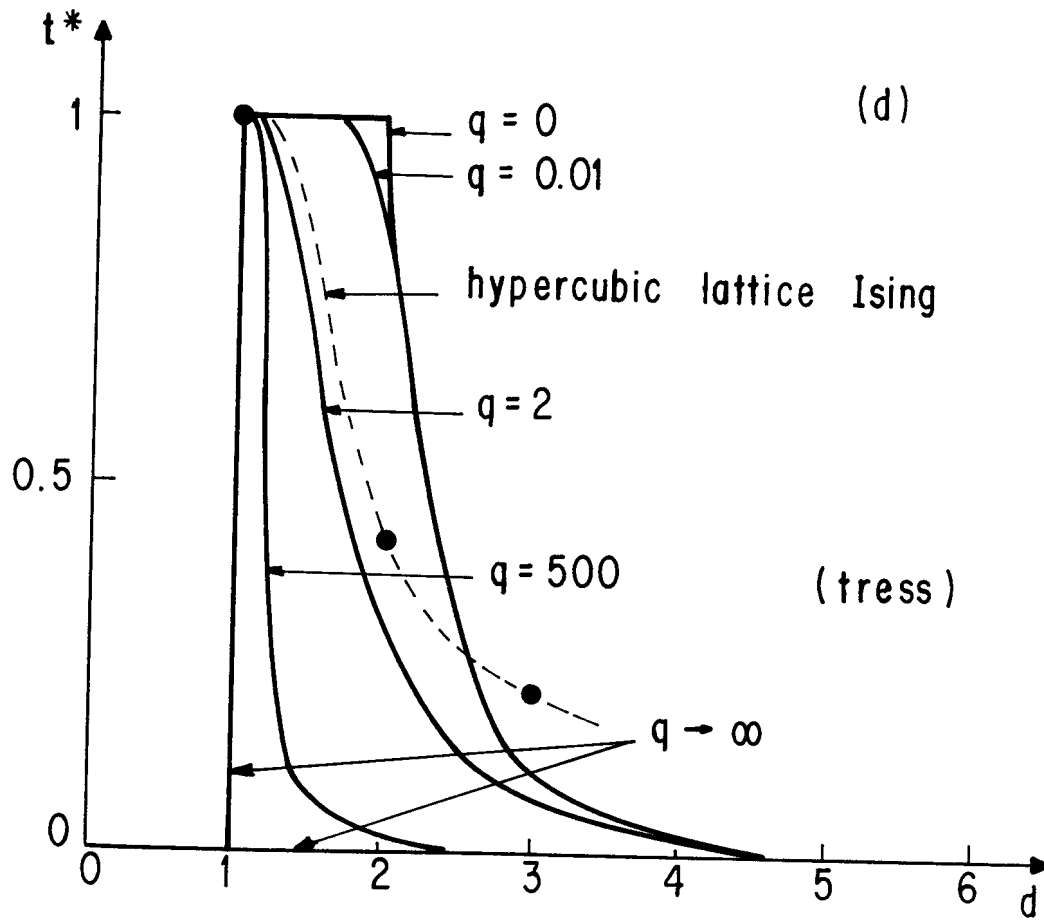


FIG. 69

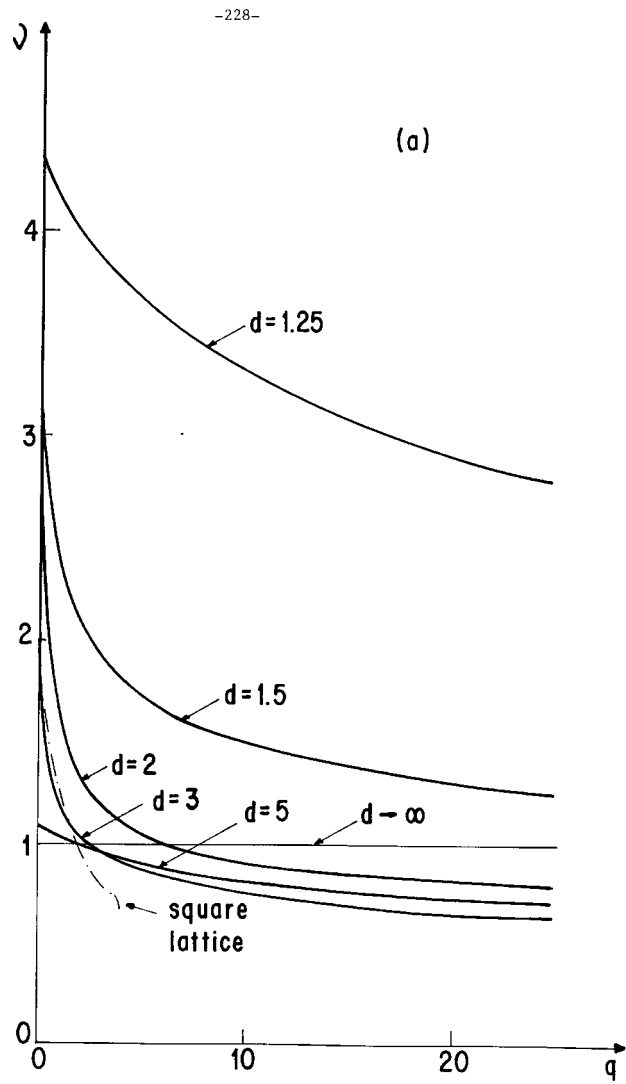


FIG. 70

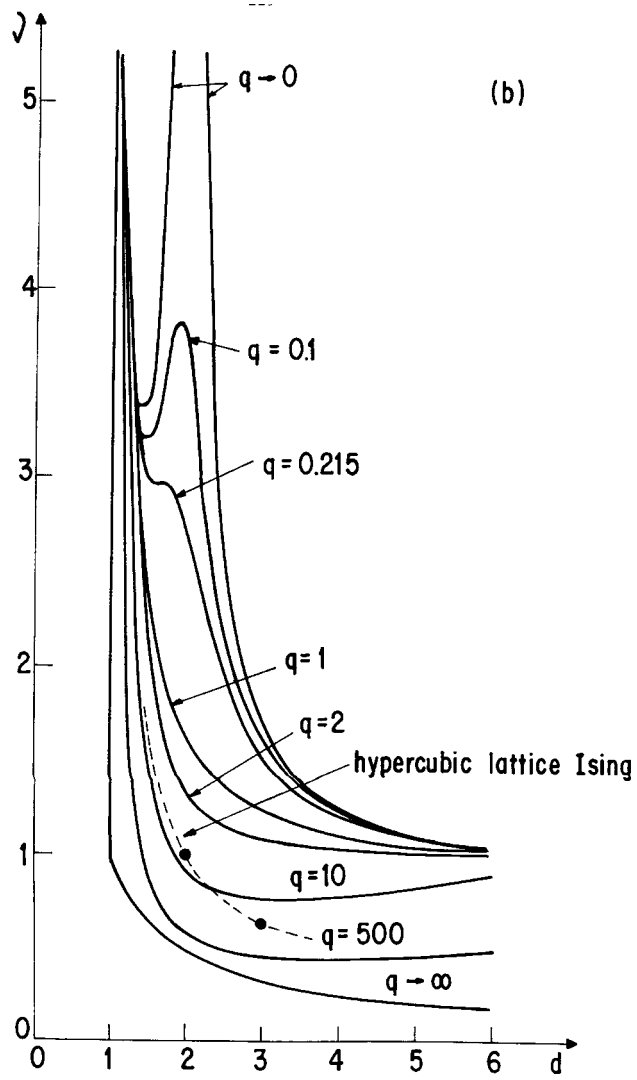


FIG. 70

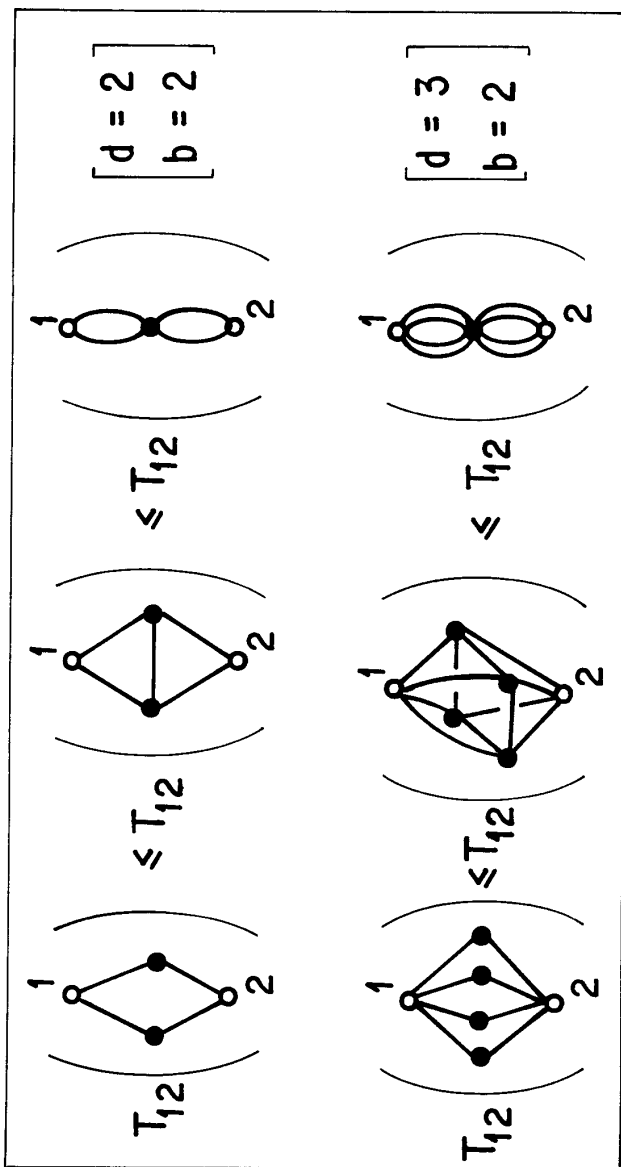


FIG. 71

(a)

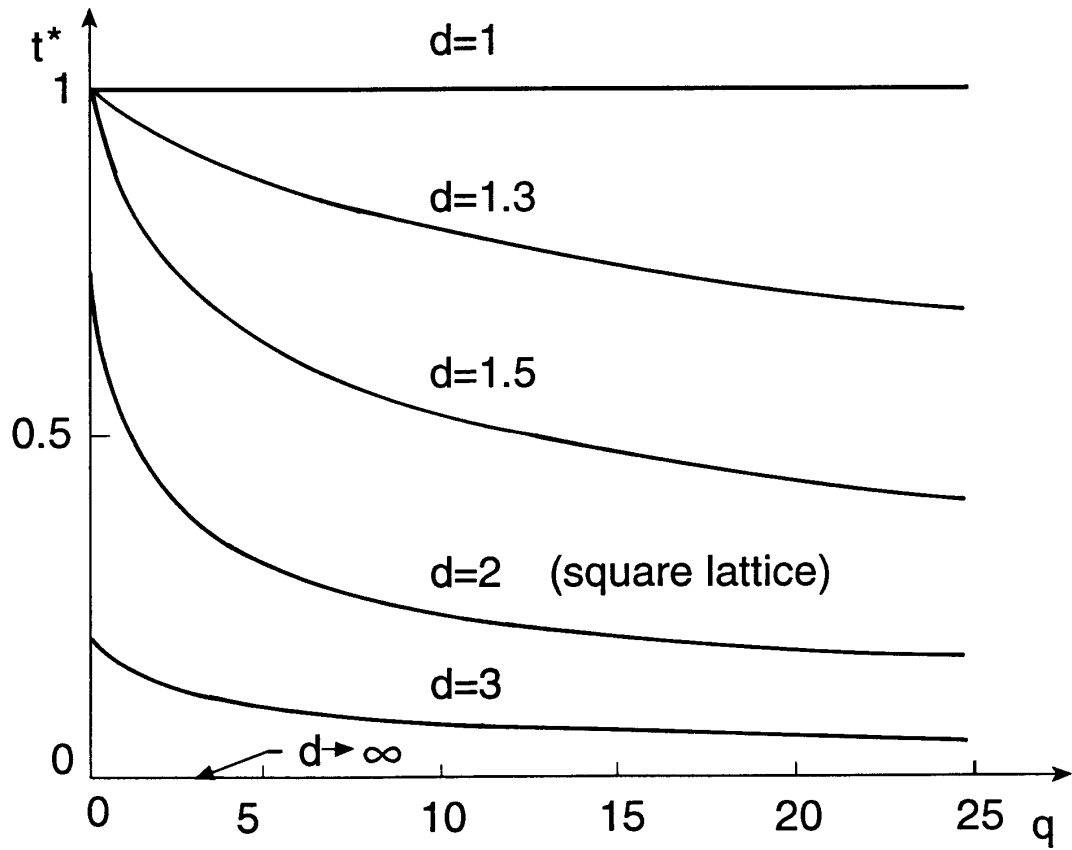


Fig. 72

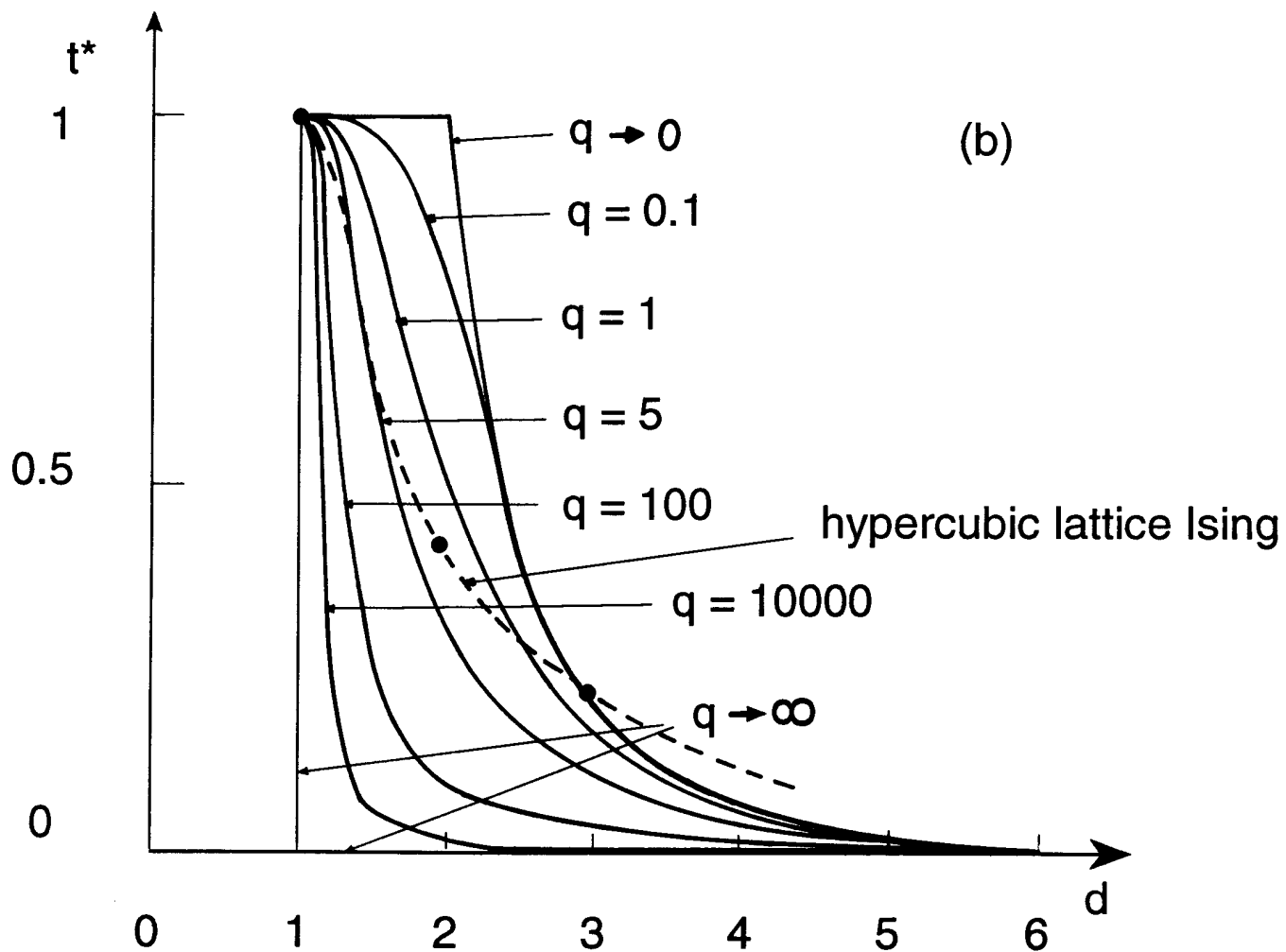


FIG. 72



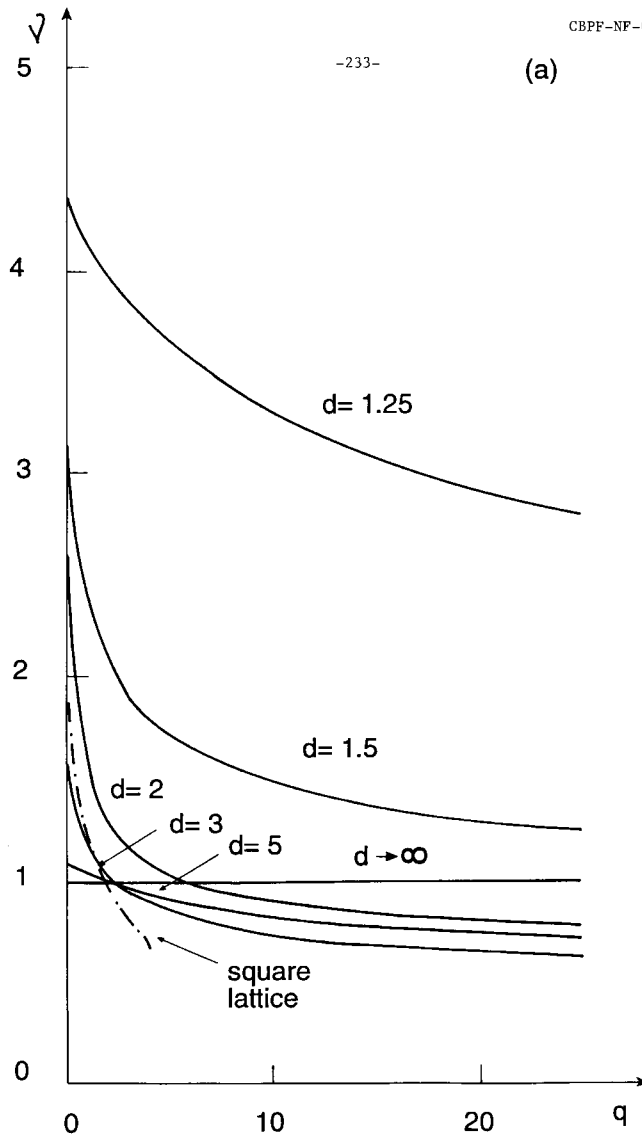


FIG. 73

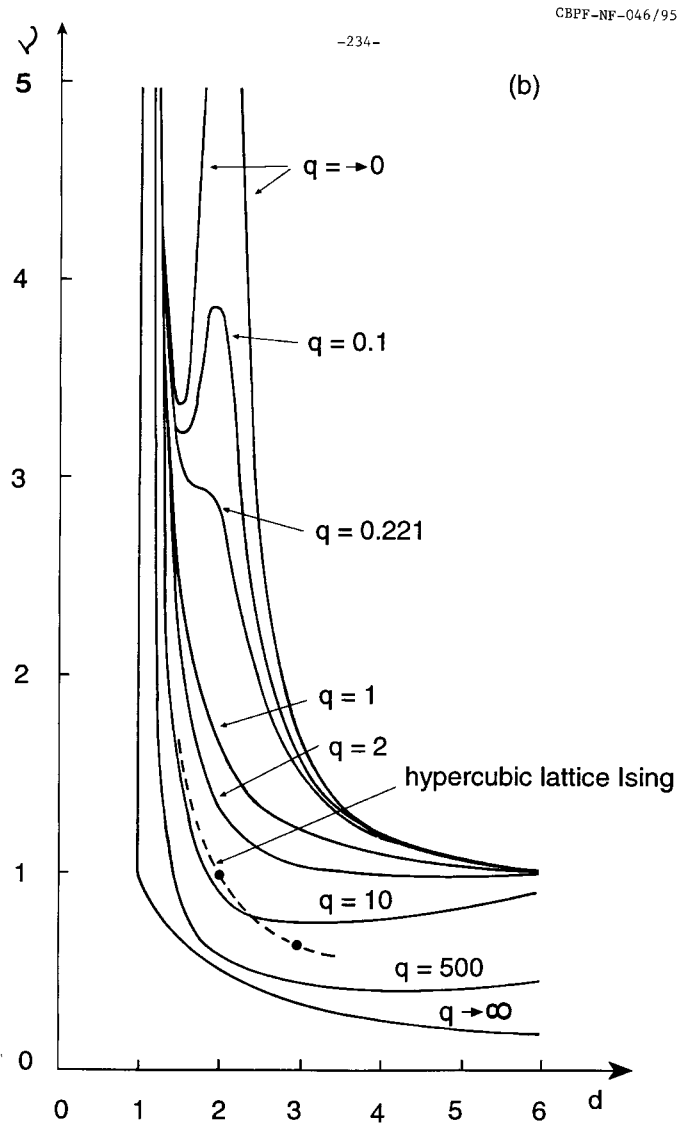


FIG. 73

TABLE I

q	$[1/T_c(1, 0)][T_c(p, 0)/dp]_{p=1}$	
	triangular	honeycomb
1	1.2472	1.7770
2	1.1877	1.5782
3	1.1506	1.4659
4	1.1246	1.3863

-236-

CBPF-NF-046/95

Configu- ration	Ground state		EQUIVA- LENT BOND
	$\frac{E^F}{ J }$	$g^F$	
	$\frac{E^{AF}}{ J }$	$g^{AF}$	
	-5	1	
	-1	2	
	-3	1	
	-1	2	
	-3	1	
	-3	1	
	-1	2	
	-5	1	
	-3	1	
	-1	2	
	-3	1	
	-3	1	
	-1	2	
	-3	1	

TABLE II

	$b = 1$	$b = 2$	$b = 3$	$\dots$	$b \rightarrow \infty$
$N = 1$				$\dots$	
$N = 2$				$\dots$	
$N = 3$				$\dots$	
$\vdots$	$\vdots$	$\vdots$	$\vdots$	$\ddots$	$\vdots$
$N \rightarrow \infty$				$\dots$	

TABLE III

TABLE IV

i=1		i=2			i=3			i=4			i=5		
b=1	n <sub>i</sub>	1		2	2	5q-10	q <sup>2</sup> -5q+6						
	d <sub>i</sub>	0		0	2q-2	q-1	q <sup>2</sup> -3q+2						

i=3		i=4		i=5		i=6		i=7		i=8		i=9	
b=3	n <sub>i</sub>	3	8	8q-6	45q-82	24q <sup>2</sup> -50q+16	2q <sup>3</sup> +62q <sup>2</sup> -223q+198	34q <sup>3</sup> -37q <sup>2</sup> -270q+422					
	d <sub>i</sub>	4q-4	4q-4	2q <sup>2</sup> -2q	8q <sup>2</sup> -10q+2	21q <sup>2</sup> -43q+22	10q <sup>3</sup> +q <sup>2</sup> -62q+51	32q <sup>3</sup> -107q <sup>2</sup> +101q-26					

i=10		i=11		i=12	
4q <sup>4</sup> +123q <sup>3</sup> -952q <sup>2</sup> +2287q-1814	66q <sup>4</sup> -593q <sup>3</sup> +2098q <sup>2</sup> +3430q+2157	13q <sup>5</sup> -144q <sup>4</sup> +671q <sup>3</sup> -1646q <sup>2</sup> +2115q-1126			
7q <sup>4</sup> +51q <sup>3</sup> -394q <sup>2</sup> +722q-386	57q <sup>4</sup> -445q <sup>3</sup> +1275q <sup>2</sup> -1565q+678	13q <sup>5</sup> -135q <sup>4</sup> +559q <sup>3</sup> -1143q <sup>2</sup> +1138q-432			

i=13	
q <sup>6</sup> -13q <sup>5</sup> +74q <sup>4</sup> -237q <sup>3</sup> +451q <sup>2</sup> -482q+224	
q <sup>6</sup> -13q <sup>5</sup> +71q <sup>4</sup> -207q <sup>3</sup> +337q <sup>2</sup> -287q+98	

i=3		i=4		i=5		i=6		i=7		i=8	
b=4	n <sub>i</sub>	0	4	18	12q+18	108-146	34q <sup>2</sup> +206q-428				
	d <sub>i</sub>	6q-6	10q-10	4q <sup>2</sup> -4q	21q <sup>2</sup> -33q+12	2q <sup>3</sup> +55q <sup>2</sup> -111q+54	20q <sup>3</sup> +42q <sup>2</sup> -164q+102				

i=9	i=10	i=11
$317q^2 - 565q + 94$	$85q^3 + 722q^2 - 2527q + 1848$	$3q^4 + 663q^3 - 528q^2 - 4096q + 5414$
$112q^3 - 291q^2 + 303q - 124$	$20q^4 + 153q^3 - 362q^2 + 105q + 84$	$93q^4 + 267q^3 - 1349q^2 + 1327q - 338$

i=12	i=13
$154q^4 + 2162q^3 - 10408q^2 + 13722q - 4972$	$8q^5 + 1374q^4 - 1342q^3 - 17055q^2 + 43669q - 29906$
$8q^6 + 443q^4 - 1118q^3 + 689q^2 - 518q + 496$	$100q^5 + 696q^4 - 1884q^3 - 3526q^2 + 10848q - 6234$

i=14	i=15
$294q^5 + 4192q^4 - 26962q^3 + 48149q^2 - 22117q - 8508$	$20q^6 + 2450q^5 - 5275q^4 - 35132q^3 + 146773q^2 - 190850q + 80802$
$3q^6 + 504q^5 + 1188q^4 - 13383q^3 + 24811q^2 - 13767q + 644$	$72q^6 + 2198q^5 - 9198q^4 + 75q^3 + 41536q^2 - 59377q + 24694$

i=16	i=17
$558q^6 + 5242q^5 - 46952q^4 + 87668q^3 + 68321q^2 - 349404q + 272188$	$56q^7 + 3227q^6 - 8611q^5 - 96709q^4 + 584490q^3 - 1293754q^2 + 1298197q - 487978$
$768q^6 + 1341q^5 - 23729q^4 + 40925q^3 + 37770q^2 - 133580q + 76505$	$90q^7 + 2704q^6 - 8166q^5 - 68824q^4 + 406429q^3 - 837363q^2 + 770924q - 265794$

i=18
$2q^8 + 766q^7 + 7052q^6 - 102324q^5 + 350816q^4 - 188187q^3 - 1365452q^2 + 2995159q - 1911544$
$2q^8 + 830q^7 + 5382q^6 - 91100q^5 + 357260q^4 - 541513q^3 + 130416q^2 + 419607q - 280884$

$$\begin{aligned} & i=19 \\ & 87q^6 + 4285q^7 - 26238q^8 - 140672q^9 + 1824305q^{10} - 7464757q^{11} + 15608746q^{12} - 16973756q^{13} + 7651698 \\ & 99q^8 + 4103q^7 - 29850q^6 - 46852q^5 + 1019541q^4 - 3949731q^3 + 7178591q^2 - 6394125q + 2218224 \end{aligned}$$

$$\begin{aligned} & i=20 \\ & 4q^9 + 1028q^8 + 6500q^7 - 246724q^6 + 2054996q^5 - 8881126q^4 + 22970358q^3 - 36171342q^2 + 32253346q - 12552920 \\ & 4q^9 + 1058q^8 + 4344q^7 - 201644q^6 + 1606302q^5 - 6374287q^4 + 14624520q^3 - 19679347q^2 + 14365400q - 4346350 \end{aligned}$$

$$\begin{aligned} & i=21 \\ & 122q^2 + 5989q^8 - 127505q^7 + 1079972q^6 - 5256762q^5 + 16379224q^4 - 33640406q^3 + 44528257q^2 - 34679637q + 12125080 \\ & 126q^9 + 5659q^8 - 118615q^7 + 965442q^6 - 4420696q^5 + 12639636q^4 - 23131342q^3 + 26357308q^2 - 16971664q + 4674146 \end{aligned}$$

$$\begin{aligned} & i=22 \\ & 6q^{10} + 1766q^9 - 36046q^8 + 329374q^7 - 1804692q^6 + 6569486q^5 - 16516720q^4 + 29705648q^3 - 33237963q^2 + 23217473q - 7426454 \\ & 6q^{10} + 1750q^9 - 35266q^8 + 314870q^7 - 1661769q^6 + 5718748q^5 - 13278244q^4 + 20718687q^3 - 20831606q^2 + 12151880q - 3099056 \end{aligned}$$

$$\begin{aligned} & i=23 \\ & 282q^{10} - 6070q^9 + 60577q^8 + 370021q^7 + 1535618q^6 - 4533514q^5 + 9656335q^4 - 14662046q^3 + 15180673q^2 - 9659534q + 2858328 \\ & 282q^{10} - 6046q^9 + 59737q^8 - 357855q^7 + 1437058q^6 - 4032690q^5 + 7983044q^4 - 10961373q^3 + 9935743q^2 - 5328872q + 1270972 \end{aligned}$$



$i=24$
$25q^{11}-582q^{10}+6334q^9-42648q^8+197920q^7-666402q^6+1664818q^5-3090972q^4+4183244q^3-3929437q^2+2301938q-635088$
$25q^{11}-582q^{10}+6318q^9-42210q^8+192692q^7-630228q^6+1503653q^5-2609179q^4+3214077q^3-2662786q^2+1326004q-297784$
$i=25$
$q^{12}-25q^{11}+294q^{10}-2156q^9+11011q^8-41375q^7+117609q^6-255411q^5+421351q^4-515486q^3+443947q^2-241344q+62452$
$q^{12}-25q^{11}+294q^{10}-2156q^9+10921q^8-40459q^7+112062q^6-233350q^5+361540q^4-404923q^3+309644q^2-144199q+30646$



TABLE VI

	b	2	3	4	5	Square lattice
	b'					(exact)
q→0	1	$\frac{4 \ln 2}{3\sqrt{q}} \cong \frac{0.924}{\sqrt{q}}$	$\frac{9 \ln 3}{11\sqrt{q}} \cong \frac{0.899}{\sqrt{q}}$	$\frac{56 \ln 4}{87\sqrt{q}} \cong \frac{0.892}{\sqrt{q}}$	?	$\frac{\pi}{3\sqrt{q}} \cong \frac{1.047}{\sqrt{q}}$
q=1		1.428	1.380	1.363	1.355	$4/3 \cong 1.333$
q=2		1.149	1.109	1.095	1.088	1
q=3		1.024	0.988	0.975	0.968	$5/6 \cong 0.833$
q=4		0.948	0.916	0.903	0.897	$2/3 \cong 0.667$
q→∞		$\frac{\ln 2}{\ln 5} \cong 0.431$	$\frac{\ln 3}{\ln 13} \cong 0.428$	$\frac{\ln 4}{\ln 25} \cong 0.431$	$\frac{\ln 5}{\ln 41} \cong 0.433$	-
q→0	2	-	$\frac{36 \ln(3/2)}{17\sqrt{q}} \cong \frac{0.859}{\sqrt{q}}$	$\frac{56 \ln(4/2)}{45\sqrt{q}} \cong \frac{0.863}{\sqrt{q}}$	?	$\frac{\pi}{3\sqrt{q}} \cong \frac{1.047}{\sqrt{q}}$
q=1		-	1.305	1.303	1.305	$4/3 \cong 1.333$
q=2		-	1.048	1.046	1.046	1
q=3		-	0.933	0.931	0.930	$5/6 \cong 0.833$
q=4		-	0.865	0.862	0.861	$2/3 \cong 0.667$
q→∞		-	$\frac{\ln(3/2)}{\ln(13/5)} \cong 0.424$	$\frac{\ln(4/2)}{\ln(25/5)} \cong 0.431$	$\frac{\ln(5/2)}{\ln(41/5)} \cong 0.435$	-
q→0	3	-	-	$\frac{504 \ln(4/3)}{167\sqrt{q}} \cong \frac{0.868}{\sqrt{q}}$	?	$\frac{\pi}{3\sqrt{q}} \cong \frac{1.047}{\sqrt{q}}$
q=1		-	-	1.301	1.306	$4/3 \cong 1.333$
q=2		-	-	1.043	1.044	1
q=3		-	-	0.928	0.928	$5/6 \cong 0.833$
q=4		-	-	0.859	0.858	$2/3 \cong 0.667$
q→∞		-	-	$\frac{\ln(4/3)}{\ln(25/13)} \cong 0.440$	$\frac{\ln(5/3)}{\ln(41/13)} \cong 0.445$	-
q→0	4	-	-	-	?	$\frac{\pi}{3\sqrt{q}} \cong \frac{1.047}{\sqrt{q}}$
q=1		-	-	-	1.311	$4/3 \cong 1.333$
q=2		-	-	-	1.046	1
q=3		-	-	-	0.928	$5/6 \cong 0.833$
q=4		-	-	-	0.857	$2/3 \cong 0.667$
q→∞		-	-	-	$\frac{\ln(5/4)}{\ln(41/25)} \cong 0.451$	-

TABLE VII

	RG <sub>31</sub>	RG <sub>51</sub>	RG <sub>53</sub>	Square lattice (exact)
q → 0	$\frac{45 \ln 3}{25\sqrt{q}} \cong \frac{0.951}{\sqrt{q}}$	$\frac{3625 \ln 5}{5996\sqrt{q}} \cong \frac{0.973}{\sqrt{q}}$	$\frac{32625 \ln(5/3)}{16264\sqrt{q}} \cong \frac{1.025}{\sqrt{q}}$	$\frac{\pi}{3\sqrt{q}} \cong \frac{1.047}{\sqrt{q}}$
q=1	1.652	1.610	1.527	4/3
q=2	1.369	1.317	1.218	1
q=3	1.244	1.188	1.082	5/6
q=4	1.170	1.110	1.000	2/3
q → ∞	$\frac{\ln 3}{\ln 5} \cong 0.683$	$\frac{\ln 5}{\ln(69/5)} \cong 0.613$	$\frac{\ln(5/3)}{\ln(69/25)} \cong 0.503$	—

TABLE VIII

(a)		q=1										
$J_y/J_x$	$J_z/J_x$	0	0.1	0.2	0.3	0.4	0.5	0.6	0.7	0.8	0.9	1.0
0	0	0.5548	0.7112	0.8349	0.9421	1.0390	1.1287	1.2129	1.2928	1.3692	1.4427	
	0	0.5548	0.7112	0.8349	0.9421	1.0390	1.1287	1.2129	1.2928	1.3692	1.4427*	
0.1	-	1.0592	1.2643	1.4255	1.5646	1.6896	1.8047	1.9125	2.0145	2.1117	2.2049	
	-	1.0229	1.2104	1.3612	1.4934	1.6139	1.7260	1.8317	1.9322	2.0284	2.1210	
0.2	-	-	1.4912	1.6689	1.8216	1.9584	2.0840	2.2013	2.3121	2.4174	2.5183	
	-	-	1.4061	1.5636	1.7024	1.8293	1.9479	2.0601	2.1670	2.2696	2.3686	
0.3	-	-	-	1.8592	2.0223	2.1682	2.3019	2.4266	2.5440	2.6557	2.7625	
	-	-	-	1.7259	1.8690	2.0002	2.1231	2.2394	2.3506	2.4575	2.5607	
0.4	-	-	-	-	2.1942	2.3476	2.4882	2.6190	2.7421	2.8591	2.9708	
	-	-	-	-	2.0158	2.1504	2.2766	2.3963	2.5107	2.6209	2.7273	
0.5	-	-	-	-	-	2.5078	2.6543	2.7905	2.9186	3.0402	3.1563	
	-	-	-	-	-	2.2882	2.4172	2.5397	2.6569	2.7698	2.8789	
0.6	-	-	-	-	-	-	2.8061	2.9472	3.0798	3.2055	3.3256	
	-	-	-	-	-	-	2.5489	2.6739	2.7935	2.9088	3.0203	
0.7	-	-	-	-	-	-	-	3.0927	3.2294	3.3590	3.4826	
	-	-	-	-	-	-	-	2.8012	2.9232	3.0406	3.1543	
0.8	-	-	-	-	-	-	-	-	3.3699	3.5031	3.6300	
	-	-	-	-	-	-	-	-	3.0472	3.1667	3.2824	
0.9	-	-	-	-	-	-	-	-	-	3.6395	3.7696	
	-	-	-	-	-	-	-	-	-	3.2882	3.4057	
1.0	-	-	-	-	-	-	-	-	-	-	3.9026	
	-	-	-	-	-	-	-	-	-	-	3.5250 <sup>§</sup>	

TABLE VIII



(b)		q=2										
$J_y/J_x$	$J_z/J_x$	0	0.1	0.2	0.3	0.4	0.5	0.6	0.7	0.8	0.9	1.0
0	0	0.4529	0.5708	0.6644	0.7462	0.8205	0.8897	0.9550	1.0172	1.0769	1.1346	
	0	0.4529	0.5708	0.6644	0.7462	0.8205	0.8897	0.9550	1.0172	1.0769	1.1346*	
0.1	-	0.7276	0.8578	0.9631	1.0555	1.1398	1.2183	1.2925	1.3631	1.4309	1.4964	
	-	0.6993	0.8165	0.9141	1.0018	1.0828	1.1591	1.2316	1.3012	1.3682	1.4332	
0.2	-	-	0.9967	1.1090	1.2075	1.2972	1.3806	1.4593	1.5341	1.6059	1.6751	
	-	-	0.9323	1.0299	1.1184	1.2009	1.2792	1.3540	1.4261	1.4958	1.5634	
0.3	-	-	-	1.2270	1.3304	1.4243	1.5116	1.5939	1.6721	1.7470	1.8192	
	-	-	-	1.1275	1.2164	1.2998	1.3791	1.4553	1.5289	1.6002	1.6696	
0.4	-	-	-	-	1.4379	1.5355	1.6262	1.7115	1.7926	1.8702	1.9449	
	-	-	-	-	1.3058	1.3898	1.4700	1.5472	1.6219	1.6944	1.7652	
0.5	-	-	-	-	-	1.6365	1.7301	1.8181	1.9018	1.9818	2.0588	
	-	-	-	-	-	1.4746	1.5556	1.6336	1.7092	1.7828	1.8546	
0.6	-	-	-	-	-	-	1.8264	1.9169	2.0029	2.0851	2.1642	
	-	-	-	-	-	-	1.6373	1.7162	1.7927	1.8671	1.9399	
0.7	-	-	-	-	-	-	-	2.0098	2.0979	2.1821	2.2630	
	-	-	-	-	-	-	-	1.7958	1.8732	1.9485	2.0221	
0.8	-	-	-	-	-	-	-	-	2.1880	2.2741	2.3568	
	-	-	-	-	-	-	-	-	1.9513	2.0274	2.1019	
0.9	-	-	-	-	-	-	-	-	-	2.3619	2.4463	
	-	-	-	-	-	-	-	-	-	2.1044	2.1796	
1.0	-	-	-	-	-	-	-	-	-	-	2.5323	
	-	-	-	-	-	-	-	-	-	-	-	2.2556 <sup>c</sup>

-247-

TABLE VIII

(c)		q=3										
$J_y/J_x$		0	0.1	0.2	0.3	0.4	0.5	0.6	0.7	0.8	0.9	1.0
$J_z/J_x$												
0	0	0.4060	0.5066	0.5869	0.6572	0.7213	0.7813	0.8380	0.8923	0.9445	0.9950	
	0	0.4060	0.5066	0.5869	0.6572	0.7213	0.7813	0.8380	0.8923	0.9445	0.9950*	
0.1	-	0.6044	0.7072	0.7918	0.8670	0.9360	1.0008	1.0622	1.1211	1.1778	1.2327	
	-	0.5820	0.6749	0.7537	0.8251	0.8917	1.9548	1.0150	1.0730	1.1291	1.1836	
0.2	-	-	0.8144	0.9028	0.9814	1.0537	1.1214	1.1857	1.2472	1.3065	1.3638	
	-	-	0.7642	0.8413	0.9123	0.9791	1.0429	1.1043	1.1636	1.2213	1.2774	
0.3	-	-	-	0.9945	1.0761	1.1510	1.2212	1.2878	1.3515	1.4128	1.4721	
	-	-	-	0.9174	0.9878	1.0547	1.1187	1.1807	1.2408	1.2993	1.3565	
0.4	-	-	-	-	1.1602	1.2374	1.3098	1.3783	1.4439	1.5070	1.5681	
	-	-	-	-	1.0580	1.1249	1.1892	1.2515	1.3122	1.3714	1.4293	
0.5	-	-	-	-	-	1.3168	1.3911	1.4614	1.5287	1.5934	1.6560	
	-	-	-	-	-	1.1918	1.2564	1.3191	1.3802	1.4399	1.4985	
0.6	-	-	-	-	-	-	1.4671	1.5391	1.6080	1.6742	1.7382	
	-	-	-	-	-	-	1.3213	1.3843	1.4459	1.5061	1.5652	
0.7	-	-	-	-	-	-	-	1.6127	1.6830	1.7506	1.8159	
	-	-	-	-	-	-	-	1.4478	1.5098	1.5705	1.6301	
0.8	-	-	-	-	-	-	-	-	1.7546	1.8235	1.8900	
	-	-	-	-	-	-	-	-	1.5723	1.6335	1.6936	
0.9	-	-	-	-	-	-	-	-	-	1.8936	1.9613	
	-	-	-	-	-	-	-	-	-	1.6952	1.7557	
1.0	-	-	-	-	-	-	-	-	-	-	2.0300	
	-	-	-	-	-	-	-	-	-	-	-	1.8169 <sup>§§</sup>

-248-

graph	degeneracy	weight	m
	1	$e^{qK}$	$2\mu$
	$q-1$	1	$(1-\frac{1}{q-1})\mu$












	1	$e^{5qK}$	$10\mu$
	$2(q-1)$	$e^{2qK}$	$(7-\frac{3}{q-1})\mu$
	$q-1$	$e^{3qK}$	$(8-\frac{2}{q-1})\mu$
	$q-1$	$e^{qK}$	$(4-\frac{6}{q-1})\mu$
	$(q-1)(q-2)$	1	$(4-\frac{6}{q-1})\mu$
	$2(q-1)$	$e^{2qK}$	$(5-\frac{5}{q-1})\mu$
	$2(q-1)(q-2)$	$e^{qK}$	$(5-\frac{5}{q-1})\mu$
	$q-1$	$e^{3qK}$	$(2-\frac{8}{q-1})\mu$
	$(q-1)(q-2)$	$e^{qK}$	$(2-\frac{8}{q-1})\mu$
	$2(q-1)(q-2)$	$e^{qK}$	$(2-\frac{8}{q-1})\mu$
	$(q-1)(q-2)(q-3)$	1	$(2-\frac{8}{q-1})\mu$

TABLE IX